

South Dakota State University

# Open PRAIRIE: Open Public Research Access Institutional Repository and Information Exchange

---

Electronic Theses and Dissertations

---

2016

## Role of T Lymphocyte Trafficking in Diabetic Cardiomyopathy

Chowdhury Sayef Abdullah  
*South Dakota State University*

Follow this and additional works at: <https://openprairie.sdstate.edu/etd>



Part of the [Pharmacy and Pharmaceutical Sciences Commons](#)

---

### Recommended Citation

Abdullah, Chowdhury Sayef, "Role of T Lymphocyte Trafficking in Diabetic Cardiomyopathy" (2016).  
*Electronic Theses and Dissertations*. 965.  
<https://openprairie.sdstate.edu/etd/965>

This Dissertation - Open Access is brought to you for free and open access by Open PRAIRIE: Open Public Research Access Institutional Repository and Information Exchange. It has been accepted for inclusion in Electronic Theses and Dissertations by an authorized administrator of Open PRAIRIE: Open Public Research Access Institutional Repository and Information Exchange. For more information, please contact [michael.biondo@sdstate.edu](mailto:michael.biondo@sdstate.edu).

ROLE OF T LYMPHOCYTE TRAFFICKING IN DIABETIC CARDIOMYOPATHY

BY

CHOWDHURY SAYEF ABDULLAH

A dissertation submitted in partial fulfillment of the requirements for the

Doctor of Philosophy

Major in Pharmaceutical Sciences

South Dakota State University

2016

## ROLE OF T LYMPHOCYTE TRAFFICKING IN DIABETIC CARDIOMYOPATHY

This dissertation is approved as a creditable and independent investigation by a candidate for the Doctor of Philosophy in Pharmaceutical Sciences degree and is acceptable for meeting the dissertation requirements for this degree. Acceptance of this dissertation does not imply that the conclusions reached by the candidate are necessarily the conclusions of the major department.

Omathanu Perumal, Ph.D.

Date

Dissertation Advisor

Omathanu Perumal, Ph.D.

Date

Head, Department of Pharmaceutical Sciences

Dean, Graduate School

Date

## ACKNOWLEDGEMENTS

I would like to express my sincere appreciation and gratitude to my advisor and mentor Dr. Zhu-Qiu Jin, former Assistant Professor of Pharmaceutical Sciences, for his supervision and guidance throughout my graduate study and research at South Dakota State University. I am grateful to Dr. Jin for giving me the training in cardiovascular pharmacology research area. Dr. Jin has taken great care to teach me the research techniques, scientific writing and presentation. I have learned and excelled in many experimental techniques during my research in Dr. Jin's laboratory. I will always appreciate Dr. Jin's contribution in my personal and professional development.

I would also like to express my heartfelt gratitude to Dr. Omathanu Perumal, Professor and Head of Department of Pharmaceutical Sciences at South Dakota State University, for serving as my advisory committee chair after Dr. Jin's departure from SDSU in Fall, 2015. Dr. Perumal spent considerable time and effort in reviewing my dissertation and in progressive discussion. His valuable suggestions improved the accuracy, presentation and readability of my dissertation.

I want to express my gratefulness to my PhD advisory committee members Dr. Xiuqing Wang, Dr. Teresa Seefeldt and Dr. Parashu Kharel for their valuable suggestions and directions throughout my dissertation research. I am really honored to have them in my advisory committee. I am especially thankful to Dr. Wang for her excellent technical assistance in flow cytometry analysis and letting me use her lab computer for flow cytometry data analysis. I am thankful to Dr. Xiangming Guan, Assistant Dean for Research/Professor of Medicinal Chemistry for providing directions and his encouragement throughout my graduate study. I am grateful to all of my course

instructors who helped me to gain advanced knowledge and skills in pharmaceutical sciences at South Dakota State University. In addition, I will always remain grateful to the Department of Pharmaceutical Sciences, College of Pharmacy at South Dakota State University for providing me the assistantship to support my graduate education and research.

Further, I am thankful to my fellow graduate students for their support and help in my research projects. I am thankful to my former lab mate Dr. Zhao Li for helping me to learn the experimental techniques and mouse handling and care. I am also thankful to Dr. Jiashu Xie for helping me with LC/MS/MS analysis. In addition, I am thankful to Dr. Shafiqur Rahman, Dr. Jayarama Gunaje, Dr. Monzurul Amin Roni, Dr. Yang Yang, Muzaffar Abbas, Rakesh Dachineni, Md. Saiful Islam, Guoqiang Ai, Mibin Kuruvilla Joseph, Siddharth Keshwarni for sharing their research expertise.

Finally, I express my sincere gratitude to my parents, Mr. Md. Bashirul Islam and Mrs. Mahfuja Begum, and younger brother Dr. Chowdhury Asif Abdullah, for their continuous encouragement, affection, well wishes and support from outside of USA to pursue my higher education.

## CONTENTS

LIST OF FIGURES .....	vii
LIST OF TABLES .....	xiv
ABBREVIATIONS .....	xvi
ABSTRACT .....	xviii
CHAPTER 1: INTRODUCTION .....	1
1.1. Diabetes and cardiovascular diseases .....	1
1.2. Diabetic cardiomyopathy .....	3
1.3. Myocardial fibrosis in diabetic cardiomyopathy .....	7
1.4. T lymphocytes involvement in myocardial fibrosis .....	12
1.5. Role of sphingosine 1-phosphate receptor 1 in T lymphocytes trafficking... 15	
1.6. Streptozotocin induced type 1 diabetic cardiomyopathy model .....	18
1.7. Cre-loxP recombination approach to generate T cell specific S1P <sub>1</sub> receptor knock out mice .....	20
1.8. Rationale and objectives .....	24
CHAPTER 2: EFFECTS OF S1P RECEPTOR 1 MODULATOR FINGOLIMOD ON CARDIAC FIBROSIS IN DIABETIC CARDIOMYOPATHY .....	27
2.1. Introduction .....	27
2.2. Materials and methods .....	29
2.3. Results .....	37
2.4. Discussion .....	76

2.5. Conclusions .....	84
CHAPTER 3: EFFECTS OF GENTIC DEPLETION OF T CELL S1P <sub>1</sub> RECEPTOR ON CARDIAC FIBROSIS IN DIABETIC CARDIOMYOPATHY	
.....	85
3.1. Introduction .....	85
3.2. Materials and methods .....	86
3.3. Results .....	92
3.4. Discussion .....	123
3.5. Conclusions .....	130
CHAPTER 4: EFFECTS OF CD4 T CELL TRANSFER TO TS1P <sub>1</sub> KO MICE ON CARDIAC FIBROSIS IN DIABETIC CARDIOMYOPATHY .....	
4.1. Introduction .....	131
4.2. Materials and methods .....	133
4.3. Results .....	140
4.4. Discussion .....	173
4.5. Conclusions .....	179
CHAPTER 5: SUMMARY .....	180
CHAPTER 6: FUTURE PROSPECTS .....	188
REFERENCES .....	190

## LIST OF FIGURES

Figure 1-1: Cellular composition of myocardium and fibrosis type .....	10
Figure 1-2: Proposed role of T lymphocytes trafficking to heart in steady state and post-myocardial infarction .....	14
Figure 1-3: Sphingosine 1-phosphate receptor 1 in T lymphocytes trafficking .....	17
Figure 1-4: Mechanism of action of streptozotocin-induced type 1 diabetes .....	19
Figure 1-5: Simplified scheme of conditional gene knock-out approach by using Cre-loxP site specific recombination system .....	22
Figure 1-6: Simplistic representation of physiological fields of study .....	24
Figure 2-1: Schematic diagram of 11-week long streptozotocin (STZ)-induced type 1 diabetes mice model and treatment protocol .....	31
Figure 2-2: Body weight (g) changes in wild-type (WT) C57BL/6 mice during 11-week experimental period .....	38
Figure 2-3: Blood glucose levels (mg/dl) in WT C57BL/6 mice at the beginning, after 4-weeks and after 11-weeks of STZ induction .....	39
Figure 2-4: Serum insulin levels (ng/mL) in WT C57BL/6 mice after 11-weeks of STZ induction .....	40
Figure 2-5: Body weight (g) changes in Rag1 KO mice during 11-week experimental period .....	42
Figure 2-6: Blood glucose levels (mg/dl) at the beginning, after 4-weeks and after 11-weeks of STZ administration in Rag1 KO mouse groups .....	43

Figure 2-7: Serum insulin levels (ng/ml) after 11-week of STZ induction in Rag1 KO mouse groups .....	44
Figure 2-8: Flow cytometry analysis of CD4 <sup>+</sup> and CD8 <sup>+</sup> T lymphocytes in peripheral blood of WT C57BL/6 mice after 11-week of experimental period .....	47
Figure 2-9: Quantification of CD4 <sup>+</sup> and CD8 <sup>+</sup> T cells percent numbers in WT C57BL/6 mice blood after 11-week of experimental period .....	48
Figure 2-10: Representative flow cytometry analysis dot plot and histogram plot of CD4 <sup>+</sup> and CD8 <sup>+</sup> T cells in Rag1 KO mice peripheral blood .....	50
Figure 2-11: Representative images of Hematoxylin and Eosin (H&E) stained heart tissue sections of WT C57BL/6 mice after 11-week of experimental period .....	52
Figure 2-12: Representative images of Hematoxylin and Eosin (H&E) stained heart tissue sections of Rag1 KO mice after 11-week of experimental period .....	53
Figure 2-13: Quantification of heart histology scores in WT C57BL/6 and Rag1 KO mice heart tissue sections .....	54
Figure 2-14: Representative images of Masson's Trichrome stained heart tissue sections of WT C57BL/6 mice after 11-week experimental period .....	56
Figure 2-15: Representative images of Masson's Trichrome stained heart tissue sections of Rag1 KO mice after 11-week experimental period .....	57
Figure 2-16: Quantification of percent fibrosis area in WT C57BL/6 and Rag1 KO mice heart after 11-weeks .....	58
Figure 2-17: Effect of FTY720 on cardiac contractile force in diabetic wild-type C57BL/6 and Rag1 KO mice hearts .....	60

Figure 2-18: Immunohistochemical detection of CD3 <sup>+</sup> T cells in heart tissue section of WT C57BL/6 mice after 11-week experimental period .....	62
Figure 2-19: FTY720 treatment effect in TGF- $\beta$ 1 expression in heart tissue sections of WT C57BL/6 and Rag1 KO mice after 11-week treatment period .....	64
Figure 2-20: Quantification of TGF- $\beta$ 1 percent staining area in WT C57BL/6 and Rag1 KO mice myocardium .....	65
Figure 2-21: Representative immunostaining images of CD34 bearing fibrocytes in heart tissue sections of WT C57BL/6 and Rag1 KO mice after 11-weeks .....	67
Figure 2-22: Quantification of percent area staining of CD34 expression in heart tissue sections of WT C57BL/6 and Rag1 KO mice after 11-weeks .....	68
Figure 2-23: Measurement of sphingosine 1-phosphate (S1P) level in the plasma samples of WT C57BL/6 and Rag1 KO mice by LC/MS/MS .....	71
Figure 2-24: Quantification of plasma S1P level in the plasma samples of WT C57BL/6 and Rag1 KO mice after 11-week experimental period .....	72
Figure 2-25: Representative immunohistochemistry images of S1P <sub>1</sub> expression in WT C57BL/6 and Rag1 KO mice myocardium after 11-weeks .....	74
Figure 2-26: Quantification of S1P <sub>1</sub> expression in WT C57BL/6 and Rag1 KO mice heart tissue sections after 11-weeks .....	75
Figure 3-1: Generation and detection of conditional T cell specific S1P receptor 1 knock out mice .....	93

Figure 3-2: Flow cytometry analysis of CD3 <sup>+</sup> T cells in spleen of littermate control and TS1P <sub>1</sub> KO mice .....	94
Figure 3-3: Flow cytometry analysis of CD4 <sup>+</sup> and CD8 <sup>+</sup> T cells in littermate control and TS1P <sub>1</sub> KO mice blood .....	95
Figure 3-4: Body weights (g) change in littermate and TS1P <sub>1</sub> KO mice during 11-week experimental period .....	97
Figure 3-5: Blood glucose levels (mg/dl) during 11-week study period in littermate and TS1P <sub>1</sub> KO mice .....	99
Figure 3-6: Flow cytometry analysis of CD4 <sup>+</sup> and CD8 <sup>+</sup> T cells in blood of littermate and TS1P <sub>1</sub> KO mice at the end of 11-weeks .....	102
Figure 3-7: Flow cytometry analysis of CD4 <sup>+</sup> Foxp3 <sup>+</sup> regulatory T cells in spleen and blood of littermate and TS1P <sub>1</sub> KO mice at the end of 11-weeks .....	104
Figure 3-8: Representative images of Hematoxylin and Eosin (H&E) stained heart tissue sections of littermate and TS1P <sub>1</sub> KO mice after 11-weeks .....	107
Figure 3-9: Quantification of heart histological scores in littermate and TS1P <sub>1</sub> KO mice after 11-weeks .....	108
Figure 3-10: Representative images of Masson's Trichrome stained heart tissue sections in littermate and TS1P <sub>1</sub> KO mice after 11-weeks .....	110
Figure 3-11: Quantification of percent fibrosis area in heart sections of littermate and TS1P <sub>1</sub> KO mice after 11-weeks .....	111

Figure 3-12: Cardiac contractility in littermate and TS1P <sub>1</sub> KO mice after 11-week study period .....	113
Figure 3-13: Immunohistochemical detection of CD3 <sup>+</sup> T cells in littermate and TS1P <sub>1</sub> KO mice heart tissue section at the end of 11-weeks .....	115
Figure 3-14: Quantification of infiltrated CD3 <sup>+</sup> T cells in heart tissue sections of littermate and TS1P <sub>1</sub> KO mice after 11-week experimental period .....	116
Figure 3-15: Immunohistochemical detection of TGF-β1 expression in littermate and TS1P <sub>1</sub> KO mice heart tissue sections after 11-weeks .....	118
Figure 3-16: Quantification of TGF-β1 expression in heart tissue sections of littermate and TS1P <sub>1</sub> KO mice after 11-week experimental period .....	119
Figure 3-17: Immunohistochemical detection of CD34 fibrocytes expression in littermate and TS1P <sub>1</sub> KO mice heart tissue sections after 11-weeks .....	121
Figure 3-18: Quantification of CD34 fibrocytes expression in heart tissue sections of littermate and TS1P <sub>1</sub> KO mice after 11-week experimental period .....	122
Figure 4-1: Schematic diagram of preparation of single-cell suspensions from littermate mouse spleen .....	135
Figure 4-2: Schematic diagram of experimental procedure to isolate CD4 <sup>+</sup> T cell from single-cell suspensions of splenocyte of littermate control mice .....	136
Figure 4-3: Schematic diagram of experimental protocol of adoptive transfer of CD4 <sup>+</sup> T cell in littermate and TS1P <sub>1</sub> KO mice followed by 11-week long streptozotocin (STZ)-induced type 1 diabetes .....	137

Figure 4-4: Representative flow cytometry histogram of CD4 <sup>+</sup> staining in total splenocytes, and in CD4 positive and CD4 negative fractions .....	141
Figure 4-5: Body weight (g) change in CD4 <sup>+</sup> T cell recipient littermate and TS1P <sub>1</sub> KO mice during 11-week study period .....	142
Figure 4-6: Blood glucose level (mg/dl) during 11-week study period in CD4 <sup>+</sup> T cell recipient littermate and TS1P <sub>1</sub> KO mice .....	145
Figure 4-7: Blood glucose level (mg/dl) at end of 11-week in diabetic TS1P <sub>1</sub> KO mice without- and with- CD4 <sup>+</sup> T cell adoptive transfer .....	146
Figure 4-8: Effects in total splenocytes number (x10 <sup>6</sup> cells/ml) in littermate and TS1P <sub>1</sub> KO mice after CD4 <sup>+</sup> T cell transfer compared to littermate and TS1P <sub>1</sub> KO mice without CD4 <sup>+</sup> T cell transfer .....	150
Figure 4-9: Quantification data of CD4 <sup>+</sup> and CD8 <sup>+</sup> T cells number in blood of littermate and TS1P <sub>1</sub> KO mice after CD4 <sup>+</sup> T cell transfer at the end of 11-weeks .....	153
Figure 4-10: Comparison of CD4 <sup>+</sup> T cells number in blood between CD4 <sup>+</sup> T cell recipient TS1P <sub>1</sub> KO mouse groups and TS1P <sub>1</sub> KO mouse groups without CD4 <sup>+</sup> T cell transfer at the end of 11 weeks .....	154
Figure 4-11: Quantification data of CD4 <sup>+</sup> Foxp3 <sup>+</sup> T cells number in spleen and blood of littermate and TS1P <sub>1</sub> KO mice after CD4 <sup>+</sup> T cell transfer at the end of 11-week experimental period .....	156
Figure 4-12: Heart histology study in H&E stained sections of CD4 <sup>+</sup> T cell recipient littermate and TS1P <sub>1</sub> KO mice after 11-week experimental period .....	159

Figure 4-13: Comparison between TS1P <sub>1</sub> KO mouse groups heart histology in H&E stained sections without- and with CD4 <sup>+</sup> T cell transfer .....	160
Figure 4-14: Fibrosis extent assessment in Trichrome stained heart sections of CD4 <sup>+</sup> T cell recipient littermate and TS1P <sub>1</sub> KO mice after 11-weeks .....	162
Figure 4-15: Comparison between TS1P <sub>1</sub> KO mouse groups fibrosis extent in Masson's Trichrome stained heart sections without- and with- CD4 <sup>+</sup> T cell transfer .....	163
Figure 4-16: Cardiac contractile force in CD4 <sup>+</sup> T cell recipient littermate and TS1P <sub>1</sub> KO mice after 11-week study period .....	164
Figure 4-17: Immunohistochemical detection of CD3 <sup>+</sup> T cells in CD4 <sup>+</sup> T cell recipient littermate and TS1P <sub>1</sub> KO mice heart sections at the end of 11 weeks .....	166
Figure 4-18: Quantification of infiltrated CD3 <sup>+</sup> T cells in myocardium of CD4 <sup>+</sup> T cell recipient littermate and TS1P <sub>1</sub> KO mice .....	167
Figure 4-19: Immunohistochemical assessment of TGF beta 1 (TGF-β1) expression in CD4 <sup>+</sup> T cell recipient littermate and TS1P <sub>1</sub> KO mice heart sections at the end of 11-weeks.....	168
Figure 4-20: Quantification of TGF-β1 expression in myocardium of CD4 <sup>+</sup> T cell recipient littermate and TS1P <sub>1</sub> KO mice .....	169
Figure 4-21: Immunohistochemical assessment of CD34 expression in CD4 <sup>+</sup> T cell recipient littermate and TS1P <sub>1</sub> KO mice heart sections at the end of 11 weeks .....	171
Figure 4-22: Quantification of CD34 expression in myocardium of CD4 <sup>+</sup> T cell recipient littermate and TS1P <sub>1</sub> KO mice .....	172

## LIST OF TABLES

Table 1-1: Summary of diabetic cardiomyopathy associated notable pathophysiological, structural and functional changes in myocardium .....	7
Table 2-1: Summary of metabolic and physiological parameters in WT C57BL/6 mice during 11-weeks .....	41
Table 2-2: Summary of metabolic and physiological parameters in Rag1 KO mice during 11-weeks .....	45
Table 2-3: Summary of CD4 <sup>+</sup> and CD8 <sup>+</sup> T cells percent numbers in peripheral blood of WT C57BL/6 mice after 11-weeks .....	49
Table 3-1: Genotyping PCR primers and reaction conditions for Cre and S1P <sub>1</sub> genes ...	87
Table 3-2: Summary of CD3 <sup>+</sup> T cells in spleen, CD4 <sup>+</sup> and CD8 <sup>+</sup> T cells number in blood of littermate control and TS1P <sub>1</sub> KO mice .....	96
Table 3-3: Summary of physiological parameter in littermate and TS1P <sub>1</sub> KO mice during 11-week experimental period .....	98
Table 3-4: Summary of metabolic parameter in littermate and TS1P <sub>1</sub> KO mice during 11-week experimental period .....	100
Table 3-5: Summary of CD4 <sup>+</sup> , CD8 <sup>+</sup> T cells percent in blood, and CD4 <sup>+</sup> Foxp3 <sup>+</sup> T cells percent in spleen and blood of littermate and TS1P <sub>1</sub> KO mice after 11-weeks .....	105
Table 4-1: Summary of physiological parameter in CD4 <sup>+</sup> T cell recipient littermate and TS1P <sub>1</sub> KO mice during 11-week experimental period .....	143
Table 4-2: Summary of metabolic parameter in CD4 <sup>+</sup> T cell recipient littermate and TS1P <sub>1</sub> KO mice during 11-week experimental period .....	147

Table 4-3: Summary of spleen weight (mg) to body weight (g) ratio in littermate and TS1P <sub>1</sub> KO mice without- and with-CD4 <sup>+</sup> T cell transfer .....	149
Table 4-4: Summary of splenocytes number (x10 <sup>6</sup> cells/ml) in littermate and TS1P <sub>1</sub> KO mice without- and with-CD4 <sup>+</sup> T cell transfer .....	151
Table 4-5: Summary of CD4 <sup>+</sup> T cells number in blood of TS1P <sub>1</sub> KO mouse groups without- and with- CD4 <sup>+</sup> T cell transfer after 11 weeks .....	155
Table 4-6: Summary of CD4 <sup>+</sup> Foxp3 <sup>+</sup> T cells number in spleen and blood of TS1P <sub>1</sub> KO mouse groups without- and with- CD4 <sup>+</sup> T cell transfer after 11-weeks .....	157

## ABBREVIATIONS

ANOVA	Analysis of variance
CD	Cluster of differentiation
CVD	Cardiovascular disease
EC <sub>50</sub>	Half maximal effective concentration
ELISA	Enzyme-linked immunosorbent assay
Fc	Contractile force
Foxp3	Forkhead box P3
FTY720	Fingolimod
GPCR	G protein-coupled receptor
H&E	Hematoxylin and eosin
IACUC	Institutional animal care and use committee
ICAM-1	Intercellular adhesion molecule-1
IHC	Immunohistochemistry
IL	Interleukin
i.p.	Intraperitoneal
KO	Knockout
LC/MS/MS	Liquid Chromatography tandem mass spectrometry

LV	Left ventricle
MI	Myocardial infarction
PKC $\theta$	Protein kinase C theta
Rag1	Recombination activating gene 1
ROS	Reactive oxygen species
S1P	Sphingosine 1-phosphate
S1P <sub>1</sub>	S1P receptor 1
SDSU	South Dakota State University
SEM	Standard error of the mean
STAT	Signal transducer and activator of transcription
STZ	Streptozotocin
TGF- $\beta$ 1	Transforming growth factor beta 1
T <sub>H</sub>	T helper cells
TNF- $\alpha$	Tumor necrosis factor alpha
TS1P <sub>1</sub> KO	T cell specific S1P <sub>1</sub> receptor knock out
VCAM-1	Vascular adhesion molecule-1
WT	Wild-type

## ABSTRACT

## ROLE OF T LYMPHOCYTE TRAFFICKING IN DIABETIC CARDIOMYOPATHY

CHOWDHURY SAYEF ABDULLAH

2016

Diabetic cardiomyopathy is a distinct pathological condition characterized by myocardial fibrosis and cardiac dysfunction in diabetic patients. The resolution of myocardial fibrosis to improve cardiac function in diabetes is an active area of research. Notably, increased T lymphocyte infiltration into myocardium has been attributed to increased cardiac fibrosis and dysfunction in diabetes. However, the experimental data on the role of T lymphocyte modulation in diabetic myocardial fibrosis is scarce. To this end, sphingosine 1-phosphate receptor 1 (S1P<sub>1</sub>) regulates the egress of mature T lymphocytes from lymphoid organs to blood and peripheral organs. Thus, the inhibition of T cells trafficking through S1P<sub>1</sub> receptor modulation is a potential translational approach to protect the heart in diabetes. We hypothesized that inhibition of T lymphocyte trafficking by modulating S1P<sub>1</sub> receptor protects diabetic heart and ameliorates fibrosis. To accomplish this overarching objective, we conducted three related studies: (1) assess the effects of fingolimod (S1P<sub>1</sub> receptor modulator) treatment in diabetes-induced myocardial fibrosis in mice; (2) study cardiac fibrosis and dysfunction in diabetes using conditional T-cell S1P<sub>1</sub> knockout (TS1P<sub>1</sub>KO) mice; (3) evaluate the effects of CD4<sup>+</sup> T cells transfer to TS1P<sub>1</sub>KO mice in diabetes-induced myocardial fibrosis and dysfunction.

We have demonstrated that FTY720 treatment induces sustained CD4<sup>+</sup> and CD8<sup>+</sup> T cells deficiency in the blood with reduced CD3<sup>+</sup> T cells infiltration into myocardium of diabetic wild-type (WT) mice. Notably, FTY720 treatment reduced cardiac fibrosis area and improved cardiac contractility in diabetic WT mice. Our results in Rag1 knock-out (KO) mice lacking mature lymphocytes, further, confirmed that systemic T lymphocytes depletion is associated with cardioprotection. However, FTY720 treatment exacerbated fibrosis and attenuated contractility in diabetic KO mice. Therefore, we utilized Cre-loxP genetic approach to generate conditional T cell specific S1P<sub>1</sub> receptor knock-out (TS1P<sub>1</sub>KO) mice to study S1P<sub>1</sub> receptor mediated T cells trafficking effects in diabetes-induced cardiac fibrogenesis.

One of the unique findings of our study is reduced cardiac fibrosis area in TS1P<sub>1</sub>KO mice in chronic diabetes. TS1P<sub>1</sub>KO mice showed profound CD4<sup>+</sup> and CD8<sup>+</sup> T cells deficiency in circulation and reduced CD3<sup>+</sup> T cells infiltration into myocardium in diabetes. We also found that diabetic TS1P<sub>1</sub>KO mice myocardium had reduced profibrotic molecular and cellular milieu. However, normoglycemic TS1P<sub>1</sub>KO buffer treated mice exhibited increased fibrosis area and reduced cardiac contractility. This result indicates the potential role of different types of lymphocytes, and lymphocyte ratio in the blood in maintaining cardiac collagen homeostasis. Although TS1P<sub>1</sub>KO mice have reduced T lymphocytes in the blood, the mice had higher circulatory B lymphocytes, which also has been implicated in myocardial fibrosis. Thus, to establish the involvement of S1P<sub>1</sub> mediated T lymphocytes trafficking in cardiac fibrosis, we conducted adoptive transfer of littermate T cells to TS1P<sub>1</sub>KO mice.

Among CD4<sup>+</sup> and CD8<sup>+</sup> T cells, all four subsets of CD4<sup>+</sup> T cells have been shown to be involved in cardiac fibrosis. Therefore, our aim was to investigate the effects of littermate CD4<sup>+</sup> T cells transfer on cardiac fibrosis and myocardial contractile force in TS1P<sub>1</sub>KO mice in both normoglycemic and hyperglycemic conditions. Our flow cytometry analysis revealed increased CD4<sup>+</sup> and CD4<sup>+</sup>Foxp3<sup>+</sup> T cells in the blood of TS1P<sub>1</sub>KO mice after CD4<sup>+</sup> T cells transfer. Strikingly, we found that CD4<sup>+</sup> T cells transfer reversed cardioprotection in hyperglycemic TS1P<sub>1</sub>KO mice, while it protected normoglycemic TS1P<sub>1</sub>KO mice heart. In both conditions, TS1P<sub>1</sub>KO mice showed increased CD3<sup>+</sup> T cells infiltration after CD4<sup>+</sup> T cell transfer. These results underpin S1P<sub>1</sub> mediated T cells trafficking in maintaining cardiac collagen homeostasis in both normoglycemic and hyperglycemic conditions.

Overall, through pharmacological and genetic approaches we have demonstrated that S1P<sub>1</sub> mediated T cells trafficking is involved in cardiac fibrogenesis in chronic diabetes. Our studies provide strong evidence of T lymphocytes S1P<sub>1</sub> receptor signaling as a translational target to protect diabetic heart and ameliorate fibrosis.

## CHAPTER 1: INTRODUCTION

### 1.1. Diabetes and cardiovascular diseases

Diabetes mellitus is characterized by hyperglycemia (increased glucose in plasma) due to defects in insulin secretion, insulin action or both.<sup>1</sup> There are two major prevalent form of diabetes, namely, type 1 and type 2 diabetes.<sup>2,3</sup> Type 1 diabetes is characterized by early onset due to autoimmune destruction of the insulin producing pancreatic beta cells.<sup>2,3</sup> Thus, type 1 diabetic patients require exogenous insulin administration to maintain their blood glucose level.<sup>3</sup> Etiological risk factors of Type 2 diabetes include obesity, aging, high calorie intake, lack of exercise and sedentary lifestyle.<sup>2,3</sup> Due to these risk factors, the tissues and cells exhibit reduced insulin sensitivity (insulin resistance) and glucose uptake in type 2 diabetes leading to increased glucose level in the blood.<sup>2,3</sup> According to the American Diabetes Association guidelines, normal fasting blood glucose level is below 100 mg/dl, while a fasting blood glucose level  $\geq 126$  mg/dl is indicative of diabetes.<sup>1</sup> According to the current estimates from World Health Organization (WHO), there are more than 300 million people affected by diabetes and is estimated to increase to more than 347 million people worldwide by 2030.<sup>4,5</sup> In the United States, 29.1 million Americans are affected by diabetes with 1.4 million newly diagnosed diabetes each year.<sup>6</sup> Type 1 diabetes accounts for approximately 5% of all diagnosed diabetes, while type 2 diabetes accounts for the other 90-95% of diagnosed diabetes cases.<sup>6,7</sup> Although there are many oral drugs available to maintain blood glucose level in diabetic patients, half of the type 2 diabetic patients ultimately rely on insulin administration to maintain the normal blood glucose level.<sup>3</sup> Thus, chronic hyperglycemia

is a hallmark of both type of diabetes and is a pivotal factor in the development of diabetic complications in patients.<sup>3</sup>

Hyperglycemia causes injury, dysfunction and failure in vital organs including heart, kidney, eye, nerves and blood vessels in diabetic patients.<sup>1,3</sup> WHO reports nearly 50% of diabetic patient's death occurs from cardiovascular disease, such as heart failure and atherosclerosis.<sup>8</sup> Epidemiological studies have reported strong association between diabetes and heart failure.<sup>7,8,9</sup> Framingham heart study conducted by the National Heart, Lung and Blood Institute of US to identify cardiovascular disease (CVD) risk factors reported two-fold and five-fold higher heart failure risk in diabetic men and women, respectively, than age matched non-diabetic control subjects.<sup>10</sup> Chronic hyperglycemia has been shown to affect cardiac function independent of other diabetes-associated CVD risk factors, such as atherosclerosis, cerebrovascular disease and hypertension.<sup>3,9,10</sup> The distinct pathologic alterations in the myocardium induced by diabetes are defined as "diabetic cardiomyopathy".<sup>9</sup> Diabetic cardiomyopathy can occur in the absence of other CVD risk factors and can contribute to heart failure development in diabetic patients.<sup>3,9</sup> Different pathological mechanisms have been shown to be involved in the development of diabetic cardiomyopathy. Nonetheless, different cellular effectors and their mechanisms of involvement in diabetic cardiomyopathy need further investigation.

## **1.2. Diabetic cardiomyopathy**

The European Society of Cardiology defines cardiomyopathy as a myocardial disorder characterized by abnormal heart muscle structure and function, in absence of coronary artery disease, hypertension, congenital heart disease and heart valve disease.<sup>11</sup> Based on etiology, cardiomyopathy can be divided into two types, primary cardiomyopathy and secondary cardiomyopathy.<sup>11</sup> Primary cardiomyopathy occurs from disease of the heart muscle cells due to genetic mutation including hypertrophic cardiomyopathy and dilated cardiomyopathy.<sup>11</sup> Secondary cardiomyopathy occurs due to systemic syndromes such as diabetes, myocarditis and alcohol overuse that negatively affect cardiac function.<sup>11</sup> Thus, diabetic cardiomyopathy is a secondary cardiomyopathy that occurs in diabetes associated chronic hyperglycemia leading to the development of the heart failure in diabetic patients.<sup>12,13</sup>

Rubler et al. first described diabetic cardiomyopathy as a distinct clinical pathophysiology prevalent in diabetic patients.<sup>9</sup> In this study, the authors reported left ventricular hypertrophy with myocardial fibrosis in diabetic patient hearts who deceased from heart failure without having coronary artery disease, hypertension or other etiological conditions underlying for observed heart failure.<sup>9</sup> Regan et al. confirmed these findings in a later study.<sup>14</sup> In line with these observations, recent larger population based studies revealed a 1.5-fold higher risk of heart failure in patients with diabetes after adjusting for multiple variables including age, sex, obesity, antihypertensive medications, atrial fibrillation, smoking habit, alcohol use, plasma cholesterol, educational level and physical activity.<sup>15</sup> Therefore, epidemiological studies further confirmed that diabetes can by itself cause development of cardiomyopathy, termed as diabetic cardiomyopathy.

Diabetic cardiomyopathy is considered as an important contributing factor for increased prevalence of heart failure in diabetic patients.<sup>12,13</sup>

The pathophysiology of diabetic cardiomyopathy development involves various pathological changes in heart under diabetes including endothelial dysfunction, myocyte apoptosis, interstitial inflammation, myocardial fibrosis and diastolic dysfunction followed by systolic dysfunction, if unresolved.<sup>13,16-18</sup> Myocardial fibrosis is a pivotal etiological factor in diabetic cardiomyopathy that underlies diastolic dysfunction development in diabetes patient heart.<sup>19-23</sup> Hyperglycemia activates and affects a diverse set of molecular and cellular pathways present in mammalian heart that ultimately leads to increased myocardial fibrosis in diabetes.<sup>24</sup> During the early stages of diabetes, the heart exhibits reduced antioxidant capacity and increased generation of reactive oxygen species (ROS) resulting in oxidative stress.<sup>25</sup> Increased ROS accumulation occurs through different metabolic pathways including increased flux of glucose into electron transport chain promoting superoxide generation by electron transfer to molecular oxygen in mitochondria, increased formation of non-enzymatic advanced glycation end products (AGEs) and activation of their receptors. Further, activation of other signaling pathways including activation of protein kinase C isoforms, and reduction of intracellular antioxidants including nicotinamide adenine dinucleotide phosphate (NADPH) and glutathione (GSH) induce overproduction of superoxide radicals.<sup>25,26</sup> Intracellular ROS, in turn, can activate redox sensitive transcription factor NF- $\kappa$ B, which is the central modulator of transcription of numerous genes including proinflammatory cytokines and adhesion molecules in the diabetic myocardium.<sup>27,28</sup> Thus, oxidative stress leads to an

ongoing inflammation in diabetic heart that is further potentiated by activation of proinflammatory pathways.

Presence of inflammation in diabetic myocardium is manifested as enhanced expression of proinflammatory cytokines including tumor necrosis factor- $\alpha$  (TNF- $\alpha$ ), interleukin-6 (IL-6), interleukin-1 $\beta$  (IL-1 $\beta$ ) and profibrotic growth factors, such as transforming growth factor- $\beta$ 1 (TGF- $\beta$ 1). Inflammation further enhances chemokines expression, such as chemokine C-C motif ligand-2 and 5 (CCL2, CCL5) and adhesion molecules expression including intercellular adhesion molecule-1 (ICAM-1), vascular adhesion molecule-1 (VCAM-1) and monocyte chemoattractant protein-1 (MCP-1).<sup>3,28-35</sup> Increased expression of adhesion molecules under chronic inflammation further enhances recruitment of blood derived immunocompetent cells including lymphocytes, monocytes, macrophages, reparative mesenchymal cells and fibrocytes into the diabetic myocardium.<sup>36,37</sup> The recruited immune cells, in turn, secrete cytokines and growth factors which potentiate, the profibrotic microenvironment development in the myocardium. Proinflammatory and profibrotic microenvironments, in turn, activate resident and recruited collagen producing fibroblasts and fibroblast progenitor cells that results in increased collagen synthesis by these cells. Increased collagen deposition in myocardium ultimately leads to fibrosis development in diabetes (Table 1-1).<sup>16,38</sup>

Increased cardiac fibrosis in diabetic myocardium underlies diastolic and systolic dysfunction in diabetes patients (Table 1-1).<sup>13,17</sup> Enhanced fibrosis reduces myocardial ventricular wall compliance and stiffens the ventricular walls that impair cardiac ventricles relaxation during diastole. Impaired cardiac ventricular relaxation, in turn, leads to diastolic dysfunction. Diastolic dysfunction further, if unresolved, leads to

systolic dysfunction underlying development of heart failure.<sup>13,17-19,39-42</sup> Prevalence of diastolic dysfunction is estimated to be as high as 40% to 60% patients with type 1 and type 2 diabetes without overt coronary artery disease.<sup>21-23</sup> Other epidemiological studies also show association between enhanced myocardial fibrosis with impaired ventricular function in diabetic patients.<sup>17</sup> Increased myocardial collagen content has been detected in insulin dependent diabetic normotensive patients as compared to age- and sex-matched control subjects, assessed by ultrasound echoreflectivity.<sup>18</sup> Similar results with increased myocardial collagen in diabetic patients have been confirmed in larger studies by Fang et al.<sup>19</sup> Thus, epidemiological studies confirmed the presence of myocardial fibrosis with cardiac dysfunction in diabetic patients. To this end, resolution of myocardial fibrosis to improve cardiac function in diabetes is an active area of research. As discussed above, the recruited effector immune cells facilitate and potentiate myocardial fibrosis. Thus, the modulation of immune cells function is a potential approach to ameliorate myocardial fibrosis in diabetes.

**Table 1-1:** Summary of diabetic cardiomyopathy associated notable pathophysiological, structural and functional changes in myocardium.

<b>Diabetic Cardiomyopathy</b>		
<b><u>Pathophysiological Changes</u></b>	<b><u>Structural Changes</u></b>	<b><u>Functional Changes</u></b>
<ul style="list-style-type: none"> <li>• Increased ROS generation</li> <li>• Increased AGEs</li> <li>• Decreased antioxidants</li> <li>• Oxidative stress</li> <li>• Increased inflammation</li> <li>• Activation of immune system</li> <li>• Increased cell death</li> <li>• Myocardial fibrosis</li> </ul>	<ul style="list-style-type: none"> <li>• Maladaptive cardiac remodeling</li> <li>• Increased LV wall thickness</li> <li>• Increased LV mass</li> </ul>	<ul style="list-style-type: none"> <li>• Impaired diastolic function</li> <li>• Impaired systolic function</li> </ul>

ROS: reactive oxygen species, AGEs: advanced glycation end products, LV: left ventricle.

### **1.3. Myocardial fibrosis in diabetic cardiomyopathy**

As discussed earlier (see section 1.2.), myocardial fibrosis is one of the hallmark pathological features in diabetic patient heart as detected by echocardiography and autopsy studies.<sup>9,11,18-23</sup> The mechanism of fibrosis induced cardiac dysfunction involves impairment of heart diastolic relaxation. Human heart works through consecutive systole (contraction) and diastole (relaxation) phases. During systole, the heart pumps the blood

throughout the body, whereas during diastole heart ventricles relax to fill blood that is pumped at the next systole. Increased cardiac fibrosis reduces ventricular wall compliance and increases stiffness that impairs normal relaxation of ventricles during diastole leading to diastolic dysfunction.<sup>42-44</sup> Excess collagen deposition in myocardium, further impedes proper contraction of the heart as electrical impulse conduction gets impaired due to collagen deposition in between cardiomyocytes.<sup>42-46</sup> Thus, enhanced myocardial fibrosis underlies the development of diastolic dysfunction preceding systolic dysfunction in diabetic patient that ultimately leads to heart failure development.<sup>47,48</sup>

Myocardial fibrosis is a complex, multifactorial process that occurs at the site of tissue injury and inflammation.<sup>36,40,46</sup> It is a natural tissue repair process that results from increased deposition of non-contractile collagen in cardiac interstitium leading to cardiac functional impairment.<sup>46</sup> Two types of cardiac fibrosis has been described reparative (replacement) fibrosis and reactive fibrosis.<sup>46</sup> Reparative fibrosis occurs after sudden cell death of a large number of cardiomyocytes resulting from myocardial infarction upon coronary artery block. On the other hand, reactive fibrosis develops in chronic inflammatory conditions, such as diabetes and hypertension. Reactive fibrosis, if unresolved, can turn into reparative fibrosis (Figure 1-1).<sup>44-46</sup> The increased synthesis of collagen during fibrogenesis involves molecular stimuli to cellular functions as discussed below.

Myocardial fibrosis is characterized by increased collagen deposition in the heart tissue.<sup>40</sup> The extracellular matrix protein (ECM) components provide support for cellular function in the heart including distribution of mechanical forces, signal transduction as well as play important role in maintaining functional cardiac shape and size.<sup>41</sup>

Myocardial ECM components consist of fibril collagen, proteoglycans and glycosaminoglycans.<sup>42</sup> The most abundant fibrillary collagen in the heart is collagen type I and type III including less abundant types of IV, V, and VI, elastin and laminin.<sup>41-43</sup> In diabetic heart, as was discussed earlier (see section 1.2), increased ROS, inflammation and growth factor stimuli result in enhanced synthesis of the ECM proteins leading to the development of cardiac fibrosis.<sup>43,44</sup> During cardiac fibrogenesis, cardiomyocytes and non-cardiomyocytes including resident cardiac fibroblasts, immune cells, vascular endothelial cells and the immunocompetent cells, closely interact with each other in fibrotic remodeling of the heart (Figure 1-1).<sup>46</sup> The fibroblasts upon stimulation by inflammatory signals produce and secrete collagen matrix proteins in excess, while other cells, such as macrophages, mast cells, lymphocytes, cardiomyocytes and vascular cells secrete profibrogenic cytokines that stimulate fibroblasts' collagen synthesizing activity.<sup>36,49</sup> Diabetes associated hyperglycemic conditions can activate, among others, fibrogenic transforming growth factor beta-1 (TGF- $\beta$ 1) signaling.<sup>50,51</sup> TGF- $\beta$ 1 is a well reported mediator in cardiac fibrosis and the most predominant isoform present in cardiovascular system among three isoforms.<sup>52-54</sup> TGF- $\beta$ 1 mediates its effects by directly inducing matrix protein synthesis by stimulating collagen producing cells, decreasing production of matrix degrading proteolytic enzymes, and modulating the expression of integrins, which increases cellular adhesions to the matrix.<sup>55,56</sup> TGF- $\beta$ 1 is present in both cardiomyocytes and cardiac fibroblasts and has been found to take part in cardiomyocyte growth, fibrosis and re-expression of fetal isoforms of myofibrillar protein genes, that are salient characteristics of pathological cardiac remodeling.<sup>57-60</sup> Further, the recruited

blood derived immune cells also participate in fibrosis by secreting cytokines, growth factors, and can transdifferentiate in collagen synthesizing fibroblasts.<sup>36,48,61</sup>

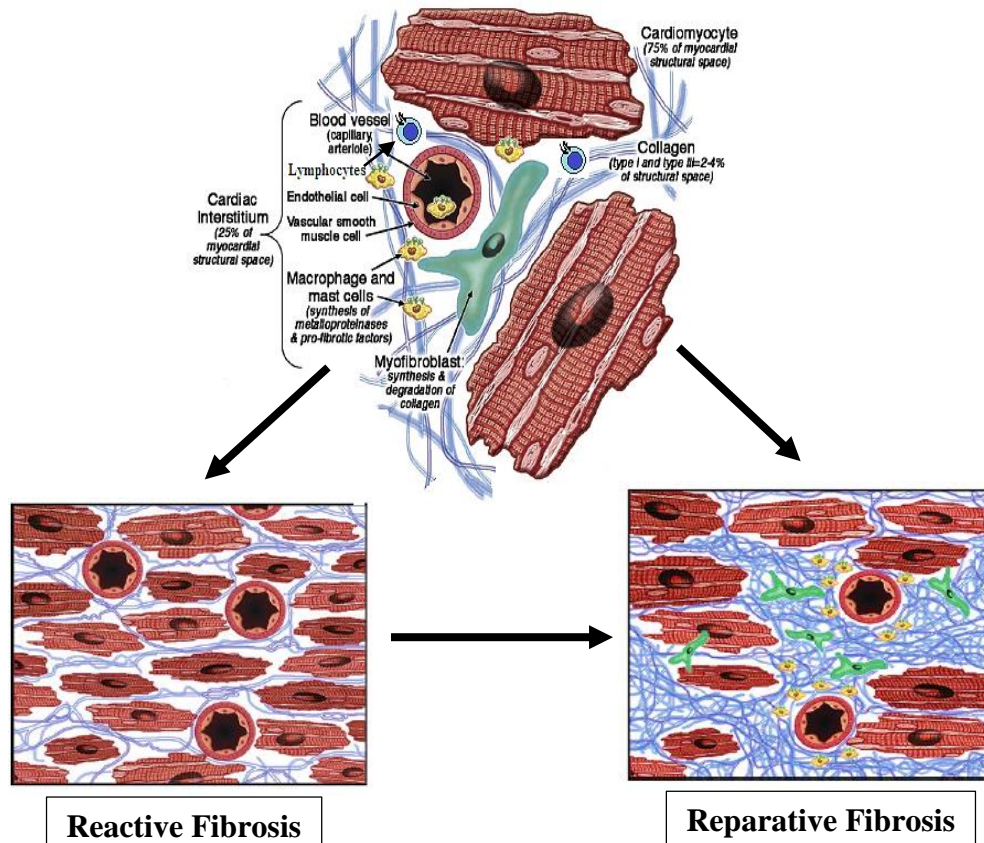


**Figure 1-1:** Cellular composition of myocardium and fibrosis type. Cardiac interstitium comprises of cardiomyocytes and non-cardiomyocytes including macrophages, lymphocytes, mast cells, myofibroblasts, endothelial cells (upper panel). Under chronic inflammation (diabetes, hypertension) or due to sudden loss of cardiomyocytes (myocardial infarction) non-contractile collagen deposited in cardiac interstitium as a natural tissue repair process results in reactive and replacement fibrosis, respectively. All cellular components in cardiac tissue participate in cardiac fibrogenesis. Adapted and modified from Mewton et al.<sup>46</sup>

Among other recruited cell types, fibrocytes are mesenchymal origin monocyte precursor cells that are recruited at the site of injury. Fibrocytes have both inflammatory properties like innate immune cells (i.e., macrophages) and tissue remodeling properties (i.e., fibroblasts).<sup>62,63</sup> Chronic inflammatory conditions promote accumulation, differentiation and trafficking of fibrocytes to the inflamed tissue. Cluster of differentiation antigen 34 (CD34) is one of the biomarkers to distinguish fibrocytes from other cells in tissues.<sup>64,65</sup> These cells are spindle shaped, adherent cells in cell culture studies. Chronic proinflammatory conditions and profibrotic microenvironment can stimulate fibrocytes to secrete collagen. Fibrocytes can also transdifferentiate into collagen synthesizing fibroblasts.<sup>61-63</sup> Altogether, fibrocytes have been reported to be important components in fibrosis generation under chronic inflammatory conditions, although a therapeutic intervention strategy to modulate fibrocytes function is yet to be established.

No specific treatment strategy to ameliorate myocardial fibrosis in diabetes has been yet determined. Inhibition of renin-angiotensin-aldosterone system by angiotensin converting enzyme (ACE) inhibitors and aldosterone antagonists have shown beneficial effect in hypertensive diabetic patient heart in the context of cardiac remodeling.<sup>66,67</sup> However, cardiac remodeling has also been observed in normotensive diabetic patients.<sup>20</sup> This indicates that further research is required to understand the mechanism of cardiac fibrosis generation to devise effective therapeutic approach to ameliorate maladaptive cardiac remodeling under diabetes.

#### 1.4. T lymphocytes involvement in myocardial fibrosis

T lymphocytes are lymphoid lineage adaptive immune cells. T lymphocytes can be divided mainly into two types, helper T cells ( $CD4^+$ ,  $T_H$ ) and cytotoxic T cells ( $CD8^+$ ,  $T_C$ ).<sup>68</sup> Based on their cytokine expression pattern and functions,  $CD4^+$  T cells can be further divided into  $T_{H1}$ ,  $T_{H2}$ ,  $T_{H17}$  and regulatory T cells ( $T_{regs}$ ).  $T_{H1}$  cells secrete mainly interferon- $\gamma$  (IFN- $\gamma$ ),  $T_{H2}$  cells secrete interleukin-4 (IL-4),  $T_{H17}$  cells secrete IL-17 and  $T_{reg}$  cells secrete TGF- $\beta$ .<sup>68</sup> In C57BL/6 mice, induction of  $T_{H1}$  lymphocytes through TCR-V $\beta$  peptide increases collagen content and cross-linking of collagen fibers with reduced collagen degrading MMP enzyme activity.<sup>69</sup> In the same report,  $T_{H2}$  induction resulted in decreased collagen content with increased collagen degrading matrix metalloproteinase (MMP) enzyme activity.<sup>69</sup> Co-culture experiments with untreated fibroblasts revealed that both  $T_{H1}$  and  $T_{H2}$  lymphocytes can affect fibroblast function, whereas  $T_{H1}$  decreases MMP-9 gene expression and  $T_{H2}$  increases MMP-9 activity.<sup>69</sup> In another study, overexpression of  $T_{H1}$  lymphocytes increased left ventricular interstitial fibrosis with diastolic dysfunction as detected by transthoracic echocardiography in mice.<sup>70</sup>  $T_{H1}$  cytokine IFN- $\gamma$  has been shown to induce interferon regulatory factor 1 (IRF1) which is a positive regulatory factor of collagen cross-linking enzyme lysyl oxidase (LOX).<sup>71</sup> Notably, chronic hypertensive BALB/c mice with predominant  $T_{H2}$  cytokine expression exhibited increased ventricular collagen and cross-linking.<sup>72</sup> Thus, depending on the physiological conditions both  $T_{H1}$  and  $T_{H2}$  cytokines can participate in cardiac fibrogenesis, whereas  $T_{H1}$  cytokines play a role in initiation phase of fibrosis and  $T_{H2}$  cytokines potentiate fibrosis in chronic conditions.<sup>72,73</sup>

More recently, in experimental heart failure model including left coronary artery occlusion induced myocardial infarction model and chronic pressure overload transverse aortic constriction model, T lymphocytes proliferation has been detected in heart draining secondary lymphoid organs i.e., lymph nodes (LNs) by flow cytometry analysis of proliferation marker Ki67 expression in T cells.<sup>74-76</sup> Increased proliferation of T cells in heart draining lymph nodes corresponds to an increased presence of lymphocytes in the heart tissue in these models.<sup>74-76</sup> Thus, it is proposed that after myocardial injury, activation of antigen presenting cells (APCs) by cardiac derived neoantigens occurs.<sup>77</sup> Activated APCs, in turn, activate T lymphocytes in heart draining lymph nodes (Figure 1-2). Activated effector T cells then migrate to injured myocardium and participate in fibrogenesis.<sup>77</sup> Increased T lymphocytes infiltration and presence in cardiac tissue has been shown to increase in collagen content and fibrosis in heart.<sup>75,76</sup> Thus, T lymphocytes has been detected as an important participant in myocardial fibrosis after cardiac injury (Figure 1-2).<sup>74-77</sup> To this end, it is intriguing to note that the modulation of T cells trafficking from lymphoid organs to blood/heart could be a potential therapeutic approach to protect heart under cardiac injury/inflammation.

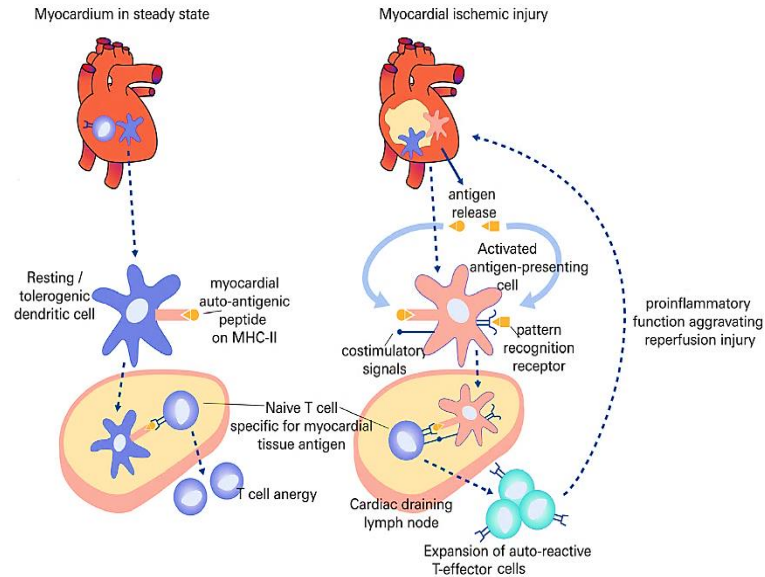


**Figure 1-2:** Proposed role of T lymphocytes trafficking to heart in steady state and post-myocardial infarction. In steady state, tolerogenic antigen presenting cells (APCs) prevent T cell activation, whereas after myocardial injury activation of APCs result in activation of T lymphocytes in heart draining lymph nodes. Adapted and modified from Hofmann et al.<sup>77</sup>

Proinflammatory cytokines have been shown to negatively affect cardiac contractility leading to heart failure.<sup>78-80</sup> Several epidemiological studies have reported that expansion of proinflammatory T lymphocytes expressing TH1 cytokine IFN- $\gamma$  in diabetic patients positively correlated with cardiac diseases including acute coronary syndrome and coronary atherosclerotic heart disease.<sup>81,82</sup> Thus, the modulation of T lymphocytes to attenuate cardiac fibrosis is a potential therapeutic avenue that needs to be further investigated.

### 1.5. Role of Sphingosine 1-phosphate receptor 1 in T lymphocytes trafficking

T lymphocytes upon maturation increase cell surface expression of sphingosine 1-phosphate receptor 1 (S1P<sub>1</sub>) in thymus.<sup>83</sup> Sphingosine 1-phosphate receptor 1 (S1P<sub>1</sub>) is a G-protein coupled receptor that signals through G<sub>ai/o</sub> subunit.<sup>84,85</sup> Upon activation, G<sub>ai/o</sub> activates phosphatidylinositol 3-kinase (PI3K) effector pathway that activates Rac pathway.<sup>84,85</sup> Rac pathway controls cell polarization, lamellipodium formation and expansion and organization of focal complexes at the frontal edge of the cell and adhesion. The endogenous natural ligand for S1P<sub>1</sub> is the bioactive lipid molecule sphingosine 1-phosphate (S1P).<sup>86,87</sup> S1P is synthesized by phosphorylation from membrane lipid sphingosine. Two isoforms of sphingosine kinase enzyme catalyzed the conversion of sphingosine to sphingosine 1-phosphate. Notably, S1P is degraded by S1P lyase enzyme in tissues due to the high expression of this enzyme. Thus, S1P concentration in tissues (e.g. thymus, lymph nodes) is low (5-20 nM) as compared to high concentration in plasma (200-900 nM).<sup>85,88</sup> This creates a concentration gradient of S1P from lymphoid tissues to systemic circulation. Thus, the increased expression of S1P<sub>1</sub> receptor on cell surface enables T lymphocytes to sense the increased chemotactic gradient of S1P in systemic circulation leading to egress from the lymphoid organs to the blood (Figure 1-3C).<sup>83-89</sup>

Under normal physiological conditions, T lymphocytes continually recirculate between secondary lymphoid organs and blood, which increases the likelihood of T cell interaction with antigen presenting cells (APCs) e.g. macrophages, dendritic cells, B lymphocytes.<sup>90</sup> T cells encounter antigen bearing APCs in secondary lymphoid organs, such as lymph nodes and spleen. Presentation of foreign antigen to T cells by APCs

activate the T cells followed by proliferation in respective secondary lymphoid organs. Activated effector T cells then migrate to target tissue to generate appropriate immune response by secreting cytokines, activating B cells through cell-cell contact (CD4<sup>+</sup> T cells) or direct cell killing (CD8<sup>+</sup> T cells).<sup>77,90</sup>

T lymphocytes trafficking through S1P-S1P<sub>1</sub> signaling axis has been utilized for therapeutic purposes. Fingolimod (FTY720) is a novel immunomodulatory drug that acts on S1P<sub>1</sub> receptor (Figure 1-3A and 1-3B).<sup>91,92</sup> It is a structural analogue of sphingosine and phosphorylated by sphingosine kinase 2 enzyme *in vivo*.<sup>93</sup> Phosphorylated FTY720 binds to S1P<sub>1</sub> as an agonist that later induces β-arrestin mediated internalization from cell surface. S1P<sub>1</sub>-FTY720 complex in cell cytosol stays longer due to metabolic stability of FTY720 against S1P lyase and promotes proteasomal degradation of the receptor.<sup>94</sup> Thus, FTY720 reduces mature single positive CD4<sup>+</sup> and CD8<sup>+</sup> T cells in blood (Figure 1-3C).<sup>95</sup> FTY720 administration in murine experimental autoimmune encephalomyelitis (EAE) model and in multiple sclerosis patients reduces autoimmune T<sub>H</sub>17 cells in blood and CNS that protects the central nervous system from autoimmune T cell mediated destruction of neural tissues.<sup>88-89,92</sup>

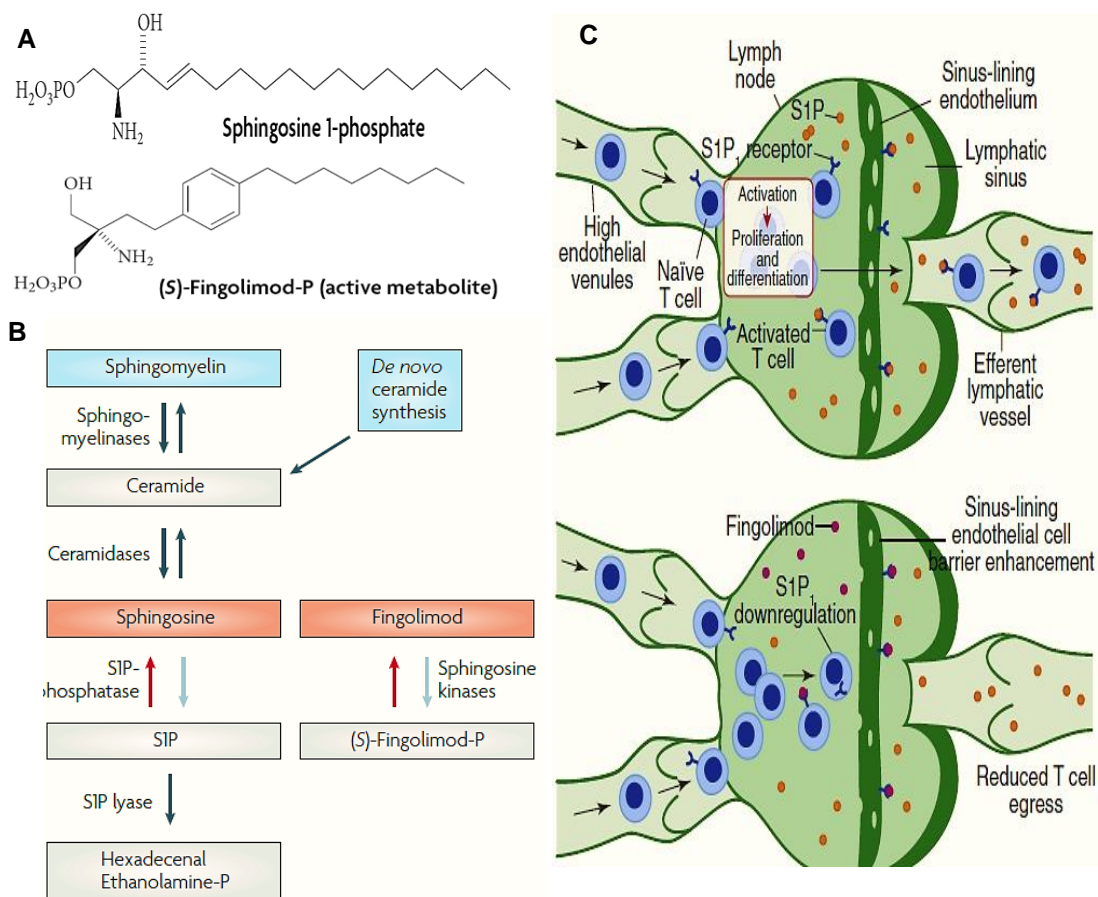


**Figure 1-3:** Sphingosine 1-phosphate receptor 1 in T lymphocytes trafficking. **(A)** Chemical structure of sphingosine 1-phosphate and phosphorylated (S)-FTY720. **(B)** Biosynthesis of sphingosine 1-phosphate from sphingomyelin. **(C)** Simplified representation of S1P-S1P<sub>1</sub> mediated egress of T lymphocytes from lymph nodes and inhibition of their egress by FTY720 to systemic circulation. Images are adapted and modified from Brinkmann et al.<sup>92</sup> (Figure 1-3A and 1-3B) and Camm et al. (Figure 1-3C).<sup>88</sup>

As discussed earlier, T lymphocytes are involved in myocardial fibrosis and dysfunction; however, therapeutic strategies to modulate T cell function in the setting of cardiac disease need to be further explored. Experimental data of modulation of T cells' role in diabetic cardiomyopathy are also lacking. Thus, in current dissertation work, we studied T cell trafficking modulation effect in myocardial fibrosis and contractility in a murine diabetic cardiomyopathy model.

### **1.6. Streptozotocin induced type 1 diabetic cardiomyopathy model**

Streptozotocin (STZ) is a glucosamine-nitrosourea that is structurally similar to glucose and is taken up by insulin producing beta cells of islets of Langerhans through cell membrane glucose transporter 2 (GLUT2) (Figure 1-4A and 1-4B).<sup>96</sup> STZ is a DNA alkylating agent that methylates guanine at O<sup>6</sup> position. This transfer of methyl group from STZ to DNA molecule results in DNA fragmentation that increases the activation of DNA repair enzyme poly (ADP-ribose) polymerase (PARP)<sup>97</sup>. Overactivation of PARP results in diminished cellular NAD<sup>+</sup> and ATP stores. The cellular energy store depletion results in beta cell necrosis.<sup>97,98</sup> Thus, STZ induced DNA methylation of pancreatic beta cells ultimately ensues destruction of insulin producing beta cells (Figure 1-4B).<sup>96-99</sup>

Streptozotocin induced mice model is a widely used type 1 diabetic mice model as these mice lack insulin producing beta cells upon STZ treatment.<sup>100</sup> STZ recipient mice promptly develop hyperglycemia (450 to 540 mg/dl) within 7 to 14 days after the first administration with marked reduction in plasma insulin levels (<20 pmol/L).<sup>14,15,100</sup> Both high dose (single dose of up to 200 mg/kg) and low dose with consecutive regimens have been reported in the literature to induce diabetes in rodents.<sup>100</sup> Animal Models of Diabetic Complications Consortium (AMDCC) recommends low dose protocol with five

consecutive injections of 50 mg/kg STZ to induce type 1 diabetes in rodents.<sup>100</sup> In the present dissertation work, a similar protocol was used to induce type 1 diabetes in mice according to AMDCC guidelines.

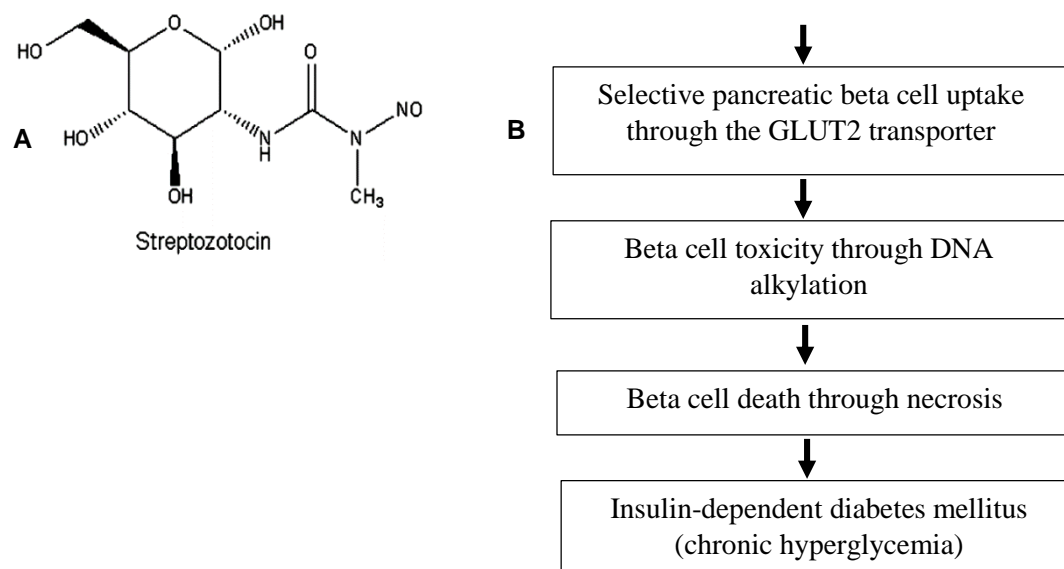


**Figure 1-4:** Mechanism of action of streptozotocin-induced type 1 diabetes. **(A)**

Chemical structure of streptozotocin. **(B)** Simplified schematic diagram of mechanism of action of streptozotocin to induce type 1 diabetes in mice. Adapted and modified from Lenzen.<sup>96</sup>

Streptozotocin (STZ) induced type 1 diabetic mouse model represents salient cellular and functional features of diabetic cardiomyopathy under hyperglycemia that makes it suitable to study molecular mechanisms and effects of therapeutic interventions.<sup>13</sup> STZ induced mice myocardium show reduced contractile protein  $\alpha$ -actin and myosin ATPase activity, altered calcium handling, impaired diastolic function and progressive systolic dysfunction corresponding to the magnitude and duration of hyperglycemia progression.<sup>12,13</sup> STZ murine myocardium has been reported to show

increased cellular ROS levels with enhanced superoxide production, increased NADPH oxidase expression and decreased GSSG/GSH ratio indicating presence of oxidative stress.<sup>12,13,32,33</sup> Increased expression of adhesion molecules, such as ICAM-1, VCAM-1 and MCP-1 in STZ rodent myocardium has been detected.<sup>32,33</sup> Impaired calcium homeostasis by myocytes has been also observed in STZ murine hearts, including attenuated expression and activity of sarcoendoplasmic reticulum  $\text{Ca}^{2+}$ -ATPase 2a enzyme with impaired calcium release and reuptake.<sup>100</sup> These molecular consequences coupled with structural abnormalities in STZ murine hearts including increased cardiac fibrosis with decline in cardiac function.<sup>13,100,101</sup>

In the present dissertation, we assessed T lymphocytes trafficking modulation effect on the extent of myocardial fibrosis and contractility by utilizing validated STZ-induced murine diabetic cardiomyopathy model.

### **1.7. Cre-loxP recombination approach to generate T cell specific S1P<sub>1</sub> receptor knock out mice**

Sphingosine 1-phosphate receptor 1 (S1P<sub>1</sub>) is a widely distributed G protein-coupled receptor in central nervous system, cardiovascular system, endothelial cells, hepatocytes and kidney tubular cells in human and rodents.<sup>85</sup> S1P<sub>1</sub> expression and activation in vascular endothelial cells are essential for new blood vessel formation and endothelial junction integrity maintenance.<sup>84,88</sup> Global knockout of S1P<sub>1</sub> receptor is lethal as mice die at early embryonic stage from hemorrhage due to leaky blood vessel formation.<sup>84,102</sup> Lack of S1P<sub>1</sub> receptor results in deformity in endothelial junction formation leading to hemorrhage.<sup>84,102</sup> Thus, cell- and tissue- specific S1P<sub>1</sub> receptor gene

knock out approach has been utilized for experimental studies. In this regard, Cre-loxP site specific genetic recombination approach is one of the successful approach.

Cre-loxP recombination system is a conditional gene inactivation approach that allows investigators to study single gene function in tissue- or cell-specific manner. It is a binary genetic system includes complementary activator and responder cassettes bearing two separate lines of transgenic mice.<sup>103,104</sup> Activator and responder cassette containing mice are then crossed to generate progeny containing both activator and responder cassettes.<sup>104</sup> The activator cassette contains Cre recombinase gene under the control of tissue specific promoter gene. The responder cassette contains flanked gene of interest by loxP sequences, usually coding region of a protein. After crossing activator and responder cassettes containing mouse strains, tissue specific Cre recombinase expression in offspring mice leads to excision of the flanked gene by loxP sites as Cre recombination action is specific at loxP sites (Figure 1-5).<sup>105,106</sup>

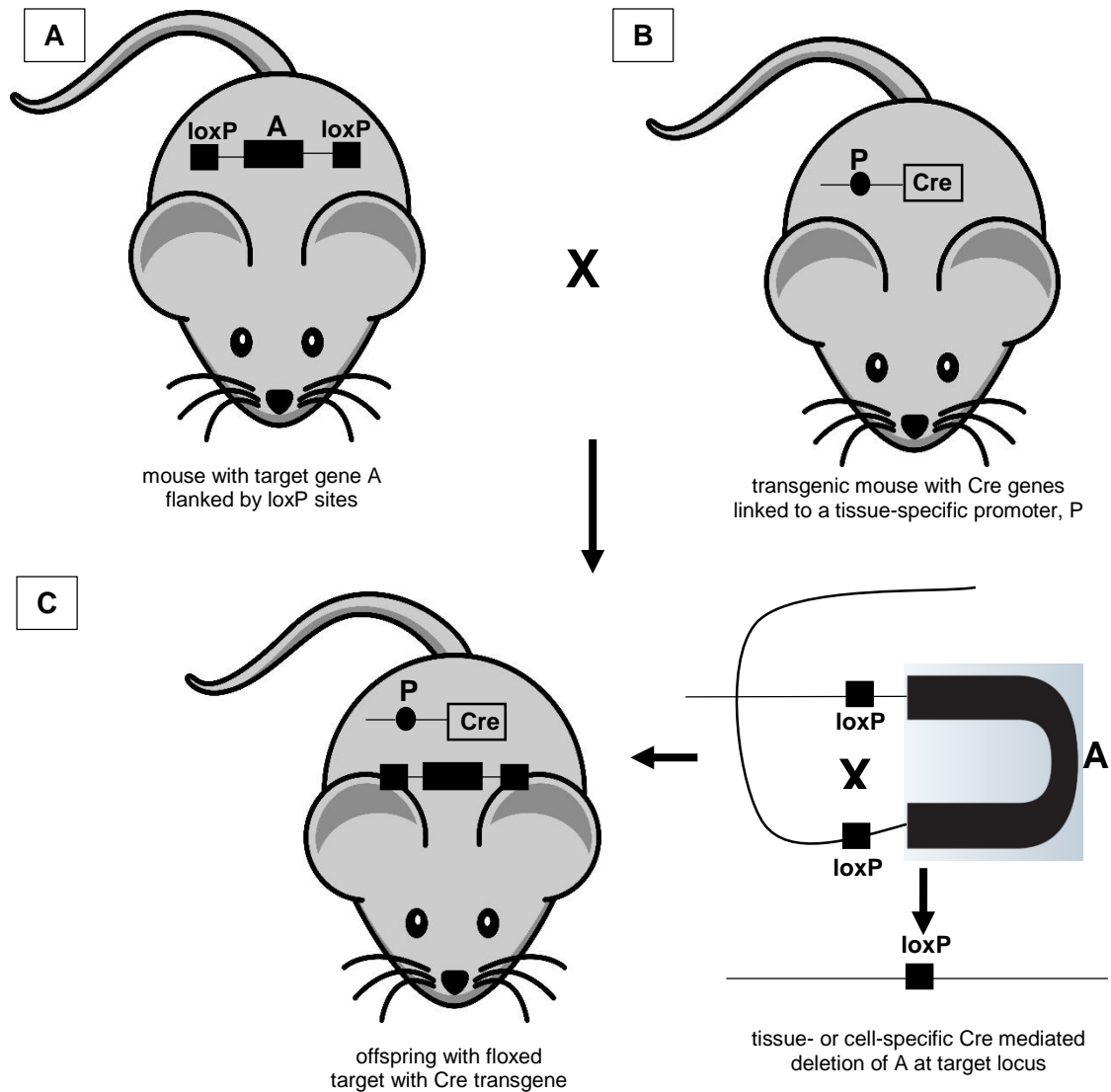


**Figure 1-5:** Simplified scheme of conditional gene knock-out approach by using Cre-loxP site specific recombination system. Mouse (A) bearing flanked specific genomic DNA sequence 'A' by two loxP sites is responder cassette containing mouse line. Mouse (B) bearing Cre transgene with a tissue- or cell-specific promoter 'P' is activator cassette containing mouse line. Cre mediated recombination under the tissue promoter 'P' occurs at two loxP sites of the particular cells of the tissue, resulting in deletion of gene 'A' specifically of the tissue- or cells- targeted offspring mice (C). Adapted and modified from Strachan et al.<sup>106</sup>

In our investigation, we generated conditional T cell specific S1P<sub>1</sub> knock out mice by crossing S1P<sub>1</sub><sup>loxP/loxP</sup> mice containing flanked exon 2 of S1P<sub>1</sub> gene with lymphocyte tyrosine kinase (Lck)-Cre promoter containing mice.<sup>83</sup> Offspring mice from the crossing that contain both a floxed target sequence and a Cre transgene were identified by genotyping PCR. T cell specific S1P<sub>1</sub> knock out mice were utilized to study effects of S1P<sub>1</sub> genetic depletion of T lymphocytes in myocardial fibrosis in STZ-induced type 1 diabetic cardiomyopathy model.

## 1.8. Rationale and objectives

As we discussed in previous sections (see section 1.4. and 1.5.), T lymphocytes are involved in myocardial fibrosis in cardiac diseases including hypertension, chronic heart failure and myocardial infarction. However, the experimental data in modulating T lymphocytes role in long term hyperglycemic condition to ameliorate cardiac fibrosis and improve cardiac contractility is scarce. In addition, the effects of T lymphocytes inhibition in fibrotic microenvironment have not been investigated in chronic diabetes. To this end, we hypothesized that modulation of T lymphocytic  $S1P_1$  receptor protects diabetic myocardium by reducing profibrotic milieu in chronic diabetic conditions. Our studies encompass broadly three areas including diabetes, immune system and cardiovascular diseases (Figure 1-6). More specifically, we studied the effects of T lymphocytes trafficking modulation in diabetic cardiomyopathy associated myocardial fibrosis (Figure 1-6).

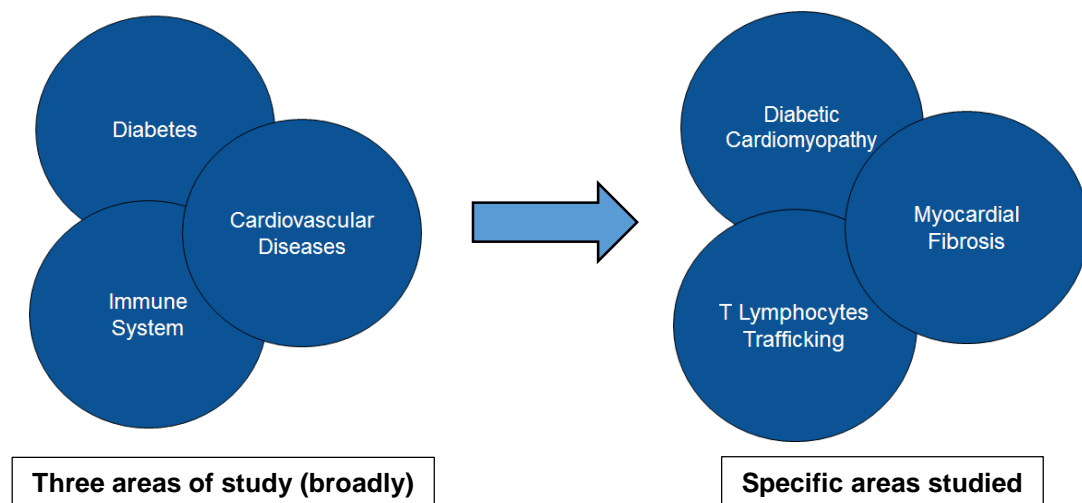


**Figure 1-6:** Simplistic representation of physiological fields of study in this dissertation.

The objectives of this dissertation are as follows:

- I. To determine the effects of pharmacological inhibition of T lymphocytes trafficking in myocardial fibrogenesis in chronic streptozotocin (STZ)-induced type 1 diabetes in mice (chapter 2).
  - a. to assess the effects of S1P<sub>1</sub> modulator-fingolimod (FTY720) administration in T lymphocytes number in the blood and extent of cardiac fibrosis in wild-type (WT) C57BL/6 mice in chronic diabetes;
  - b. to assess myocardial fibrosis and cardiac function in recombination activating gene 1 knock-out (Rag1 KO) mice as complementary to WT C57BL/6 mice under chronic diabetes;
  - c. to determine the effects of T lymphocytes trafficking modulation in profibrotic cellular and molecular milieu in diabetic myocardium of WT and KO mice.
  
- II. To investigate the effects of T cell specific S1P<sub>1</sub> receptor genetic depletion in T lymphocytes trafficking in the blood and cardiac fibrosis in STZ-induced diabetic cardiomyopathy model (chapter 3).
  - a. to generate T cell specific S1P<sub>1</sub> receptor knockout (TS1P<sub>1</sub>KO) mice and study T lymphocytes number in the blood and secondary lymphoid organs of TS1P<sub>1</sub>KO mice;
  - b. to study fibrotic remodeling in TS1P<sub>1</sub>KO mice under STZ-induced diabetic cardiomyopathy model;

- c. to assess profibrotic cellular and molecular expression in TS1P<sub>1</sub>KO mice myocardium under chronic diabetes;
- III. To evaluate the effects of CD4<sup>+</sup> T cells transfer to TS1P<sub>1</sub>KO mice in myocardial fibrosis under chronic diabetes (chapter 4).
- a. to isolate CD4<sup>+</sup> T cells from littermate mice spleen and adoptive transfer of isolated CD4<sup>+</sup> T cells to TS1P<sub>1</sub>KO mice;
  - b. to study the effects of CD4<sup>+</sup> T cells transfer in T cells number in the blood and myocardium in TS1P<sub>1</sub>KO mice;
  - c. to assess myocardial fibrosis in TS1P<sub>1</sub>KO mice after CD4<sup>+</sup> T cells transfer in STZ-induced diabetic cardiomyopathy model.

## CHAPTER 2: EFFECTS OF S1P RECEPTOR 1 MODULATOR FINGOLIMOD ON CARDIAC FIBROSIS IN DIABETIC CARDIOMYOPATHY

### 2.1. Introduction

As discussed in chapter 1, cardiovascular dysfunction resulting in heart failure is a prevalent cause of morbidity and mortality in diabetic patients.<sup>2,10</sup> Diabetic cardiomyopathy, first reported by Rubler et al., refers to structural and functional abnormalities in diabetic heart as characterized by myocyte apoptosis, interstitial inflammation, myocardial fibrosis and ventricular dysfunction independent of other cardiovascular disease risk factors e.g., age, gender, hypertension, coronary artery disease, congenital heart disease and valvular heart disease.<sup>9,15,16,24,31,32,107,108</sup> Myocardial fibrosis, one of the cardinal features of diabetic cardiomyopathy, contributes to increased ventricular stiffness which leads to contractile dysfunction in failing diabetic hearts.<sup>46,109</sup> Epidemiological studies have shown increased proinflammatory T cell subsets expansion in diabetic patient blood that correlates with adverse cardiac events including acute coronary syndrome.<sup>79,110</sup> Recent investigations in murine pressure-overload-induced heart failure model have shown the presence of T lymphocytes in injured cardiac tissue associated with exacerbated fibrosis.<sup>76</sup> Increased T lymphocytes infiltration in diabetic myocardium has been detected that correlates with enhanced collagen deposition in myocardium with increased ventricular stiffness.<sup>111</sup> T lymphocytes secrete proinflammatory cytokines, growth factors that activate profibrotic cells.<sup>73</sup> Stimulated profibrotic cells, such as fibroblasts and fibrocytes, secrete excess collagen that facilitates fibrosis development in heart.<sup>73,163</sup> Although different approaches including antibody-induced neutralization or genetic knockout of signaling protein of T cells have

demonstrated reduced fibrosis in murine heart failure models, therapeutic interventions to protect hearts in T cell mediated injury need to be explored. Modulation of T cell trafficking and its effect in long term diabetic fibrogenesis are not known yet. Further, the crosstalk between T cells and other cellular components in myocardial fibrosis is not completely understood. Therefore, we hypothesized that the modulation of T cell trafficking could protect heart from diabetes-associated fibrosis and cardiac dysfunction. In this chapter, we investigated T cell trafficking modulation by using novel immunomodulator drug fingolimod (FTY720) in wild-type C57BL/6 mice through streptozotocin-induced type 1 diabetic cardiomyopathy model. Rag1 knock-out mice that lacks mature lymphocytes were used as a complementary genetic approach of wild-type C57BL/6 mice.<sup>113</sup>

Sphingosine 1-phosphate receptor 1 (S1P<sub>1</sub>) is a cell membrane resident G protein-coupled receptor. Sphingosine 1-phosphate (S1P) is the endogenous ligand for S1P receptor 1. Mature T lymphocytes upregulate the expression of sphingosine 1-phosphate receptor for egress from lymphoid organs to circulation.<sup>114</sup> Interaction of S1P and S1P<sub>1</sub> is crucial for egress of mature T lymphocytes from lymphoid organs to circulation. FTY720 is a S1P analogue which binds to S1P<sub>1</sub> as an agonist. The binding of FTY720 to S1P<sub>1</sub> down-modulates cell surface S1P<sub>1</sub> receptor on T cells and disables the T cells to sense the chemotactic gradient of endogenous ligand S1P in circulation. Thus, FTY720 induces lymphopenia by sequestering lymphocytes in secondary lymphoid organs.<sup>91,95,115</sup> Additionally, S1P and S1P<sub>1</sub> signaling have been implicated in inflammation mediation in myocardial injury.<sup>116</sup> Notably, S1P<sub>1</sub> expression status in diabetic myocardium has not yet been reported. Thus, chronic FTY720 administration effects in long term experimental

diabetes settings in the context of myocardial fibrotic remodeling and cardiac function needs to be explored.

In this dissertation, we evaluated the effects of chronic administration of FTY720 on cardiac fibrosis and cardiac function in streptozotocin-induced diabetic wild-type and Rag1 knockout mice at the end of 11-week experimental period. In this study, we assessed outcomes of FTY720 treatment in murine diabetic cardiomyopathy model. We determined T lymphocytes number in heart and circulation by flow cytometry analysis. We conducted immunohistological studies to detect CD34 expressing fibrocytes localization, profibrotic TGF- $\beta$ 1 and S1P<sub>1</sub> expression in myocardium after long term diabetes. We studied heart histology and measured fibrosis area in heart sections at the end of experimental period. We, further, evaluated the cardiac function of the mouse heart using *ex vivo* Langendorff's heart perfusion system.

## **2.2. Materials and Methods**

### **2.2.1. Animals**

This investigation was carried out in accordance with the *Guide for the Care and Use of Laboratory Animals* set forth by U.S. National Research Council (Eighth Edition, 2011). All experimental procedures involving research animals were approved by the Institutional Animal Care and Use Committee (IACUC) at South Dakota State University (SDSU). Eight-week old male wild-type (WT) C57BL/6 mice weighing 22-25 g were purchased from the Charles River Laboratories (Wilmington, MA, USA) and two breeding pairs of Rag1 knockout (KO) mice weighing ~20 g lacking mature lymphocytes were obtained from The Jackson Laboratory (Bar Harbor, ME, USA). Rag1 KO mice were bred in the Animal Research Wing (ARW) at SDSU. All the mice were housed in

the ARW facility at SDSU and given *ad libitum* standard rodent chow food (5001; LabDiet, St. Louis, MO, USA) and water. Rag1 KO mice were kept in a specific pathogen free room and had free access to autoclaved food (5010; LabDiet) and water.

### **2.2.2. Type 1 diabetes induction and physiological assessment**

Streptozotocin (STZ) is a glucosamine-nitrosourea antibiotic that destroys insulin secreting pancreatic beta cells rendering recipient animal diabetic.<sup>125</sup> In present study, we used multiple low doses of STZ to induce type 1 diabetes in mice. Briefly, streptozotocin (STZ) (S0103; Sigma-Aldrich, MO, USA) was administered through intraperitoneal (i.p.) injection at a dose of 50 mg/kg body weight in 0.1 M sodium citrate buffer (pH 4.5) for 5 consecutive day to induce Type 1 diabetes while the control group received only buffer (i.p). Body weights (g) were measured by an electric balance twice each week (OHAUS® Scout-Pro™, OHAUS, NJ, USA). Blood glucose levels (mg/dl) were measured in blood samples from tail veins at the beginning, 4- and 11-week post STZ injection by using a blood glucose meter (CONTOUR®, Bayer Healthcare LLC, IN, USA). STZ recipient mice with fasting blood glucose level over 200 mg/dl were considered as diabetic.

### **2.2.3. Experimental protocol**

Age-matched WT and KO mice were divided into three groups: control, untreated diabetic (STZ), diabetic treated with FTY720 (FTY720+STZ). All mice went through 11-week study period as described earlier.<sup>117</sup> FTY720 (10006292; Cayman Chemical, MI, USA) was administered by i.p. injection at 0.3 mg/kg body weight every day for first four weeks. After that, there was an interim three week no treatment period, and then FTY720 administration was resumed for another four week till the end of 11-weeks (Figure 2-1).

Serum insulin levels were measured after 11-week by using an ultrasensitive mouse insulin ELISA kit according to manufacturer's instructions (90080; Crystal Chem Inc., IL, USA).

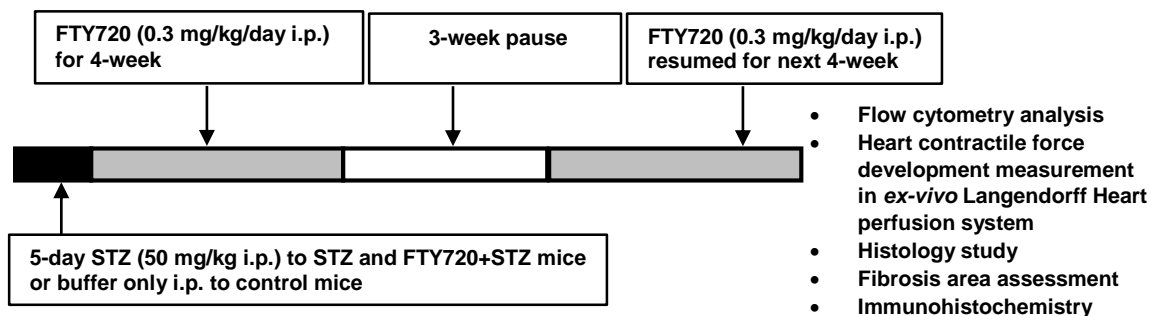


**Figure 2-1:** Schematic diagram of 11-week long streptozotocin (STZ)-induced type 1 diabetes mice model and treatment protocol.

#### 2.2.4. Flow cytometry analysis

CD4<sup>+</sup> and CD8<sup>+</sup>T lymphocytes were measured in blood by two-color flow cytometry analysis at the end of 11-weeks. The blood samples were collected into heparinized blood collection tubes (367884, BD Biosciences, NJ) and mixed well to achieve anti-coagulation. The anti-mouse fluorescein isothiocyanate (FITC) conjugated CD4 (561828; IgG2b; BD Pharmingen, CA) and anti-mouse phycoerythrin (PE)-CD8a (561095; IgG2a; BD Pharmingen) antibodies were added into the freshly prepared 100  $\mu$ L of heparinized blood. Respective isotype controls for both FITC- (553988; IgG2b; BD Pharmingen) and PE-conjugated antibodies (551799; IgG2a; BD Pharmingen) were used to set detector compensation at the instrument during analysis. The tubes were then incubated for 30 min(s) at room temperature in the dark for antibody staining. Red blood cells lysis and cell fixation were done by adding 2 mL of 1x 1-step fix/lyse solution (00-

5333; eBioscience, San Diego, CA, USA) and incubated for 15 min(s) at room temperature in the dark. After incubation, cells were washed by centrifugation (Eppendorf 5810R, Hauppauge, NY) at 500 x g for 5 min(s) at room temperature with 2 mL of flow cytometry staining buffer (00-4222; eBioscience) twice. The supernatants were discarded. The remaining cell pellets were re-suspended with 200  $\mu$ L of flow cytometry staining buffer and proceeded to flow cytometry analysis. Positively stained CD4<sup>+</sup> and CD8<sup>+</sup> cell populations were counted on a BD FACSCalibur flow cytometry system (BD Biosciences, San Jose, CA, USA). Data acquisition and analysis were done by BD CellQuest Pro Software (BD Biosciences).

### **2.2.5. Hemodynamics Study**

At the end of 11-week experimental period, mice were weighed, heparin (500 U kg<sup>-1</sup>) was injected i.p. and then anesthetized with phenobarbital (120 mg kg<sup>-1</sup>, i.p.). Surgical anesthesia was assessed by the absence of toe pinch reflex in anesthetized mice before starting the operation. Hearts were then rapidly excised and washed in ice-cold arresting solution (NaCl 120 mmol L<sup>-1</sup>, KCl 30 mmol L<sup>-1</sup>), and cannulated via the aorta with a 20 gauge stainless steel blunt needle. Heart perfusions were carried out at 70 mmHg pressure on a modified Langendorff apparatus using Krebs–Henseleit solution (NaCl 118.5 mmol L<sup>-1</sup>, NaHCO<sub>3</sub> 25.0 mmol L<sup>-1</sup>, KCl 4.75 mmol L<sup>-1</sup>, KH<sub>2</sub>PO<sub>4</sub> 1.18 mmol L<sup>-1</sup>, MgSO<sub>4</sub> 1.19 mmol L<sup>-1</sup>, D-glucose 11.0 mmol L<sup>-1</sup>, CaCl<sub>2</sub> 1.41 mmol L<sup>-1</sup>) supplemented with 95% O<sub>2</sub> and 5% CO<sub>2</sub> at 37°C.<sup>118</sup> Cardiac contractility was measured by a force displacement transducer (Model T03; Grass, Warwick, RI, USA) attached to the apex of the heart with a thin thread and a metal hook. The cardiac contractility was recorded with Biopac MP 100 data system (Goleta, CA, USA).

### **2.2.6. Hematoxylin and eosin (H&E) and Masson's trichrome staining of heart sections**

After cardiac contractile force measurement, hearts were perfused and fixed with freshly prepared 4% paraformaldehyde in 0.1 M phosphate buffered saline, pH 7.4 for 10 minutes. Hearts were removed after perfusion and placed in 4% paraformaldehyde overnight at 4°C. Paraffin-embedded (5 µm) heart sections were prepared. Hematoxylin & Eosin and Masson's trichrome staining were done according to standard procedures. Heart histology was examined in H&E stained slides using Zeiss Axio Imager A1 upright microscope. Each heart section was graded based on the presence of eosinophilic interstitial collagen fibers, interstitial cellular infiltration, myocardial cell necrosis and myofiber striation and organization on a five-point scale for each characteristic from 0 to 4.<sup>120,121</sup> The composite scores were expressed from 0 to 16 for each group. Trichrome stained whole heart sections images were taken using Leica EZ4 HD stereomicroscope (Leica Microsystems, Buffalo Grove, IL, USA). The percent of fibrosis area in whole heart sections was quantified by using NIH Image J software (Bethesda, MA, USA).<sup>117</sup>

### **2.2.7. Immunohistochemistry of heart sections**

Immunohistochemical detection of CD3, S1P<sub>1</sub>, TGF-β1 and CD34 expression was conducted with CD3 (10 µg/mL, sc-20047; Santa Cruz Biotechnology, Inc., CA), S1P<sub>1</sub> (15 µg/mL, MAB7089; R&D Systems, Inc., Minneapolis, MN), TGF-β1 (15 µg/mL, MAB240; R&D Systems, Inc.) and CD34 (10 µg/mL, MA5-17825; Pierce Biotechnology, Rockford, IL, USA) primary antibodies in 5 µm thick paraffin-embedded heart tissue sections. We used R&D systems mouse/rat cell and tissue staining HRP-DAB kit (CTS002/CTS017; R&D Systems) according to primary antibodies host species to

amplify and visualize primary antibody staining localization in heart tissue sections. Briefly, heart sections were first deparaffinized and hydrated through consecutive washes with xylene and graded alcohol series. Antigen unmasking was done through heat-induced epitope retrieval (HIER) procedure by heating the slides at 95 °C with 10 mM sodium citrate buffer (pH 6.0) for 40 minutes. Slides were cooled to room temperature and were washed with 1x Tris-buffered saline containing 0.01% v/v Tween 20 (1x TBST, pH 7.4). Endogenous peroxidase activity was quenched by incubating with peroxidase blocking reagent (R&D Systems) for 5 minutes. Sections were washed and blocked with blocking solution composed of 1% w/v bovine serum albumin, 1% v/v normal goat serum, 1% v/v donkey serum, 0.3% v/v Triton X-100 and 0.05% v/v Tween 20 in 1x phosphate buffered saline for 1 hour at room temperature. Avidin and biotin were blocked according to the manufacturer's instructions (R&D Systems). Sections were then incubated with respective primary antibodies diluted in blocking solution overnight at 4 °C in sealed humid boxes. After overnight incubation, sections were washed with 1x TBST and incubated with secondary biotinylated antibody for 30 minutes at room temperature. Sections were then washed with 1x TBST and incubated with high sensitivity streptavidin conjugated to horseradish peroxidase (HSS-HRP) (Part 865006; R&D systems) for 30 minutes at room temperature. After incubation, sections were washed and incubated with 3, 3' diaminobenzidine (DAB) for 2 minutes. DAB is a chromogenic substrate for HRP, and enzymatic conversion of DAB by peroxidase enzyme yields brown color precipitation at antigen localization site. Sections were gently washed under running tap water for 5 minutes and counterstained with Mayer's hematoxylin (MHS16; Sigma-Aldrich, St. Louis, MO, USA) for nuclear staining. Finally,

sections were mounted with histological mounting medium Permount® (SP15; Fisher Scientific, Fair Lawn, NJ, USA). All experiments were done in triplicate. In all experiments, the slides incubated only with blocking solution was used as negative control to ensure specificity of IHC detection. To count immunopositive CD3<sup>+</sup> cells, 30 fields for each stained slide were pictured at bright-field under high magnification (400x) in Zeiss Axio Imager.A1 upright microscope equipped with Zeiss Achromplan objective lens (Carl Zeiss). Myocardium infiltrating cells number was calculated by counting the cells in imaged 400x fields and was expressed as cells/field.<sup>75</sup> TGF-β1, S1P<sub>1</sub> and CD34 positive staining percent area were quantified in ten images and averaged.<sup>122</sup> Stained sections were examined under Zeiss Axio microscope and imaged with AxioCam MRc 5 digital camera. Images were used to quantify positively stained regions in heart section.

#### **2.2.8. Plasma S1P quantification by LC/MS/MS**

At the end of 11-weeks, blood samples were collected from mice in EDTA blood collection tubes (367856, BD Biosciences, NJ) and mixed well to achieve anti-coagulation. The tubes were centrifuged immediately at 1300 x g at room temperature and plasma samples were collected from the top. The mice plasma samples were stored at -80 °C until further analysis. Sphingosine 1-phosphate (S1P) levels in plasma were measured using liquid chromatography-tandem mass spectrometry method (LC/MS/MS).<sup>123,124</sup> Briefly, S1P was extracted from 10 μL of plasma by methanol extraction. After dilution with methanol, final concentration was 10% plasma, 90% methanol, and 30 ng/ml of internal standard D-erythro-sphingosine-1-phosphate (C17 base) (860641; Avanti Polar Lipids, Alabaster, AL, USA). Sample tubes were then vortexed and centrifuged at 14,000 rpm for 10 minutes at 4 °C. Supernatants were

collected and analyzed by LC/MS/MS. S1P and internal standard were eluted with isocratic mobile phase consisting of 70% acetonitrile/30% water/0.1% formic acid mobile phase at a flow rate of 0.25 ml/min through Waters XBridge™ Phenyl Column (150 cm length x 2 mm internal diameter; i.d., 5 µm particle size) with a C18 guard column (4 mm length x 2 mm i.d.) (Waters Corporation, Milford, MA, USA). The runtime for each injection was 4 min(s). The retention time for S1P and internal standard were about 1.87 and 1.75, respectively. All the components of mobile phase were LC/MS grade reagents (Optima; Fisher Scientific, Fair Lawn, NJ, USA). Separation and LC/MS/MS analysis was carried out using Agilent 1100 series HPLC system (Agilent Technologies, Waldbronn, Germany) coupled with Finnigan TSQ Quantum Ultra triple quadrupole mass spectrometer (Thermo Electron Corporation, San Jose, CA, USA) operating in positive ion mode. S1P and internal standard were monitored by Multiple Reaction Monitoring (MRM) at 380.31 → 264.31 m/z and 366.26 → 250.27 m/z, respectively. S1P peak area was divided by the percent recovery of the internal standard in each sample to reconcile the loss. The concentration of S1P was calculated from loss-adjusted S1P peak area using a loss-adjusted standard curve of S1P (860492; Avanti Polar Lipids). The linearity of standard curve to calculate S1P concentration was determined by R<sup>2</sup> value of 0.99.

### **2.2.9. Data analyses**

Data was expressed as mean  $\pm$  SEM. One-way ANOVA was used for statistical analysis followed by Tukey's post hoc test for multiple comparisons of group means.

Two-tailed unpaired student's t-test was done, where applicable. Data were analyzed in GraphPad Prism Software (v5.01, 2007). A P value of less than 0.05 was considered statistically significant and indicated with an asterisk (\*) or a number (#) sign.

## **2.3. Results**

### **2.3.1. Assessment of metabolic and physiological parameters in diabetic mice**

In WT mice, both untreated (STZ, n=9) and FTY720 treated (FTY720+STZ, n=9) STZ recipient mice demonstrated lower body weight gain compared to only buffer recipient (Control, n=8) mice throughout the 11-week treatment period (Figure 2-2). There was no statistically significant difference in body weight between groups at the beginning. After 11-week, control mice gained 8.67 % higher body weight than STZ and 14.63% higher body weight than FTY720+STZ mice (Table 2-1, Figure 2-2).

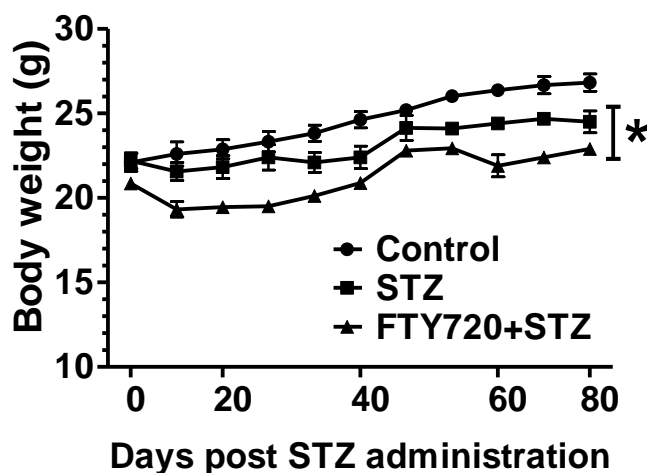


**Figure 2-2:** Body weight (g) changes in wild-type (WT) C57BL/6 mice during 11-week experimental period. Streptozotocin recipient both STZ and FTY720+STZ mouse groups exhibited less body weight gain during treatment period. Sample size, n=8-9 mice in each group, \*P < 0.05 as compared to control mice at the end of 11-weeks. The data is expressed as mean  $\pm$  SEM.

Blood glucose level was higher both in STZ ( $466.7 \pm 22.4$  mg/dl vs.  $159.3 \pm 8.21$  mg/dl, \*\*P < 0.01, after 4-week) and FTY720+STZ ( $563.4 \pm 10.92$  mg/dl vs.  $159.3 \pm 8.21$  mg/dl, \*\*P < 0.01, after 4-week) mice than control mice post STZ induction, although at the beginning there was no statistically significant difference in blood glucose levels between these groups (Table 2-1, Figure 2-3). After 11-week, STZ and FTY720+STZ mice remained hyperglycemic compared with control mice (Table 2-1, Figure 2-3).

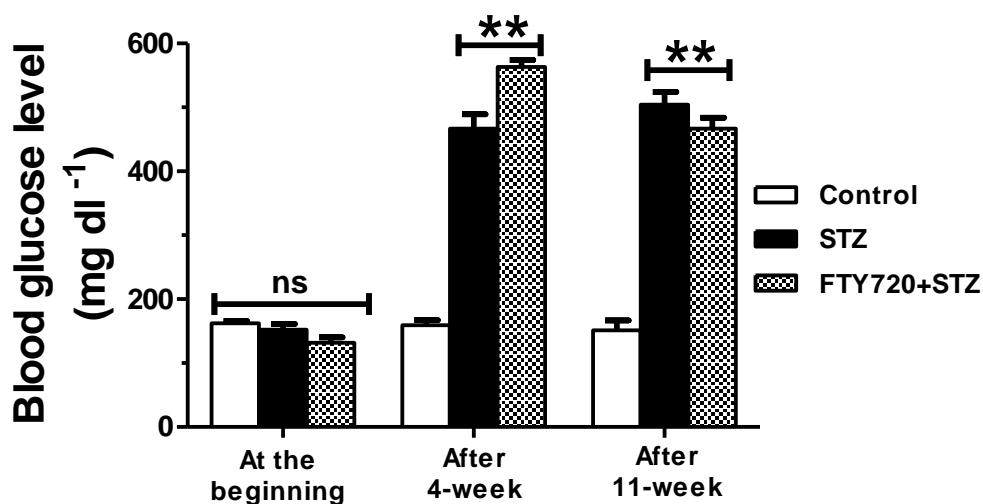


**Figure 2-3:** Blood glucose levels (mg/dl) in WT C57BL/6 mice at the beginning, after 4-week and after 11-week of STZ induction. Sample size, n = 8-9 mice per each group, \*\*P < 0.01 as compared to control mice after 4-weeks and after 11-weeks of post STZ-induction. The data is expressed as mean  $\pm$  SEM.

Hyperglycemic STZ ( $0.41 \pm 0.02$  ng/ml vs.  $0.66 \pm 0.08$  ng/ml, \*P < 0.05) and FTY720+STZ ( $0.38 \pm 0.03$  ng/ml vs.  $0.66 \pm 0.08$  ng/ml, \*P < 0.05) mice had lower serum insulin level compared to control mice at the end of the treatment period (Figure 2-4). In sum, FTY720 treatment did not improve body weight, blood glucose and serum insulin levels in diabetic WT mice compared to untreated diabetic mice.

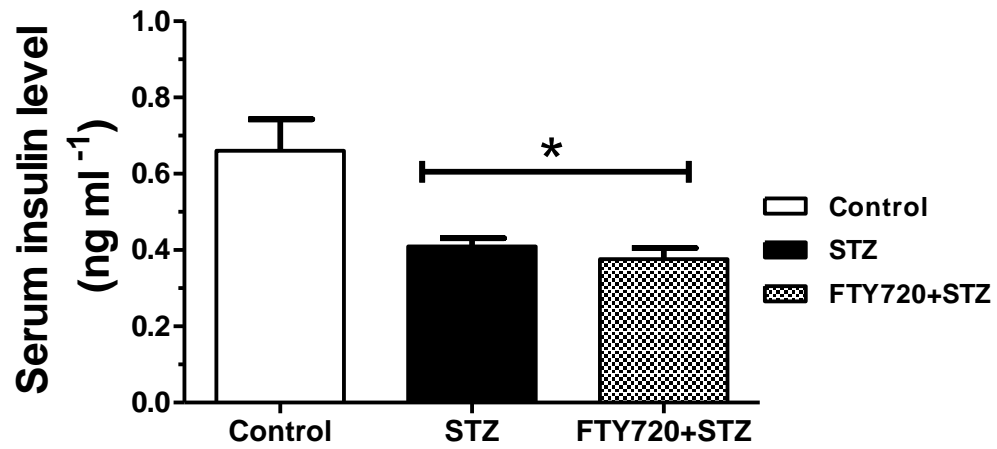


**Figure 2-4:** Serum insulin levels (ng/mL) in WT C57BL/6 mice after 11-week of STZ induction. Sample size, n = 8-9 mice per each group, \*P < 0.05 between control and STZ & FTY720+STZ mice after 11-week of post STZ-induction. The data is expressed as mean  $\pm$  SEM.

**Table 2-1:** Summary of metabolic and physiological parameters in WT C57BL/6 mice after 11-week experimental period.

	<b>Control</b>	<b>STZ</b>	<b>FTY720+STZ</b>
At the beginning (before STZ induction)			
<b><i>Body wt. (g)</i></b>	22.1±0.53	22.2±0.47	20.86±0.23
<b><i>Blood glucose level (mg/dl)</i></b>	162.38±3.59	152.33±9.05	131.67±8.68
After 4-week of STZ induction			
<b><i>Body wt. (g)</i></b>	23.33±0.60	22.4±0.75	19.50±0.15
<b><i>Blood glucose level (mg/dl)</i></b>	159.29±8.21	466.67±22.41**	563.44±10.92**
After 11-week of STZ induction			
<b><i>Body wt. (g)</i></b>	26.83±0.51	24.5±0.65*	22.9±0.34*
<b><i>Blood glucose level (mg/dl)</i></b>	151.29±15.39	504.00±20.29**	466.56±17.38**
<b><i>Serum insulin level (ng/ml)</i></b>	0.66±0.08	0.41±0.02*	0.38±0.03*

The data is expressed as mean ± SEM. Sample size, n = 8-9 mice in each group. \*P < 0.05 and \*\*P < 0.01 as compared to control group. STZ, streptozotocin; FTY720, fingolimod.

In Rag1 KO mice, both untreated (STZ) and FTY720 treated diabetic (FTY720+STZ) mice showed lower body weight gain during study period similar to WT C57BL/6 mice. Rag1 STZ and FT720+STZ mice had 13.90% and 10.20% lower body weight than age-matched non-diabetic control mice, respectively, at the end of 11-week after STZ administration ( $23.97 \pm 1.09$  g vs.  $27.84 \pm 0.62$  g and  $25 \pm 0.51$  g vs.  $27.84 \pm 0.62$  g,  $^{\#}P < 0.05$ ; n=4-6 mice in each group) (Figure 2-5).

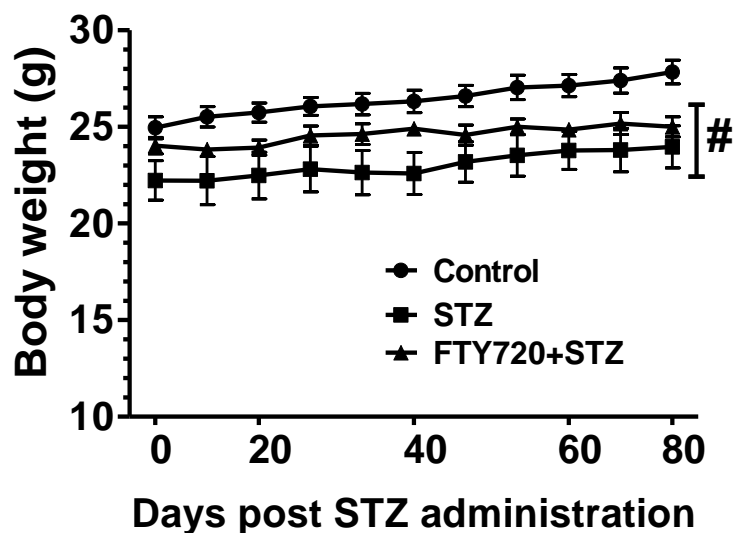


**Figure 2-5:** Body weight (g) changes in Rag1 KO mice throughout 11-week experimental period. Sample size n =4-6 mice in each group,  $^{\#}P < 0.05$  as compared to control mice. The data is expressed as mean  $\pm$  SEM.

There was no significant difference in blood glucose levels between Rag1 KO mouse groups at the beginning (Figure 2-6, Table 2-2). After STZ induction, STZ (374.8±37.05 mg/dl vs. 155.7±6.06 mg/dl, <sup>##</sup>P < 0.01) and FTY720+STZ (443.75±72.42 mg/dl vs. 155.7±6.06 mg/dl, <sup>##</sup>P < 0.01) mice exhibited higher blood glucose level as measured after 4-weeks. Both STZ and FTY720+STZ groups remained hyperglycemic at the end of 11-week compared to control group (Figure 2-6, Table 2-2).

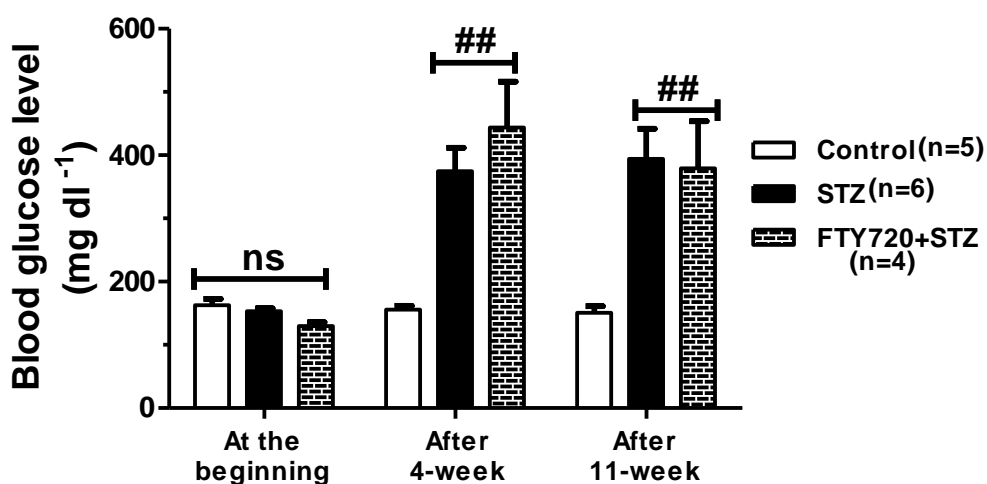


**Figure 2-6:** Blood glucose levels (mg/dl) at the beginning, after 4-week and after 11-week of STZ administration in Rag1 KO mouse groups. Sample size, n =4-6 mice in each group, <sup>##</sup>P < 0.01 as compared to control mice. The data is expressed as mean ± SEM.

Along with hyperglycemia, diabetic KO mice had lower serum insulin level than control mice (0.78±0.12 ng/ml vs. 0.43±0.02 ng/ml, <sup>#</sup>P < 0.05) (Figure 2-7, Table 2-2). In summary, FTY720 treatment in Rag1 KO diabetic mice, did not exhibit significant improvement in body weight, and remained hyperglycemic as compared to control mice.

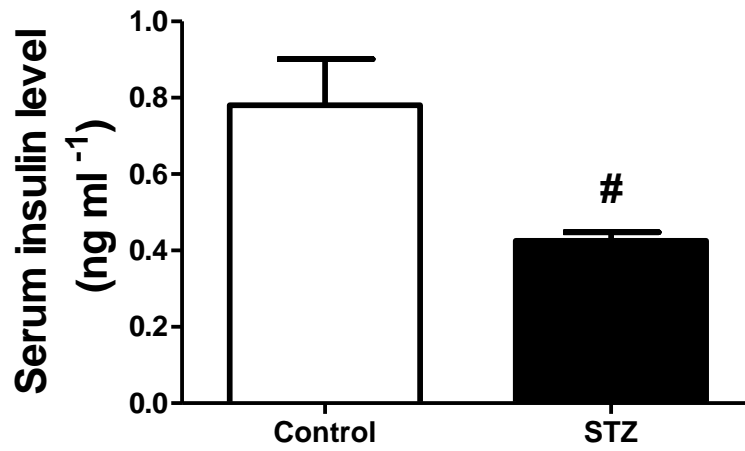


**Figure 2-7:** Serum insulin levels (ng/ml) after 11-week of post STZ induction in Rag1 KO mouse groups. Sample size, n =5 mice in each group, #P < 0.05 as compared to control mice. The data is expressed as mean  $\pm$  SEM.

**Table 2-2:** Summary of metabolic and physiological parameters in Rag1 KO mice after 11-week of experimental period.

	Control	STZ	FTY720+STZ
At the beginning (before STZ induction)			
<i>Body wt. (g)</i>	24.95±0.58	22.23±1.02	25.43±0.40
<i>Blood glucose level (mg/dl)</i>	162.50±10.00	153.29±4.48	129.75±6.05
After 4-week of STZ induction			
<i>Body wt. (g)</i>	26.06±0.47	22.82±1.19	24.73±0.52
<i>Blood glucose level (mg/dl)</i>	155.67±6.06	374.83±37.05 <sup>##</sup>	443.75±72.42 <sup>##</sup>
After 11-week of STZ induction			
<i>Body wt. (g)</i>	27.84±0.61	23.97±1.09 <sup>#</sup>	25.00±0.51 <sup>#</sup>
<i>Blood glucose level (mg/dl)</i>	150.80±10.27	394.00±47.86 <sup>##</sup>	379.00±74.88 <sup>##</sup>
<i>Serum insulin level (ng/ml)</i>	0.66±0.08	0.41±0.02 <sup>#</sup>	

The data is expressed as mean ± SEM. Sample size, n = 4-6 mice in each group. <sup>#</sup>P<0.05 and <sup>##</sup>P < 0.01 as compared to control group.

STZ, streptozotocin; FTY720, fingolimod.

### 2.3.2. Effects of FTY720 treatment in CD4<sup>+</sup> and CD8<sup>+</sup> T cells number in the blood

Sphingosine 1-phosphate (S1P) is an endogenous-bioactive lipid molecule that acts on five G-protein coupled receptors, S1P<sub>1-5</sub>. The concentration of S1P in plasma and lymph is 200 to 900 nM. Due to metabolic degradation of S1P in tissues, its concentration is 5 to 20 nM in tissues. This difference in concentrations of S1P between systemic circulation and tissues creates a concentration gradient of S1P.<sup>85,88</sup> Single positive CD4<sup>+</sup> and CD8<sup>+</sup> T lymphocytes upregulate S1P<sub>1</sub> receptor expression on their cell membrane upon maturation in lymphoid organs.<sup>114</sup> The upregulation of S1P<sub>1</sub> enables T lymphocytes to egress from lymphoid organs to blood and lymph through chemotactic response towards higher concentration of S1P present in systemic circulation. FTY720 (Fingolimod) acts as ‘functional antagonist’ to S1P<sub>1</sub> (EC<sub>50</sub> 0.2 nM).<sup>88</sup> Fingolimod binds to S1P<sub>1</sub> and causes its internalization following subsequent degradation of the receptor in T lymphocytes.<sup>92</sup> Thus, T lymphocytes chemotactic movement to blood is inhibited by FTY720 that causes sequestration of T cells in lymphoid organs. In our present study, we counted both CD4<sup>+</sup> helper T cells and CD8<sup>+</sup> cytotoxic T cells in blood by flow cytometry (Table 2-3, Figure 2-8 and Figure 2-9). FTY720 treatment in WT diabetic mice, significantly reduced both CD4<sup>+</sup> (control, n=3, 12.02±1.06 %, STZ, n=4, 12.79±1.42 %, FTY720+STZ, n=4, 0.19±0.03 %; \*\*P < 0.01 when FTY720+STZ compared with control and STZ group, data after 4-week) and CD8<sup>+</sup> T cells in blood (control, n=3, 7.97±0.68 %, STZ, n=4, 7.89±1.07 %, FTY720+STZ, n=4, 0.32±0.04 %; \*\*P < 0.01 when FTY720+STZ compared with control and STZ group, data after 4-week). The observed lymphopenia in FTY720 treated group sustained after 11-week (CD4 T cells: control, n=6, 9.10±1.44 %, STZ, n=8, 8.87±0.81%, FTY720+STZ, n=7, 0.24±0.07%;

\*\*P < 0.01 when FTY720+STZ compared with control and STZ group, data after 11-week; CD8<sup>+</sup> T cells: control, n=6, 6.89±1.40 %, STZ, n=8, 5.80±0.78 %, FTY720+STZ, n=7, 0.75±0.21 %; \*\*P < 0.01 when FTY720+STZ compared with control and STZ group, data after 11-week) (Table 2-3, Figure 2-8 and Figure 2-9).

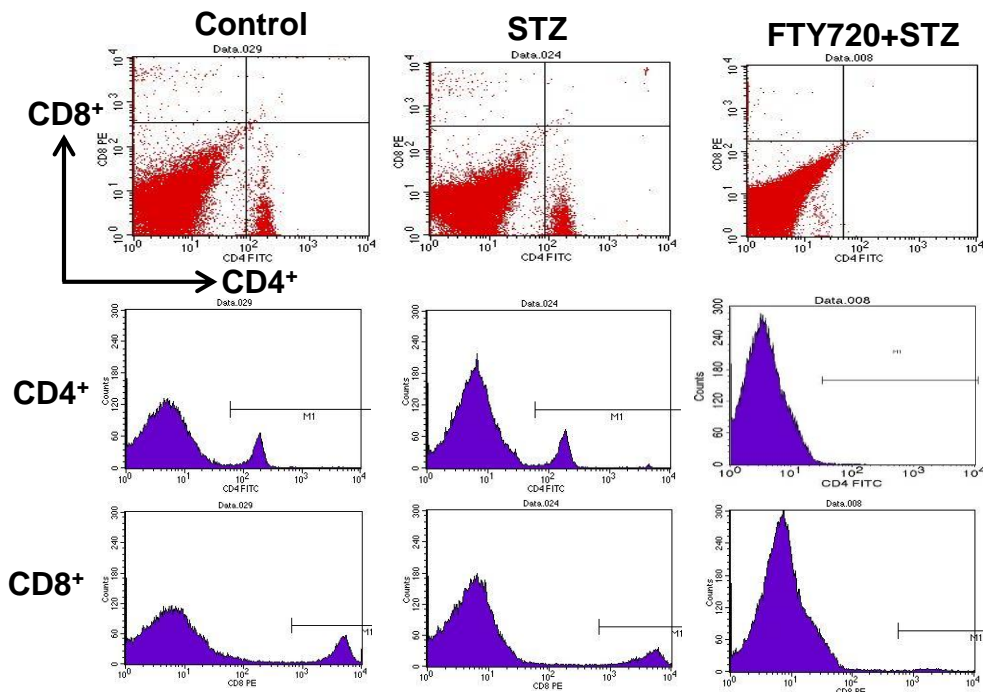


**Figure 2-8:** Flow cytometry analysis of CD4<sup>+</sup> and CD8<sup>+</sup> T lymphocytes in peripheral blood of WT C57BL/6 mice after 11-week experimental period. Representative dot plot (upper panel) and histogram plot (lower two panel) of flow cytometry analysis of CD4<sup>+</sup> and CD8<sup>+</sup> T lymphocytes in WT C57BL/6 mice blood. FTY720 treatment noticeably depleted both CD4<sup>+</sup> and CD8<sup>+</sup> T cells in peripheral blood compartment as observed in lower right (CD4<sup>+</sup> stained cells) and upper left (CD8<sup>+</sup> stained cells) quadrants in dot plot and in M1 gate in histogram.

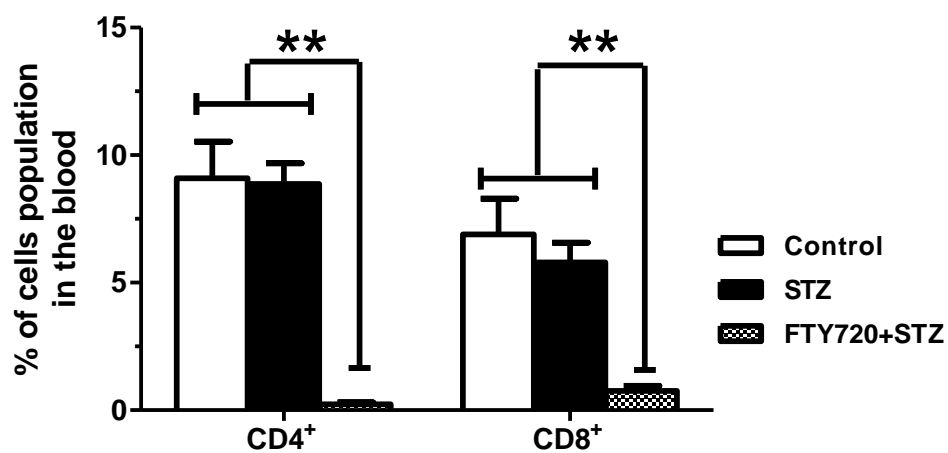


**Figure 2-9:** Quantification of CD4<sup>+</sup> and CD8<sup>+</sup> T cells percent numbers in WT C57BL/6 mice blood after 11-week of experimental period. \*\*P < 0.01 as compared to control and STZ groups, n = 6-8 mice per group. The data is expressed as mean ± SEM.

**Table 2-3:** Summary of CD4<sup>+</sup> and CD8<sup>+</sup> T cells percent numbers in peripheral blood of WT C57BL/6 mice after 11-weeks.

	<b>Control</b>	<b>STZ</b>	<b>FTY720+STZ</b>
After 4-week of STZ induction			
<i>CD4<sup>+</sup> (relative % of total cell populations)</i>	12.02±1.06 (n=3)	12.79±1.42 (n=4)	0.19±0.03** (n=4)
<i>CD8<sup>+</sup> (relative % of total cell populations)</i>	7.97±0.68 (n=3)	7.89±1.07 (n=4)	0.32±0.04** (n=4)
After 11-week of STZ induction			
<i>CD4<sup>+</sup> (relative % of total cell populations)</i>	9.1±1.44 (n=6)	8.87±0.81 (n=8)	0.24±0.07** (n=7)
<i>CD8<sup>+</sup> (relative % of total cell populations)</i>	6.89±1.40 (n=6)	5.80±0.78 (n=8)	0.75±0.21** (n=7)

The data is expressed as mean ± SEM. The value of ‘n’ represents number of mice in each group. \*\*P<0.01 as compared with control and STZ mice. STZ, streptozotocin; FTY720, fingolimod.

Recombination activating gene 1 (Rag1) encodes recombinase enzyme Rag1 which along with Rag2 mediate recombination in development process of both B and T cells receptor repertoire. In Rag1 deficient mice, recombination does not occur which thwart lymphocytes development at early stage. Thus, Rag1 deficient mice does not have any mature B or T lymphocytes.<sup>113</sup> In our present study, flow cytometry analysis of Rag1 KO mice blood did not yield any detectable CD4<sup>+</sup> and CD8<sup>+</sup> T cells (Figure 2-10).

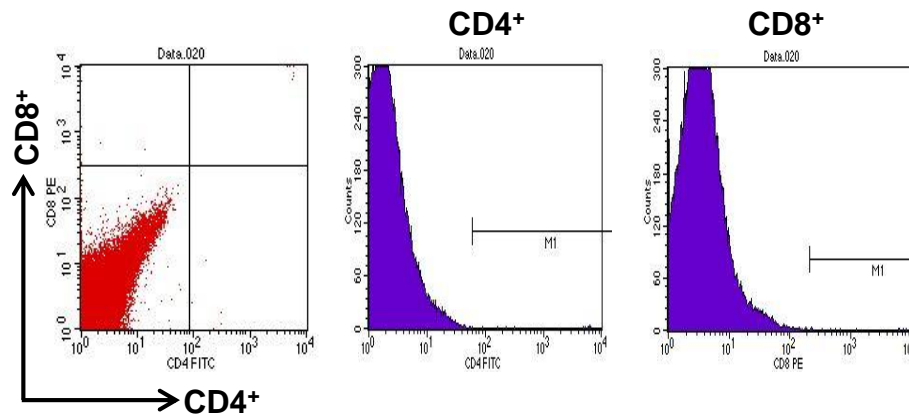


**Figure 2-10:** Representative flow cytometry analysis dot plot and histogram plot of CD4<sup>+</sup> and CD8<sup>+</sup> T cells in Rag1 KO mice peripheral blood. There was no detectable CD4<sup>+</sup> and CD8<sup>+</sup> T cells in Rag1 KO mice blood. Experiments are representative of triplicate samples.

### 2.3.3. Effects of FTY720 treatment on heart histology

After 11-week diabetic period, heart sections from all the groups were prepared and H&E staining was done to evaluate heart histology. H&E stained sections were observed under microscope and graded on histological parameters. WT diabetic mice heart exhibited noticeable cardiomyocyte loss, large interstitial space indicating edema, focal and diffuse increased cellularity and myofiber disorganization in myocardium in comparison to control group. In contrast, FTY720 treatment in WT diabetic mice protected heart histology with improved myocytes organization and structure (Figure 2-11). FTY720 treated WT diabetic mice heart had reduced cumulative histology score compared to WT STZ mice (control [n=5]  $2.2 \pm 0.80$ ; STZ [n=6],  $9.67 \pm 0.49$ ; FTY720+STZ [n=5],  $3.4 \pm 0.75$ , #P < 0.05 when FTY720+STZ compared with STZ) (Figure 2-13).

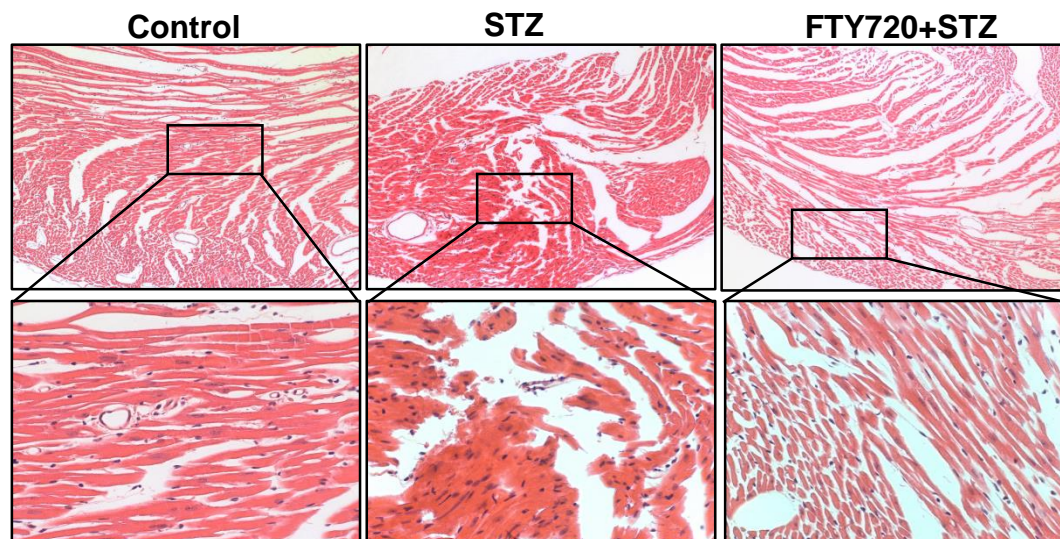


**Figure 2-11:** Representative images of Hematoxylin and Eosin (H&E) stained heart tissue sections of WT C57BL/6 mice after 11-week of experimental period. Untreated WT diabetic mice heart sections exhibited altered cardiac architecture and disorganization of myocytes as compared to control group. FTY720 treatment preserved cardiac histology under diabetes. Upper panel magnification is 100x, lower panel magnification is 400x. Images are representative of n=5-6 mice heart tissue sections in each group.

Diabetic Rag1 KO mice (STZ, n=5) heart exhibited protected heart histology under hyperglycemic conditions. KO STZ mice heart histology score had no significant difference compared with control group (n=6) (control,  $3.33 \pm 0.42$ ; STZ,  $3.00 \pm 0.45$ ;  $P > 0.05$ ) (Figure 2-12). Notably, treatment with FTY720 exacerbated heart histology with marked myocytes breakage and disorganization in KO diabetic mice (FTY720+STZ, n=3;  $10.33 \pm 0.33$ ) (Figure 2-12 and Figure 2-13).

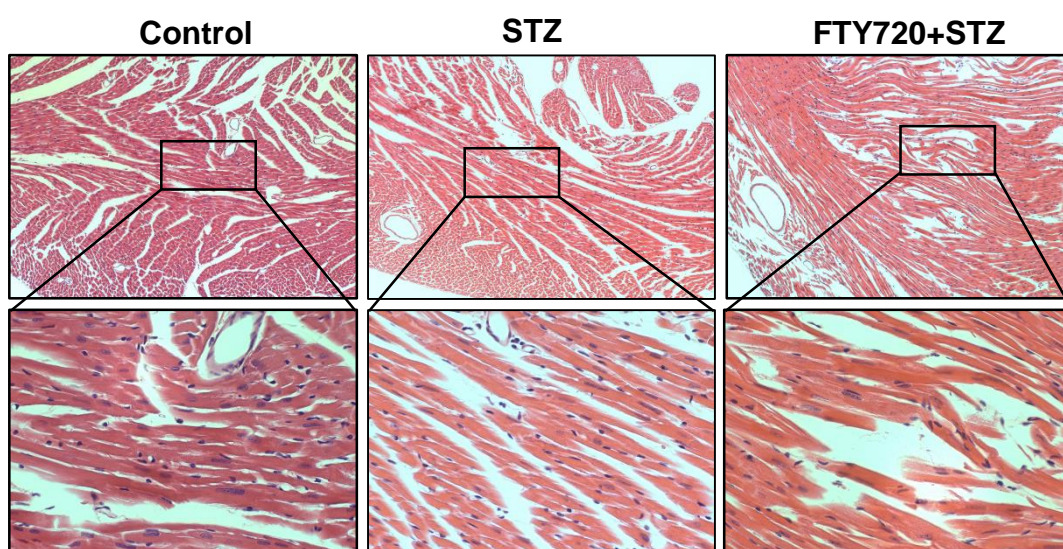


**Figure 2-12:** Representative images of Hematoxylin and Eosin (H&E) stained heart tissue sections of Rag1 KO mice after 11-week of experimental period. Rag1 KO diabetic mice heart showed no significant difference in heart histology than control mice. Noticeably, FTY720 treatment in diabetic Rag1 KO mice exhibited altered cardiac histology with marked myocytes disarray. Upper panel magnification is 100x, lower panel magnification is 400x. Images are representative of n=3-6 mice heart tissue sections in each group.

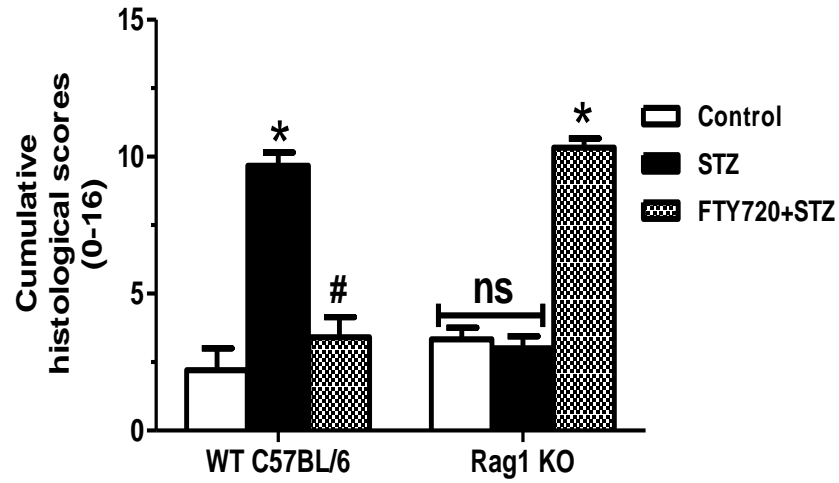
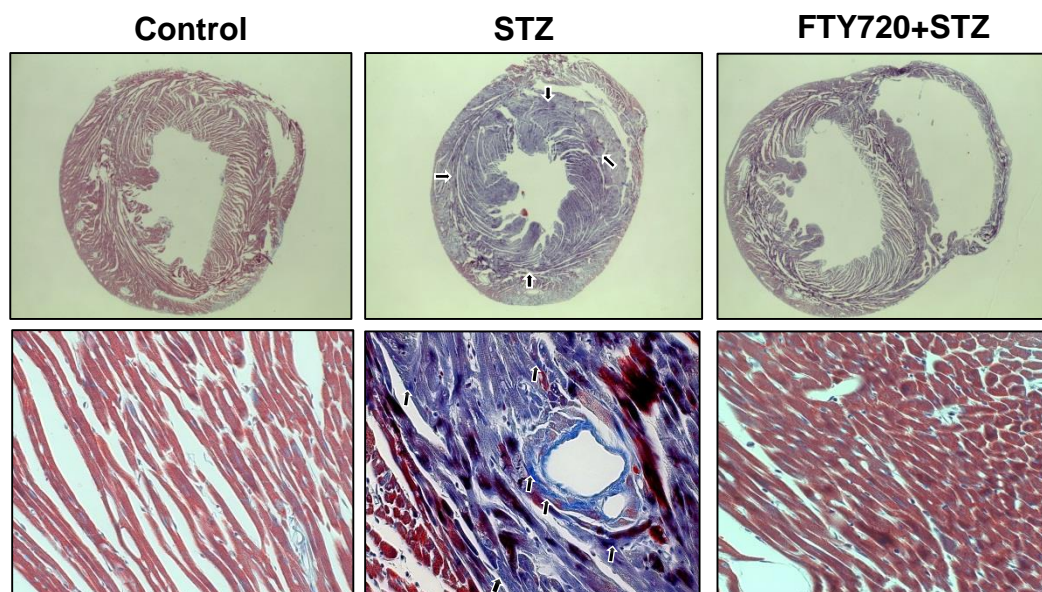


**Figure 2-13:** Quantification of heart histology scores in WT C57BL/6 and Rag1 KO mice heart tissue sections. In WT mice, Control vs. STZ, \* $P < 0.05$  and FTY720+STZ vs. STZ, # $P < 0.05$ . In KO mice, control vs. STZ ( $P = ns$ ) and STZ vs. FTY720+STZ, \* $P < 0.05$ . Sample size,  $n = 3-6$  mice in each group. The data is expressed as mean  $\pm$  SEM.

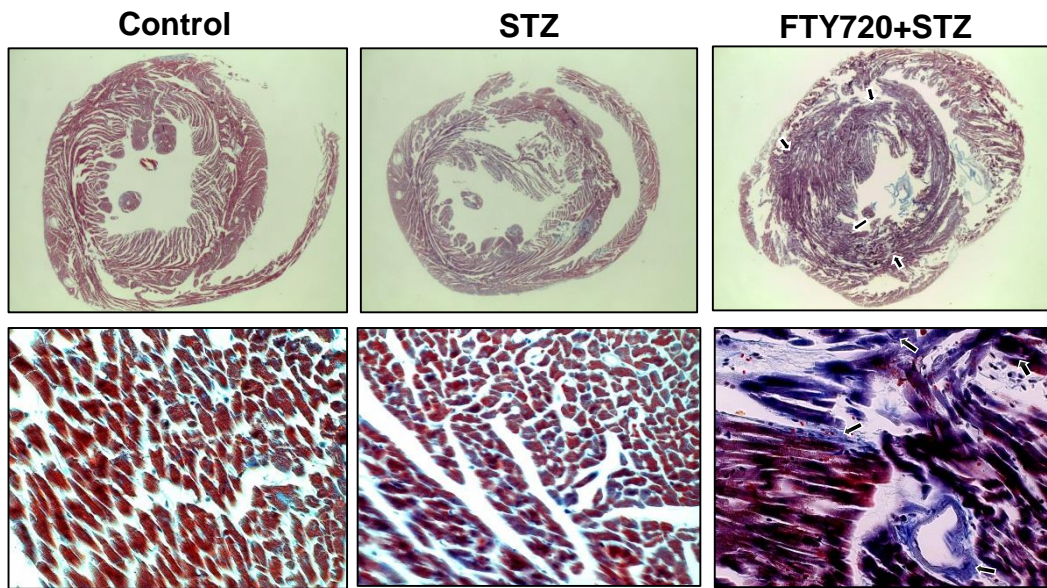
#### 2.3.4. Effects of FTY720 treatment on myocardial fibrosis

Fibrosis area was measured in paraffin-embedded whole heart sections stained with Masson's Trichrome staining. Blue color represents collagen deposition in heart sections (Figure 2-14 and 2-15). After 11-weeks, WT diabetic mice had increased collagen deposition in myocardium and perivascular area compared to control group ( $38.09 \pm 4.35$  % vs.  $7.40 \pm 1.23$  %, \* $P < 0.05$ ) (Figure 2-14 and 2-16). FTY720 treatment in WT diabetic mice significantly reduced interstitial and perivascular fibrosis compared to untreated diabetic mice ( $9.40 \pm 2.23$  % vs.  $38.09 \pm 4.35$ %, # $P < 0.05$ ) (Figure 2-14 and 2-16).

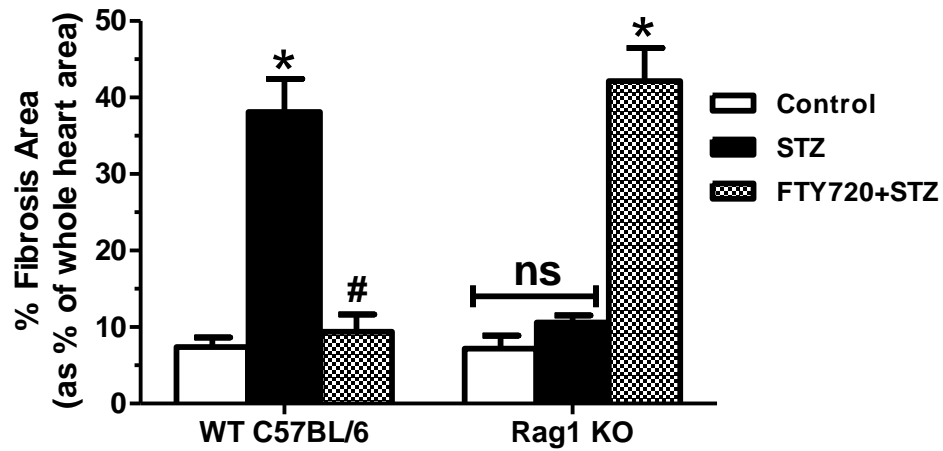
Rag1 KO control and STZ mice do not have any significant difference in total fibrosis percent area ( $7.20 \pm 1.72$  % vs.  $10.60 \pm 0.91$  %,  $P = ns$ ) (Figure 2-15 and 2-16). FTY720 treatment in Rag1 KO diabetic mice markedly increased interstitial fibrosis area compared to untreated KO diabetic mice ( $42.16 \pm 4.30$  % vs.  $10.60 \pm 0.91$  %, \* $P < 0.05$ ). (Figure 2-15 and 2-16).



**Figure 2-14:** Representative images of Masson's Trichrome stained heart tissue sections of WT C57BL/6 mice after 11-week experimental period. Arrows indicate collagen staining as blue color. Diabetic WT mice myocardium exhibited increased interstitial and perivascular fibrosis. FTY720 treatment reduced markedly fibrosis development in diabetic WT mice heart sections. Upper panel magnification is 16x, lower panel magnification is 400x. Images are representative of n=5-7 mice heart tissue sections in each group.



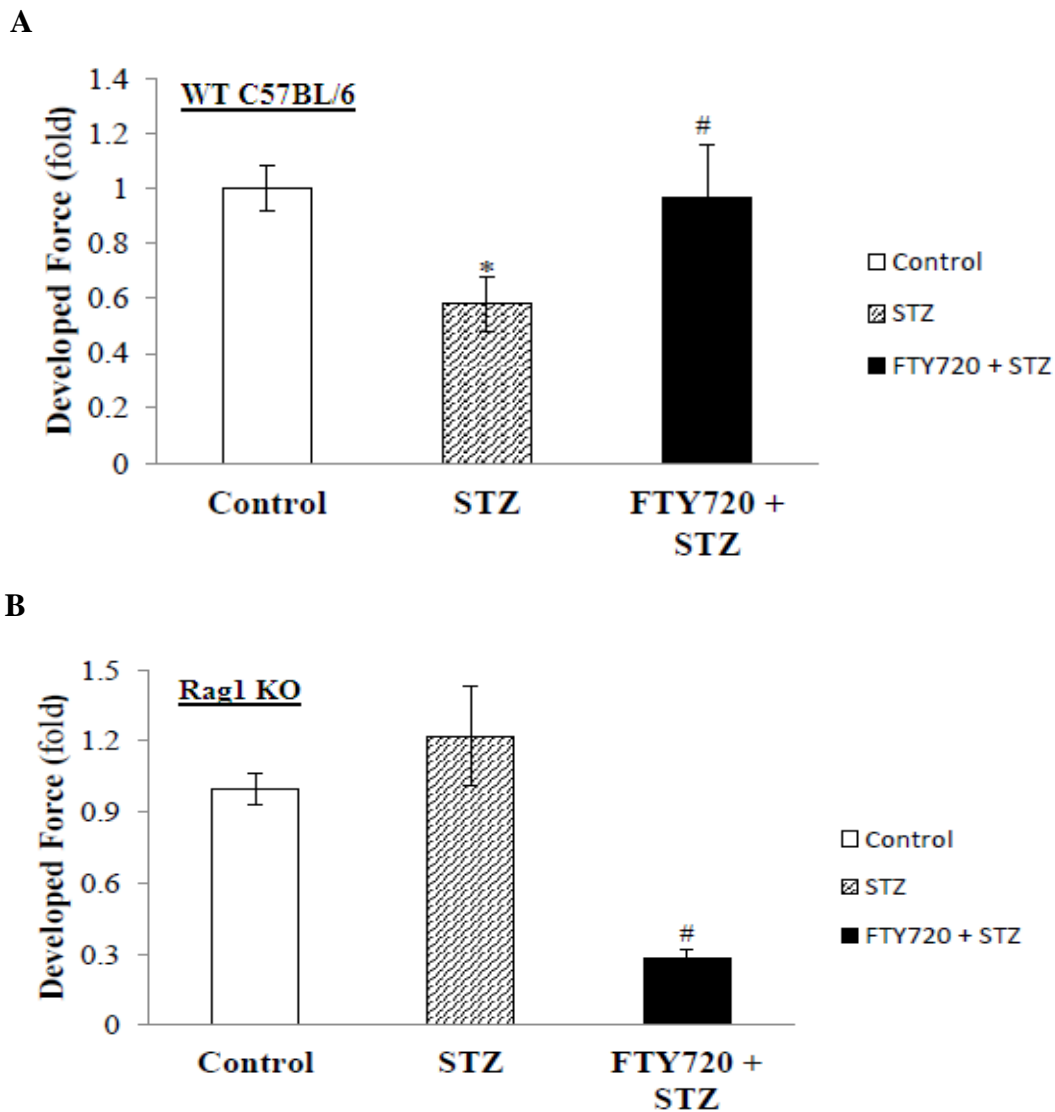
**Figure 2-15:** Representative images of Masson's Trichrome stained heart tissue sections of Rag1 KO mice after 11-week experimental period. Untreated Rag1 KO diabetic mice heart did not exhibit increased fibrosis compared with control mice, while FTY720 treatment in this mice strain developed increased fibrosis. Arrow indicates collagen deposition. Upper panel magnification is 16x, lower panel magnification is 400x. Images are representative of n=3-6 mice heart tissue sections in each group.



**Figure 2-16:** Quantification of percent fibrosis area in WT C57BL/6 and Rag1 KO mice heart after 11-weeks. In WT mice, control (n=6) vs. STZ (n=7), \*P < 0.05; control (n=6) vs. FTY720+STZ (n=5), #P < 0.05. In Rag1 KO mice, control (n=6) vs. STZ (n=5), P = ns, STZ vs. FTY720+STZ (n=3), \*P < 0.05. The data is reported as mean  $\pm$  SEM.

### **2.3.5. Effects of FTY720 treatment on cardiac contractility**

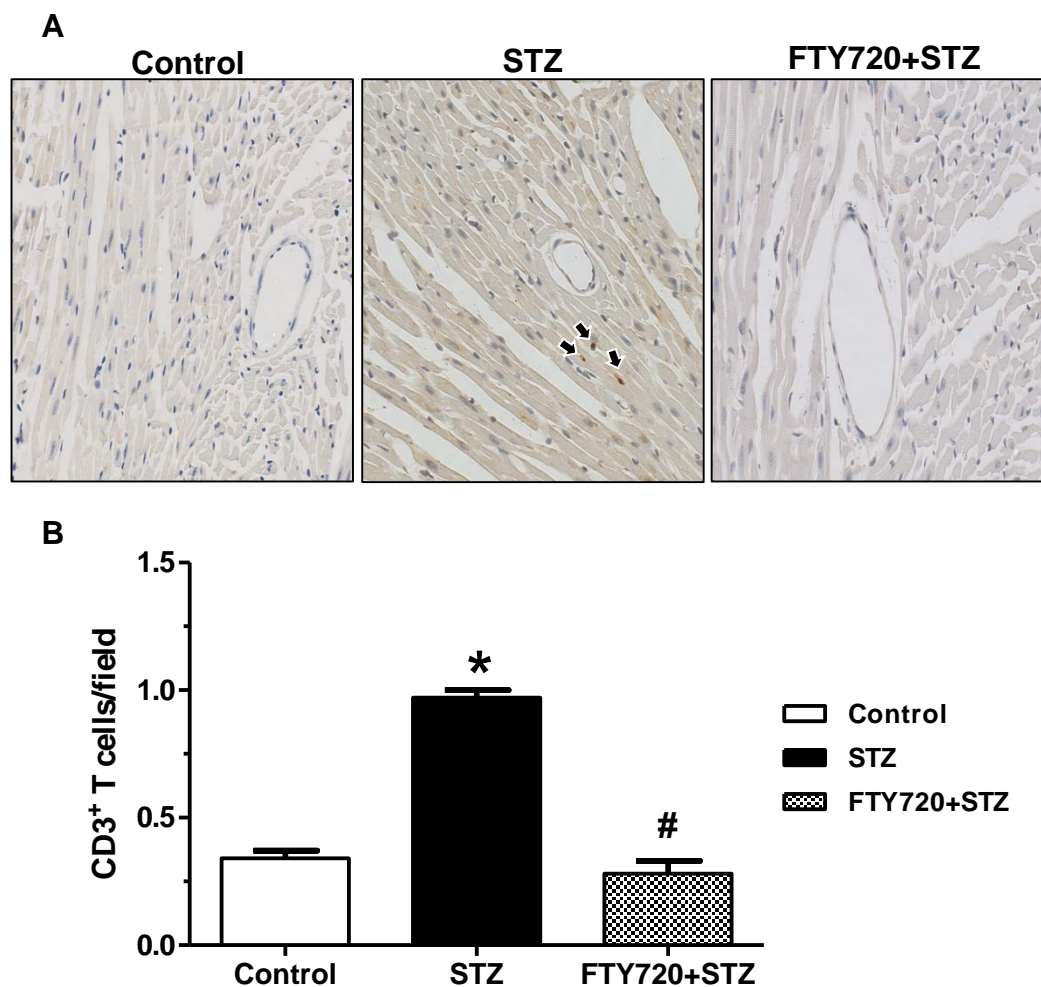
We determined the force of contraction development in an *ex-vivo* Langendorff's heart perfusion system after 11-weeks. The data is expressed as fold change in contractile force development compared to control. Cardiac dysfunction was observed in STZ-induced diabetic WT C57BL/6 mice. There was no alternation in myocardial contractility between STZ-induced diabetic Rag1 KO mice and control Rag1 KO mice (Figure 2-17B). Chronic treatment with FTY720 improved cardiac contractile force in diabetic WT C57BL/6 mice but reduced contractile force in diabetic Rag1 KO mice (Figure 2-17A and 2-17B).



**Figure 2-17:** Effect of FTY720 on cardiac contractile force in diabetic WT C57BL/6 and (A) and Rag1 knockout mice (B) hearts. Chronic Treatment with FTY720 preserved the cardiac function of diabetic WT hearts but attenuated contractile force of diabetic Rag1 KO mice. The contractile force was expressed as fold change relative to control. Sample size, n = 4-9 mice in each group. The data is expressed as mean  $\pm$  SEM. \*P < 0.05, control vs. STZ; #P < 0.05, STZ vs. FTY720+STZ.

### 2.3.6. FTY720 reduces CD3<sup>+</sup> T cells infiltration into the myocardium

Although normal heart does not exhibit appreciable amount of CD3<sup>+</sup> T lymphocytes, under pathological conditions T cells can infiltrate the heart.<sup>76</sup> To detect CD3<sup>+</sup> T lymphocytes in diabetic myocardium, we carried out immunostaining with mouse monoclonal CD3 IgG antibody. CD3<sup>+</sup> T cells were barely detected in WT control hearts. On the other hand, we observed increased CD3<sup>+</sup> T cells presence in interstitial space with close proximity to cardiomyocytes in diabetic WT mice, indicating T cells direct involvement in cardiac injury under diabetes (Figure 2-18A). FTY720 treatment reduced detectable CD3<sup>+</sup> T cells in WT diabetic mice myocardium (STZ, 0.97±0.03 cells/field vs. FTY720+STZ, 0.28±0.05 cells/field; #P<0.05) (Figure 2-18B). Rag1 KO heart sections exhibited no CD3<sup>+</sup> T cell staining.

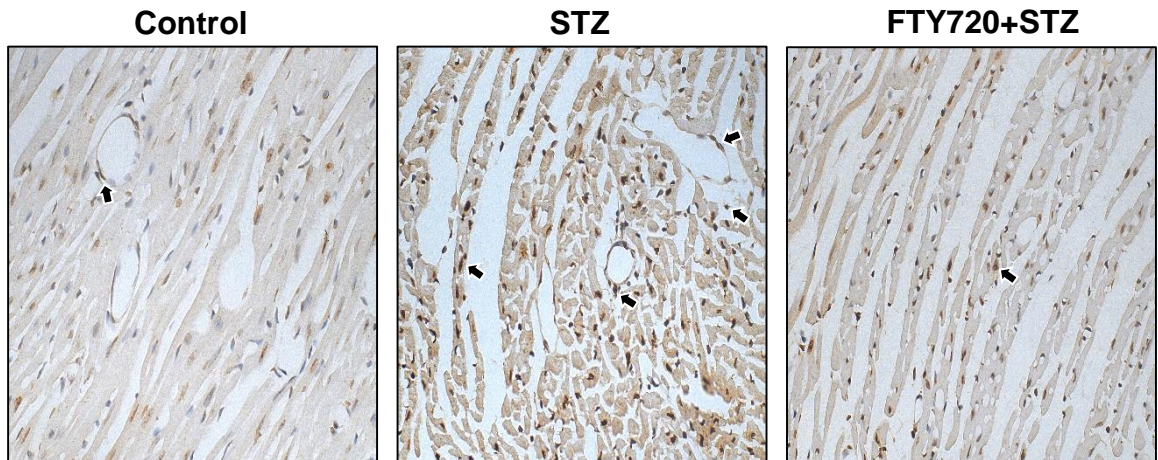
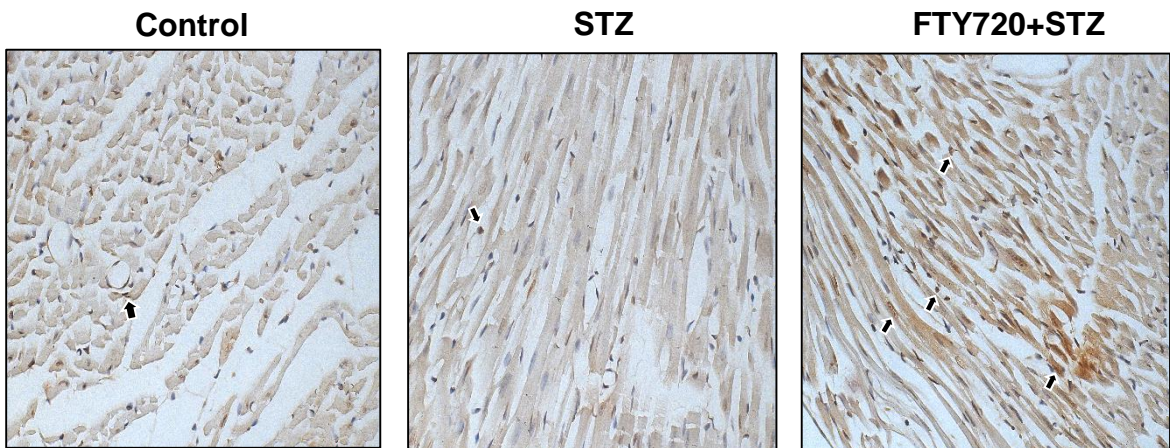


**Figure 2-18:** Immunohistochemical detection of CD3<sup>+</sup> T cells in heart tissue section of WT C57BL/6 mice after 11-week experimental period. **(A)** Increased infiltration of CD3<sup>+</sup> T cells in diabetic WT C57BL/6 mice myocardium were observed. FTY720 treatment reduced CD3<sup>+</sup> T cells number in diabetic WT mice myocardium. Black arrows indicate detected CD3<sup>+</sup> T cells in mice myocardium. Images are representative of three independent experiments. The magnification is 400x. **(B)** Results are from three independent experiments. The data is expressed as mean ± SEM. Control vs. STZ; \*P < 0.05; STZ vs. FTY720+STZ; #P < 0.05.

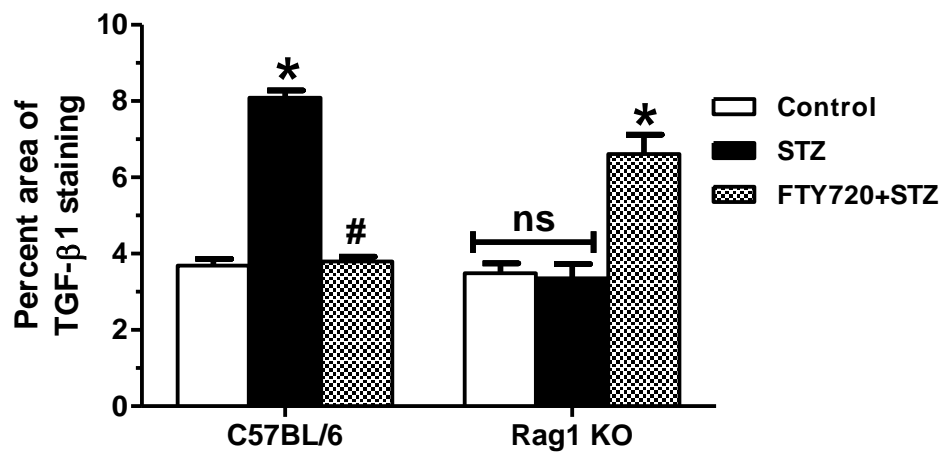
### 2.3.7. FTY720 reduces TGF- $\beta$ 1 expression in diabetic WT myocardium

Transforming growth factor beta 1 (TGF- $\beta$ 1) is a profibrotic cytokine that can activate fibrotic pathway in heart that induces fibrosis.<sup>126</sup> To measure total TGF- $\beta$ 1 expression in cardiac tissue, we conducted immunohistochemistry and quantified the intensity and staining area. TGF- $\beta$ 1 expression was increased in diabetic WT mice myocardium after 11-week diabetic period compared to control mice (8.09 $\pm$ 0.19 % staining area vs. 3.69 $\pm$ 0.17 % staining area, \*P<0.05) (Figure 2-19A and 2-20). FTY720 treatment significantly reduces TGF- $\beta$ 1 expression in diabetic heart compared to untreated diabetic mice (3.80 $\pm$ 0.12 % staining area vs. 8.09 $\pm$ 0.19 % staining area, #P<0.05) (Figure 2-19A and 2-20).

In contrast, diabetic Rag1 KO mice heart sections exhibited statistically no significant difference in TGF- $\beta$ 1 expression than control mice (3.48 $\pm$ 0.26 % staining area vs. 3.35 $\pm$ 0.38 % staining area, P=ns). FTY720 treatment in Rag1 KO hyperglycemic mice increased TGF- $\beta$ 1 expression in myocardium compared to untreated diabetic mice (6.61 $\pm$ 0.51% vs. 3.35 $\pm$ 0.38%, \*P<0.05) (Figure 2-19B and 2-20).

**A WT C57BL/6****B Rag1 KO**

**Figure 2-19:** FTY720 treatment effect in TGF- $\beta$ 1 expression in heart tissue sections of WT C57BL/6 and Rag1 KO mice after 11-week treatment period. **(A)** Representative immunohistochemical images show reduced TGF- $\beta$ 1 expression in WT FTY720 treated diabetic mice compared to untreated diabetic mice. **(B)** TGF- $\beta$ 1 expression was reduced in diabetic Rag1 KO mice, while FTY720 treatment increased TGF- $\beta$ 1 expression in Rag1 KO mice heart sections. Black arrows indicate TGF- $\beta$ 1 expression localization in myocardium. Images are representative of three independent experiments. The magnification is 400x.

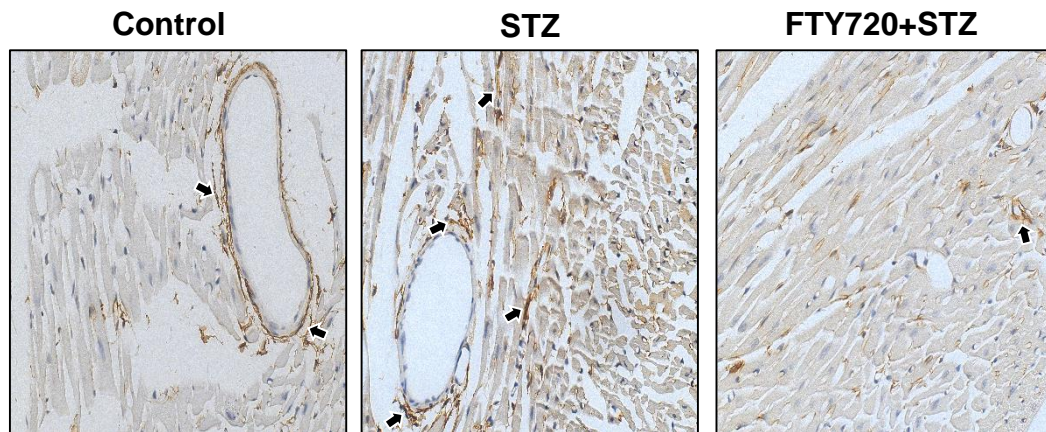


**Figure 2-20:** Quantification of TGF- $\beta$ 1 percent staining area in WT C57BL/6 and Rag1 KO mice myocardium. Results are from three independent experiments. The data is expressed as mean  $\pm$  SEM. In WT mice, Control vs. STZ, \* $P < 0.05$ , STZ vs. FTY720+STZ, # $P < 0.05$ . In Rag1 KO mice, control vs. STZ,  $P = ns$ , Control, STZ vs FTY720+STZ, \* $P < 0.05$ .

### 2.3.8. Effects of FTY720 treatment on CD34 fibrocyte expression in the myocardium

Fibrocytes are circulatory, spindle shaped, monocyte-derived profibrotic cells that augment fibrotic conditions. Chronic injury invokes fibrocytes recruitment at the site of inflammation.<sup>62</sup> CD34 surface expression can be considered as a biomarker for fibrocytes.<sup>62,63</sup> We detected CD34 expression pattern and quantified expression level by immunostaining in mice heart sections. In WT control mice, CD34 expressing cells predominantly appeared in perivascular region, while in diabetic WT mice, CD34 expressing cells appeared in interstitial space of myocardium and closely adherent to myocytes (Figure 2-21A). The total expression of CD34 in myocardium was increased in untreated diabetic mice heart tissue compared with control mice ( $6.59 \pm 0.20\%$  vs.  $2.97 \pm 0.44\%$ , \* $P < 0.05$ ) (Figure 2-22). Fingolimod treatment markedly reduced CD34 expressing cells presence in diabetic myocardium compared to untreated diabetic mice ( $3.11 \pm 0.21\%$  vs.  $6.59 \pm 0.20\%$ , # $P < 0.05$ ) (Figure 2-21A and 2-22).

Rag1 KO control and diabetic mice heart sections exhibited minimal expression of CD34 cells in myocardium ( $2.35 \pm 0.05\%$  vs.  $2.27 \pm 0.20\%$ ,  $P = \text{ns}$ ) (Figure 2-21B and 2-22). FTY720 treatment increased CD34 cells expression in interstitial space of diabetic Rag1 KO mice heart compared to untreated KO diabetic mice ( $4.45 \pm 0.12\%$  vs.  $2.27 \pm 0.20\%$ , \* $P < 0.05$ ) (Figure 2-21B and 2-22).

**A** WT C57BL/6**B** Rag1 KO

**Figure 2-21:** Representative immunostaining images of CD34 bearing fibrocytes in heart tissue sections of WT C57BL/6 and Rag1 KO mice after 11-weeks. **(A)** In WT control mice, CD34 fibrocytes are localized in perivascular area, while in WT diabetic mice heart CD34 cells are found increasingly adjacent to myocardium. FTY720 treatment reduced CD34 cells in myocardium of WT diabetic mice. **(B)** Rag1 KO control and diabetic mice myocardium have minimal CD34 expressing cells. FTY720 treatment in Rag1 KO diabetic mice significantly increased CD34 cells expression in the mouse heart sections. Black arrows indicate CD34 cells detected by immunostaining. Images are from three independent experiments. The magnification is 400x.

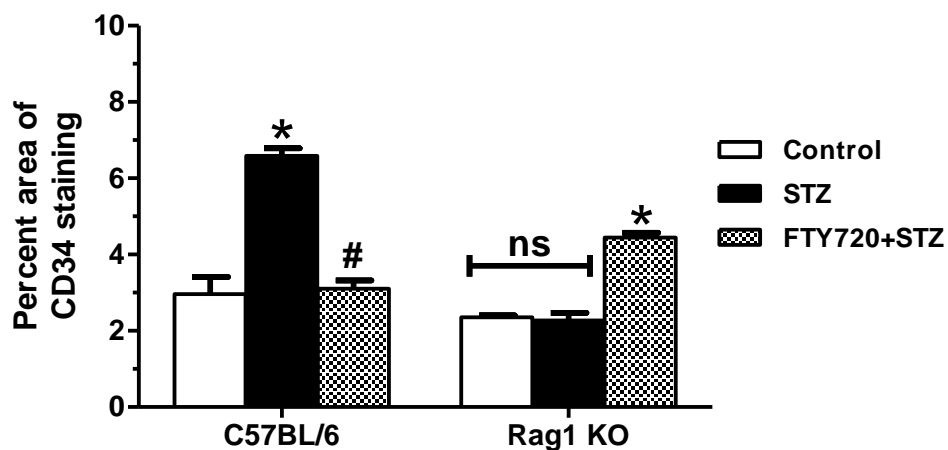


**Figure 2-22:** Quantification of percent area staining of CD34 expression in heart tissue sections of WT C57BL/6 and Rag1 KO mice after 11-weeks. Results are from three independent experiments. The data is expressed as mean  $\pm$  SEM. Control vs. STZ; \*P < 0.05 and STZ vs. FTY720+STZ; #P < 0.05 in WT mice. Control vs. STZ, P = ns, STZ vs. FTY720+STZ; \*P < 0.05 in Rag1 KO mice.

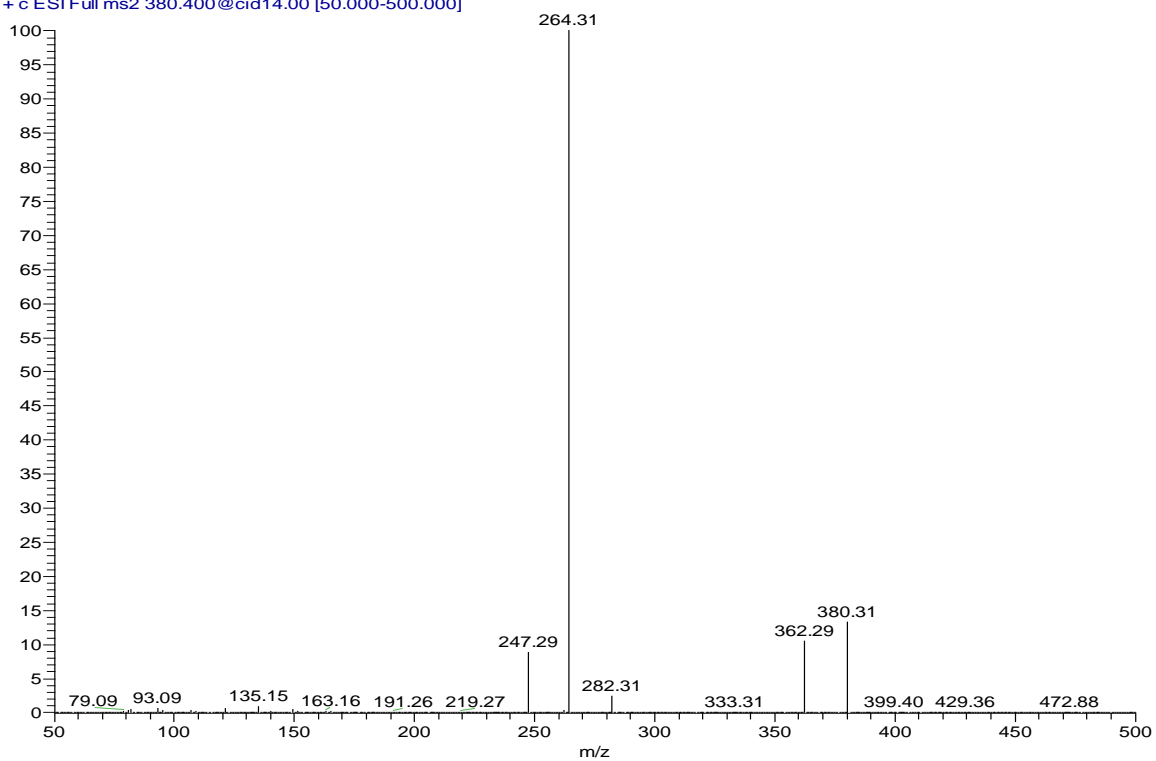
### **2.3.9. Increased plasma S1P levels and S1P<sub>1</sub> expression in myocardium in diabetic mice**

Chronic inflammatory conditions in mice, such as colitis-associated cancer and myocardial infarction, lead to increased S1P synthesis at the site of tissue injury/inflammation.<sup>116,130</sup> In addition, S1P<sub>1</sub> receptor expression has been detected to increase at the site of tissue injury/inflammation. This phenomenon indicates presence of a positive feedback loop of S1P-S1P<sub>1</sub> signaling in inflamed tissue.<sup>116,130</sup> To this end, it is noteworthy that long term diabetes is associated with chronic systemic and local inflammation. Thus, in the present study we measured mice plasma S1P level by using LC/MS/MS technique and also detected S1P<sub>1</sub> expression in the myocardium.

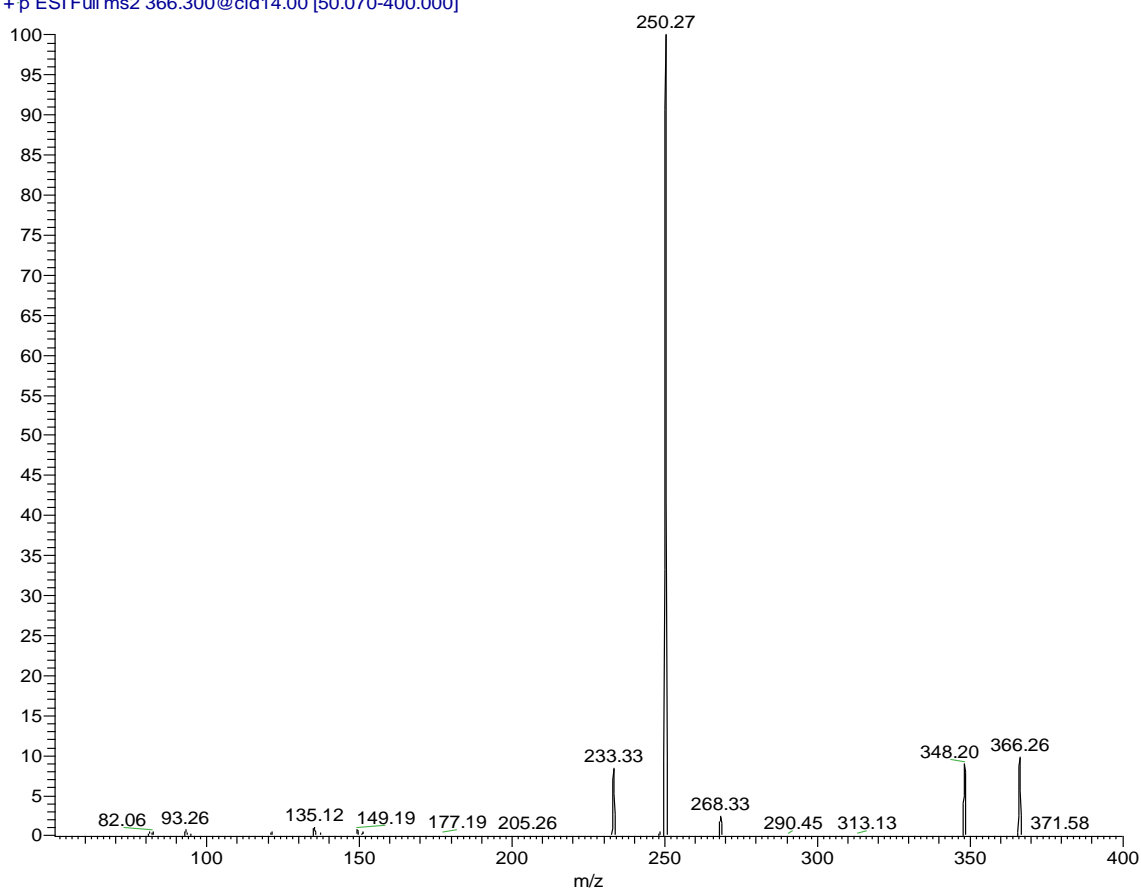
Hyperglycemia increased plasma S1P level in both WT and KO mice (Figure 2-23A, 2-23B and 2-24A, 2-24B, \*P<0.05, as compared with control mice). In WT mice, plasma S1P level was increased in diabetic mice compared to control mice (0.61±0.02 μM vs. 0.42±0.05 μM, \*P < 0.05) (Figure 2-24A). FTY720 treatment reduced plasma S1P level about 1.20 –fold, but yielded no statistical significant difference with diabetic mice S1P level (0.51±0.05 μM vs. 0.61±0.02 μM, P > 0.05) (Figure 2-24A). Similarly, Rag1 KO diabetic mice have increased S1P levels compared to control mice (0.70±0.02 μM vs. 0.50±0.04 μM, \*P < 0.05) (Figure 2-24B).

**A**

S1P\_Product #1-82 RT: 0.00-1.00 AV: 82 NL: 2.61E7  
T: + c ESI Full ms2 380.400@cid14.00 [50.000-500.000]



S1P\_IS\_Product #1-81 RT: 0.01-0.99 AV: 81 NL: 1.52E7  
T: + p ESI Full ms2 366.300@cid14.00 [50.070-400.000]



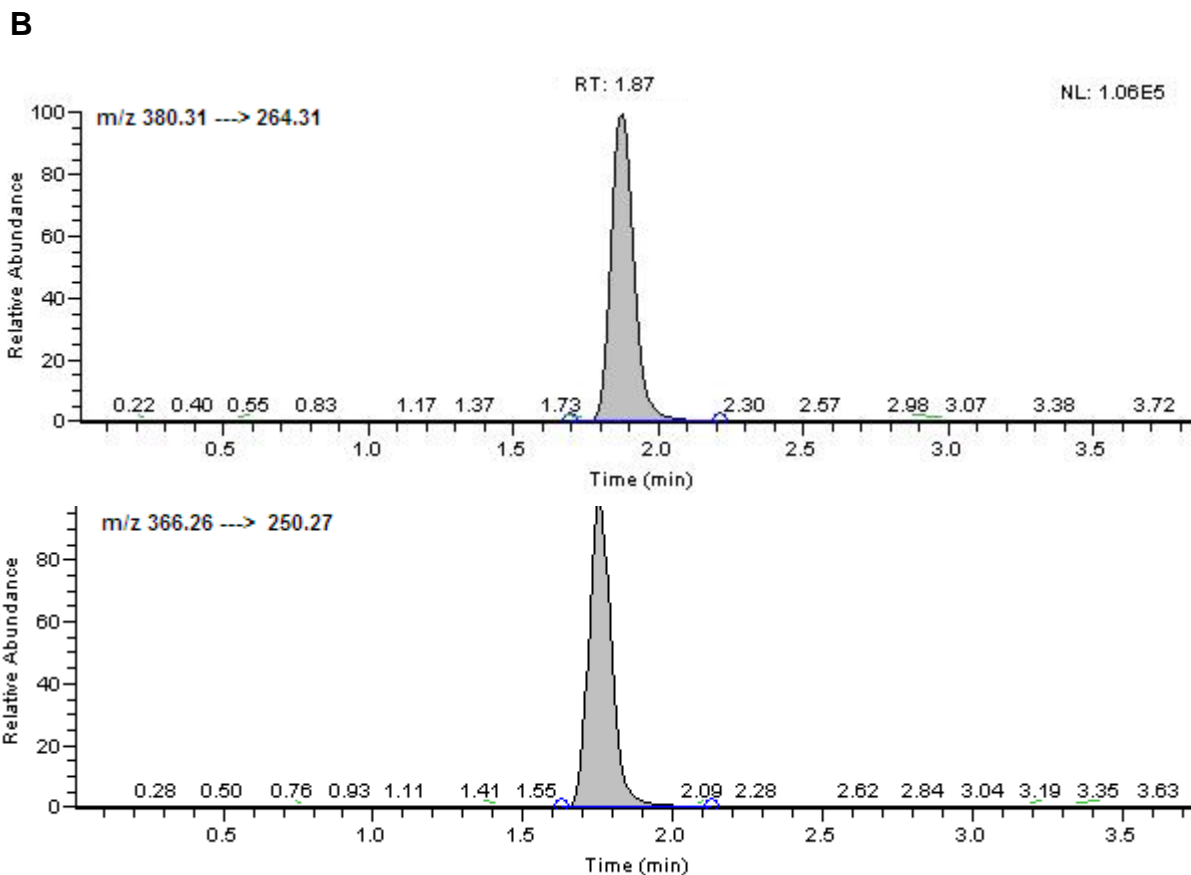


**Figure 2-23:** Measurement of sphingosine 1-phosphate (S1P) level in the plasma samples of WT C57BL/6 and Rag1 KO mice by LC/MS/MS. (A) Representative full-scan product ion mass spectra of  $[M+H]^+$  for S1P (upper panel) and internal standard (IS) C17-S1P (lower panel). (B) Representative SRM chromatograms of S1P (upper panel) and IS (lower panel).

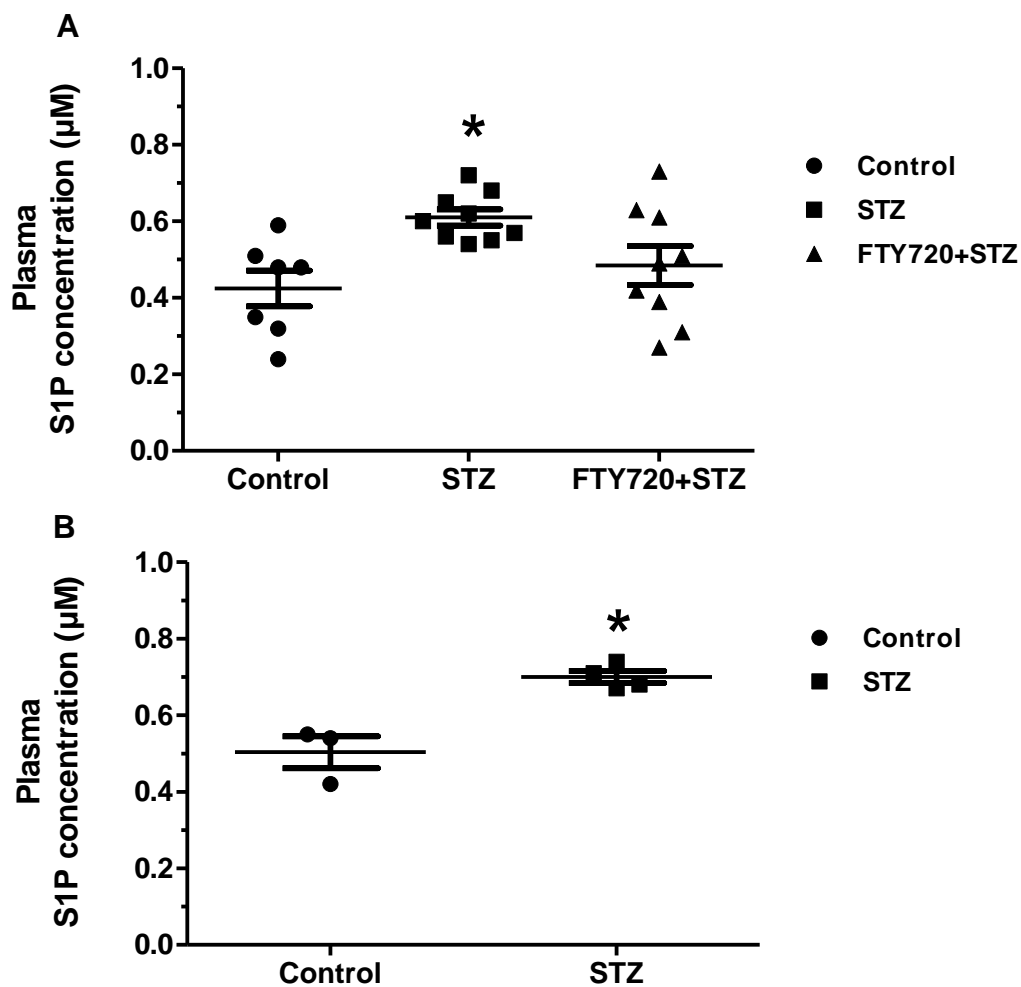


**Figure 2-24:** Quantification of plasma S1P level in the plasma samples of WT C57BL/6 and Rag1 KO mice after 11-week experimental period. **(A)** In WT mice, Control (n=7) vs. STZ (n=9), \*P < 0.05, STZ (n=9) vs. FTY720+STZ (n=8), P > 0.05. **(B)** In Rag1 KO mice, control (n=3) vs. STZ (n=4), \*P < 0.05. The data is expressed as mean ± SEM.

We further detected sphingosine 1-phosphate receptor 1 (S1P<sub>1</sub>) expression in heart tissue sections by immunohistochemistry and quantified the expression level. S1P<sub>1</sub> expression was detected in cardiomyocytes, cells in interstitial spaces and in endothelial cells in control mouse heart tissue (Figure 2-25A). Hyperglycemia increased S1P<sub>1</sub> expression in cardiomyocytes in WT STZ mice compared to control mice (6.13±0.27% vs. 3.13±0.18%, \*P<0.05) (Figure 2-25A and 2-26). Fingolimod treatment markedly reduced S1P<sub>1</sub> expression in cardiomyocytes and limits the expression mainly on the endothelial cells compared to untreated diabetic mice (3.15±0.08% vs. 6.13±0.27%, #P<0.05) (Figure 2-25A and 2-26).

Similar S1P<sub>1</sub> expression profile was observed in Rag1 KO heart sections. Untreated Rag1 KO diabetic mice heart sections exhibited increased S1P<sub>1</sub> expression (5.30±0.18 % [STZ] vs. 3.29±0.25 % [control], \*P < 0.05), while FTY720 treatment reduces S1P<sub>1</sub> expression (3.10±0.36 % [FTY720+STZ] vs. 5.30±0.18 % [STZ], #P < 0.05) (Figure 2-25B and 2-26).

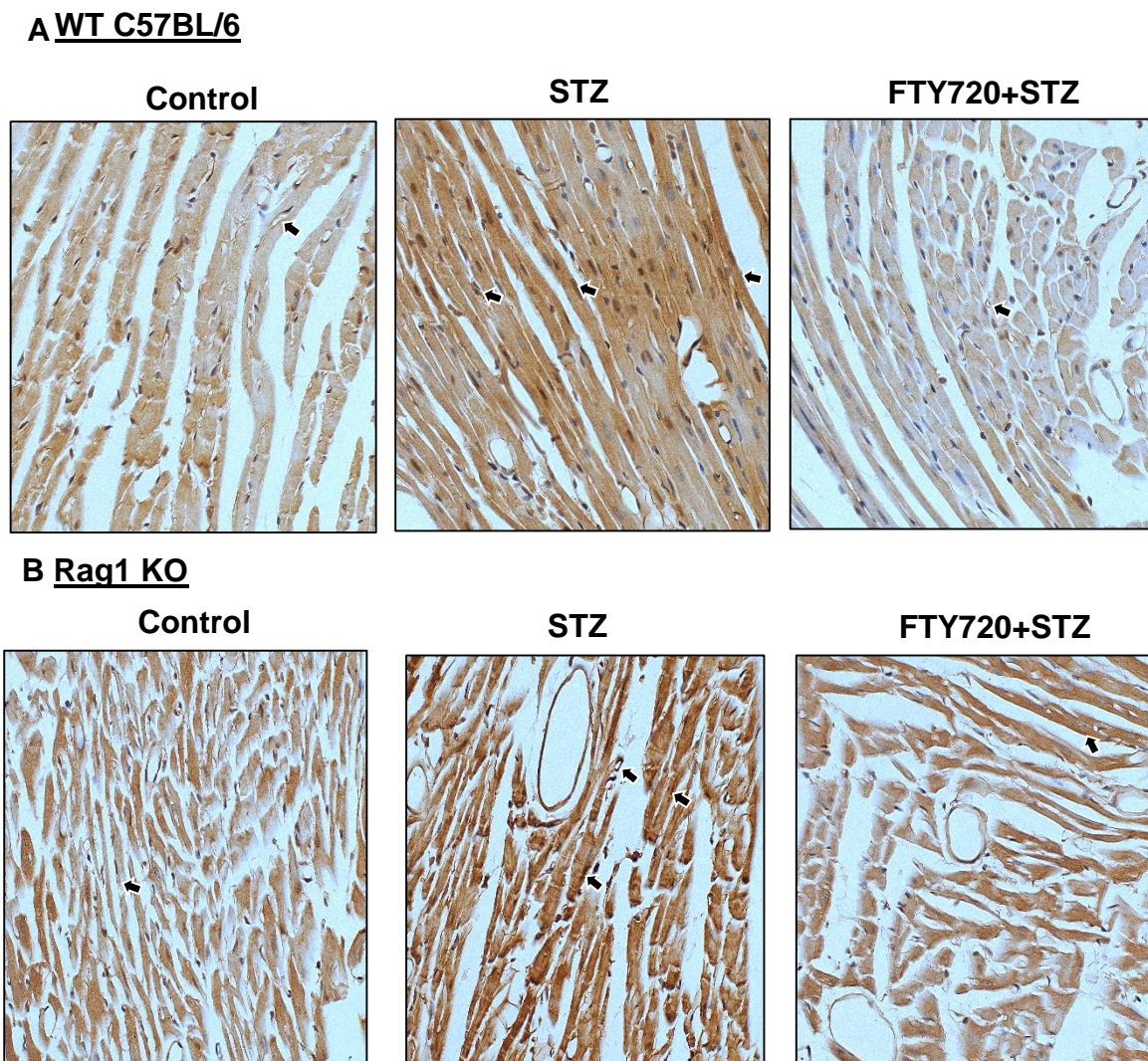


**Figure 2-25:** Representative immunohistochemistry images of S1P<sub>1</sub> expression in WT C57BL/6 and Rag1 KO mice myocardium after 11-weeks. Both WT C57BL/6 (**A**) and Rag1 KO (**B**) diabetic mice heart sections exhibited increased S1P<sub>1</sub> expression. FTY720 treatment limits cardiomyocyte expression of S1P<sub>1</sub> in both WT (**A**) and KO (**B**) mice myocardium. Images are representative of triplicate experiments for each group. The magnification is 400x.

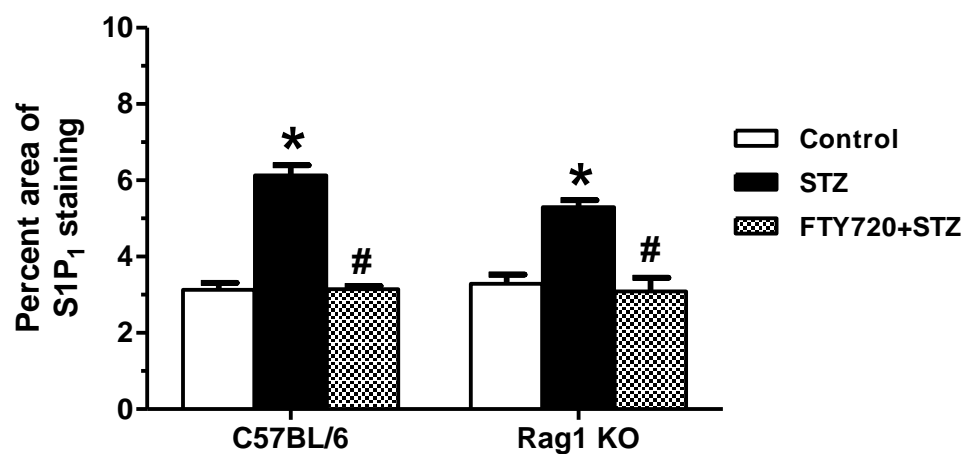


**Figure 2-26:** Quantification of S1P<sub>1</sub> expression in WT C57BL/6 and Rag1 KO mice heart tissue sections after 11-weeks. Results are from three independent experiments. The data is expressed as mean  $\pm$  SEM. Control vs. STZ, \*P < 0.05, STZ vs. FTY720+STZ, #P < 0.05 in WT and KO mice.

## 2.4. Discussion

Recent studies have reported that the T lymphocytes infiltration is an important component in myocardial fibrogenesis in murine myocardial infarction model and pressure overload transverse aortic constriction models.<sup>74,76</sup> In the present study, we for the first time report the chronic administration of FTY720 treatment reduced cardiac fibrosis area and improved contractility under chronic hyperglycemic condition compared to untreated diabetic mice in wild-type (WT) C57BL/6 mice. FTY720 treatment induced sustained reduction of CD4<sup>+</sup> and CD8<sup>+</sup> T lymphocytes in the blood and was associated with reduced CD3<sup>+</sup> T cells infiltration into heart tissue of diabetic WT mice compared to untreated WT diabetic mice. Cardiac protection and anti-fibrosis were also observed in diabetic Rag1 knock-out (KO) mice without any mature lymphocytes. Remarkably, FTY720 caused heart injury in diabetic Rag1 KO mice.

FTY720, also known as fingolimod, is an orally active immunomodulator drug approved by FDA for relapsing multiple sclerosis.<sup>92</sup> FTY720 is a synthetic structural analogue of endogenous sphingosine, becomes activated *in vivo* upon phosphorylation by sphingosine kinase 2 and then acts on all five S1P receptors (S1P<sub>1-5</sub>).<sup>92,93,128</sup> FTY720 binds with S1P<sub>1</sub> receptor with high affinity (0.3 nM); causes ligand induced internalization and degradation of the receptor (functional antagonism).<sup>88,89</sup> Mature T cells express higher S1P<sub>1</sub> receptor on their cell surface that enables these cells to sense the increased concentration gradient of endogenous ligand sphingosine 1-phosphate (S1P) in blood and lymph than in lymphoid tissues.<sup>85,89</sup> Thus, S1P-S1P<sub>1</sub> driven chemotaxis enables T cells exit from lymphoid organs to periphery. Fingolimod downmodulates mature T lymphocytes cell surface S1P<sub>1</sub> receptor and sequesters the T

cells in lymphoid organs. Thus, FTY720 inhibits the recirculation of T cells between lymphoid organs and blood.<sup>95</sup> In experimental autoimmune encephalomyelitis, FTY720 alters lymphocytes trafficking directed towards central nervous system and thus provides protection from immune assault mediated by T lymphocytes.<sup>92,95</sup> Similarly, we found that FTY720 causes both CD4<sup>+</sup> and CD8<sup>+</sup> T cells sustained depletion in blood as shown in this study, and maintained the pronounced lymphopenia at the end of 11-week study period. To correlate circulatory T cells deficiency effect with heart T cells infiltration, we conducted immunostaining to detect myocardium infiltrating CD3<sup>+</sup> T cells. WT diabetic mice myocardium increased CD3<sup>+</sup> T cells presence in interstitial space that was reduced in FTY720 treatment WT diabetic mice. FTY720 protected diabetic WT mouse hearts against hyperglycemia-induced injury. Trichrome staining showed less fibrosis area in heart sections of FTY720 treatment diabetic WT mice compared to untreated diabetic mice. These cardiac protective effects are consistent with the study in diabetic Rag1 KO mice that lacks mature lymphocytes.

After 11-weeks, diabetic Rag1 KO mouse hearts showed integrated cardiac structure with less fibrosis and preserved contractile force. Fibrosis development involves complex network of cellular and molecular milieu. We further investigated CD34 bearing fibrocytes localization in cardiac tissue. Diabetic mice myocardium exhibited increased myocytes adherent CD34 fibrocytes with increased expression of profibrotic mediator TGF- $\beta$ 1. Diabetic WT mice under FTY720 treatment as well as Rag1 KO diabetic mice showed significantly less fibrocytes presence in interstitial space of myocytes with reduced TGF- $\beta$ 1 expression. Elevated sphingosine 1-phosphate receptor 1 (S1P<sub>1</sub>) signaling has been implicated in potentiating inflammation in murine myocardium after

left anterior coronary artery ligation induced myocardial infarction within 4-weeks.<sup>116</sup> Similarly, both WT and KO mice under long term hyperglycemia in present study exhibited increased S1P<sub>1</sub> expression in heart tissue after 11-weeks. This increment is reversed in both mice strain under FTY720 treatment. Paradoxically, FTY720 administration in KO diabetic mice attenuates cardioprotection as observed in untreated diabetic KO mice: FTY720 treatment increases fibrotic area, worsens cardiac histology and reduces contractile force in KO diabetic mice. Increased CD34 infiltration with increased TGF- $\beta$ 1 expression has been observed in these mouse hearts. These findings indicate that FTY720 can modulate myocardial fibrosis through different mechanisms depending on the presence of T lymphocytes discussed later.

Diabetic heart generates increased reactive oxygen species (ROS) due to metabolic perturbations in presence of hyperglycemia.<sup>3,26</sup> Increased ROS induces proinflammatory signaling that activates endothelial cells.<sup>3</sup> Activated endothelial cells as well as inflamed myocardium express increased adhesion molecules expression (e.g. vascular cell adhesion molecule 1; intercellular adhesion molecule 1) as observed in STZ-induced diabetic rodent myocardium.<sup>129</sup> Increased adhesion molecules expression recruits inflammatory mononuclear cells in heart that participate in inflammation potentiation and fibrosis generation. Increased infiltration of CD3<sup>+</sup> T cells into heart tissue, as early as 2-week, has been reported in a STZ-induced diabetic rodent model that is associated with increased collagen deposition into myocardium with declined left ventricular contractility.<sup>111</sup> Increased endothelial cell adhesion molecule ICAM-1 and increased T cells recruitment into heart tissue were detected in pressure overload TAC heart.<sup>76</sup> T cells as an adaptive immune system cell continually recirculate between secondary lymphoid

organs e.g. spleen and lymph nodes as well as periphery that maximizes their interaction with antigen bearing antigen-presenting cells e.g. macrophages, B cells, dendritic cells. The continuous recirculation of T cells is necessary for activation, proliferation and subsequent generation of immune response in target organ. This concept has been implicated in recent report where T cells proliferation have been detected in heart draining lymph nodes of mice underwent MI and TAC surgery induced injury after activation through heart derived neoantigens e.g. myocytes debris encountering.<sup>77</sup> In these models, increased T cells recruitment into heart was associated with increased fibrosis. From our lab, we have also reported earlier that the inhibition of PKC- $\theta$ , a selectively T cell expressed protein kinase C family protein necessary for T cell activation, by a cell permeable peptide inhibitor in STZ-induced diabetic cardiomyopathy model reduces T cells presence into cardiac tissue associated with antifibrotic effect.<sup>117</sup> Despite these findings, the effect of T cells trafficking modulation in long term diabetes associated fibrogenesis is still not known. In our present chapter work, we for the first time report that FTY720 induced T cells reduction in blood is associated with reduced myocardial fibrosis under long term 11-week diabetic period.

Fibrocytes are circulating monocyte-derived CD34 expressing cells that appear in injured tissue and can secrete extracellular matrix (ECM) protein as well as under chronic profibrotic milieu e.g. TGF- $\beta$ 1, apoptotic debris etc. and can differentiate in to ECM protein synthesizing fibroblasts.<sup>62</sup> To determine fibrocytes localization in diabetic heart tissue, we used CD34 as a biomarker for immunostaining of fibrocytes. One of the unique findings of our current work is that FTY720 treatment reduced interstitial appearance of CD34 expressing fibrocytes in diabetic myocardium. Similarly, diabetic KO mice without

FTY720 treatment exhibited minimal expression of CD34 cells in their heart tissue. In addition, profibrotic mediator TGF- $\beta$ 1 expression is markedly reduced in FTY720 treatment diabetic WT mice heart. Rag1 KO diabetic mice heart sections showed similar expression profile of TGF- $\beta$ 1. Altogether, our findings for the first time demonstrate that simultaneous high magnitude presence of T cells and fibrocytes in diabetic myocardium results in profibrotic microenvironment as manifested by increased TGF- $\beta$ 1 expression and increased myocardial fibrosis. Fingolimod causes reduction of T lymphocytes in circulation and heart tissue that is associated with attenuation in TGF- $\beta$ 1 expression and CD34 fibrocytes in diabetic cardiac tissue.

S1P-S1P<sub>1</sub> signaling has been reported as a proinflammatory mediator in colitis-associated cancer<sup>127</sup> and more recently, in the long term myocardial infarction murine model.<sup>116</sup> In this paradigm, increased S1P level under inflammatory condition increases S1P<sub>1</sub> expression that causes persistent activation of transcription factor STAT3 which further potentiates proinflammatory molecules gene expression. Thus, we measured S1P level by LC/MS/MS in plasma and quantified S1P<sub>1</sub> expression in heart tissue by immunohistochemistry. Increased plasma S1P levels were observed in both diabetic WT and KO mice. Although FTY720 treatment reduced about 1.20-fold S1P level in diabetic mice, the statistical test did not show any significant difference between untreated and treated diabetic mice blood. This result is consistent with earlier reports as in heart injury model FTY720 treatment did not reduce serum S1P level.<sup>116,127</sup> Further, diabetic myocardium showed increased expression of S1P<sub>1</sub> receptor suggesting activation of S1P-S1P<sub>1</sub> inflammatory loop in present long term diabetic model. Here, we for the first time demonstrate increased S1P<sub>1</sub> expression in diabetic myocardium. Notably, FTY720

reduces increased S1P<sub>1</sub> expression in cardiomyocytes in both WT and KO mice.

Recently, Zhang et al. reported FTY720 reduces S1P<sub>1</sub> expression in mouse heart tissue after myocardial infarction and protects the heart from inflammation, dysfunction and cardiac remodeling.<sup>116</sup>

Surprisingly, FTY720 treatment in diabetic Rag1 KO mice exacerbated fibrosis, worsened cardiac histology and decreased cardiac force of contraction with discernible disarray and loss of myofibers compared with untreated diabetic KO mice. There could be two possible explanations to describe this paradoxical result. First, fate of cell membrane S1P<sub>1</sub> receptor in presence of sustained FTY720 in extracellular space, and second, FTY720 actions on other S1P receptors. S1P<sub>1</sub> receptor is widely distributed in different tissues/cells and involved in many important physiological functions including maintenance of vascular tone and maturation and endothelial cell barrier regulation.<sup>85</sup> Cell surface residing receptor internalization and re-insertion to cell membrane is a way of G protein-coupled receptors regulation that maintains receptor responsiveness in case of sustained ligand presence in extracellular space. FTY720 binds to S1P<sub>1</sub> and internalizes the receptor and causes ubiquitinylation and proteasomal degradation unlike natural ligand S1P induced S1P<sub>1</sub> internalization, in which case receptor surface expression recycled back shortly.<sup>84,94</sup> FTY720 induced downregulation and degradation of S1P<sub>1</sub> receptor can be a possible cause of contradicting results in reported studies. In lipopolysaccharide-induced murine inflammatory lung injury model, treatment with single dose of FTY720 (0.1 mg kg<sup>-1</sup> body weight, i.p.) after 1 hour of lipopolysaccharide administration, prevented pulmonary vascular leakage by endothelial barrier enhancement as examined after 24 hours.<sup>130</sup> In another study, FTY720 (0.5 mg kg<sup>-1</sup> body

weight, i.p.) administration before and after 24 hour lipopolysaccharide induction; at 48 hour examination of bronchoalveolar lavage showed increased total protein concentration, suggesting increased pulmonary vascular leak.<sup>131</sup> In the same study, authors reported in bleomycin induced lung injury model (fibrosis independent of T cells), FTY720 (0.5 mg kg<sup>-1</sup> body weight, i.p.) three times for 2 weeks increased collagen deposition and fibrosis compared with control mice. Notably, in later investigation higher dose and chronic administration of FTY720 opposes pulmonary vascular protection as seen in single dose FTY720. As lungs are more susceptible to endothelial barrier disruption due to presence of extensive microvascular network associated with alveolar air spaces might be the reason for observed effect. In contrast, cardiac microvascular endothelial cells in STZ-induced diabetic rats have reduced S1P<sub>1</sub> expression and increased membrane translocation of S1P<sub>3</sub>.<sup>132</sup> The opposing roles of S1P<sub>1</sub> and S1P<sub>3</sub> in endothelial cells have been reported in STZ-induced rodent model.<sup>132</sup> Activation of S1P<sub>1</sub> has been implicated in promoting angiogenesis whereas S1P<sub>3</sub> stimulation leads to impaired barrier function.<sup>132</sup> We have observed similar S1P<sub>1</sub> expression pattern in diabetic mouse heart section in present work. Although FTY720 reduces total S1P<sub>1</sub> expression in diabetic myocardium, but maintained its expression on endothelial cells in WT diabetic mice (Figure 2-25). This discrepancy in FTY720 effects on S1P<sub>1</sub> receptor on T cells and cardiac microvascular endothelial cells might be due to the differential association of the receptor with specific molecules in lipid rafts, cellular niche where G protein-coupled receptor specific signaling and internalization/recycling tasks occur, in different cell types.<sup>84</sup> In another paradigm, FTY720 (1 mg kg<sup>-1</sup> body weight, immediately before) protects WT mice brain in transient middle cerebral artery occlusion, but

abolishes protection in Rag1 KO mice.<sup>133</sup> This implies that FTY720-mediated protection in acute transient cerebral ischemia and reperfusion results from not by direct neuroprotection rather its effect on neurovasculature and its interaction with immune cells. In our present study, although Rag1 KO mice heart does not have any T cells but FTY720 treatment causes increased TGF- $\beta$ 1, CD34 expression with increased collagen deposition in heart. These results indicate FTY720 in absence of T cells may activate different fibrotic pathway, while in presence of T cells by inhibiting T cells infiltration and profibrotic milieu into the heart it exerts cardioprotection in diabetes. In this regard, both pharmacokinetic and pharmacodynamic characteristics of FTY720 should be taken into consideration. FTY720 is a lipophilic drug molecule with large volume of distribution ( $V_D$  is 1116-1737 L) and long elimination half-life ( $t_{1/2}$  is 4.5 days).<sup>134,135</sup> Thus, in our present study continuous systemic administration of FTY720 might create a sustained drug pool in the blood to act on its target receptors. Keller et al. reported that FTY720 in dose dependent manner (0.1-1  $\mu$ M) can activate S1P<sub>3</sub> receptor on fibroblasts that causes differentiation into collagen producing myofibroblasts.<sup>136</sup> In summary, FTY720 treatment induced increased fibrosis area in Rag1 KO diabetic mice indicates that the drug might activate other fibrotic pathways in absence of lymphocytes either by affecting S1P<sub>1</sub> receptor functions in heart or by acting on other S1P receptors.

## 2.5. Conclusions

In summary, the important findings of the present study are: (1) diabetic myocardium exhibited profibrotic milieu manifested by increased T cells infiltration with increased TGF- $\beta$ 1 and CD34 expressing fibrocytes into myocardium, (2) fingolimod (FTY720) reduced T lymphocytes infiltration into the myocardium, inhibited profibrotic milieu in myocardium and attenuated fibrotic remodeling with improved cardiac contractility in WT diabetic mice, (3) FTY720 induced cardiac fibrosis in Rag1 KO mice indicates the potential role of FTY720 in activating fibrotic remodeling in absence of lymphocytes under diabetes.

Nonetheless, FTY720 is a non-specific S1P<sub>1</sub> receptor agonist, and S1P<sub>1</sub> receptor expression not exclusive to T lymphocytes only. Therefore, for the next set of experiments, we utilized conditional T cell specific S1P<sub>1</sub> receptor knock out (TS1P<sub>1</sub>KO) mice through Cre-loxP approach. These studies are discussed in the next chapter.

## CHAPTER 3: EFFECTS OF GENETIC DEPLETION OF T CELL S1P<sub>1</sub> RECEPTOR ON CARDIAC FIBROSIS IN DIABETIC CARDIOMYOPATHY

### 3.1. Introduction

In chapter 2, we discussed that chronic administration of sphingosine 1-phosphate receptor 1 (S1P<sub>1</sub>) modulator, FTY720, profoundly reduced circulatory CD4<sup>+</sup> and CD8<sup>+</sup> T cells number in wild-type (WT) C57BL/6 diabetic mice. FTY720 treatment reduced CD3<sup>+</sup> T cells infiltration in diabetic WT mice myocardium compared to untreated diabetic mice. Further, FTY720 treated diabetic WT mice myocardium showed attenuated profibrotic TGF-β1 and CD34 expressing cells expression compared to untreated diabetic mice heart. Rag1 knock out mice, lacking mature B and T lymphocytes, exhibited less fibrosis and preserved contractility under diabetic conditions. Interestingly, FTY720 treatment in Rag1 KO diabetic mice increased fibrosis area and attenuated contractility. These contrary results indicate that FTY720 may target different mechanistic pathways in the absence of lymphocytes to induce cardiac fibrosis. Notably, FTY720 is not only selective to S1P<sub>1</sub> receptor among five S1P receptors, but can also act on other S1P receptors (S1P<sub>2,3,4,5</sub>).<sup>88,92,128,136</sup> FTY720 can induce transdifferentiation of fibroblasts to myofibroblasts similar to TGF-β at concentrations of 0.1 to 1 μM by acting through S1P<sub>3</sub> receptor.<sup>136</sup> In another recent report, FTY720 was shown to cause contraction of fibroblasts by targeting S1P<sub>2</sub> receptor.<sup>128</sup> Thus, FTY720 may induce fibrosis by activating other fibrotic pathways that override lymphocytes depletion associated cardioprotection in Rag1 knock out mice under diabetes.

In this chapter of the dissertation, we have reported the use of Cre-loxP mediated genetic recombination approach to generate conditional T cell specific S1P<sub>1</sub> receptor knock out mice (TS1P<sub>1</sub>KO). Use of this genetic tool enables us to deplete S1P<sub>1</sub> receptor gene specifically on T lymphocytes. To this end, our goal is to demonstrate that the modulation of S1P<sub>1</sub> mediated T lymphocytes trafficking protects heart under diabetic conditions. Littermate and TS1P<sub>1</sub>KO mice undergone chronic STZ-induced type 1 diabetic cardiomyopathy model. At the end point of experimental period (11-weeks), we studied heart histology, assessed fibrosis area, and measured cardiac contractility in *ex-vivo* Langendorff perfusion system. CD3<sup>+</sup> T cells number, profibrotic molecular and cellular milieu were assessed through evaluation of TGF-β1 and CD34 expression by immunohistochemistry in heart tissue.

## **3.2. Materials and Methods**

### **3.2.1. T cell specific S1P receptor 1 knock out mice generation**

To achieve conditional T cell specific sphingosine 1-phosphate receptor 1 (S1P<sub>1</sub>) depletion we used reported Cre-LoxP approach.<sup>83,137</sup> Specific depletion of S1P<sub>1</sub> on T cell was achieved by crossing S1P<sub>1</sub><sup>loxP/loxP</sup> mice (The Jackson Laboratory, Bar Harbor, ME), carrying modified S1P<sub>1</sub> gene with two loxP sequences flanking exon 2 (coding region of S1P<sub>1</sub>), with lymphocyte tyrosine kinase (Lck) promoter bearing Cre mice (Taconic, Hudson, NY).<sup>83</sup> The offspring mice were genotyped to detect TS1P<sub>1</sub>KO mice bearing S1P<sub>1</sub><sup>loxP/loxP</sup> allele with the Lck-Cre gene and littermate control mice with S1P<sub>1</sub><sup>WT</sup> allele with Cre by genotyping polymerase chain reaction. Briefly, genomic DNA was extracted from ear punch tissues by using sodium hydroxide and Tris-HCl buffer.<sup>138</sup> Presence of

Cre transgene and S1P<sub>1</sub> alleles in extracted genomic DNA from offspring mice, primers and PCR conditions were used as described in table 3-1.

**Table 3-1:** Genotyping PCR primers and reaction conditions for Cre and S1P<sub>1</sub> genes.

Genes	Primers	PCR Reaction Conditions
<i>Cre</i>	Forward (5'-->3'): CCTGGAAAATGCTTCTGTCCGTTTG	Initial denaturation: 95 °C for 5 minutes
	Reverse (5'-->3'): ACGAACCTGGTCGAAATCAGTGCG	30 cycles of Denaturation: 95 °C for 1 minute Annealing: 56 °C for 1 minute 30 seconds Extension: 72 °C for 2 minutes; followed by Final extension: 72 °C for 8 minutes
<i>S1P<sub>1</sub></i>	Forward (5'-->3'): GAGCGGAGGAAGTTAAAAGTG	Initial denaturation: 94 °C for 3 minutes
	Reverse (5'-->3'): CCTCCTAAGAGATTGCAGCAA	35 cycles of Denaturation: 94 °C for 30 seconds Annealing: 55 °C for 30 seconds Extension: 72 °C for 30 seconds; followed by Final extension: 72 °C for 2 minutes

In both cases, primer sequences and PCR conditions were followed according to the manufacturers' instruction (S1P<sub>1</sub>: The Jackson Laboratory; Cre: Taconic). All primer pairs were acquired from Eurofins MWG Operon (Huntsville, AL). PCR reactions were carried out by using KAPA LongRange HotStart kit (KK3501, Kapa Biosystems Inc. Wilmington, MA) in a thermal cycler (MasterCycler Personal, Eppendorf). After PCR amplification, DNA bands were detected in 3% w/v agarose gel electrophoresis containing 0.02 % v/v ethidium bromide and imaged at ChemiDoc™ XRS+ system coupled with Image Lab software (Bio-Rad, Hercules, CA). Mutant S1P<sub>1</sub><sup>loxP</sup> allele

amplified at 250-bp and wild-type S1P<sub>1</sub> allele at 200-bp (The Jackson Laboratory). Mice carrying mutant S1P<sub>1</sub><sup>loxP</sup> allele with Cre transgene were TS1P<sub>1</sub>KO mice. Blood samples from all the mouse used in the present study were analyzed by flow cytometry to confirm appropriate use of mouse type. All mice were housed in specific pathogen free room in Animal Research Wing (ARW) facility at South Dakota State University (SDSU) and given free access to autoclaved food (5010, LabDiet) and water. Mice used in the present investigation were handled and cared for according to the *Guide for the Care and Use of Laboratory Animals* by U.S. National Research Council (Eighth Edition, 2011). All the experimental procedures were approved by Institutional Animal Care and Use Committee at SDSU.

### **3.2.2. Induction of Type 1 diabetes**

We used repeated low doses of streptozotocin (STZ) to induce type 1 diabetes in mice as described in chapter 2. Briefly, streptozotocin (S0103, Sigma-Aldrich, MO) at a dose of 50 mg/kg body weight in 0.1 M sodium citrate buffer (pH 4.5) was administered intraperitoneally for five day at the beginning. Both littermate control and TS1P<sub>1</sub>KO mice were divided into vehicle and STZ treated (diabetic) groups. Vehicle group received 0.1 M sodium citrate buffer (pH 4.5) only. All mice then underwent 11-week long study period. Body weights (g) were measured twice each week in an electric balance machine (OHAUS® Scout-Pro™, OHAUS, NJ, USA). Blood glucose levels (mg/dl) were measured in the blood samples from tail vein of mice in a glucose meter (CONTOUR®, Bayer Healthcare LLC, IN) at three time points: at the beginning, 4- and 11-week post STZ induction. STZ recipient mice with blood glucose levels above 200 mg/dl were considered hyperglycemic.

### 3.2.3. Flow cytometry analysis of CD4<sup>+</sup> and CD8<sup>+</sup> T cells

We measured helper CD4<sup>+</sup> and cytotoxic CD8<sup>+</sup> T cells proportions in peripheral blood of all mice by two color flow cytometry analysis as described in chapter 2 in a BD FACSCalibur flow cytometer (BD Biosciences, San Jose, CA). Data was acquired and analyzed by BD CellQuest Pro software (BD Biosciences).

### 3.2.4. Flow cytometry analysis of regulatory T cells

We measured percentage of CD4<sup>+</sup>Foxp3<sup>+</sup> regulatory T cells (T<sub>reg</sub> cells) in spleen and blood after 11-weeks. Single-cell suspension of spleen was prepared from freshly dissected spleen from anesthetized mice. Spleen was cut into 1 mm<sup>3</sup> pieces and passed through 70 μm nylon cell strainer (352350, Corning Inc. NY) by gentle press with a rubber plunger. The dissociated cells were collected in isolation buffer containing 0.5% w/v bovine serum albumin (A2153, Sigma-Aldrich, MO) and 2 mM EDTA in 0.01 M PBS (P3813, Sigma-Aldrich). The cell suspension was centrifuged at 300 x g for 10 minutes at RT. Supernatant was discarded and incubated at RT for 5 minutes with 5 mL of 1 x RBC lysis buffer (00-4333, eBioscience) per spleen. Cell suspension was washed twice in isolation buffer by centrifugation at 500 x g for 10 minutes at RT. The cell pellet was re-suspended in 10 mL isolation buffer and counted in Cellometer Auto T4 (Nexcelom, MA). One million (1 x 10<sup>6</sup>) cells were taken in 100 μL FCS buffer into each tube for staining. For staining in blood, 100 μL of heparinized blood was prepared as described above. Red blood cells were lysed with 2 mL of 1 x RBC lysis buffer by incubating for 5 minutes at RT. Both splenocytes (1 x 10<sup>6</sup>) and blood (100 μL) were dual stained with fluorescein isothiocyanate (FITC)-conjugated anti-mouse CD4 (11-0041-82, eBioscience) and phycoerythrin (PE)-conjugated anti-mouse Foxp3 (12-5773,

eBioscience) antibodies. Respective isotype controls FITC-IgG2b (11-4732, eBioscience) and PE-IgG2a were used to set compensations at detectors of flow cytometer. We used anti-mouse/rat Foxp3 staining set (Catalog# 72-5775, eBioscience) for Foxp3 staining according to manufacturer's instructions (eBioscience, CA). Briefly, first staining with CD4 antibody was carried out at RT for 30 minutes followed by washing with 2 mL of FCS buffer at 500 x g for 5 minutes twice. The cells were then prepared for intracellular staining by re-suspending in 1 mL of fixation/permeabilization buffer at 4 °C for 30 minutes in dark. The cells were then washed with 2 mL of 1 x permeabilization buffer at 500 x g for 5 minutes at RT twice. The cell pellets were re-suspended with 100 µL of 1 x permeabilization buffer and incubated with Foxp3 antibody for 30 minutes at 4 °C in dark. The cells were washed with 2 mL of 1 x permeabilization buffer followed by 2 mL of FCS buffer at 500 x g at RT. The cell pellets were re-suspended in 200 µL of FCS buffer. Flow cytometry analysis was carried out in BD FACSCalibur flow cytometer coupled with CellQuest Pro software (BD Biosciences).

### **3.2.5. Cardiac contractility measurement**

We assessed cardiac contractile force (g) in all mice after 11-week diabetic period in a modified Langendorff heart perfusion system *ex-vivo*, as described in chapter 2. Developed cardiac contractile force (Fc) and the maximal rate of development of contractile force ( $\pm dFc/dt_{max}$ ) were recorded and analyzed with Biopac MP 100 data system (Goleta, CA, USA).

### **3.2.6. Evaluation of heart histology and fibrosis area**

Heart histology was studied in H&E stained, and fibrosis area was determined in Masson's trichrome stained heart sections at the end of 11-weeks. H&E stained sections

were examined under bright field microscope (Carl Zeiss, Germany), and histological scores were given to each heart sections based on the observed characteristics, such as, (i) presence of eosinophilic interstitial collagen fibers, (ii) extent of cellularity in interstitial space of myocardium, (iii) myocardial cell necrosis/loss, (iv) myofiber striation and myocytes organization on a five-point scale for each characteristic from 0 to 4.<sup>120,121</sup> The cumulative scores were expressed from 0 to 16 for each group. Trichrome stained heart sections images were acquired through a Leica EZ4 HD stereomicroscope as a whole (Leica Microsystems, Buffalo Grove, IL, USA). The percentage of fibrosis area relative to whole heart area was quantified by using NIH Image J (Bethesda, MA) software as described by Zhao et al.<sup>117</sup>

### **3.2.7. Immunohistochemical (IHC) analysis of heart sections**

CD3<sup>+</sup> T cells, TGF- $\beta$ 1 and CD34 bearing cells expression were analyzed in myocardium by immunohistochemistry in paraffin-embedded 5  $\mu$ m tissue sections with CD3 (10  $\mu$ g/mL, sc-20047; Santa Cruz Biotechnology, Inc., CA), TGF- $\beta$ 1 (15  $\mu$ g/mL, MAB240; R&D Systems, Inc., Minneapolis, MN) and CD34 (10  $\mu$ g/mL, MA5-17825; Pierce Biotechnology, Rockford, IL, USA) primary antibodies. R&D systems mouse/rat cell and tissue staining HRP-DAB kit (CTS002/CTS017; R&D Systems) were used to amplify positive signals and visualize corresponding to mouse/rat primary antibodies. Detailed procedure was described in chapter 2. To count immunopositive CD3<sup>+</sup> cells, 30 fields of stained heart sections were pictured at bright-field under 400x magnification in an upright microscope (Carl Zeiss, Germany). Myocardium infiltrating cells number (cells/field) was calculated by counting the cells number in imaged 400x fields.<sup>75</sup> TGF- $\beta$ 1

and CD34 positive staining percent area were quantified and averaged in 10 fields of 400x magnification images by using NIH ImageJ software (Bethesda, MD).<sup>119,139</sup>

### **3.2.8. Data analyses**

Data was expressed as mean  $\pm$  SEM. One-way ANOVA was used for statistical analysis of data followed by Tukey's post hoc test of group means. Data was analyzed in GraphPad Prism Software (v5.01, 2007). A P value of less than 0.05 was considered statistically significant and is indicated with an asterisk (\*) or a number (#) or a currency ( $\alpha$ ) sign when comparing between different groups.

## **3.3. Results**

### **3.3.1. T cell specific S1P receptor 1 knock-out mice showed lymphopenia**

All offspring mice from S1P<sub>1</sub><sup>loxP/loxP</sup> and Lck-Cre breeding pair were genotyped by PCR and immunophenotyped for CD3<sup>+</sup> T cells in spleen, CD4<sup>+</sup> and CD8<sup>+</sup> T cells in blood by flow cytometry. Lymphocyte tyrosine kinase driven Cre recombinase deletes coding region of sphingosine 1-phosphate receptor 1 (S1P<sub>1</sub>) at exon 2 in offspring mutant mice specifically on T cells (Figure 3-1A). Figure 3-1B demonstrated PCR amplicons band for S1P<sub>1</sub> gene and Cre gene in offspring mice after genomic DNA amplification by using specific primer sets for mentioned genes. Mice bearing S1P<sub>1</sub> mutant allele amplified at 250-bp with Cre transgene presence were T cell specific S1P receptor 1 knock out (TS1P<sub>1</sub>KO) mice (Figure 3-1B). Littermate control mice with S1P<sub>1</sub> WT allele amplified at 217-bp with Cre transgene were used.

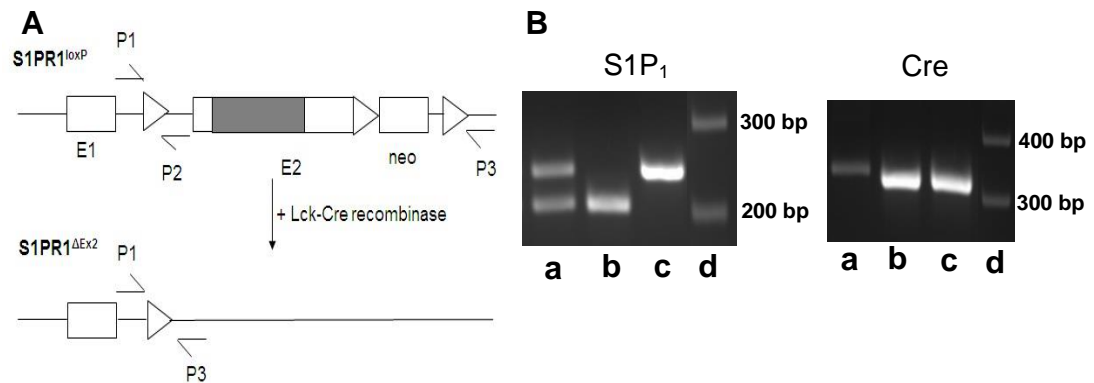


**Figure 3-1:** Generation and detection of conditional T cell specific S1P receptor 1 knock out mice. **(A)** Mice carrying flanked S1P<sub>1</sub> gene at exon 2 (coding region of S1P<sub>1</sub> gene) by loxP sites are cross-bred with mice carrying Lck promoter driven Cre recombinase, results in T cell specific S1P<sub>1</sub> genetic depletion in progenies. Figure adapted and modified from Allende et al.<sup>83</sup> **(B)** Left panel: PCR bands for S1P<sub>1</sub> gene and right panel: PCR bands for Cre transgene amplification in genomic DNA extracted from offspring mice. Left panel: lane ‘a’ represents heterozygote, lane ‘b’ represents wild-type and lane ‘c’ represents mutant band of S1P<sub>1</sub> gene. In two panel combination, lane ‘b’ represents littermate control mice genotype and lane ‘c’ represents TS1P<sub>1</sub>KO mice genotype. In both panels, lane ‘d’ represents DNA ladder.

Mature T lymphocytes express S1P<sub>1</sub> on their cell surface to exit from thymus and secondary lymphoid organs to blood and lymph. As TS1P<sub>1</sub>KO mice T cells lack S1P<sub>1</sub> due to Cre mediated recombination at genomic level, T cells mature in thymus but could not exit in periphery as reported earlier.<sup>83</sup> In our present study, thus, we counted CD3<sup>+</sup> T cells proportions in spleen of littermate control and TS1P<sub>1</sub>KO mice. TS1P<sub>1</sub>KO mice exhibited

near 2.73-fold decrease in CD3<sup>+</sup> T cells percent in spleen as compared to littermate control mice (Figure 3-2A and 3-2B, Table 3-2). Similarly, TS1P<sub>1</sub>KO mice had about 90% less CD4<sup>+</sup> and CD8<sup>+</sup> T cells in blood as compared with littermate control mice (Figure 3-3A and 3-3B, Table 3-2).

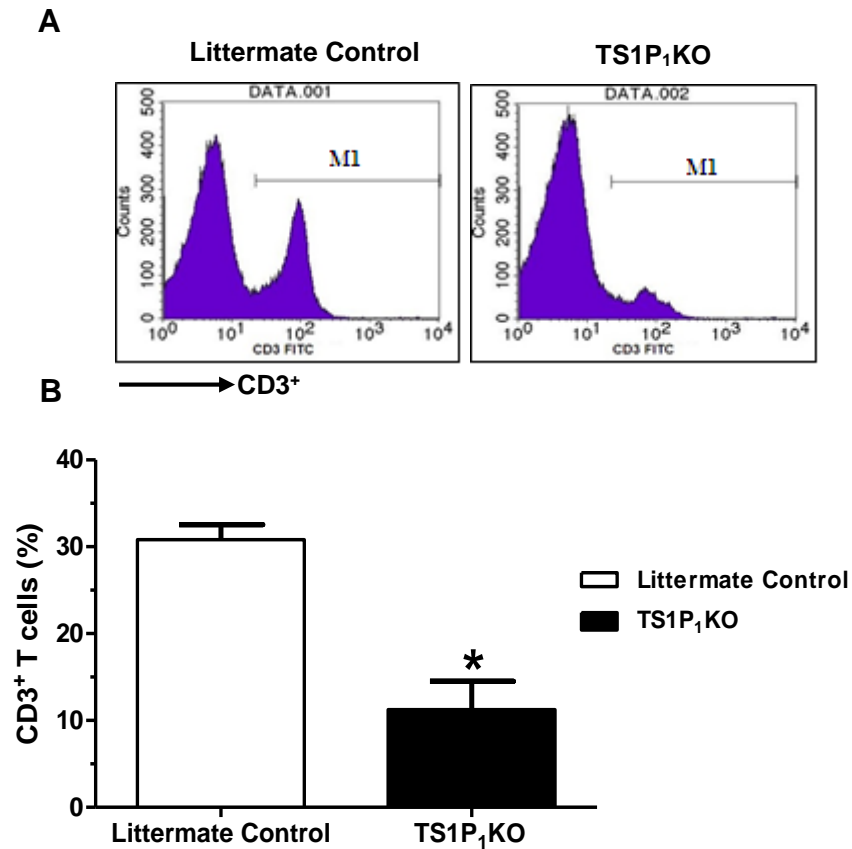


**Figure 3-2:** Flow cytometry analysis of CD3<sup>+</sup> T cells in spleen of littermate control and TS1P<sub>1</sub>KO mice. **(A)** Representative flow cytometry histogram plot exhibit depleted CD3<sup>+</sup> T cells in TS1P<sub>1</sub>KO mice spleen than littermate mice under M1 gate. **(B)** Quantification of CD3<sup>+</sup> T cells number in littermate control and TS1P<sub>1</sub>KO mice spleen. Data are representative of three independent experiments. \*P<0.05 between littermate control and TS1P<sub>1</sub>KO mice. The data is expressed as mean ± SEM.

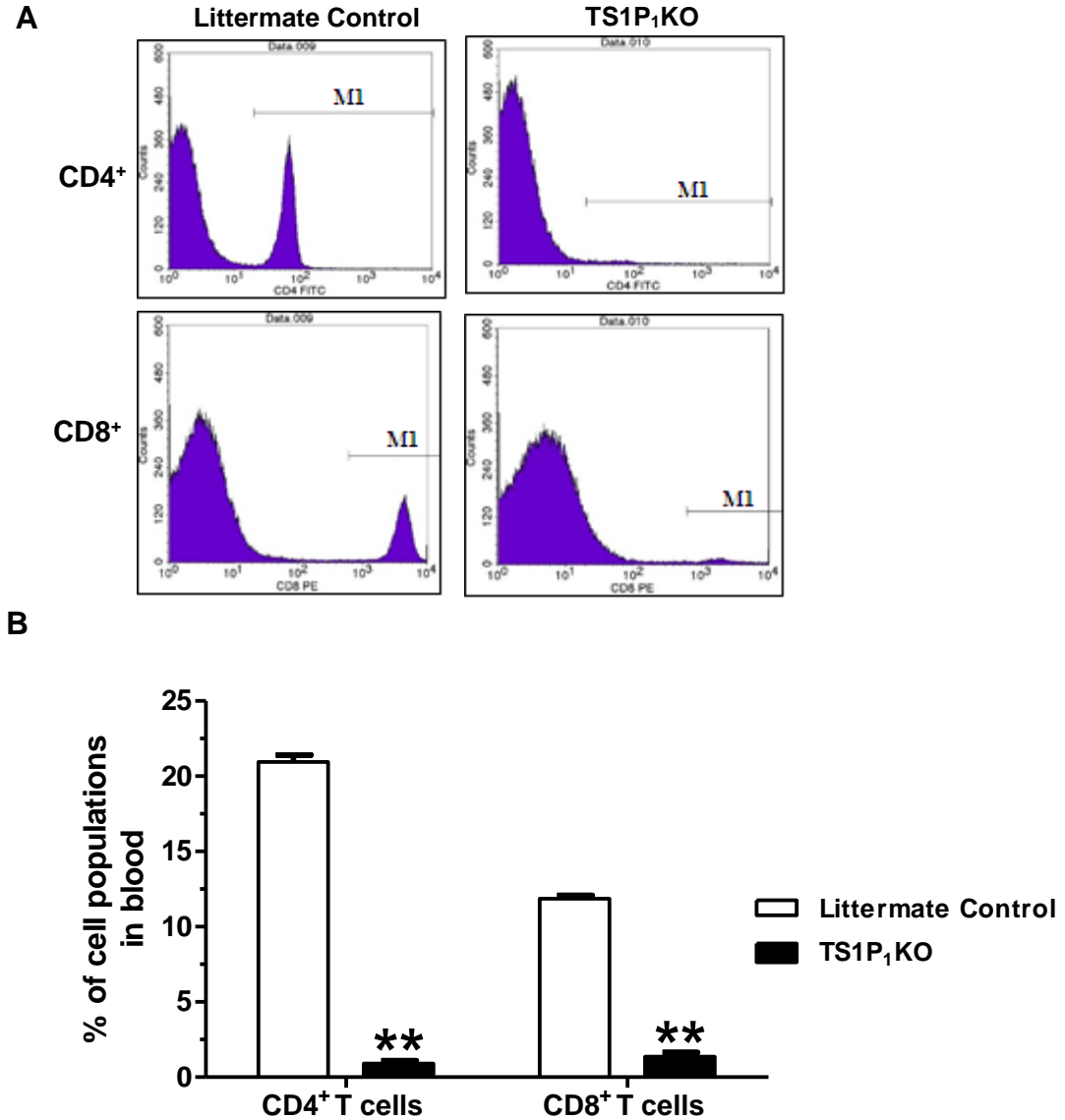


**Figure 3-3:** Flow cytometry analysis of CD4<sup>+</sup> and CD8<sup>+</sup> T cells in littermate control and TS1P<sub>1</sub>KO mice blood. **(A)** Histogram plot show remarkable deficiency of both CD4<sup>+</sup> and CD8<sup>+</sup> T cells in TS1P<sub>1</sub>KO mice blood compared to littermate mice under M1 gate. **(B)** Quantification of CD4<sup>+</sup> and CD8<sup>+</sup> T cells number in littermate and TS1P<sub>1</sub>KO mice blood. \*\*P < 0.01 between littermate and TS1P<sub>1</sub>KO mice, n= 5-6 mice in each group. The data is expressed as mean ± SEM.

**Table 3-2:** Summary of CD3<sup>+</sup> T cells in spleen, CD4<sup>+</sup> and CD8<sup>+</sup> T cells number in blood of littermate control and TS1P<sub>1</sub>KO mice.

	Littermate Control	TS1P <sub>1</sub> KO
<i>CD3<sup>+</sup> T cells in spleen</i>	30.80±1.75 (n=3)	11.27±3.25* (n=3)
<i>(% of cell populations)</i>		
<i>CD4<sup>+</sup> T cells in blood</i>	20.94±0.47 (n = 5)	0.91±0.17** (n = 5)
<i>(% of cell populations)</i>		
<i>CD8<sup>+</sup> T cells in blood</i>	11.86±0.21 (n = 6)	1.37±0.26** (n = 6)
<i>(% of cell populations)</i>		

The data is expressed as mean ± SEM. The value of ‘n’ represents number of mice in each group. \*P < 0.05 and \*\*P < 0.01 as compared to littermate control mice.

### 3.3.2. Physiological characteristics assessment

Streptozotocin (STZ) is a nitrosourea compound that alkylates DNA and is pancreatic β-cells toxic due to its transport through glucose transporter 2 into these cells.<sup>96,125</sup> Thus, STZ administration in mice destroys insulin producing β-cells rendering them hyperglycemic.<sup>96</sup> STZ-induced type 1 diabetic model exhibits salient pathological changes in heart corresponding to clinical diabetic cardiomyopathy manifested by increased oxidative stress and inflammation and increased collagen deposition in cardiac interstitium with cardiac ventricular dysfunction. In the present work, both littermate control and TS1P<sub>1</sub>KO mice were divided into vehicle treated and STZ treated groups. There was no significant difference in body weight between littermate vehicle and

littermate STZ mice, and TS1P<sub>1</sub>KO vehicle and TS1P<sub>1</sub>KO STZ mice at the beginning before STZ induction (Figure 3-4, Table 3-3). After STZ administration, through 11-week both littermate and KO STZ recipient mice showed less body weight gain trend compared to only vehicle treated mice (Figure 3-4). After 11-weeks, littermate STZ mice had 15.29% reduced body weight compared with littermate vehicle mice, and TS1P<sub>1</sub>KO STZ mice have 17.75% reduced body weight compared to TS1P<sub>1</sub>KO vehicle mice (Figure 3-4, Table 3-3). There was no significant difference between littermate STZ and TS1P<sub>1</sub>KO STZ mice body weight at the end of 11-weeks (Figure 3-4, Table 3-3).

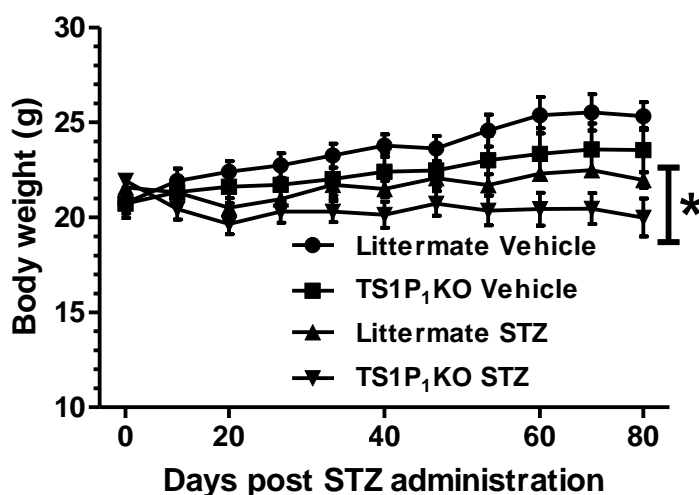


**Figure 3-4:** Body weights (g) change in littermate and TS1P<sub>1</sub>KO mice during 11-week experimental period. Both littermate and TS1P<sub>1</sub>KO STZ-recipient mice exhibited lower body weight gain throughout 11-weeks. Both littermate and TS1P<sub>1</sub>KO STZ mice had significantly low body weights (g) at the end of 11-week compared to littermate and TS1P<sub>1</sub>KO vehicle mice, respectively. \*P<0.05 between vehicle and STZ groups of littermate and TS1P<sub>1</sub>KO mice. Sample size n = 6-10 mice in each group. The data is expressed as mean  $\pm$  SEM.

**Table 3-3:** Summary of physiological parameter in littermate and TS1P<sub>1</sub>KO mice during 11-week experimental period.

	<b>Littermate Vehicle</b>	<b>TS1P<sub>1</sub>KO Vehicle</b>	<b>Littermate STZ</b>	<b>TS1P<sub>1</sub>KO STZ</b>
	<b>(n=6)</b>	<b>(n=6)</b>	<b>(n=10)</b>	<b>(n=8)</b>
<i>At the beginning</i>				
<i>(before STZ induction)</i>				
Body wt. (g)	20.45±0.78	20.73±0.53	21.58±0.52	21.93±0.35
<i>After 4-week of STZ induction</i>				
Body wt. (g)	22.73±0.64	21.72±0.83	20.95±0.49	20.30±0.59
<i>After 11-week of STZ induction</i>				
Body wt. (g)	25.30±0.73	23.54±1.15	21.97±0.40*	19.99±1.003*

The data is expressed as mean ± SEM. \*P < 0.05 between vehicle and STZ groups of littermate and TS1P<sub>1</sub>KO mice. The value of ‘n’ represents number of mice in each group.

There was no significant difference between littermate and TS1P<sub>1</sub>KO mice blood glucose levels (mg/dl) at the beginning (Figure 3-5, Table 3-4). STZ administration rendered both littermate and TS1P<sub>1</sub>KO mice hyperglycemic as measured in 4-weeks. Hyperglycemia was sustained in STZ recipient littermate and TS1P<sub>1</sub>KO mice at the end of 11-weeks (Figure 3-5, Table 3-4). There was no significant difference between littermate STZ and TS1P<sub>1</sub>KO STZ mice blood glucose levels at the end of 11-weeks (Figure 3-5, Table 3-4).

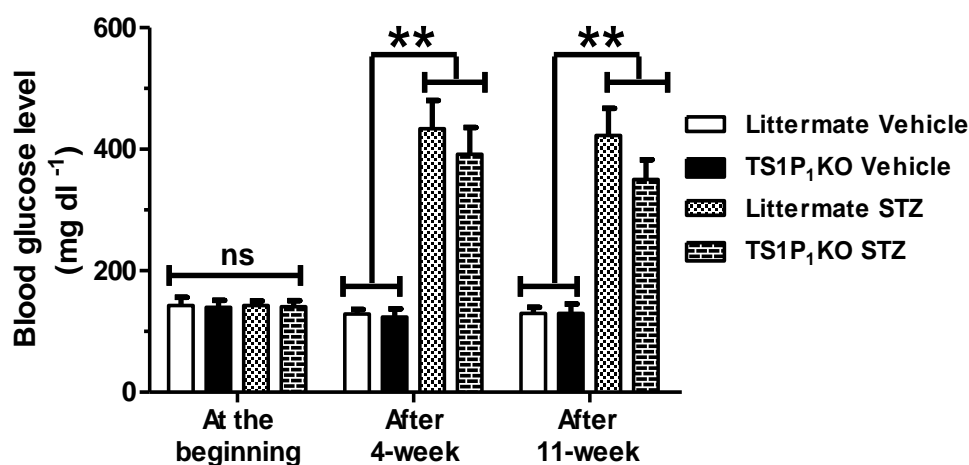


**Figure 3-5:** Blood glucose levels (mg/dl) during 11-week study period in littermate and TS1P<sub>1</sub>KO mice. Bar graph shows blood glucose levels (mg/dl) at the beginning, after 4-week and after 11-week. Sample size, n = 6-10 mice in each group. \*\*P < 0.01 between vehicle and STZ groups of littermate and TS1P<sub>1</sub>KO mice, respectively. The data is expressed as mean ± SEM.

**Table 3-4:** Summary of metabolic parameter in littermate and TS1P1KO mice during 11-week experimental period.

	Littermate Vehicle (n=6)	TS1P1KO Vehicle (n=6)	Littermate STZ (n=10)	TS1P1KO STZ (n=8)
<i>At the beginning</i>				
<i>(before STZ induction)</i>				
Blood glucose level (mg/dl)	142.67±13.59	139.83±11.33	142.70±7.32	140.63±10.15
<i>After 4-week of STZ induction</i>				
Blood glucose level (mg/dl)	128.5±7.61	123.67±13.52	433.50±46.57**	391.63±44.30**
<i>After 11- week of STZ induction</i>				
Blood glucose level (mg/dl)	129.67±9.87	129.50±15.96	422.80±44.69**	350.00±32.98**

The data is expressed as mean ± SEM. \*\*P < 0.01 between vehicle and STZ groups of littermate and TS1P1KO mice. The value of ‘n’ represents number of mice in each group.

### 3.3.3. Flow cytometry analysis of T lymphocyte subsets

Flow cytometry analysis was used to determine CD4<sup>+</sup> and CD8<sup>+</sup> T cells in the blood and CD4<sup>+</sup>Foxp3<sup>+</sup> T cells in spleen and blood after 11-weeks (Figure 3-6 and 3-7). TS1P<sub>1</sub>KO vehicle and STZ mice had about 90% reduction of both CD4<sup>+</sup> (CD4<sup>+</sup> T cells: littermate vehicle, 12.93±3.98 %, littermate STZ, 12.10±1.75 % vs. TS1P<sub>1</sub>KO vehicle, 1.37±0.02 %, TS1P<sub>1</sub>KO STZ, 1.21±0.61 %, n=4-5 mice in each group, \*\*P < 0.01) and CD8<sup>+</sup> (CD8<sup>+</sup> T cells: littermate vehicle, 7.73±1.43%, littermate STZ, 7.11±0.80 % vs. TS1P<sub>1</sub>KO vehicle, 1.61±0.13 %, TS1P<sub>1</sub>KO STZ, 1.29±0.44%, n=4-5 mice in each group, \*\*P < 0.01) T cells in blood after 11-week experimental period (Figure 3-6A and 3-6B, Table 3-5). This data demonstrates sustained T lymphocytes deficiency in TS1P<sub>1</sub>KO mice circulation.

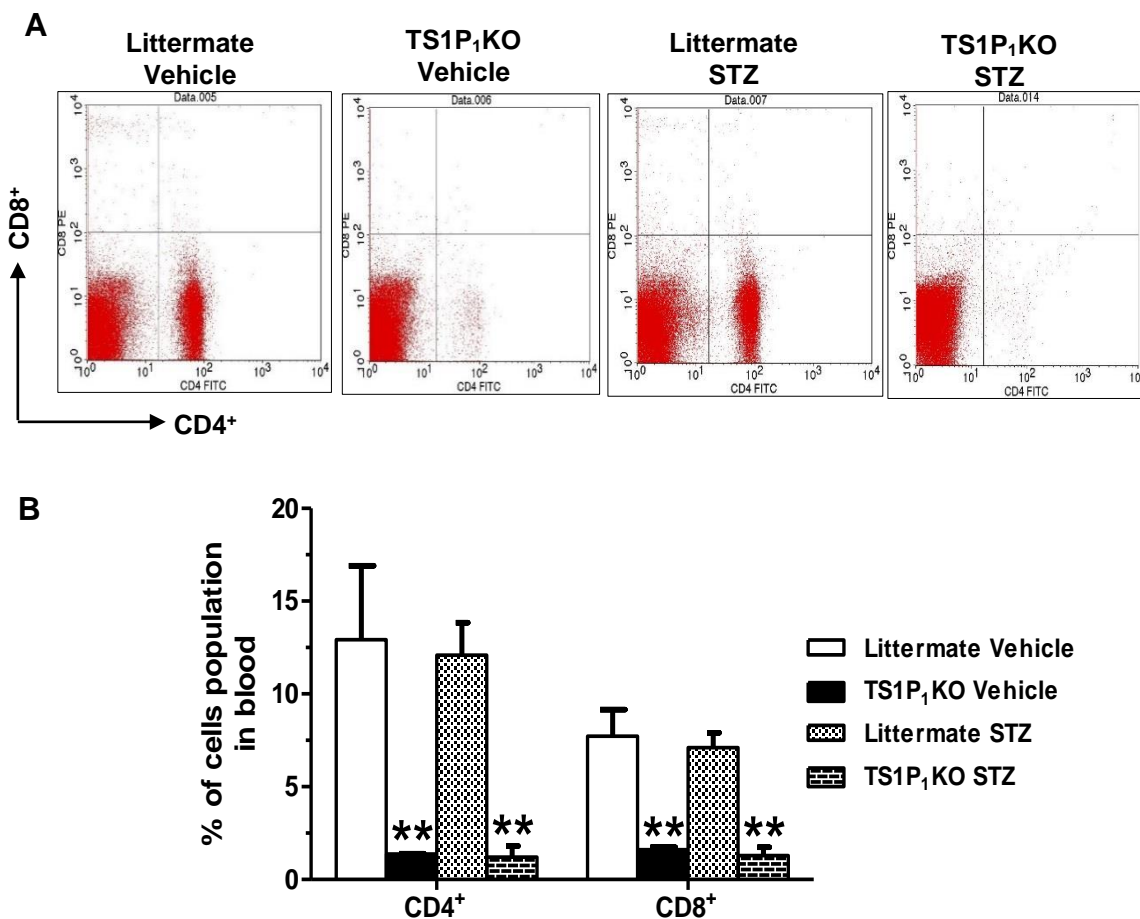


**Figure 3-6:** Flow cytometry analysis of CD4<sup>+</sup> and CD8<sup>+</sup> T cells in blood of littermate and TS1P<sub>1</sub>KO mice at the end of 11-weeks. **(A)** Representative flow cytometry dot plots showing CD4<sup>+</sup> (in lower right quadrant) and CD8<sup>+</sup> (in upper left quadrant) T cells in the blood of littermate and TS1P<sub>1</sub>KO mice. TS1P<sub>1</sub>KO mice exhibited noticeable less CD4<sup>+</sup> and CD8<sup>+</sup> T cells in the blood. **(B)** Both vehicle and STZ groups of TS1P<sub>1</sub>KO mice had significantly reduced CD4<sup>+</sup> and CD8<sup>+</sup> T cells number than littermate vehicle and STZ mice, respectively. \*\*P<0.01 between littermate and TS1P<sub>1</sub>KO mouse groups. Sample size, n = 3-5 mice in each group. The data is expressed as mean ± SEM.

Further, we counted CD4<sup>+</sup>FoxP3<sup>+</sup> T cells proportion percent in spleen and blood by two-color flow cytometry. In littermate diabetic mice, CD4<sup>+</sup>FoxP3<sup>+</sup> T cells were increased by 1.60-fold in spleen (3.15±0.22 % vs. 1.97±0.27 %, n=3, #P < 0.05) and 1.82-fold in blood (1.58±0.19 % vs. 0.87±0.21 %, n=3, #P < 0.05) compared to littermate vehicle mice after 11-weeks (Figure 3-7A and 3-7B). In contrast, similar to reduced CD3<sup>+</sup> T cells in spleen and CD4<sup>+</sup> and CD8<sup>+</sup> T cells in blood, TS1P<sub>1</sub>KO vehicle mice had 2.94-fold (in spleen) and 4.58-fold (in blood) decreased (spleen: 0.67±0.12 % vs. 1.97±0.27 %, n=3, \*P < 0.05, blood: 0.19±0.03 % vs. 0.87±0.21 %, n=3, \*P < 0.05) and TS1P<sub>1</sub>KO STZ mice had 2.28-fold (in spleen) and 3.76-fold (in blood) decreased (spleen: 1.38±0.37 % vs. 3.15±0.22 %, n=3, \*P < 0.05, blood: 0.42±0.18 % vs. 1.58±0.19 %, n=3, \*P < 0.05) CD4<sup>+</sup>Foxp3<sup>+</sup> T cells compared to littermate vehicle and STZ mice, respectively (Figure 3-7A and 3-7B, Table 3-5). There was no statistically significant difference between TS1P<sub>1</sub>KO vehicle and STZ mice (spleen: 1.38±0.37 % vs. 0.67±0.12 %, n=3, P value = 0.1407, blood: 0.42±0.18 % vs. 0.19±0.03 %, n=3, P value = 0.2624) in CD4<sup>+</sup>Foxp3<sup>+</sup> T cells percent in spleen and blood, although about 2-fold increase in average percent of cells was observed in TS1P<sub>1</sub>KO diabetic mice (Figure 3-7A and 3-7B, Table 3-5).

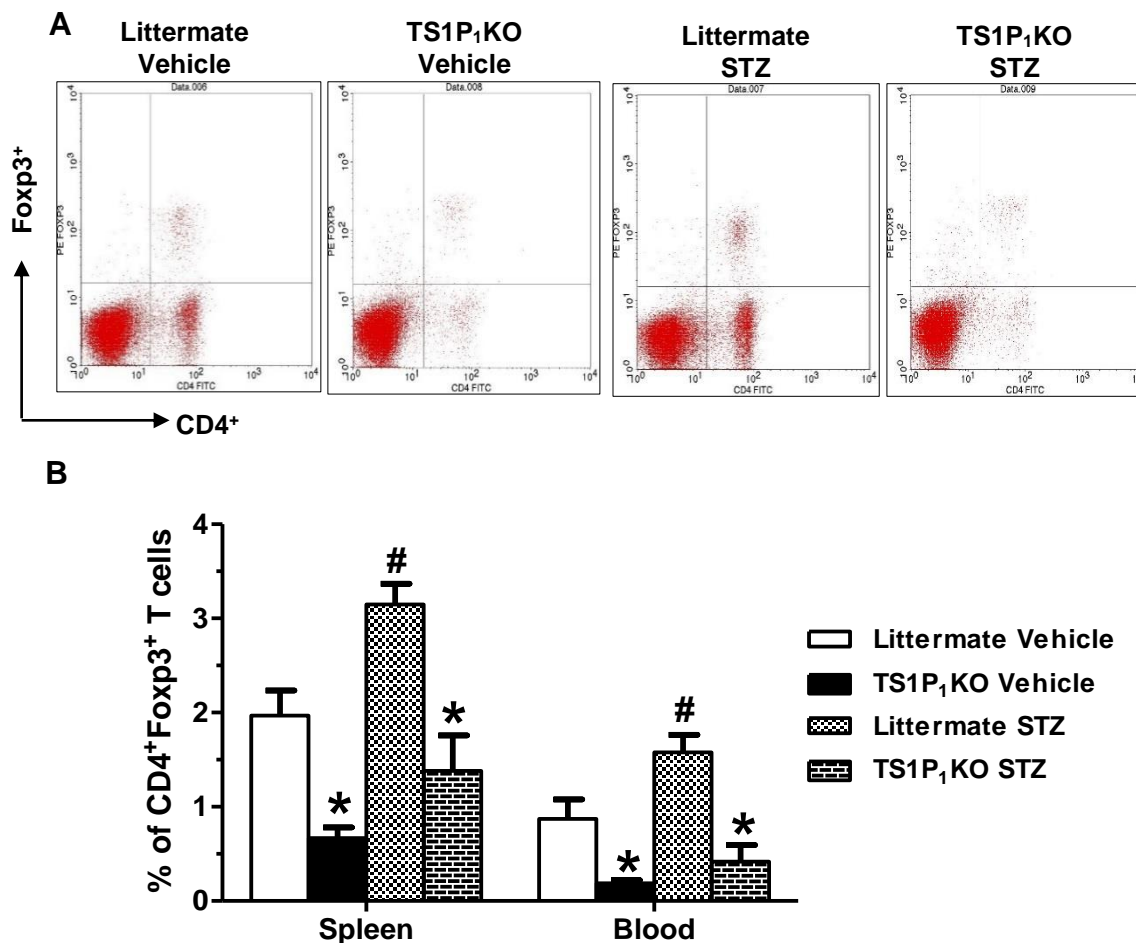


**Figure 3-7:** Flow cytometry analysis of CD4<sup>+</sup>Foxp3<sup>+</sup> regulatory T cells in spleen and blood of littermate and TS1P<sub>1</sub>KO mice at the end of 11-weeks. **(A)** Representative flow cytometry dot plots showing CD4<sup>+</sup>Foxp3<sup>+</sup> T cells staining (in upper right quadrant) in littermate and TS1P<sub>1</sub>KO mice spleen after 11 weeks. **(B)** Diabetic littermate mice had increased CD4<sup>+</sup>Foxp3<sup>+</sup> T cells number in spleen and blood compared to littermate vehicle mice. Both vehicle and STZ mice of TS1P<sub>1</sub>KO had reduced CD4<sup>+</sup>Foxp3<sup>+</sup> T cells in spleen and blood than littermate vehicle and STZ mice, respectively, at the end of 11-weeks. #P<0.05 littermate STZ vs. littermate vehicle, and \*P<0.05 between TS1P<sub>1</sub>KO vehicle, STZ and littermate vehicle, STZ mice. The data is expressed as mean ± SEM. Sample size, n = 3 mice in each group.

**Table 3-5:** Summary of CD4<sup>+</sup>, CD8<sup>+</sup> T cells percent in blood, and CD4<sup>+</sup>Foxp3<sup>+</sup> T cells percent in spleen and blood of littermate and TS1P<sub>1</sub>KO mice after 11-weeks.

	Littermate Vehicle	TS1P <sub>1</sub> KO Vehicle	Littermate STZ	TS1P <sub>1</sub> KO STZ
<i>CD4<sup>+</sup> T cells in blood</i>	12.93±3.98	1.37±0.02**	12.10±1.75	1.21±0.61**
<i>CD8<sup>+</sup> T cells in blood</i>	7.73±1.43	1.61±0.13**	7.11±0.80	1.29±0.44**
<i>CD4<sup>+</sup>Foxp3<sup>+</sup> T cells in spleen</i>	1.97±0.27	0.67±0.12*	3.15±0.22 <sup>#</sup>	1.38±0.37*
<i>CD4<sup>+</sup>Foxp3<sup>+</sup> T cells in blood</i>	0.87±0.21	0.19±0.03*	1.58±0.19 <sup>#</sup>	0.42±0.17*

All values represent percent (%) of cell population. The data is expressed as mean ± SEM. n = 3-5 mice in each group. \*P < 0.05 and \*\*P < 0.01 between vehicle and STZ groups of littermate and TS1P<sub>1</sub>KO mice. <sup>#</sup>P < 0.05 between vehicle and STZ groups of littermate mice. Percent of CD4<sup>+</sup>Foxp3<sup>+</sup> T cells, spleen: P = 0.14 between TS1P<sub>1</sub>KO vehicle and TS1P<sub>1</sub>KO STZ mice, blood: P = 0.26 between TS1P<sub>1</sub>KO vehicle and TS1P<sub>1</sub>KO STZ mice.

### 3.3.4. Assessment of cardiac histology and fibrosis area

Hematoxylin and Eosin (H&E) stained heart sections were prepared after 11-weeks. H&E stained sections were examined microscopically at magnification of 400x and graded based on morphology, organization, presence of cellularity in myocardium, myocytes loss presence of collagen fiber. Littermate STZ (diabetic) mice exhibited deteriorated myocardium structure manifested by myocytes loss and increased interstitial space with presence of increased cellularity compared with littermate vehicle mice (cumulative histology score; littermate STZ (n=9):  $9.56 \pm 0.58$  vs. littermate vehicle (n=4):  $3 \pm 0.41$ , \*P < 0.05) (Figure 3-8 and 3-9). TS1P<sub>1</sub>KO STZ mice (diabetic) heart exhibited preserved myocardial structural phenotype as compared with littermate diabetic mice (TS1P<sub>1</sub>KO STZ (n=7):  $3 \pm 0.58$  vs. littermate STZ (n=9):  $3 \pm 0.41$ , #P < 0.05) (Figure 3-8 and 3-9). Notably, TS1P<sub>1</sub>KO vehicle mice showed altered heart phenotype demonstrated by loss of interstitial space between myocytes with thickening of vascular smooth muscle cells and perivascular edema compared with littermate vehicle mice (TS1P<sub>1</sub>KO vehicle (n=4):  $9.5 \pm 0.87$  vs. littermate vehicle (n=4):  $3 \pm 0.41$ , <sup>α</sup>P < 0.05) (Figure 3-8 and 3-9).

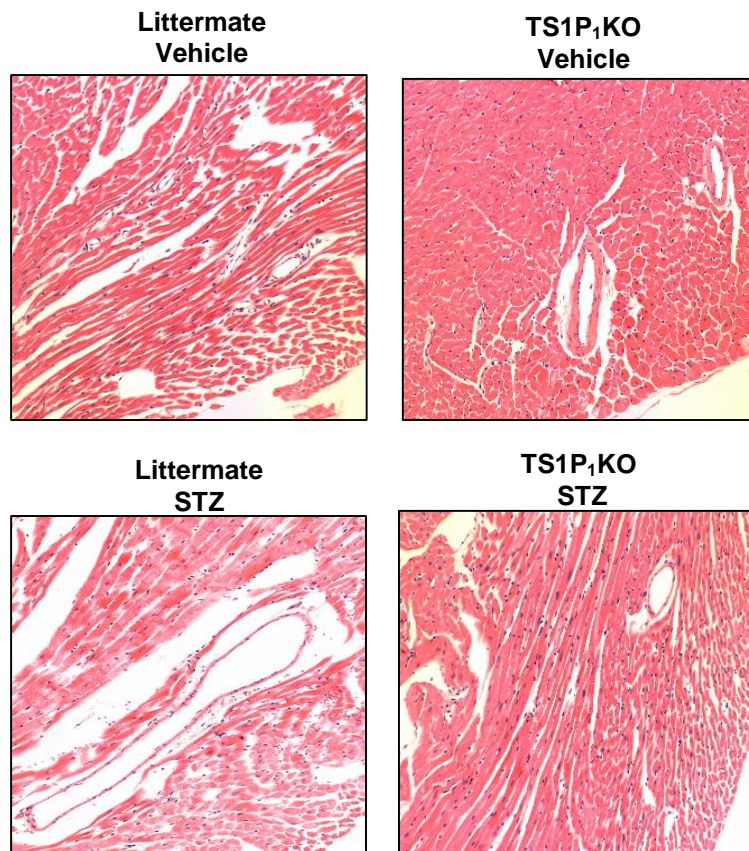


**Figure 3-8:** Representative images of Hematoxylin and Eosin (H&E) stained heart tissue sections of littermate and TS1P<sub>1</sub>KO mice after 11-weeks. Littermate STZ mice heart section showed discernible myocytes loss with increased cellularity and disorganization in myocardium after 11-week experimental period. TS1P<sub>1</sub>KO mice heart sections exhibited preserved heart histology under diabetes. Interestingly, TS1P<sub>1</sub>KO vehicle mice exhibited altered cardiac phenotype with congested myocytes and thickening of perivascular smooth muscles. Images are representative of heart sections of 4-9 mice in each group. The magnification is 200x.

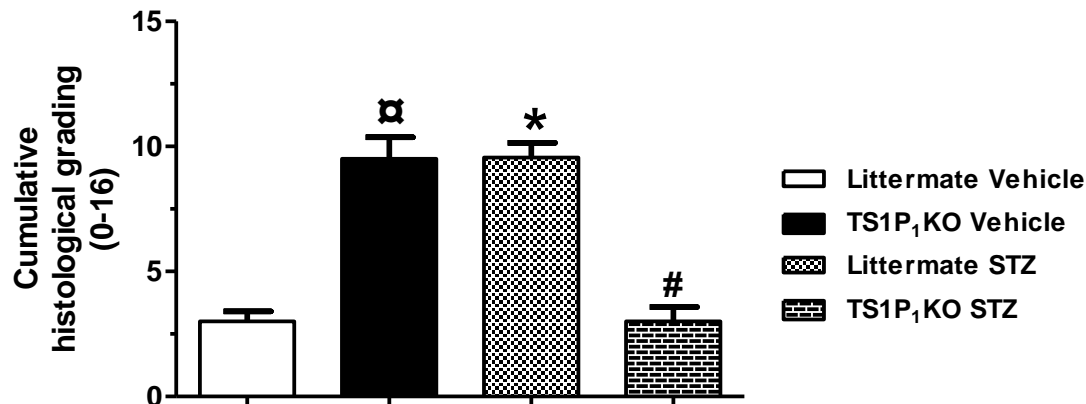


**Figure 3-9:** Quantification of heart histological scores in littermate and TS1P<sub>1</sub>KO mice after 11-weeks. \*P < 0.05 between littermate vehicle and littermate STZ mice, #P < 0.05 between TS1P<sub>1</sub>KO STZ and littermate STZ mice, <sup>□</sup>P < 0.05 between littermate vehicle and TS1P<sub>1</sub>KO vehicle mice. The data is expressed as mean ± SEM, n = 4-9 mice in each group.

Collagen deposition was quantified semi-quantitatively in Masson's Trichrome stained heart sections of all mice after 11-week experimental period. Diabetic littermate mice (n=9) showed increased fibrosis area relative to whole heart area compared to littermate vehicle mice (n=4) ( $46.48 \pm 8.06$  % vs.  $7.65 \pm 0.86$  %, \*P < 0.05) (Figure 3-10 and 3-11). Diabetes induced increase of collagen deposition in interstitial and perivascular area in littermate diabetic mice. TS1P<sub>1</sub>KO vehicle mice (n=4) heart showed increased fibrosis area as compared with littermate vehicle mice (n=4) ( $46.03 \pm 7.16$  % vs.  $7.65 \pm 0.86$  %, <sup>#</sup>P < 0.05) (Figure 3-10 and 3-11). Notably, TS1P<sub>1</sub>KO diabetic mice (n=7) heart showed less fibrosis area compared to littermate diabetic mice ( $6.15 \pm 0.62$  % vs.  $46.48 \pm 8.06$  %, <sup>#</sup>P < 0.05) (Figure 3-10 and 3-11).

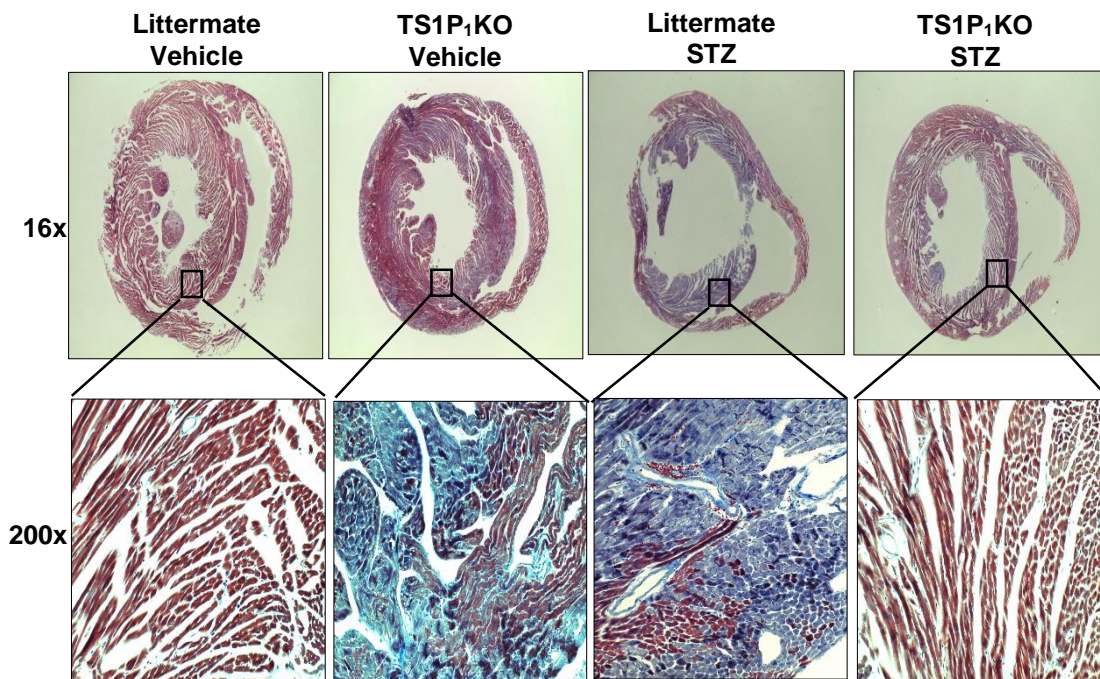


**Figure 3-10:** Representative images of Masson's Trichrome stained heart tissue sections in littermate and TS1P<sub>1</sub>KO mice after 11-weeks. Upper panel shows whole heart sections (magnification is 16x) and lower panel shows magnified section images (magnification is 200x). Littermate STZ mice had increased perivascular and interstitial fibrosis area compared with littermate vehicle mice. TS1P<sub>1</sub>KO STZ mice had noticeable less fibrosis than littermate STZ. Interestingly, TS1P<sub>1</sub>KO vehicle mice heart sections exhibited increased fibrosis than littermate vehicle mice.

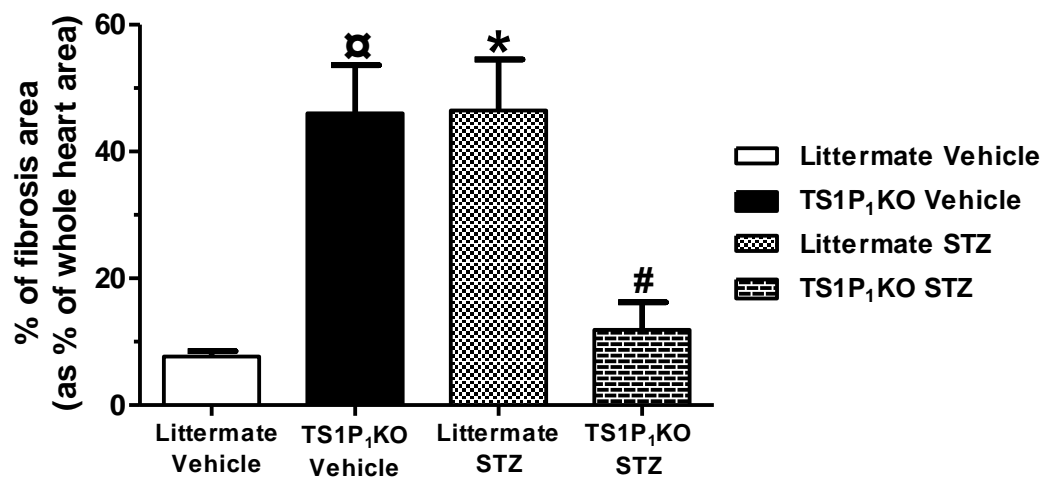


**Figure 3-11:** Quantification of percent fibrosis area in heart sections of littermate and TS1P<sub>1</sub>KO mice after 11-weeks. \*P<0.05 in littermate STZ vs. littermate vehicle mice, #P<0.05 in TS1P<sub>1</sub>KO STZ vs. littermate STZ mice and αP<0.05 in TS1P<sub>1</sub>KO vehicle vs. littermate vehicle mice. Sample size, n = 4-9 mice in each group. The data is expressed as mean ± SEM.

### 3.3.5. TS1P<sub>1</sub>KO mice exhibits improved cardiac contractility under hyperglycemia

We determined the cardiac force of contraction in an *ex-vivo* Langendorff's heart perfusion system. The data is expressed as a fold change in contractile force development compared to littermate control mice. Littermate diabetic mice showed 29.37% reduction in contractility as compared with littermate vehicle mice (P = 0.19) (Figure 3-12).

TS1P<sub>1</sub>KO mice exhibited 33.07% increase in force of contraction development than littermate diabetic mice (P=0.06) (Figure 3-12). Interestingly, TS1P<sub>1</sub>KO vehicle mice have attenuated contractility compared to littermate vehicle mice (\*P < 0.05) (Figure 3-12).

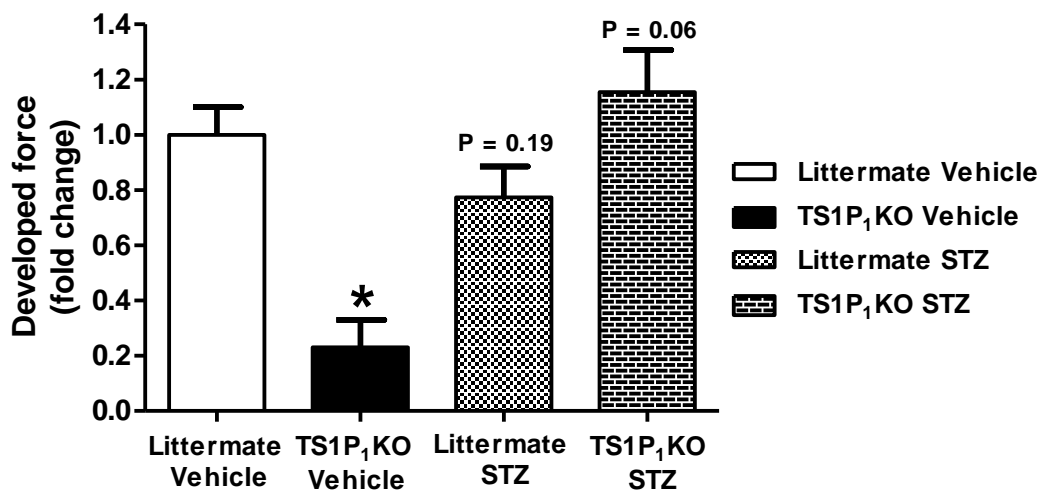


**Figure 3-12:** Cardiac contractility in littermate and TS1P<sub>1</sub>KO mice after 11-week study period. Littermate STZ mice (n=8) showed reduction in contractile force compared to littermate vehicle mice (n=5) (P value is 0.19 between these two groups). TS1P<sub>1</sub>KO STZ mice (n=5) showed improved contractile force compared to littermate STZ mice (n=8) (P = 0.06 between these two groups). TS1P<sub>1</sub>KO vehicle mice (n=6) have significantly attenuated force of contraction than littermate vehicle mice (\*P < 0.05). The contractile force is expressed as fold change relative to control. The data is expressed as mean ± SEM.

### **3.3.6. Reduced CD3<sup>+</sup> T cells infiltration in diabetic TS1P<sub>1</sub>KO mice myocardium**

We detected CD3<sup>+</sup> T cells in myocardium by immunostaining with anti-mouse CD3 antibody. Increased CD3<sup>+</sup> T cells infiltration has been observed in myocardium of littermate STZ mice ( $1.75 \pm 0.15$  cells/field vs.  $0.86 \pm 0.04$  cells/field,  $n=3$  independent experiments,  $*P < 0.05$ ) than littermate control mice (Figure 3-13 and 3-14). TS1P<sub>1</sub>KO STZ mice myocardium exhibited significantly less CD3<sup>+</sup> T cells ( $0.84 \pm 0.09$  cells/field vs.  $1.75 \pm 0.15$  cells/field,  $n=3$  independent experiments,  $^{\#}P < 0.05$ ) than littermate STZ mice (Figure 3-13 and 3-14).

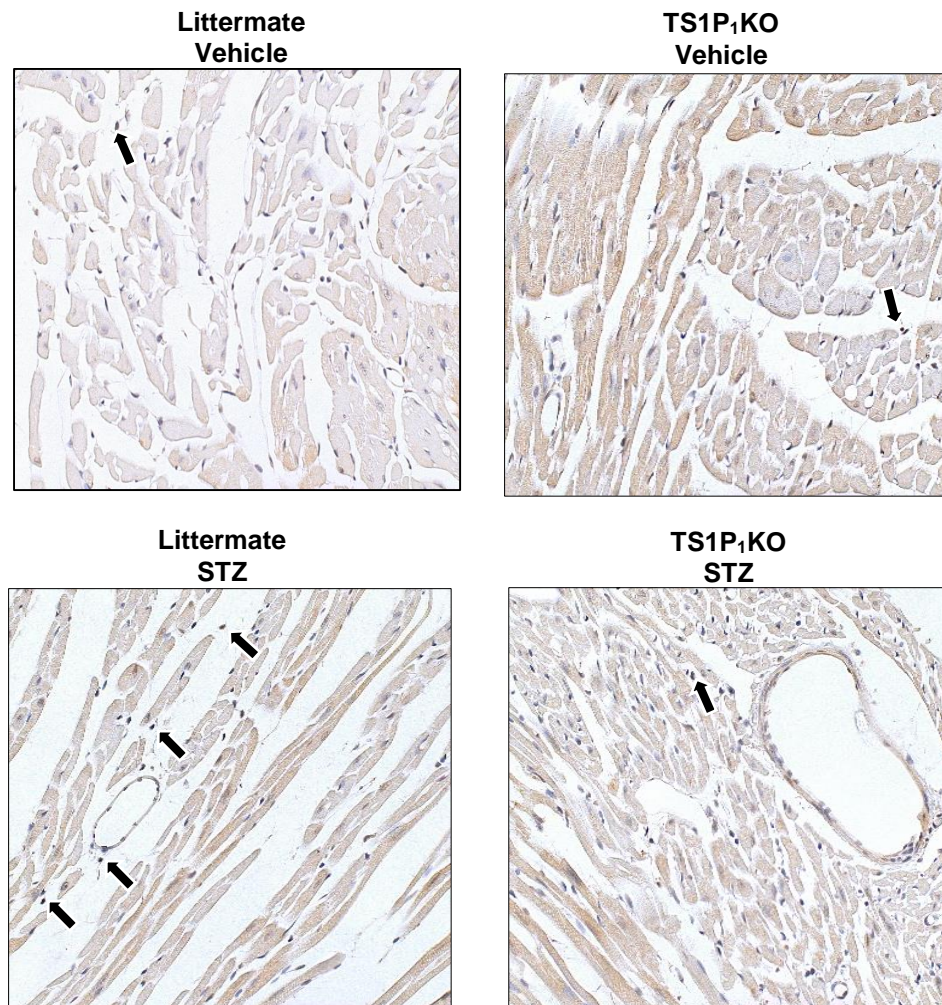


**Figure 3-13:** Immunohistochemical detection of CD3<sup>+</sup> T cells in littermate and TS1P<sub>1</sub>KO mice heart tissue section at the end of 11-weeks. Littermate STZ mice heart section show increased infiltration of CD3<sup>+</sup> T cells into cardiac tissue compared to littermate vehicle mice. TS1P<sub>1</sub>KO STZ mice myocardium do not have noticeable CD3<sup>+</sup> T cells infiltration compared to littermate STZ mice. Images are representative of three independent experiments.

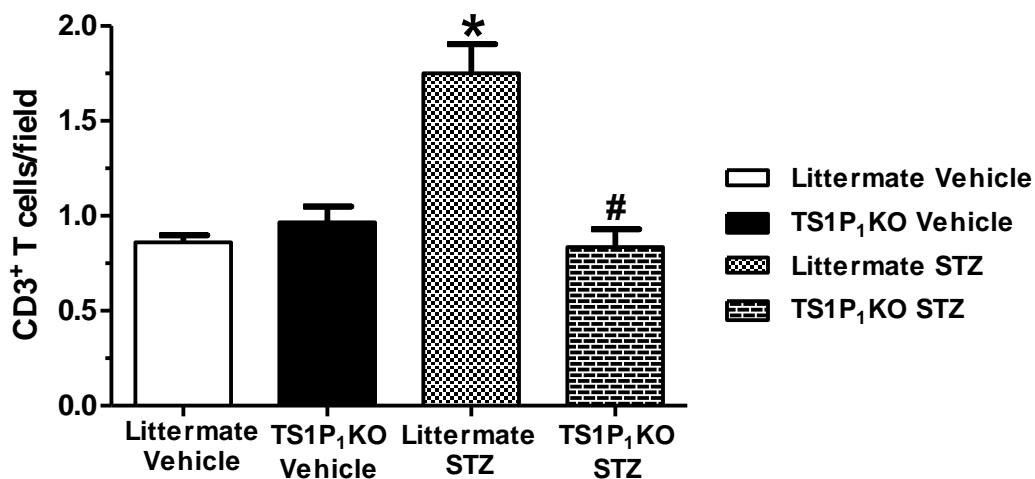


**Figure 3-14:** Quantification of infiltrated CD3<sup>+</sup> T cells in heart tissue sections of littermate and TS1P<sub>1</sub>KO mice after 11-week experimental period. CD3<sup>+</sup> T cells number (cells per 400x magnification field) was significantly higher in littermate STZ mice heart section than littermate vehicle mice. \*P < 0.05 between littermate STZ and littermate vehicle mice. TS1P<sub>1</sub>KO STZ mice heart tissue have reduced CD3<sup>+</sup> T cells infiltration as compared to littermate STZ mice. \*P < 0.05 between TS1P<sub>1</sub>KO STZ and littermate STZ mice. Results are from three independent experiments. The data is presented as mean ± SEM.

### 3.3.7. Reduced TGF- $\beta$ 1 expression in TS1P<sub>1</sub>KO diabetic mice myocardium

We determined profibrotic cytokine transforming growth factor beta 1 (TGF- $\beta$ 1) expression in myocardium of all mice group after 11-week diabetic period. TGF- $\beta$ 1 expression was increased in littermate diabetic mice cardiac tissue compared to littermate vehicle mice (6.79 $\pm$ 0.59 % staining area vs. 2.64 $\pm$ 0.23 % staining area, \*P < 0.05) (Figure 3-15 and 3-16). TS1P<sub>1</sub>KO diabetic mice exhibited reduced TGF- $\beta$ 1 expression in myocardium after 11 weeks as compared with littermate diabetic mice (3.54 $\pm$ 0.10 % staining area vs. 6.79 $\pm$ 0.59 % staining area, #P < 0.05) (Figure 3-15 and 3-16). In contrast, TS1P<sub>1</sub>KO vehicle mice myocardium exhibited increment of TGF- $\beta$ 1 expression as compared with littermate vehicle mice (6.78 $\pm$ 0.71 % staining area vs. 2.64 $\pm$ 0.23 % staining area,  $\alpha$ P < 0.05) (Figure 3-15 and 3-16).

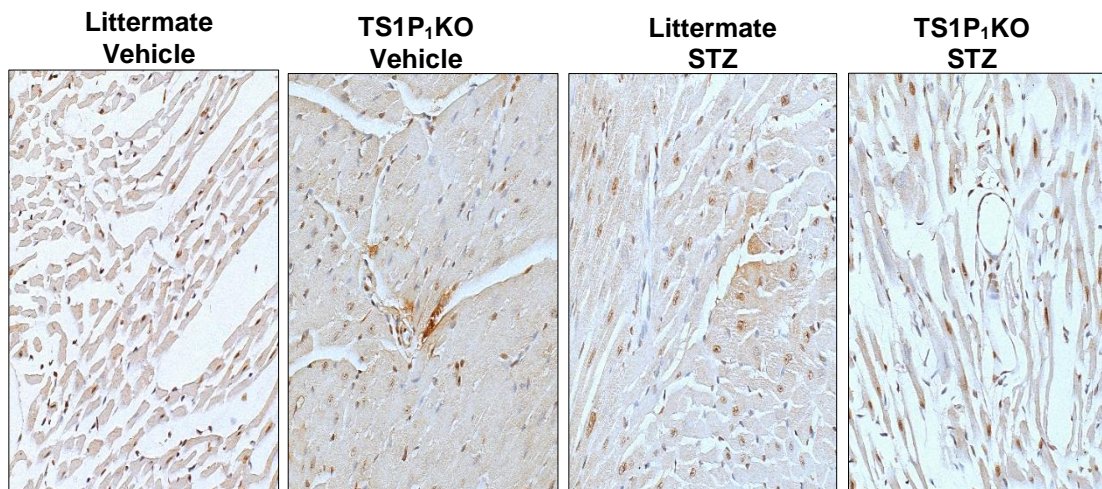


**Figure 3-15:** Immunohistochemical detection of TGF- $\beta$ 1 expression in littermate and TS1P<sub>1</sub>KO mice heart tissue sections after 11-weeks. Representative images of TGF- $\beta$ 1 immuno-staining. Littermate STZ mice myocardium show increased TGF- $\beta$ 1 expression compared to littermate vehicle mice. TS1P<sub>1</sub>KO STZ mice myocardium exhibit reduced TGF- $\beta$ 1 expression than littermate STZ mice. Notably, TS1P<sub>1</sub>KO vehicle mice myocardium exhibit increased TGF- $\beta$ 1 expression than littermate vehicle mice. The magnification for all images is 400x.

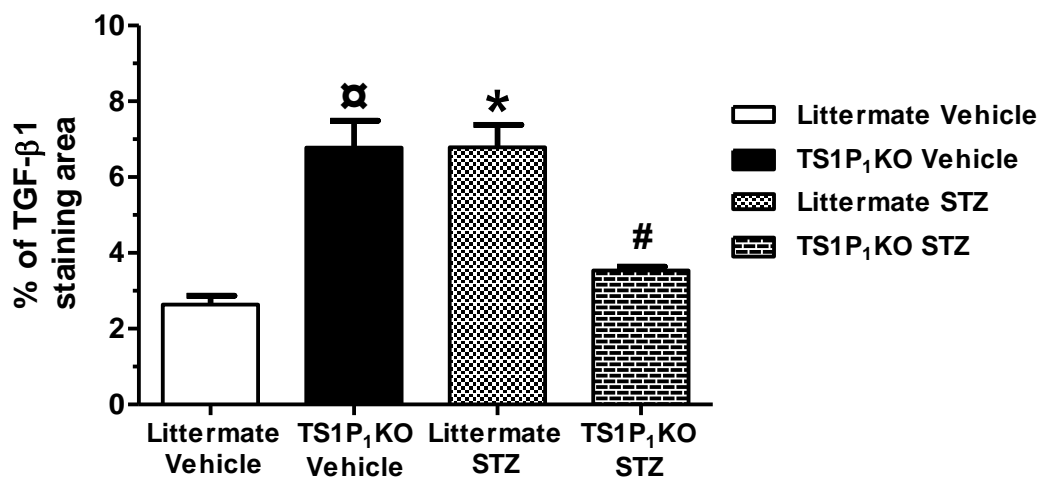


**Figure 3-16:** Quantification of TGF-β1 expression in heart tissue sections of littermate and TS1P<sub>1</sub>KO mice after 11-week experimental period. Results are from three independent experiments. The data is expressed as mean ± SEM. \*P < 0.05 between littermate vehicle and littermate STZ, #P < 0.05 between littermate STZ and TS1P<sub>1</sub>KO STZ and αP < 0.05 between littermate vehicle and TS1P<sub>1</sub>KO vehicle.

### 3.3.8. TS1P<sub>1</sub>KO mice myocardium have less CD34 cells in diabetes

Fibrocytes under chronic inflammation are recruited through chemokine interactions to the site of injury. Recruited fibrocytes can synthesize extracellular matrix protein and transdifferentiate into collagen producing myofibroblasts. CD34 is a surface antigen that is expressed by fibrocytes and can be used as a biomarker to detect these cells from other cell types. In our present work, we detected CD34 expressing cells in mice myocardium after 11-week of experimental period. Littermate STZ mice myocardium exhibited higher CD34 expressing cells than littermate vehicle mice ( $6.25 \pm 0.28$  % staining area vs.  $2.74 \pm 0.12$  % staining area,  $*P < 0.05$ ) (Figure 3-17 and 3-18). Notably, diabetic TS1P<sub>1</sub>KO mice myocardium exhibited less CD34 expressing cells than littermate diabetic mice ( $2.97 \pm 0.17$  % staining area vs.  $6.25 \pm 0.28$  % staining area,  $^{\#}P < 0.05$ ) (Figure 3-17 and 3-18). In contrast, TS1P<sub>1</sub>KO vehicle mice myocardium have increased CD34 expressing cells compared to littermate vehicle mice ( $6.52 \pm 0.47$  % staining area vs.  $2.74 \pm 0.12$  % staining area,  $^{\#}P < 0.05$ ) (Figure 3-17 and 3-18).

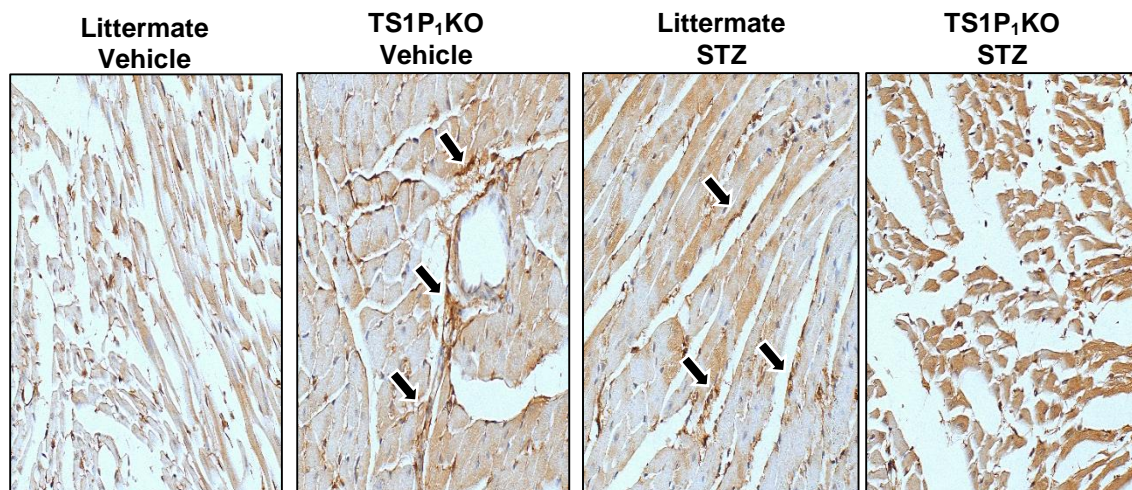


**Figure 3-17:** Immunohistochemical detection of CD34 fibrocytes expression in littermate and TS1P<sub>1</sub>KO mice heart tissue sections after 11-weeks. Representative images of CD34 fibrocytes immunostaining. Littermate STZ mice myocardium show increased CD34 expressing cells than littermate vehicle mice. Notably, diabetic TS1P<sub>1</sub>KO mice myocardium exhibit reduction of CD34 expression than littermate diabetic mice. In contrast, TS1P<sub>1</sub>KO vehicle mice myocardium exhibit increased CD34 expression compared to littermate vehicle mice. The magnification for all images is 400x.

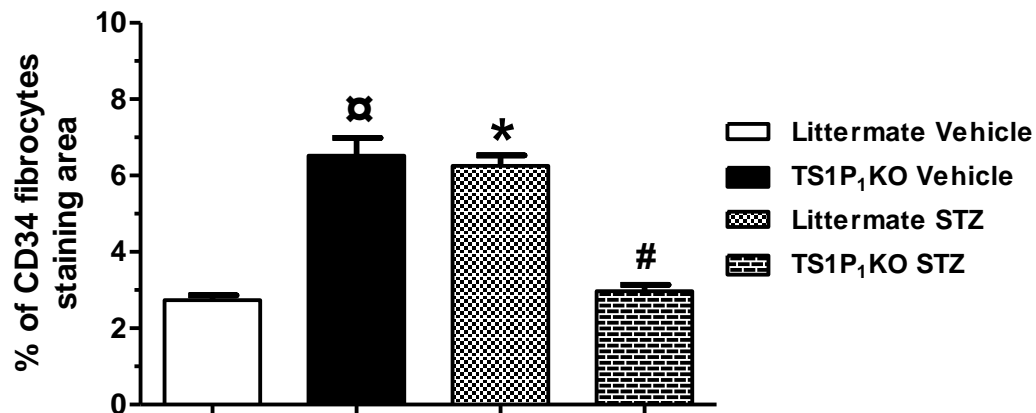


**Figure 3-18:** Quantification of CD34 fibrocytes expression in heart tissue sections of littermate and TS1P<sub>1</sub>KO mice after 11-week experimental period. Results are from three independent experiments. The data is expressed as mean  $\pm$  SEM. \*P < 0.05 between littermate vehicle and littermate STZ, #P < 0.05 between littermate STZ and TS1P<sub>1</sub>KO STZ and  $\alpha$ P < 0.05 between littermate vehicle and TS1P<sub>1</sub>KO vehicle.

### 3.4. Discussion

In the present study, we for the first time demonstrated that conditional T cell specific sphingosine 1-phosphate receptor 1 genetic depletion associated T lymphocytes deficiency in circulation exerts cardioprotection with reduced myocardial fibrosis under chronic hyperglycemia compared to littermate diabetic mice.

Several lines of investigation demonstrated T lymphocytes involvement in cardiac injury and cardiac remodeling in experimental cardiac injury settings.<sup>77</sup> In chronic pressure overload murine transverse aortic constriction model, increased activated/effector CD4<sup>+</sup>CD44<sup>high</sup> T cells have been detected in heart tissue with increased cardiac collagen content and cardiac dysfunction after 6-week of this model.<sup>75</sup> In murine myocardial infarction (MI) model, increased CD4<sup>+</sup>Ki67<sup>+</sup> T cells have been detected in heart draining mediastinal lymph nodes after 7-day of MI injury.<sup>74</sup> Increased CD4<sup>+</sup>IFN- $\gamma$ <sup>+</sup> T cells have been detected in 7-day post-MI heart tissues. In this report, the authors demonstrated that presence of CD4<sup>+</sup> T cells increases collagen deposition in heart as CD4 knock out mice showed reduction of collagen density after MI injury.<sup>74</sup> Becher et al. demonstrated that diabetic rodent myocardium have augmented infiltration of CD3<sup>+</sup> T lymphocytes within 6-week of diabetes induction by STZ that positively correlated with increased ventricular stiffness and decreased systolic and diastolic left ventricular function.<sup>111</sup> Increased proinflammatory T cell subsets, such as CD4<sup>+</sup>IFN- $\gamma$ <sup>+</sup>, CD4<sup>+</sup>CD28<sup>null</sup>, in peripheral blood of human diabetic patients associated with adverse cardiac events.<sup>78,79,110</sup> Thus, modulation of T cell function and abundance can be a potential therapeutic strategy to protect heart under chronic diabetic conditions. To this

end, the effects of T cells trafficking modulation by means of molecular mechanism to heart in diabetes has not been precisely determined yet.

In chapter 2, we demonstrated that fingolimod (FTY720), a novel immunomodulator drug, causes sustained CD4<sup>+</sup> and CD8<sup>+</sup> T cells deficiency in the blood of C57BL/6 mice that is associated with reduced fibrosis area and improved cardiac contractility. FTY720 acts as a functional antagonist on mature T lymphocytic cell membrane G protein coupled receptor, sphingosine 1-phosphate receptor 1 (S1P<sub>1</sub>).<sup>88,89,92</sup> Binding of phosphorylated FTY720 to S1P<sub>1</sub> receptor causes internalization of the receptor from cell membrane to cytosol and promotes proteasomal degradation there. The absence of S1P<sub>1</sub> receptor on cell membrane disables T lymphocytes to sense the increased chemotactic gradient of sphingosine 1-phosphate (S1P) present in blood and lymph that results in sequestration of mature lymphocytes in primary (thymus) and secondary lymphoid organs, such as spleen, and lymph nodes. Thereby, FTY720 creates substantial T lymphocytes deficiency in systemic circulation. For this immunomodulatory function, fingolimod (FTY720) is approved for treatment of relapsing-remitting multiple sclerosis. FTY720 treatment reduces autoimmune T<sub>H</sub>17 cells in circulation and reduces infiltrating autoreactive T lymphocytes in central nervous system. Therefore, administration of FTY720 protects the central nervous system from autoimmune T cell mediated destruction in these patients and in experimental autoimmune encephalomyelitis rodents.<sup>91,92</sup> To this point, it is noteworthy that S1P<sub>1</sub> receptor is widely expressed in different type of cells, other than T lymphocytes, including vascular endothelial cells, cardiomyocytes and both innate and adaptive immune cells.<sup>85,140</sup> Although FTY720 reduced myocardial fibrosis in C57BL/6 mice, administration of

FTY720 exacerbated cardiac histology and increased fibrosis area in Rag1 knockout mice (lacking mature B and T lymphocytes) under diabetic conditions. FTY720 can act on other four S1P receptors (S1P<sub>2,3,4,5</sub>) besides S1P<sub>1</sub> (EC<sub>50</sub> value is 0.2 nM) in varying affinity (EC<sub>50</sub> value for S1P<sub>2</sub> is >10000 nM and for S1P<sub>3</sub> is 5 nM).<sup>88</sup> Opposite results between C57BL/6 and Rag1 KO mice of FTY720 treatment indicate that the drug targets different fibrotic pathway in complete absence of lymphocytes under chronic hyperglycemia. Notably, FTY720 at higher concentrations (0.1-1  $\mu$ M) can activate S1P<sub>3</sub> receptor in fibroblasts that causes them to differentiate into collagen producing myofibroblasts.<sup>136</sup> In isolated murine S1P<sub>3</sub> knock out fibroblasts, FTY720 did not increase myofibroblast differentiation marker alpha smooth muscle actin ( $\alpha$ -SMA), whereas FTY720 was able to increase  $\alpha$ -SMA expression in wild-type mice fibroblasts. Primary human fibroblasts express mRNAs for different S1P receptors in the following order: S1P<sub>3</sub> >> S1P<sub>1</sub> > S1P<sub>2</sub> > S1P<sub>5</sub> > S1P<sub>4</sub>. Treatment with S1P<sub>1</sub>-, S1P<sub>3</sub>-, S1P<sub>4</sub>- and S1P<sub>5</sub>- antisense oligonucleotide to isolated primary human fibroblasts resulted in substantial reduction of respective protein levels. Notably, FTY720 mediated myofibroblast differentiation only abrogated in S1P<sub>3</sub> ASO treated fibroblasts. Further, it has been found that FTY720 activates Smad3 pathway in fibroblasts acting through S1P<sub>3</sub> receptor in fibroblasts leading to myofibroblast differentiation.<sup>136</sup> In a more recent report, FTY720 has been shown to activate S1P<sub>2</sub> receptor to induce myofibroblast contraction *in vitro*.<sup>128</sup> Thus, nonselective functions of FTY720 on S1P receptor subtypes make it obscure to dissect the mechanism through which it increases fibrosis area in Rag1 knock out mice, devoid of mature B and T lymphocytes. These circumstances set the premise

for our current study objective to dissect the effects of genetic S1P<sub>1</sub> receptor deficiency in T lymphocytes in murine diabetic cardiomyopathy model.

In the present study through genetic loss-of-function approach we generated T cell specific S1P<sub>1</sub> knockout (TS1P<sub>1</sub>KO) mice. TS1P<sub>1</sub>KO mice showed profound deficiency of CD3<sup>+</sup> T cells in spleen and reduced CD4<sup>+</sup> and CD8<sup>+</sup> T cells in blood than littermate control mice. Immunohistochemical analysis in cardiac tissue revealed the presence of fibrotic milieu in littermate mice myocardium under 11-week diabetic period. Littermate diabetic mice myocardium showed increased presence of CD3<sup>+</sup> T cells with concomitant increase of profibrotic cytokine TGF-β1 expression and fibroblast progenitor CD34 expressing fibrocytes presence after 11-week of chronic hyperglycemia. Comparatively, TS1P<sub>1</sub>KO mice myocardium showed less CD3<sup>+</sup> T cells infiltration with reduced TGF-β1 and CD34 expression in myocardium with improved cardiac contractile force than littermate diabetic mice after the same length of diabetic period. Additionally, CD4<sup>+</sup>Foxp3<sup>+</sup> T cells number were increased in spleen and blood of diabetic littermate mice. CD4<sup>+</sup>Foxp3<sup>+</sup> T cells are considered as regulatory T cells (T<sub>reg</sub> cells) that maintain immune tolerance by suppressing excessive immune reaction at periphery. S1P<sub>1</sub> mediated signaling has been shown to negatively regulate T<sub>reg</sub> cells development in thymus and periphery through Akt-mTOR pathway activation, whereas it promotes T<sub>H</sub>1 helper T cells differentiation.<sup>141,142</sup> It is beyond the scope of our present study objectives to elucidate S1P<sub>1</sub> mediated T cells differentiation effect on cardiac fibrosis in diabetes. However, it is important to note that, Zhen et al. reported increased T<sub>reg</sub> cells in STZ-induced diabetic mice spleen and blood with activated/memory phenotype. Notably, T<sub>reg</sub> cells from STZ treated mice showed reduced immunosuppressive ability than buffer recipient control

mice after 4-month diabetic period.<sup>143</sup> The authors observations indicate that under chronic hyperglycemia T cells phenotype changed towards more effector phenotype. Several epidemiological studies reported increased proinflammatory T cells in periphery in diabetic patients that correlate with the adverse cardiac outcomes.<sup>78,79</sup> To this end, based on the results of the present study, our conclusion is deficiency of T lymphocytes in TS1P<sub>1</sub>KO mice under chronic hyperglycemia ameliorates fibrosis and preserves heart histology as compared with littermate diabetic mice.

Mature T lymphocytes continually recirculate between secondary lymphoid organs and systemic circulation. This movement increases the probability of interaction of T cells with antigen presenting cells (APCs), such as macrophages and dendritic cells.<sup>90</sup> T lymphocytes encounter with antigen bearing APCs activates T cells that results in proliferation of activated T cells in respective lymph nodes. Effector T cells then can migrate to inflamed tissue and participate in potentiating the immune response by secreting cytokines, growth factors, and through direct cell-cell contact. T lymphocytes trafficking has been found to be involved in murine myocardial injury models.<sup>77,144</sup> After left coronary artery ligation in mouse heart, heart draining lymph nodes have increased CD4<sup>+</sup> T cells proliferation and infiltration into the myocardium.<sup>74</sup> Another report demonstrated that in murine chronic transverse aortic constriction model, increased CD3<sup>+</sup> T cells infiltration was associated with increased fibrosis area and cardiac dysfunction.<sup>75,76</sup> In our present study, TS1P<sub>1</sub>KO mice have reduced CD4<sup>+</sup> and CD8<sup>+</sup> T cells in circulation, as T cells in these mice have decreased S1P<sub>1</sub> mRNA expression due to Lck driven Cre-mediated recombination of S1P<sub>1</sub> gene at the coding region.<sup>83</sup> CD4<sup>+</sup> and CD8<sup>+</sup> T cells in these mice sequester in thymus and have reduced in secondary lymphoid

organs as shown consistent with the literature.<sup>83</sup> We observed less CD3<sup>+</sup> T lymphocytes infiltration in diabetic TS1P<sub>1</sub>KO mice myocardium than littermate diabetic mice.

Altogether, altered T lymphocytes trafficking in TS1P<sub>1</sub>KO mice is a contributing factor for the observed cardioprotection under long term hyperglycemia.

Surprisingly, TS1P<sub>1</sub>KO vehicle mice myocardium exhibited increased collagen deposition in myocardium with altered heart histology and attenuated cardiac force of contraction. Although TS1P<sub>1</sub>KO vehicle mice myocardium did not exhibit increased presence of T cells compared with littermate vehicle mice, TGF- $\beta$ 1 and CD34 bearing cells expression were increased in these mouse myocardium. These contrasting results indicate the complexity of cardiac fibrotic remodeling and important contributions of different types of immune cells to maintain the collagen homeostasis in heart under both physiological and pathological conditions. To this point, it is noteworthy that TS1P<sub>1</sub>KO mice have increased circulatory B lymphocytes (B220<sup>+</sup> lymphocytes) in their blood as immune compensatory mechanism of reduced circulating T cells.<sup>83</sup> Lack of programmed cell death protein-1 (PD-1<sup>-/-</sup>) in mice resulted in severe form of dilated cardiomyopathy with increased interstitial fibrosis, disarrayed and disrupted myofilaments.<sup>145</sup> PD-1 acts as negative regulator of lymphocytes proliferation. Increased IgG autoantibodies against cardiac proteins were deposited in PD-1<sup>-/-</sup> murine myocardium. Strikingly, PD1<sup>-/-</sup> mice generated in Rag2<sup>-/-</sup> background (mice lacking mature B and T lymphocytes) did not develop dilated cardiomyopathy.<sup>145</sup> Interestingly, B lymphocytes have been also implicated in heart failure development by secreting autoantibodies against cardiomyocytes.<sup>146</sup> Similarly, our results presented in chapter 2 and earlier<sup>117</sup> demonstrate that Rag1 knock-out mice lacking mature B and T lymphocytes exhibit resistance against

diabetes induced fibrosis and cardiac dysfunction as compared to C57BL/6 mice with normal B and T cells compartment. TS1P<sub>1</sub>KO mice had significantly lower T cells in circulation and lymphoid organs due to the lack of S1P<sub>1</sub> in T cells that increases B cells number in circulation.<sup>83</sup> Altered B and T cells number in the circulation might contribute to develop fibrosis in TS1P<sub>1</sub>KO vehicle mice, as B lymphocytes secreted antibodies have shown detrimental effects on cardiomyocytes.<sup>146</sup>

Proinflammatory cytokines, such as TNF- $\alpha$ , IL-1 $\beta$  and IL-6, can cause cardiac dysfunction by negatively affecting cardiac contractility and cardiac extracellular matrix compartment remodeling. To this end, the inhibition of proinflammatory cytokine TNF- $\alpha$  is not proven efficacious in a human clinical trial.<sup>147</sup> Thus, a more comprehensive understanding of molecular and cellular basis of heart failure development should be investigated in different models of cardiac dysfunction to devise better and effective therapeutic interventions. In our present study, T cell trafficking modulation by genetic depletion of T cell S1P receptor 1 protects heart in chronic diabetes. To this end, T cells S1P<sub>1</sub> receptor is a potential therapeutic target to modulate T cells trafficking in chronic inflammatory conditions, such as diabetes and hypertension, to ameliorate cardiac fibrosis. In this regard, several newer, more specific S1P<sub>1</sub> receptor modulator drug molecules have shown promising results. For instance, unlike S1P<sub>1</sub> receptor non-specific agonist FTY720, ponesimod (Actelion, Switzerland), a selective S1P<sub>1</sub> agonist (EC<sub>50</sub> value is 5.7 nM), is now under Phase III clinical trial for depleting T lymphocytes in circulation.<sup>149</sup> Ponesimod has been shown efficacious in preventing T cell mediated tissue damage in rodent delayed-type hypersensitivity of the skin and adjuvant-induced rodent

arthritis model.<sup>148,149</sup> Thus, specific S1P<sub>1</sub> receptor modulator drugs can be used more effectively to modulate T lymphocytes trafficking in clinical practices.

### 3.5. Conclusions

In summary, key findings of our present investigation are: (1) presence of T lymphocytes normal trafficking between lymphoid organs and circulation is an important determinant of cardiac fibrotic remodeling both under physiological and pathological conditions; (2) T cell specific genetic S1P receptor 1 deficiency reduces circulatory T lymphocytes in TS1P<sub>1</sub>KO mice; (3) TS1P<sub>1</sub>KO mice myocardium exhibits less CD3<sup>+</sup> T cells with reduced fibrosis area, preserved cardiac histology and improved cardiac contractility under chronic diabetes.

However, our present study did not assess the role of specific subset of T lymphocytes in diabetic myocardial fibrogenesis. In the next study, we isolated CD4<sup>+</sup> T cells from wild-type littermate mice, and intravenously transfer the isolated CD4<sup>+</sup> T cells to TS1P<sub>1</sub>KO mice. We evaluated cardiac fibrotic response in TS1P<sub>1</sub>KO mice after CD4<sup>+</sup> T cells transfer in chronic diabetes. These studies are discussed in the next chapter.

## CHAPTER 4: EFFECTS OF CD4 T CELL TRANSFER TO TS1P<sub>1</sub>KO MICE ON CARDIAC FIBROSIS IN DIABETIC CARDIOMYOPATHY

### 4.1. Background

In chapter 3, we demonstrated that conditional T cell specific sphingosine 1-phosphate receptor 1 (S1P<sub>1</sub>) genetic depletion results in marked reduction of both single positive CD4<sup>+</sup> and CD8<sup>+</sup> T lymphocytes in systemic circulation. T-cell specific S1P<sub>1</sub> knock-out mice (TS1P<sub>1</sub>KO) in long term streptozotocin (STZ)-induced type 1 diabetic cardiomyopathy model exerted less fibrosis and improved cardiac contractility compared to diabetic littermate mice. We found less CD3<sup>+</sup> T cells invasion into diabetic TS1P<sub>1</sub>KO mice heart sections compared to diabetic littermate mice. The expression of profibrotic cytokine TGF-β1 and CD34 fibrocytes were also reduced in diabetic TS1P<sub>1</sub>KO mice heart sections compared to diabetic littermate mice. However, our studies did not elucidate specific subset of T lymphocytes role in myocardial fibrogenesis in long term diabetes. Among the helper CD4<sup>+</sup> and cytotoxic CD8<sup>+</sup> T lymphocytes, CD4<sup>+</sup> T lymphocytes have been found to be responsible for cardiac fibrosis generation in various cardiovascular diseases including hypertension, myocardial infarction and myocarditis.<sup>36</sup> To date, four distinct CD4<sup>+</sup> T lymphocyte subsets have been reported including T<sub>H</sub>1, T<sub>H</sub>2, T<sub>H</sub>17 and regulatory T cells.<sup>68</sup> All the CD4<sup>+</sup> T cell subsets have been reported to be involved in cardiac fibrosis.<sup>36</sup> The expression of T helper type 1 (T<sub>H</sub>1) CD4<sup>+</sup> T cells increases collagen content and have been shown to increase procollagen synthesis in cardiac fibroblasts.<sup>69</sup> T helper type 2 (T<sub>H</sub>2) CD4<sup>+</sup> T cells cytokines IL-4 and IL-13 have been reported to be pro-fibrotic stimulators leading to synthesis of collagen in fibroblasts.<sup>36,150</sup> T helper type 17 (T<sub>H</sub>17) cells have been implicated in cardiac fibrosis in

autoimmune inflammatory myocarditis.<sup>151</sup> On the other hand, regulatory T cells attenuate cardiac fibrosis in experimental models of hypertension, angiotensin-induced cardiomyopathy and myocardial infarction.<sup>152,153,154</sup> The attenuation of inflammation by regulatory T cells has been implicated as a mechanism to reduce myocardial fibrosis under pathological conditions.<sup>36</sup> CD4<sup>+</sup> T lymphocytes have also been reported to facilitate fibrocytes development from blood derived monocytes and increase the collagen deposition in murine kidney.<sup>155</sup>

Several epidemiological studies have reported the expansion of pro-inflammatory CD4<sup>+</sup> T lymphocytes in diabetic patients with increased systemic inflammation and adverse cardiovascular outcomes including acute coronary events.<sup>78,79,110</sup> The time course analysis in rodent STZ-induced diabetic cardiomyopathy model has shown increased CD3<sup>+</sup> T lymphocytes into myocardium as early as 2-week after STZ induction.<sup>111</sup> As both mature CD4<sup>+</sup> and CD8<sup>+</sup> T lymphocytes express CD3<sup>+</sup> on their cell surface,<sup>156</sup> ambiguity exists to precisely determine the cellular origin of infiltrating CD3<sup>+</sup> T cells in the myocardium under chronic diabetes.

TS1P<sub>1</sub>KO mice, due to genetic depletion of T cell specific S1P receptor 1, have substantially reduced CD4<sup>+</sup> and CD8<sup>+</sup> T cells in blood and cardioprotection with less myocardial fibrosis in long term diabetic cardiomyopathy model (Chapter 3). Because CD4<sup>+</sup> T cells have been shown to participate in cardiac fibrosis, we hypothesized that adoptive transfer of CD4<sup>+</sup> T cells from littermate mice to TS1P<sub>1</sub>KO mice reverses the cardioprotective and antifibrotic effect in chronic diabetes. Evaluating the effects of adoptive transfer of CD4<sup>+</sup> T lymphocytes on myocardial fibrosis in chronic diabetes will help to elucidate the role of CD4<sup>+</sup> T cells more precisely, which in turn will facilitate

future therapeutic strategy to ameliorate cardiac fibrosis in diabetes. In this study, we isolated splenic CD4<sup>+</sup> T cells from littermate mice and reconstituted purified CD4<sup>+</sup> T cells into TS1P<sub>1</sub>KO mice intravenously. CD4<sup>+</sup> T cells recipient mice underwent long term STZ-induced diabetes. At the end point of experimental period, we evaluated cardiac contractility in an *ex-vivo* Langendorff's heart perfusion system, we also studied heart histology and fibrosis area. In addition, we assessed myocardium infiltrating CD3<sup>+</sup> T cells number, profibrotic TGF-β1 and CD34 expressing fibrocyte expression in cardiac tissue by immunohistological studies.

## **4.2. Materials and Methods**

### **4.2.1. T cell specific S1P receptor 1 knock out mice**

T cell specific S1P receptor 1 knock out (TS1P<sub>1</sub>KO) mice from S1P<sub>1</sub><sup>loxP/loxP</sup> mice and Lck-Cre mice breeding colony were genotyped and immunophenotyped as described in chapter 3. We housed all mice in specific pathogen free room in Animal Research Wing (ARW) facility at SDSU. Mice were given *ad libitum* rodent autoclaved food (5010, LabDiet) and water. The animals were handled and cared in accordance with the *Guide for the Care and Use of Laboratory Animals* by U.S. National Research Council (Eighth Edition, 2011). All experimental procedures were approved by Institutional Animal Care and Use Committee (IACUC) at SDSU.

#### **4.2.2. Isolation of CD4<sup>+</sup> T cells and adoptive transfer**

We isolated CD4<sup>+</sup> T cells by positive selection from the littermate control mice spleen by using microbeads conjugated with CD4<sup>+</sup> antibody from Miltenyi Biotech (Auburn, CA). Briefly, freshly excised spleen from anesthetized littermate control mice was cut into 1 mm<sup>3</sup> pieces and passed through 70 µm nylon cell strainer (352350, Corning Inc. NY). The dissociated cells were collected in isolation buffer containing 0.5% w/v bovine serum albumin (A2153, Sigma-Aldrich, MO) and 2 mM EDTA in 0.01 M PBS (P3813, Sigma-Aldrich). The single-cell suspensions were centrifuged at 300 x g for 10 minutes at room temperature (RT). Supernatants were discarded and red blood cells were lysed by incubating at RT for 5 minutes with 5 mL of 1 x RBC lysis buffer (00-4333, eBioscience) for each spleen. After incubation, the single-cell suspensions were washed twice in isolation buffer by centrifugation at 500 x g for 10 minutes at RT. The cell pellets were re-suspended in 10 ml isolation buffer and cell numbers were counted in Cellometer Auto T4 (Nexcelom, MA) in prepared single-cell suspension of splenocytes (Figure 4-1).

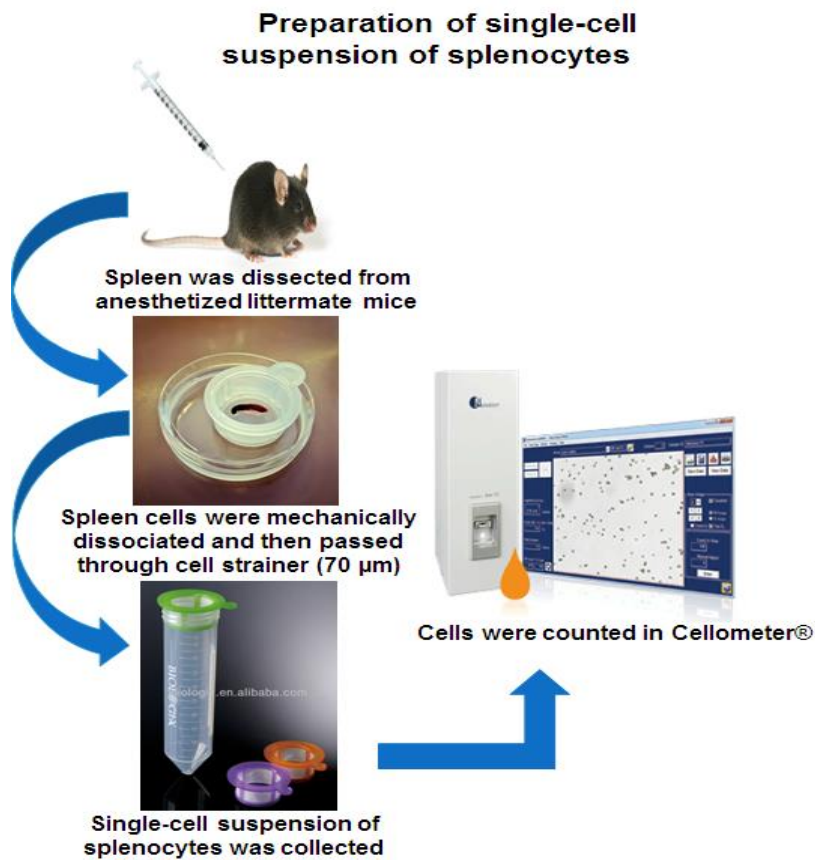


**Figure 4-1:** Schematic diagram of preparation of single-cell suspensions from littermate mouse spleen. The images used in the figure were taken from multiple web based sources for schematic representation.

The prepared single-cell suspension of splenocytes was then incubated with 10 µL of mouse CD4 antibody-microbeads (130-049-201, Miltenyi Biotec) per  $10^7$  cells at 4 °C for 15 minutes. Cells were washed by centrifugation with isolation buffer at 300 x g for 10 minutes at RT. The cell pellets were re-suspended with 500 µL of isolation buffer per  $10^8$  cells and proceeded to magnetic separation. The magnetically labeled cells were passed through MS column (130-042-201, Miltenyi Biotec) attached to a magnet (130-042-102, Miltenyi Biotec) by washing with 500 µL isolation buffer for three times.

Specific CD4 microbeads labeled cells were then collected by removing the MS column from the magnet followed by immediate flushing of the column with a rubber plunger. The collected CD4 positive T cells were counted, and viability was measured by trypan blue exclusion assay. We also assessed the isolated CD4<sup>+</sup> T cells purity by flow cytometry using anti-mouse CD4 antibody (11-0041-82, eBioscience). The isolated CD4<sup>+</sup> T cell viability and purity were ~90-95% in each case (Figure 4-2).

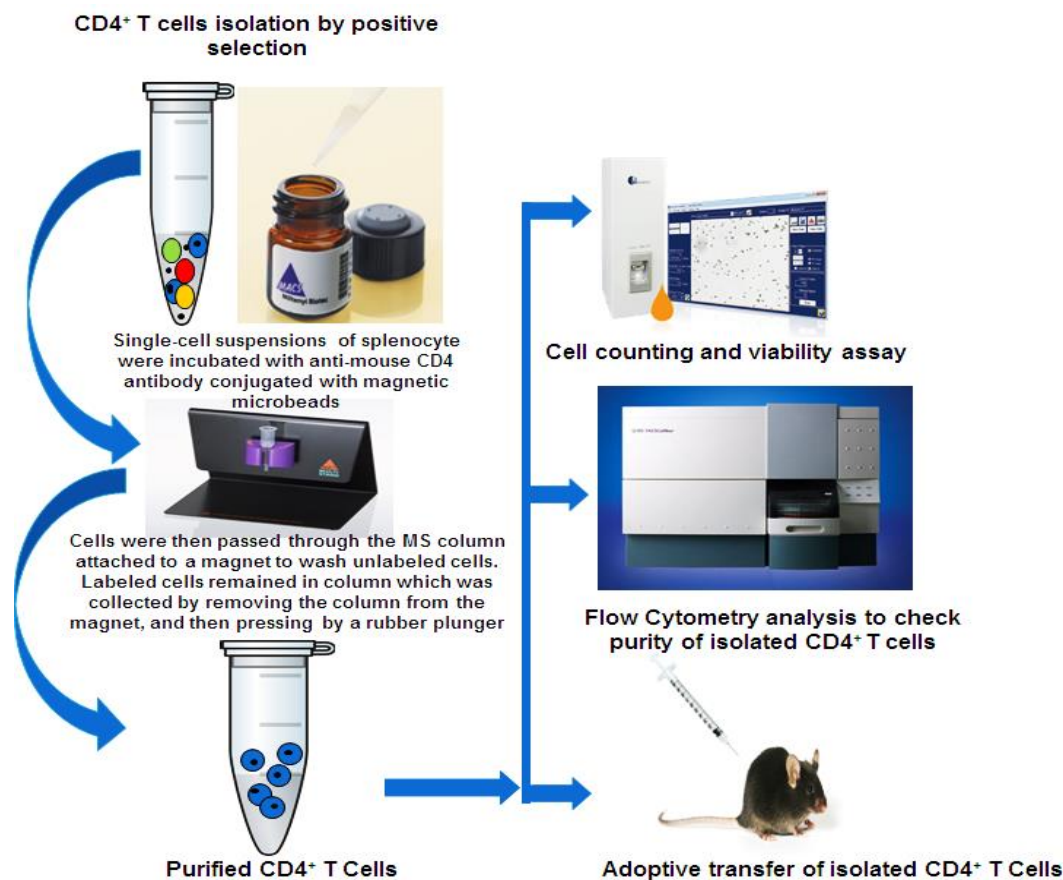


**Figure 4-2:** Schematic diagram of experimental procedure to isolate CD4<sup>+</sup> T cells from single-cell suspensions of splenocyte of littermate control mice. The images used in the figure were taken from multiple web based sources for schematic presentation.

One million ( $10^6$ )  $CD4^+$  T cells prepared by the above mentioned procedure in 0.01 M PBS was intravenously transferred through tail vein to littermate and TS1P<sub>1</sub>KO mice. After  $CD4^+$  T cells transfer, littermate and TS1P<sub>1</sub>KO mice were observed for one week. After one week, both strains were divided into vehicle and streptozotocin treated group. The groups is represented as ‘ $CD4^+$ mouse type & treatment name’. All mice underwent similar 11-week long experimental protocol as described in chapter 3. The experimental protocol is shown below (Figure 4-3).

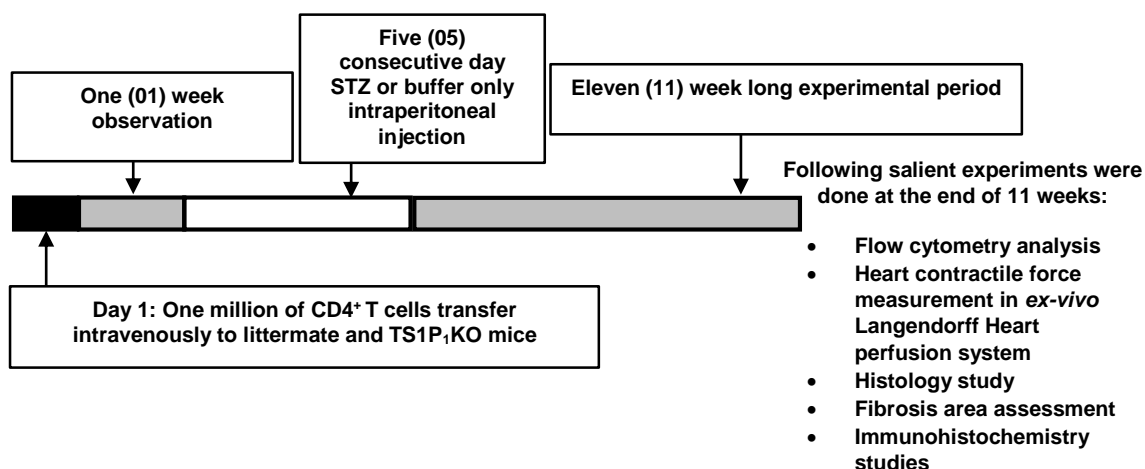


**Figure 4-3:** Schematic diagram of experimental protocol of adoptive transfer of  $CD4^+$  T cells in littermate and TS1P<sub>1</sub>KO mice followed by 11-week long streptozotocin (STZ)-induced type 1 diabetes.

#### 4.2.3. Flow cytometry analysis of $CD4^+$ and $CD8^+$ T cells in peripheral blood

We measured helper  $CD4^+$  and cytotoxic  $CD8^+$  T cells proportions in peripheral blood of mice by two color flow cytometry analysis as described in chapter 2 in a BD FACSCalibur flow cytometer (BD Biosciences, CA). Data was acquired and analyzed by BD CellQuest Pro software (BD Biosciences, CA).

#### 4.2.4. Flow cytometry analysis of regulatory T cells

We measured relative percentage of CD4<sup>+</sup>Foxp3<sup>+</sup> regulatory T cells (T<sub>reg</sub> cells) in spleen and blood after 11-week study period in mice according to the procedures described in chapter 3. Flow cytometry analysis was carried out in BD FACSCalibur flow cytometer coupled to CellQuest Pro software (BD Biosciences).

#### 4.2.5. Cardiac contractility assessment

We assessed cardiac contractile force (g) in the mice after 11-week experimental period in a modified Langendorff's heart perfusion system *ex-vivo*, as described in chapter 2. Cardiac contractile force was recorded and analyzed with Biopac MP 100 data system (Goleta, CA, USA). The fold change in cardiac contractile force relative to littermate vehicle mice was measured.

#### 4.2.6. Heart histology and analysis of cardiac fibrosis

Paraffin-embedded 5 μm thick heart sections of littermate and TS1P<sub>1</sub>KO mouse groups were prepared at the end of 11-weeks. Heart histology in Hematoxylin & Eosin stained, and fibrosis area in Masson's trichrome stained heart sections were studied at the end of 11-weeks. H&E stained sections were examined under bright field illumination in a upright microscope (Carl Zeiss, Germany), and score was given for each heart section for (i) the presence of eosinophilic interstitial collagen fibers, (ii) extent of cellularity in interstitial space of myocardium, (iii) myocardial cell necrosis/loss, (iv) myofiber striation and myocytes organization on a five-point scale for each characteristics from 0 to 4.<sup>120,121</sup> The cumulative scores were expressed from 0 to 16 for each group. Trichrome stained whole heart sections image was acquired using a Leica EZ4 HD stereomicroscope (Leica Microsystems, Buffalo Grove, IL, USA). The percentage of fibrosis area relative

to the whole heart area was quantified by using NIH Image J (Bethesda, MA) software as described by Zhao et al.<sup>117</sup>

#### **4.2.7. Immunohistochemical analysis on littermate and TS1P1KO mice heart sections**

CD3<sup>+</sup> T cells, TGF- $\beta$ 1 and CD34 bearing cell expression were analyzed in myocardium by immunohistochemistry in paraffin embedded 5  $\mu$ m tissue sections with CD3 (10  $\mu$ g/mL, sc-20047; Santa Cruz Biotechnology, Inc., CA), TGF- $\beta$ 1 (15  $\mu$ g/mL, MAB240; R&D Systems, Inc., Minneapolis, MN) and CD34 (10  $\mu$ g/mL, MA5-17825; Pierce Biotechnology, Rockford, IL, USA) primary antibodies. R&D systems mouse/rat cell and tissue staining HRP-DAB kit (CTS002/CTS017; R&D Systems) were used to amplify positive signals and visualize by using corresponding mouse/rat primary antibodies. The detailed procedure is described in chapter 2. To count immunopositive CD3<sup>+</sup> cells, 30 fields of stained heart sections were pictured at bright-field under 400x magnification in an upright microscope (Carl Zeiss, Germany). Myocardium infiltrating cells number was calculated by counting the cells number in imaged 400x fields (cells/field).<sup>75</sup> TGF- $\beta$ 1 and CD34 positive staining percent area were quantified in 10 fields of 400x magnification images by using NIH ImageJ software (Bethesda, MD) and the averaged percent of staining area is presented.<sup>119,139</sup>

#### **4.2.8. Data analyses**

All the data was expressed as mean  $\pm$  SEM. One-way ANOVA was used for statistical analysis followed by Student-Newman-Keuls post hoc test for multiple comparisons of group means to evaluate statistical significance. Two-tailed unpaired Student's t-test was done, where applicable. Data was analyzed in GraphPad Prism software (v5.01, 2007). A P value of less than 0.05 was considered statistically significant, and indicated with an asterisk (\*) or a number (#) sign.

### **4.3. Results**

#### **4.3.1. Isolated CD4<sup>+</sup> T cell number and purity by flow cytometry analysis**

Total cell number was  $7.03 \pm 0.45$  million cells per milliliter (n=14) in single-cell suspensions of splenocytes from littermate control mice. Isolated CD4<sup>+</sup> T cell numbers were  $5.09 \pm 0.46$  million cells per milliliter (n=14) from single-cell suspensions. The purity of isolated CD4<sup>+</sup> T cells was about 90-95% as analyzed by CD4<sup>+</sup> antigen expression in cells of CD4 positive and CD4 negative fraction from MS column effluent by flow cytometry analysis (Figure 4-4).

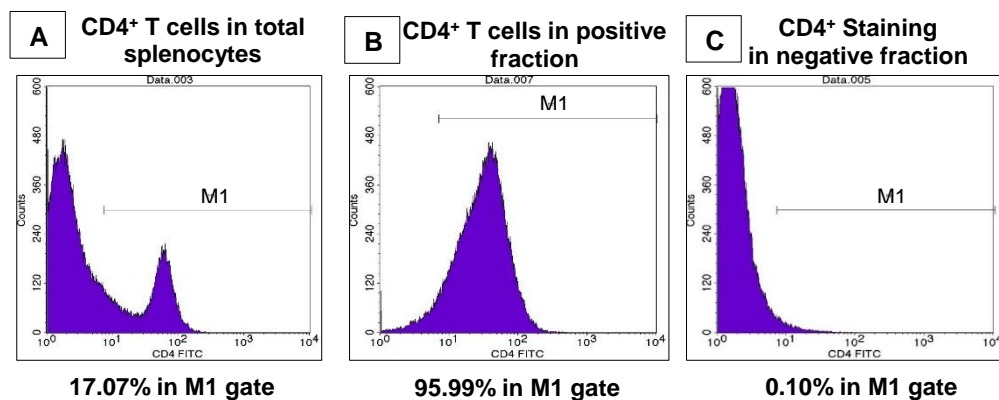


**Figure 4-4:** Representative flow cytometry histogram represents CD4<sup>+</sup> T cells staining and number in total isolated splenocytes of littermate control mice (panel A). CD4<sup>+</sup> T cells staining in positive fraction after separation through MACS positive selection method exhibited only CD4<sup>+</sup> staining in positive fraction (panel B). CD4<sup>+</sup> T cells staining in negative fraction after separation, yielded negligible CD4<sup>+</sup> staining (panel C).

#### 4.3.2. Assessment of physiological parameters in chronic diabetes

We measured body weight (g) twice each week and blood glucose level (mg/dl) at the beginning, after 4-week and after 11-week during experimental period. In our present study, both littermate control and TS1P<sub>1</sub>KO mice were divided into vehicle treated and streptozotocin (STZ) treated groups where all mice received one million CD4<sup>+</sup> T cells isolated from littermate mice spleen. Both littermate and TS1P<sub>1</sub>KO mice recipient of streptozotocin (STZ) exhibited less body weight gain compared to vehicle treated mice during 11-week study period. CD4<sup>+</sup> T cells recipient littermate and TS1P<sub>1</sub>KO groups had no significant difference in body weight at the beginning (Figure 4-5, Table 4-1). But after STZ injection, CD4<sup>+</sup> T cells recipient littermate STZ mice showed 39.68% reduced body weight compared to littermate vehicle mice and TS1P<sub>1</sub>KO STZ mice had 35.83%

reduced body weight compared to TS1P<sub>1</sub>KO vehicle mice at the end of 11-weeks (Figure 4-5, Table 4-1). This reduction was 2.59-fold less (39.68 % vs. 15.29 %) in body weight for littermate STZ and 2.01-fold less (35.83 % vs. 17.75 %) in body weight for KO STZ mice compared to respective STZ mice of both strain without CD4<sup>+</sup> T cells transfer (Figure 4-5, Table 4-1).

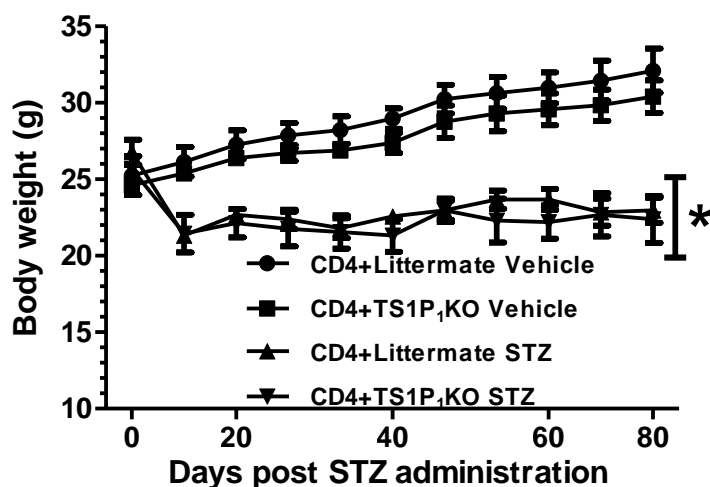


**Figure 4-5:** Body weight (g) change in CD4<sup>+</sup> T cells recipient littermate and TS1P<sub>1</sub>KO mice during 11-week study period. Both CD4<sup>+</sup> T cells recipient littermate and TS1P<sub>1</sub>KO STZ mice exhibited lower body weight gain trend throughout 11-week, and showed significantly lower body weight (g) at the end of 11-week compared to littermate and TS1P<sub>1</sub>KO vehicle mice. \*P<0.05 vs. CD4+littermate vehicle and CD4+TS1P<sub>1</sub>KO vehicle mice, respectively. Sample size n = 4-5 mice per each group. All data are expressed as means ± SEM at each time point.

**Table 4-1:** Summary of physiological parameter in CD4<sup>+</sup> T cells recipient littermate and TS1P<sub>1</sub>KO mice during 11-week experimental period.

	CD4+Littermate Vehicle (n=5)	CD4+TS1P <sub>1</sub> KO Vehicle (n=5)	CD4+Littermate STZ (n=4)	CD4+TS1P <sub>1</sub> KO STZ (n=4)
<i>At beginning</i>				
<i>(before STZ</i>				
<i>induction)</i>				
Body wt. (g)	25.24±1.27	24.62±0.33	26.78±0.82	25.68±0.31
<i>After 4-week of STZ</i>				
<i>induction</i>				
Body wt. (g)	27.86±0.82	26.72±0.52	22.38±0.63*	21.75±1.14
<i>After 11-week of</i>				
<i>STZ induction</i>				
Body wt. (g)	32.1±1.45	30.4±1.07	22.98±0.82*	22.38±1.53*

The data is expressed as mean ± SEM. \*P < 0.05 between vehicle and STZ groups of CD4<sup>+</sup> T cells recipient littermate and TS1P<sub>1</sub>KO mice. The values of 'n' represent number of mice in each group.

At the beginning of the study, there was no significant difference in blood glucose level (mg/dl) among CD4<sup>+</sup> T cells recipient littermate and TS1P<sub>1</sub>KO mice (Figure 4-6, Table 4-2). However, STZ induction exhibited significantly higher blood glucose level in both littermate and TS1P<sub>1</sub>KO mice compared to respective vehicle only treated mice of two strains after 4-weeks (Figure 4-6, Table 4-2). Hyperglycemia persisted significantly after 11-week in both littermate and TS1P<sub>1</sub>KO STZ mice compared to vehicle treated mice (Figure 4-6, Table 4-2). Notably, TS1P<sub>1</sub>KO STZ mice recipient of CD4<sup>+</sup> T cells showed 1.50-fold increased high blood glucose level compared to without CD4<sup>+</sup> T cells recipient TS1P<sub>1</sub>KO STZ mice (CD4<sup>+</sup>TS1P<sub>1</sub>KO STZ, [n=4], 527.75±41.16 mg/dl vs. TS1P<sub>1</sub>KO STZ, [n=7], 350±32.98 mg/dl, #P<0.05) (Figure 4-7).

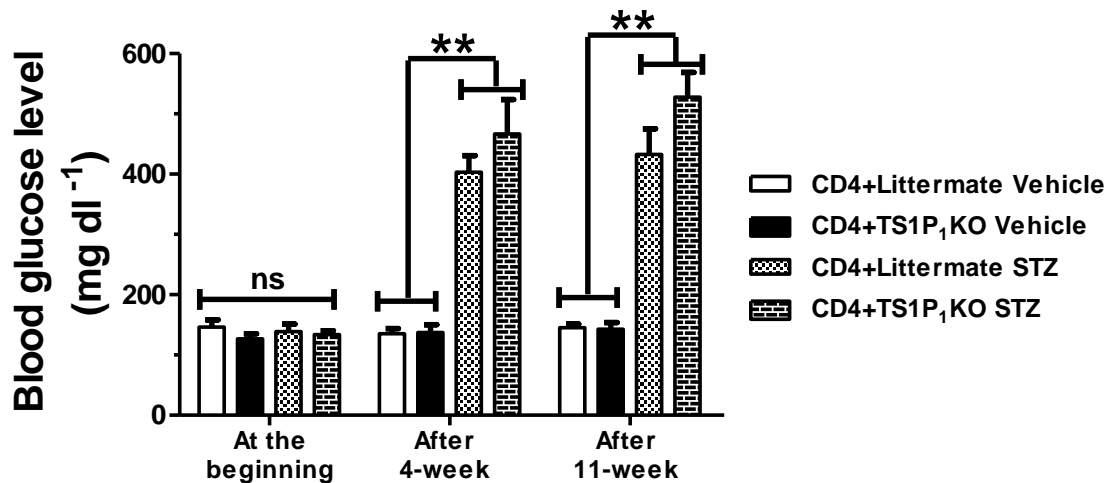


**Figure 4-6:** Blood glucose level (mg/dl) during 11-week study period in CD4<sup>+</sup> T cells recipient littermate and TS1P<sub>1</sub>KO mice. Bar graphs show blood glucose level (mg/dl) at the beginning, after 4-week and after 11-week of streptozotocin (STZ) administration in all mice. Sample size, n = 5-4 mice per each group. \*\*P < 0.01 between vehicle and STZ groups of CD4<sup>+</sup> T cells recipient littermate and TS1P<sub>1</sub>KO mice blood glucose level after 4-week and after 11-week of STZ induction. The data is expressed as mean ± SEM.

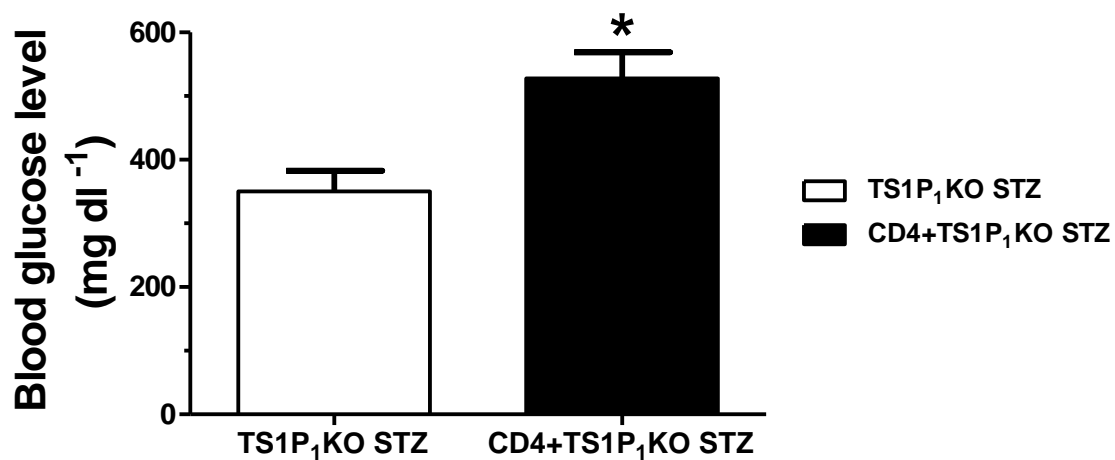


**Figure 4-7:** Blood glucose level (mg/dl) at end of 11-week in diabetic TS1P<sub>1</sub>KO mice without- and with- CD4<sup>+</sup> T cells adoptive transfer. CD4<sup>+</sup> T cells recipient TS1P<sub>1</sub>KO STZ mice (n=4) exhibited significantly higher blood glucose level compared to TS1P<sub>1</sub>KO STZ mice without CD4<sup>+</sup> T cells transfer (n=4) at the end of 11 weeks, \*P < 0.05. The data is expressed as mean ± SEM.

**Table 4-2:** Summary of metabolic parameter in CD4<sup>+</sup> T cells recipient littermate and TS1P<sub>1</sub>KO mice during 11-week experimental period.

	CD4+Littermate Vehicle (n=5)	CD4+TS1P <sub>1</sub> KO Vehicle (n=5)	CD4+Littermate STZ (n=4)	CD4+TS1P <sub>1</sub> KO STZ (n=4)
<i>At the beginning</i>				
<i>(before STZ induction)</i>				
Blood glucose level (mg/dl)	146±12.03	126.80±8.35	138.50±12.84	133.75±6.70
<i>After 4-week of STZ induction</i>				
Blood glucose level (mg/dl)	135.40±8.27	137.40±12.63	403±27.97**	466.75±56.76**
<i>After 11-week of STZ induction</i>				
Blood glucose level (mg/dl)	145.20±5.83	142.60±11.14	432.50±42.52**	527.75±41.16**

The data is expressed as mean ± SEM. \*\*P < 0.01 between vehicle and STZ groups of CD4<sup>+</sup> T cells recipient littermate and TS1P<sub>1</sub>KO mice.

### 4.3.3. Flow cytometry analysis of T lymphocyte subsets

We measured dissected spleen wet weight (mg) and calculated spleen weight (mg) to body weight (g) ratio in both without- and with- CD4<sup>+</sup> T cells recipient mice to detect gross splenic structural remodeling in long term diabetes. One-way ANOVA followed by Tukey's post hoc test yielded no significant difference between spleen weight (mg) to body weight (g) ratio between littermate and TS1P<sub>1</sub>KO mice without- and with-CD4<sup>+</sup> T cells transfer (Table 4-3). Notably, splenocytes number (x10<sup>6</sup> cells/mL) was significantly increased, as analyzed by student's two-tailed t-test, in littermate and TS1P<sub>1</sub>KO vehicle mice after CD4<sup>+</sup> T cells transfer compared to littermate and TS1P<sub>1</sub>KO vehicle mice without CD4<sup>+</sup> T cells transfer. Although, littermate STZ mice had 12.84% and TS1P<sub>1</sub>KO STZ mice had 21.34% increased splenocytes number (x10<sup>6</sup> cells/mL) after CD4<sup>+</sup> T cells transfer compared to littermate vehicle and TS1P<sub>1</sub>KO vehicle mice without CD4<sup>+</sup> T cells transfer, two-tailed t-test did not yield significant differences between these two groups (Figure 4-8, Table 4-4).

**Table 4-3:** Summary of spleen weight (mg) to body weight (g) ratio in littermate and TS1P<sub>1</sub>KO mice without- and with- CD4<sup>+</sup> T cells transfer.

<b>Groups</b>	<b>Spleen wt. (mg)/body wt. (g)</b>
Littermate Vehicle (n=4)	2.97±0.37
TS1P <sub>1</sub> KO Vehicle (n=5)	2.61±0.24
Littermate STZ (n=8)	2.82±0.23
TS1P <sub>1</sub> KO STZ (n=6)	2.72±0.27
CD4+Littermate Vehicle (n=5)	2.43±1.69
CD4+TS1P <sub>1</sub> KO Vehicle (n=5)	2.48±0.32
CD4+Littermate STZ (n=4)	2.79±0.29
CD4+TS1P <sub>1</sub> KO STZ (n=4)	2.15±0.23

The data is expressed as mean ± SEM. ‘n’ value represents number of mice in each group.

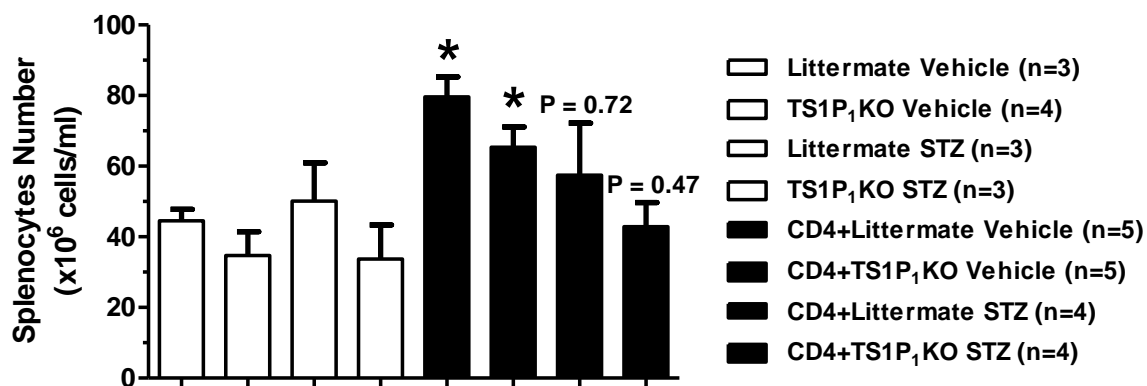


**Figure 4-8:** Effects in total splenocytes number ( $\times 10^6$  cells/ml) in littermate and TS1P<sub>1</sub>KO mice after CD4<sup>+</sup> T cells transfer compared to littermate and TS1P<sub>1</sub>KO mice without CD4<sup>+</sup> T cells transfer. Both littermate and TS1P<sub>1</sub>KO vehicle mice had significantly increased splenocytes number after CD4<sup>+</sup> T cells transfer compared to littermate and TS1P<sub>1</sub>KO vehicle mice, respectively, without CD4<sup>+</sup> T cells transfer, \* $P < 0.05$ . Diabetic littermate ( $P = 0.72$ ) and TS1P<sub>1</sub>KO mice ( $P = 0.47$ ) had increased splenocytes number after CD4<sup>+</sup> T cells transfer compared to littermate and TS1P<sub>1</sub>KO STZ mice, respectively, without CD4<sup>+</sup> T cells transfer. The data is expressed as mean  $\pm$  SEM. 'n' value represents number of mice in each group.

**Table 4-4:** Summary of splenocytes number ( $\times 10^6$  cells/ml) in littermate and TS1P<sub>1</sub>KO mice without- and with- CD4<sup>+</sup> T cells transfer.

<b>Groups</b>	<b>Splenocytes number (<math>\times 10^6</math> cells/ml)</b>
Littermate Vehicle (n=3)	44.5 $\pm$ 3.32
TS1P <sub>1</sub> KO Vehicle (n=4)	34.73 $\pm$ 6.74
Littermate STZ (n=3)	50.1 $\pm$ 10.89
TS1P <sub>1</sub> KO STZ (n=3)	33.73 $\pm$ 9.65
CD4+Littermate Vehicle (n=5)	79.64 $\pm$ 5.68*
CD4+TS1P <sub>1</sub> KO Vehicle (n=5)	65.35 $\pm$ 5.80*
CD4+Littermate STZ (n=4)	57.48 $\pm$ 14.69
CD4+TS1P <sub>1</sub> KO STZ (n=4)	42.88 $\pm$ 6.83

The data is expressed as mean  $\pm$  SEM. \*P < 0.05 compared to littermate vehicle and TS1P<sub>1</sub>KO vehicle without CD4<sup>+</sup> T cells transfer. 'n' value represents number of mice in each group.

After CD4<sup>+</sup> T cells adoptive transfer, although CD4<sup>+</sup> and CD8<sup>+</sup> T cell numbers in TS1P<sub>1</sub>KO mouse groups blood remained significantly lower than littermate mouse groups, CD4<sup>+</sup> T cells number in TS1P<sub>1</sub>KO mice was increased by 1.58-fold in vehicle and 1.95-fold in STZ mice compared to TS1P<sub>1</sub>KO vehicle and STZ groups, respectively, without CD4<sup>+</sup> T cells transfer at the end of 11-weeks (Figure 4-9A, 4-9B, 4-10 and Table 4-5). CD8<sup>+</sup> T cell numbers did not show any significant difference between these two categories of mouse. Similarly, CD4<sup>+</sup>Foxp3<sup>+</sup> T cells number had increased in spleen of both CD4<sup>+</sup> T cells recipient TS1P<sub>1</sub>KO vehicle and STZ groups than TS1P<sub>1</sub>KO mice without CD4<sup>+</sup> T cells transfer (Figure 4-11A, 4-11B and Table 4-6). CD4+littermate STZ mice had increased CD4<sup>+</sup>Foxp3<sup>+</sup> T cells than CD4+littermate vehicle mice after 11-weeks (Figure 4-11B). Both CD4+TS1P<sub>1</sub>KO vehicle and CD4+TS1P<sub>1</sub>KO STZ mice had reduced CD4<sup>+</sup>Foxp3<sup>+</sup> T cells than CD4+littermate vehicle and CD4+littermate STZ mice, respectively, at the end of 11-weeks (Figure 4-11B). In blood, there was no significant difference between CD4<sup>+</sup>Foxp3<sup>+</sup> T cells numbers between groups after CD4<sup>+</sup> T cells transfer (Figure 4-11B). Although in CD4+TS1P<sub>1</sub>KO vehicle mice had 2.63-fold increased CD4<sup>+</sup>Foxp3<sup>+</sup> T cells in blood than TS1P<sub>1</sub>KO vehicle mice without CD4<sup>+</sup> T cells transfer (Table 4-6).

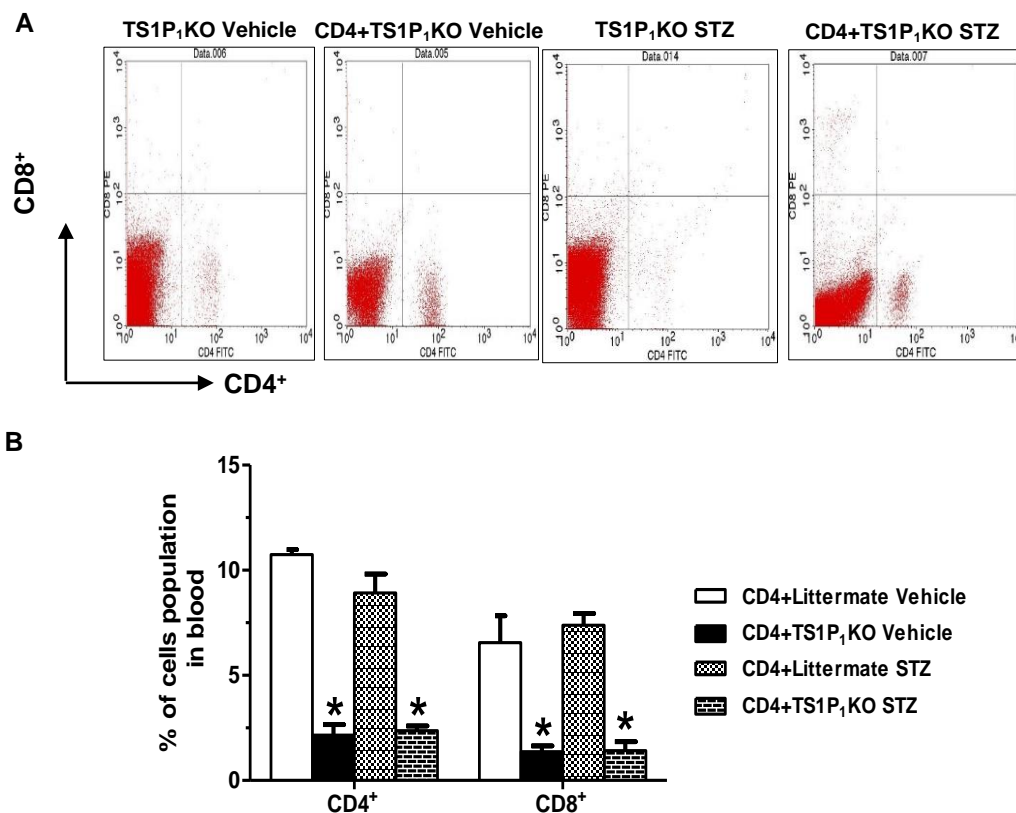


**Figure 4-9:** Quantification data of CD4<sup>+</sup> and CD8<sup>+</sup> T cells number in blood of littermate and TS1P<sub>1</sub>KO mice after CD4<sup>+</sup> T cells transfer at the end of 11-weeks. **(A)**

Representative flow cytometry dot plot show increased CD4<sup>+</sup> T cells in lower right quadrant of TS1P<sub>1</sub>KO vehicle and STZ mice blood after CD4<sup>+</sup> T cells transfer compared to TS1P<sub>1</sub>KO vehicle and STZ mice, respectively, without CD4<sup>+</sup> T cells transfer at the end of 11-weeks. **(B)** Quantification of flow cytometry data of CD4<sup>+</sup> and CD8<sup>+</sup> T cells in CD4<sup>+</sup> T cells recipient mice blood after 11-weeks. \*P<0.05 between CD4+littermate vehicle and CD4+TS1P<sub>1</sub>KO vehicle mice, and CD4+littermate STZ and CD4+TS1P<sub>1</sub>KO STZ mice, n = 3-4 mice per group. The data is expressed as mean ± SEM.

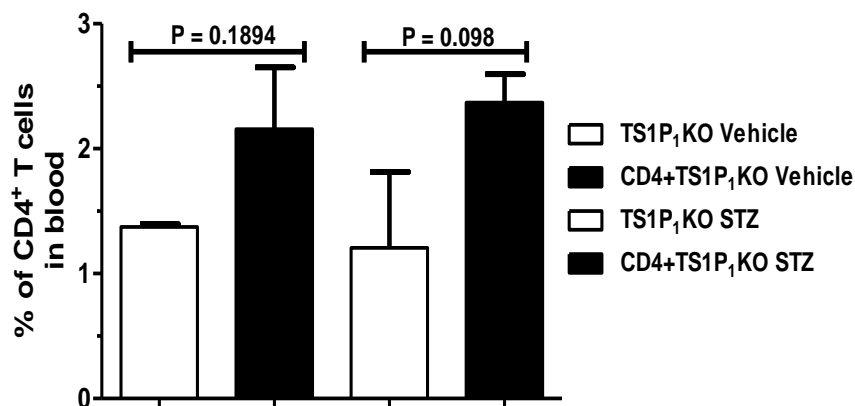


**Figure 4-10:** Comparison of CD4<sup>+</sup> T cells number in blood between CD4<sup>+</sup> T cells recipient TS1P<sub>1</sub>KO mouse groups and TS1P<sub>1</sub>KO mouse groups without CD4<sup>+</sup> T cells transfer at the end of 11-weeks. After CD4<sup>+</sup> T cells transfer both TS1P<sub>1</sub>KO vehicle and TS1P<sub>1</sub>KO STZ mice exhibited increased number of CD4<sup>+</sup> T cells in blood at the end of 11 weeks compared to TS1P<sub>1</sub>KO vehicle and TS1P<sub>1</sub>KO STZ mice without CD4<sup>+</sup> T cells transfer. The data is expressed as mean  $\pm$  SEM.  $P = 0.1894$  between TS1P<sub>1</sub>KO vehicle and CD4+TS1P<sub>1</sub>KO vehicle mice, and  $P = 0.098$  between TS1P<sub>1</sub>KO STZ and CD4+TS1P<sub>1</sub>KO STZ mice,  $n = 3-4$  mice per group.

**Table 4-5:** Summary of CD4<sup>+</sup> T cells number in blood of TS1P<sub>1</sub>KO mouse groups without- and with- CD4<sup>+</sup> T cells transfer after 11-weeks.

<b>Groups</b>	<b>CD4<sup>+</sup> T cells in blood (% of cell populations)</b>
TS1P <sub>1</sub> KO Vehicle (n=3)	1.37±0.02
CD4+TS1P <sub>1</sub> KO Vehicle (n=3)	2.16±0.50 (36.57% increase, P =0.1894)
TS1P <sub>1</sub> KO STZ (n=3)	1.21±0.61
CD4+TS1P <sub>1</sub> KO STZ (n=4)	2.37±0.23 (48.95% increase, P =0.098)

The data is expressed as mean ± SEM. ‘n’ value represents number of mice in each group. P = 0.1894 between TS1P<sub>1</sub>KO vehicle and CD4+TS1P<sub>1</sub>KO vehicle mice, and P = 0.098 between TS1P<sub>1</sub>KO STZ and CD4+TS1P<sub>1</sub>KO STZ mice, n = 3-4 mice per group.

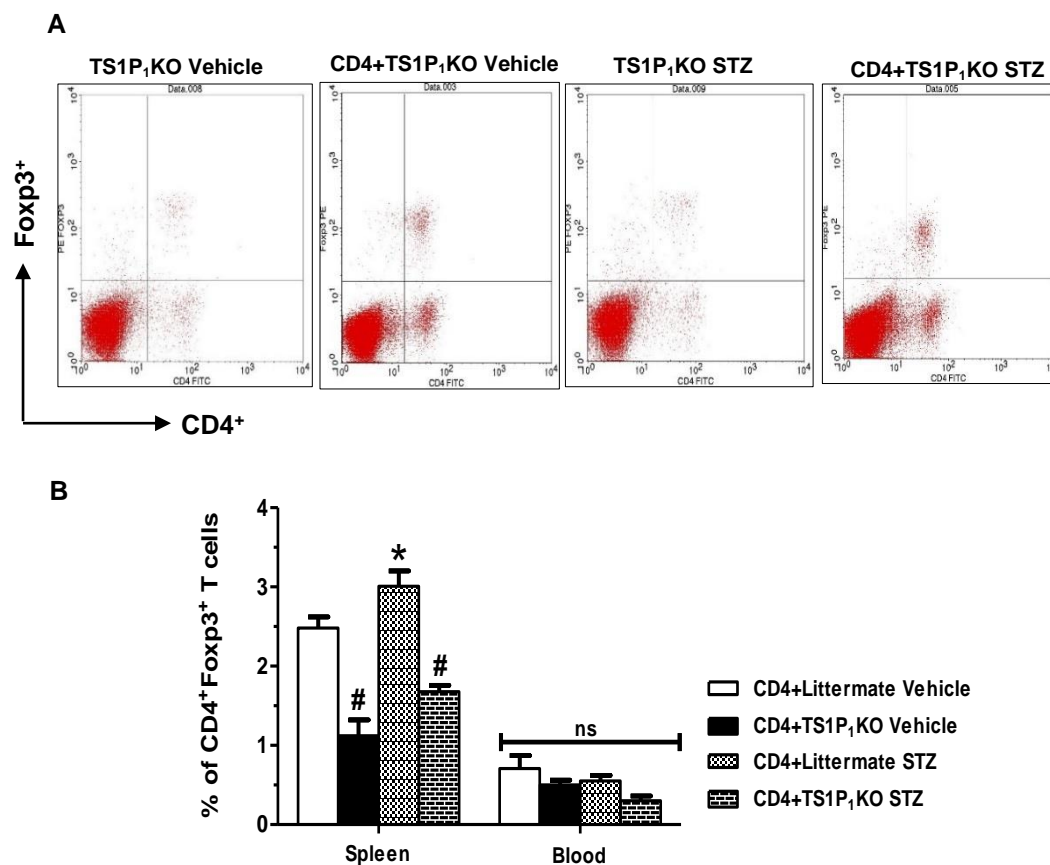


**Figure 4-11:** Quantification data of CD4<sup>+</sup>Foxp3<sup>+</sup> T cells number in spleen and blood of littermate and TS1P<sub>1</sub>KO mice after CD4<sup>+</sup> T cells transfer at the end of 11-week experimental period. **(A)** Representative flow cytometry dot plot show noticeable increase in CD4<sup>+</sup> T cells (lower right quadrant) and CD4<sup>+</sup>Foxp3<sup>+</sup> T cells (upper right quadrant) presence in TS1P<sub>1</sub>KO vehicle and STZ mice spleen after CD4<sup>+</sup> T cells transfer compared to TS1P<sub>1</sub>KO vehicle and STZ mice, respectively, without CD4<sup>+</sup> T cells transfer at the end of 11-weeks. **(B)** Quantification of flow cytometry data of CD4<sup>+</sup>Foxp3<sup>+</sup> T cells in CD4<sup>+</sup> T cells recipient mice spleen and blood after 11-weeks. \*P<0.05 between CD4+littermate vehicle and CD4+littermate STZ mice, and #P < 0.05 between CD4+littermate vehicle and CD4+TS1P<sub>1</sub>KO vehicle, and CD4+littermate STZ and CD4+TS1P<sub>1</sub>KO STZ mice, n = 4-5 mice per group. The data is expressed as mean ± SEM.

**Table 4-6:** Summary of CD4<sup>+</sup>Foxp3<sup>+</sup> T cells number in spleen and blood of TS1P<sub>1</sub>KO mouse groups without- and with- CD4<sup>+</sup> T cells transfer after 11-weeks.

<b>Groups</b>	<b>CD4<sup>+</sup>Foxp3<sup>+</sup> T cells (% of cell populations)</b>
<b>Spleen</b>	
TS1P <sub>1</sub> KO Vehicle (n=3)	0.67±0.12
CD4+TS1P <sub>1</sub> KO Vehicle (n=5)	1.12±0.20 (40.18% increase, P=0.16)
TS1P <sub>1</sub> KO STZ (n=3)	1.38±0.37
CD4+TS1P <sub>1</sub> KO STZ (n=4)	1.68±0.08 (17.86% increase, P=0.40)
<b>Blood</b>	
TS1P <sub>1</sub> KO Vehicle (n=3)	0.19±0.03
CD4+TS1P <sub>1</sub> KO Vehicle (n=4)	0.50±0.06 (62% increase, *P<0.05)
TS1P <sub>1</sub> KO STZ (n=3)	0.42±0.18
CD4+TS1P <sub>1</sub> KO STZ (n=4)	0.30±0.06

CD4<sup>+</sup> T cells recipient TS1P<sub>1</sub>KO vehicle and TS1P<sub>1</sub>KO STZ mice showed increased CD4<sup>+</sup>Foxp3<sup>+</sup> T cells in spleen compared to TS1P<sub>1</sub>KO vehicle and TS1P<sub>1</sub>KO STZ mice, respectively, without CD4<sup>+</sup> T cells transfer. CD4<sup>+</sup> T cells recipient TS1P<sub>1</sub>KO vehicle mice showed increased CD4<sup>+</sup>Foxp3<sup>+</sup> T cells in blood compared to TS1P<sub>1</sub>KO vehicle without CD4<sup>+</sup> T cells transfer. P values calculated through two-tailed student's t-test. The data is expressed as mean ± SEM. The value of 'n' represents number of mice in each group.

#### **4.3.4. CD4<sup>+</sup> T cells transfer exacerbates cardiac disorganization in TS1P<sub>1</sub>KO mice under diabetes**

We prepared Hematoxylin and Eosin (H&E) stained heart sections after 11-week experimental period. H&E stained sections were examined microscopically and graded based on cardiomyocyte morphology, organization, degree of cellularity in interstitial space, myocyte loss, and presence of collagen fibers in interstitial space. CD4<sup>+</sup> T cells recipient TS1P<sub>1</sub>KO STZ mice (CD4<sup>+</sup>TS1P<sub>1</sub>KO STZ, n=4) hearts showed exacerbated myocytes organization with discernible disarray compared to TS1P<sub>1</sub>KO STZ mice without CD4<sup>+</sup> T cells transfer (cumulative heart histology score: 9.25±0.95 vs. 3±0.58, \*P < 0.05) (Figure 4-12A, 4-12B and 4-13A, 4-13B). Noticeably, CD4<sup>+</sup> T cells recipient TS1P<sub>1</sub>KO vehicle mice (n=5) showed improved heart histology compared to TS1P<sub>1</sub>KO vehicle mice without CD4<sup>+</sup> T cells transfer (n=4) (3±0.76 vs. 9.5±0.87, \*P < 0.05) (Figure 4-12A, 4-12B and 4-13A, 4-13B).

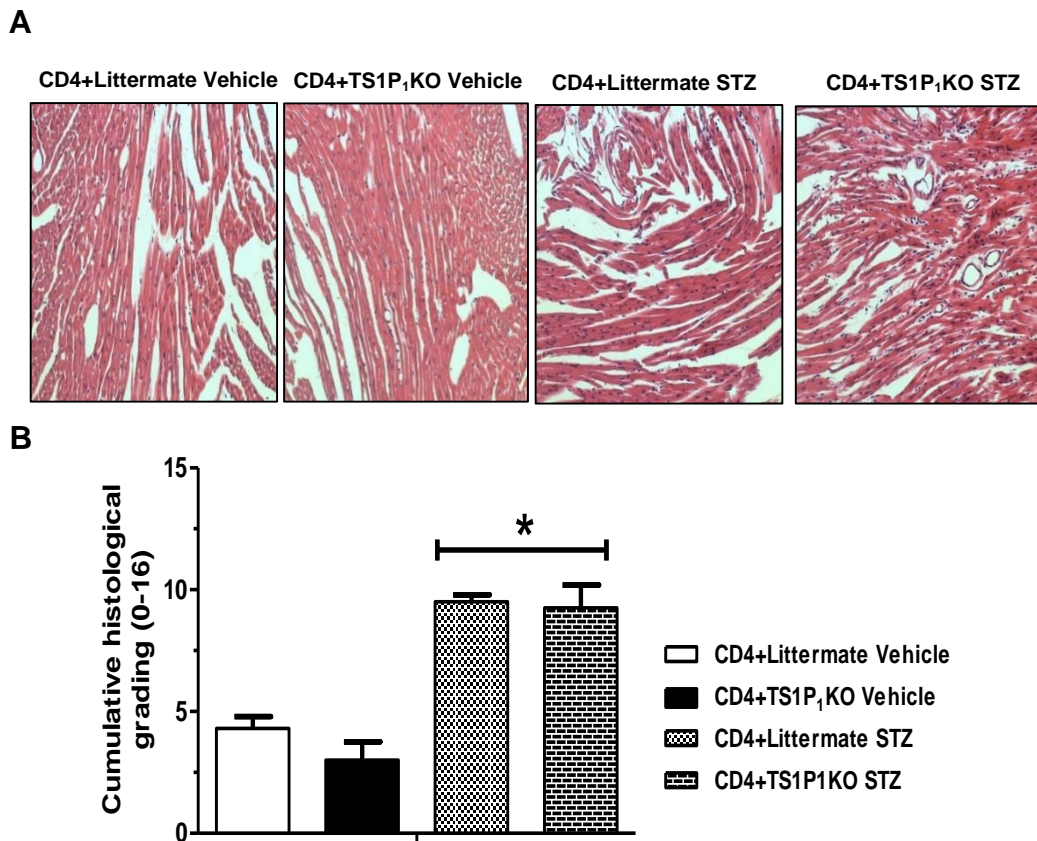


**Figure 4-12:** Heart histology study in H&E stained sections of CD4<sup>+</sup> T cells recipient littermate and TS1P<sub>1</sub>KO mice after 11-week experimental period. **(A)** Diabetic CD4+littermate STZ and CD4+TS1P<sub>1</sub>KO STZ mice heart sections showed discernible disorganization of myocytes in myocardium after 11-week diabetes period. TS1P<sub>1</sub>KO mice vehicle heart sections exhibited improved heart histology under diabetes after CD4<sup>+</sup> T cells transfer. The magnification is 200x. **(B)** Bar graphs represents cumulative heart histology score of littermate and TS1P<sub>1</sub>KO mice heart sections after CD4<sup>+</sup> T cells transfer at the end of 11-weeks. \*P<0.05 between CD4+littermate vehicle and CD4+littermate STZ mice, and between CD4+TS1P<sub>1</sub>KO vehicle and CD4+TS1P<sub>1</sub>KO STZ mice. The data is expressed as mean ± SEM, n = 4-5 mice in each group.

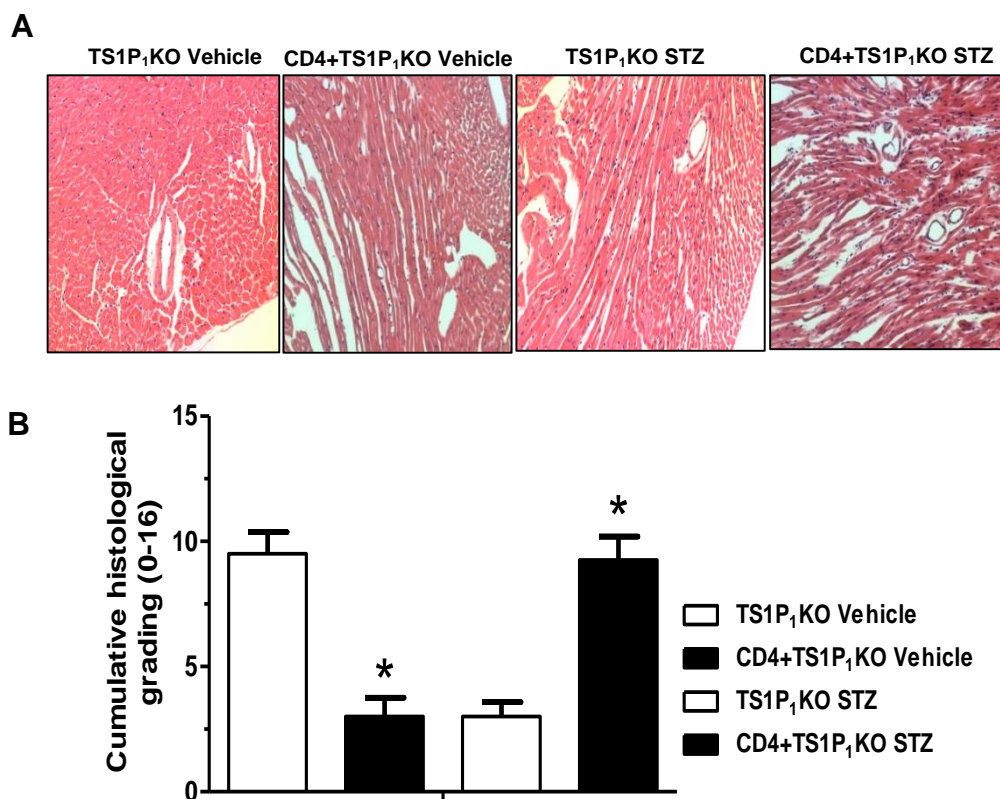


**Figure 4-13:** Comparison between TS1P<sub>1</sub>KO mouse groups heart histology in H&E stained sections without- and with CD4<sup>+</sup> T cells transfer. **(A)** Representative H&E stained heart sections images (magnification is 200x). Diabetic CD4<sup>+</sup> TS1P<sub>1</sub>KO STZ mice heart sections showed discernible disorganization of myocytes in myocardium after 11-week diabetes period compared to TS1P<sub>1</sub>KO STZ mice without CD4<sup>+</sup> T cells transfer. In contrast, TS1P<sub>1</sub>KO vehicle mice heart sections exhibited improved heart histology under diabetes after CD4<sup>+</sup> T cells transfer compared to TS1P<sub>1</sub>KO vehicle mice without CD4<sup>+</sup> T cells transfer. **(B)** Quantification of cumulative heart histology score of TS1P<sub>1</sub>KO mice heart sections at the end of 11-weeks. \*P<0.05 between CD4<sup>+</sup> TS1P<sub>1</sub>KO vehicle and TS1P<sub>1</sub>KO vehicle mice, and between CD4<sup>+</sup>TS1P<sub>1</sub>KO STZ and TS1P<sub>1</sub>KO STZ mice. The data is expressed as mean ± SEM, n = 4-7 mice in each group.

#### **4.3.5. CD4<sup>+</sup> T cells transfer increases fibrosis area in TS1P<sub>1</sub>KO diabetic mice**

We assessed fibrosis area in Tri-chrome stained heart sections after 11-week diabetic period. CD4<sup>+</sup> T cells transfer to TS1P<sub>1</sub>KO mice exacerbated fibrotic area in diabetic TS1P<sub>1</sub>KO STZ mice (n=4) compared to TS1P<sub>1</sub>KO STZ mice (n=7) without CD4<sup>+</sup> T cells transfer (37.11±3.22 % vs. 11.86±4.34 %, \*P < 0.05) (Figure 4-14A, 4-14B, 4-15A and 4-15B). Notably, CD4<sup>+</sup> T cell recipient TS1P<sub>1</sub>KO vehicle mice (n=4) heart sections showed less fibrotic area compared to TS1P<sub>1</sub>KO vehicle mice (n=4) without CD4<sup>+</sup> T cells transfer (12.74±2.22 % vs. 46.03±7.60 %, \*P < 0.05) (Figure 4-14A, 4-14B, 4-15A and 4-15B).

#### **4.3.6. CD4<sup>+</sup> T cells transfer attenuates cardiac contractility in TS1P<sub>1</sub>KO diabetic mice**

We determined cardiac contractility in *ex-vivo* Langendorff heart perfusion system at the end of 11-weeks. The contractile force was expressed as fold change compared to littermate control mice. After CD4<sup>+</sup> T cells transfer, diabetic TS1P<sub>1</sub>KO mice had shown 22% lower contractile force compared to CD4<sup>+</sup>littermate control mice (P=0.57) (Figure 70). In contrast, TS1P<sub>1</sub>KO vehicle mice exhibited 47.09% higher contractile force after CD4<sup>+</sup> T cells transfer compared to CD4<sup>+</sup>littermate vehicle mice (\*P>0.05) (Figure 4-16).

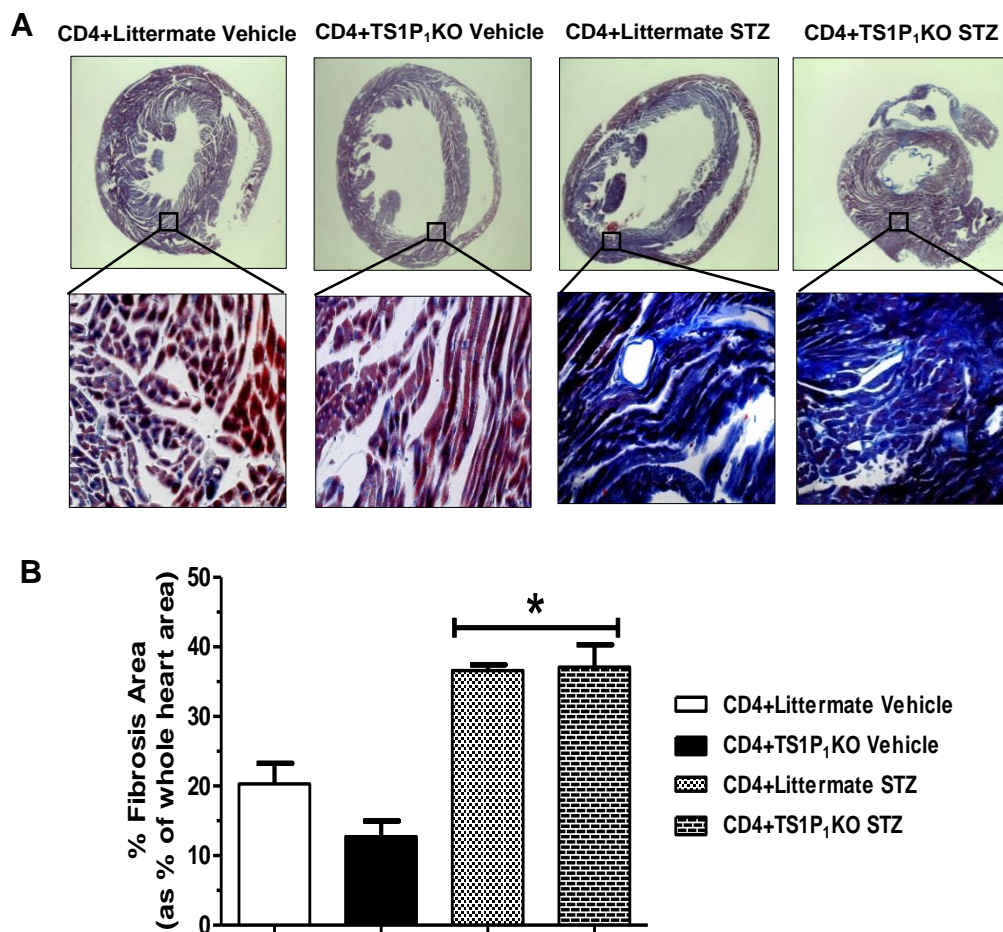


**Figure 4-14:** Fibrosis extent assessment in Trichrome stained heart sections of CD4<sup>+</sup> T cells recipient littermate and TS1P<sub>1</sub>KO mice after 11-weeks. **(A)** Upper panel represents whole heart sections (magnification 16x) and lower panel represents magnified section images (magnification 400x). CD4<sup>+</sup> T cells transfer enhanced perivascular and interstitial fibrosis area in diabetic TS1P<sub>1</sub>KO mice. Notably, CD4<sup>+</sup> T cells transfer to TS1P<sub>1</sub>KO vehicle mice, attenuates fibrosis area. **(B)** Quantification of percent fibrosis area. \*P<0.05 in CD4+littermate STZ vs. CD4+littermate vehicle mice, \*P<0.05 in CD4+TS1P<sub>1</sub>KO STZ vs. CD4+TS1P<sub>1</sub>KO vehicle mice. The data is expressed as mean ± SEM. n = 4 mice in each group.

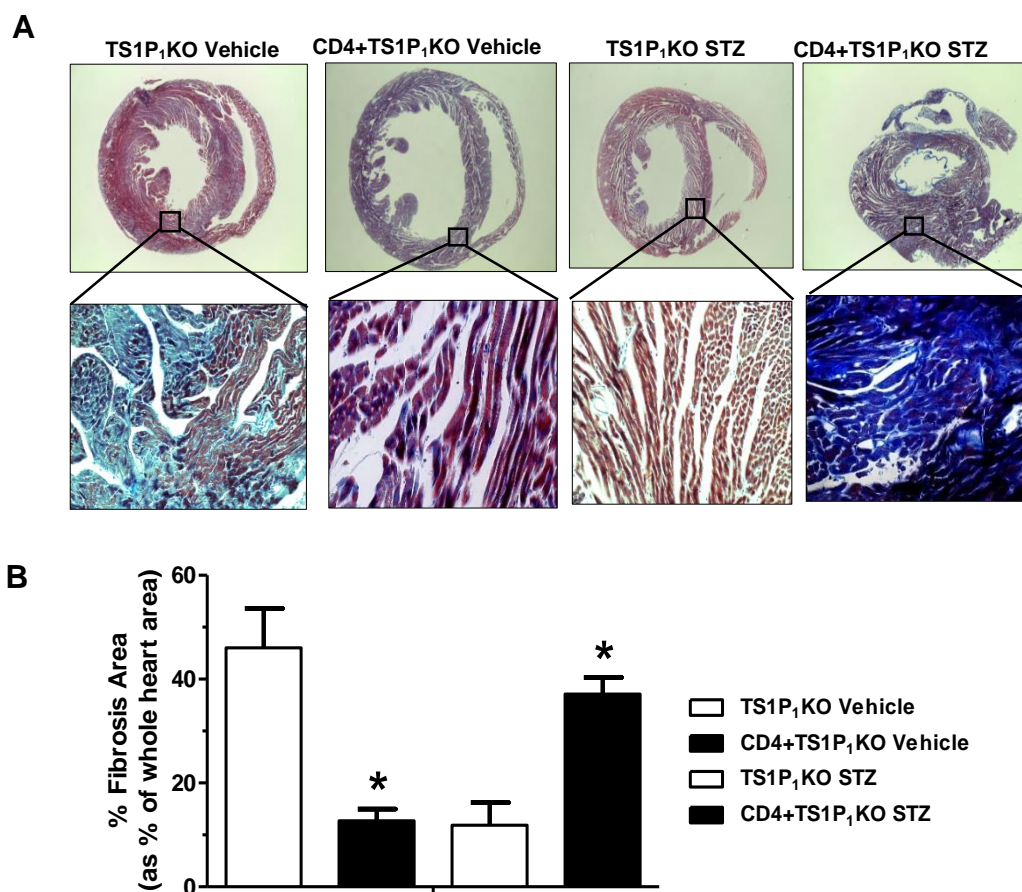


**Figure 4-15:** Comparison between TS1P<sub>1</sub>KO mouse groups fibrosis extent in Masson's Trichrome stained heart sections without- and with CD4<sup>+</sup> T cells transfer. **(A)** Diabetic CD4<sup>+</sup> TS1P<sub>1</sub>KO STZ mice heart sections exhibited enhanced fibrosis after 11-week diabetic period compared to TS1P<sub>1</sub>KO STZ mice without CD4<sup>+</sup> T cells transfer. In contrast, TS1P<sub>1</sub>KO vehicle mice heart sections exhibited attenuated fibrosis area after CD4<sup>+</sup> T cells transfer compared to TS1P<sub>1</sub>KO vehicle mice without CD4<sup>+</sup> T cells transfer. **(B)** Quantification of fibrosis area in TS1P<sub>1</sub>KO mice heart sections. \*P<0.05 in CD4<sup>+</sup> TS1P<sub>1</sub>KO vehicle and TS1P<sub>1</sub>KO vehicle mice, and in CD4<sup>+</sup>TS1P<sub>1</sub>KO STZ and TS1P<sub>1</sub>KO STZ mice. The data is expressed as mean ± SEM, n = 4-7 mice in each group.

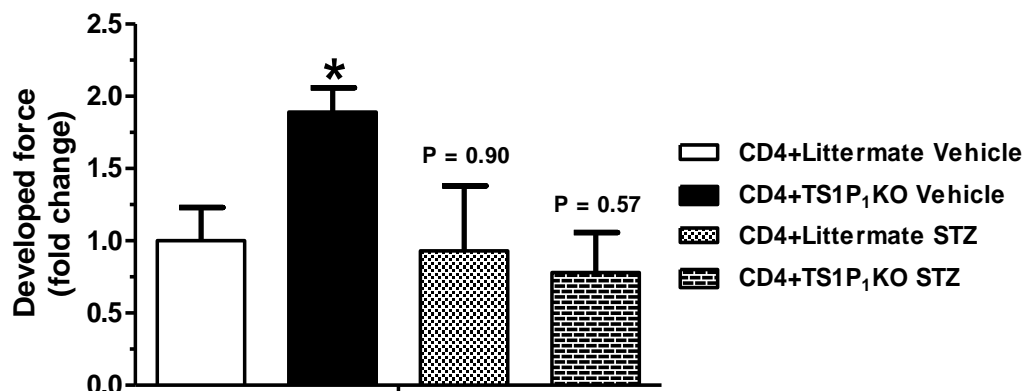


**Figure 4-16:** Cardiac contractile force in CD4<sup>+</sup> T cells recipient littermate and TS1P<sub>1</sub>KO mice after 11-week study period. CD4<sup>+</sup> T cells recipient TS1P<sub>1</sub>KO STZ mice showed reduced cardiac contractile force compared to CD4+littermate vehicle mice (P=0.57). In contrast, CD4<sup>+</sup> T cells recipient TS1P<sub>1</sub>KO vehicle mice exhibited increased contractility compared to CD4+littermate vehicle mice. The data is expressed as mean ± SEM.

Sample size, n=3 mice in each group.

#### **4.3.7. Increased infiltration of CD3<sup>+</sup> T cells in TS1P<sub>1</sub>KO mouse hearts after reconstitution of CD4<sup>+</sup> T cells**

We detected CD3<sup>+</sup> T cells in heart tissue by immunostaining with mouse monoclonal CD3 antibody and counted the infiltrated CD3<sup>+</sup> T cells in 30 high magnification fields (400x) for each heart sections (Figure 4-17). After CD4<sup>+</sup> T cells transfer, in both vehicle and STZ group of TS1P<sub>1</sub>KO mice showed increased CD3<sup>+</sup> T cells in myocardium (vehicle: 1.56±0.06 cells/field vs. 0.97±0.08 cells/field, \*P < 0.05, and STZ: 1.84±0.05 cells/field vs. 0.84±0.09 cells/field, n=3 independent experiments, #P < 0.05) than TS1P<sub>1</sub>KO vehicle and TS1P<sub>1</sub>KO STZ group, respectively, without CD4<sup>+</sup> T cells transfer (Figure 4-17, 4-18A and 4-18B).

#### **4.3.8. CD4<sup>+</sup> T cells recipient diabetic TS1P<sub>1</sub>KO mice heart show increased TGF beta 1 expression**

Transforming growth factor beta 1 expression was assessed in immunostained heart sections by computer assisted morphometric analysis. After CD4<sup>+</sup> T cell transfer, TS1P<sub>1</sub>KO STZ mice heart sections exhibited increased TGF-β1 expression (5.45±0.08 % staining area vs. 3.54±0.10 % staining area, #P < 0.05, n= 3 experiments as compared to TS1P<sub>1</sub>KO STZ without CD4<sup>+</sup> T cells transfer (Figure 4-19, 4-20A and 4-20B). In contrast, TGF-β1 expression was reduced in TS1P<sub>1</sub>KO vehicle mice after CD4<sup>+</sup> T cells transfer (2.78±0.15 % staining area vs. 6.78±0.71 % staining area, \*P < 0.05, n= 3 experiments compared to TS1P<sub>1</sub>KO vehicle mice without CD4<sup>+</sup> T cells transfer (Figure 4-19, 4-20A and 4-20B).

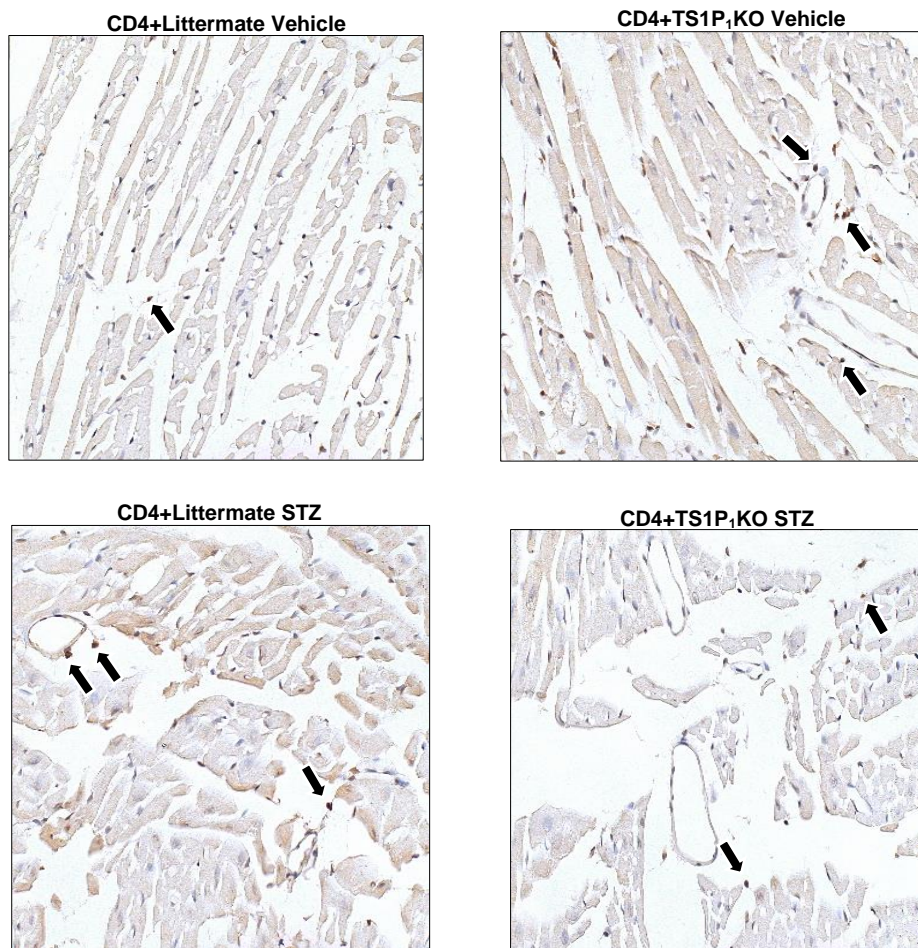


**Figure 4-17:** Immunohistochemical detection of CD3<sup>+</sup> T cells in CD4<sup>+</sup> T cells recipient littermate and TS1P<sub>1</sub>KO mice heart sections at the end of 11-weeks. CD4<sup>+</sup> T cells recipient TS1P<sub>1</sub>KO vehicle and TS1P<sub>1</sub>KO STZ mice heart sections have increased infiltration of CD3<sup>+</sup> T cells after 11-week of experimental period compared to littermate vehicle mice. Images are representative of three independent experiments. The magnification is 400x.

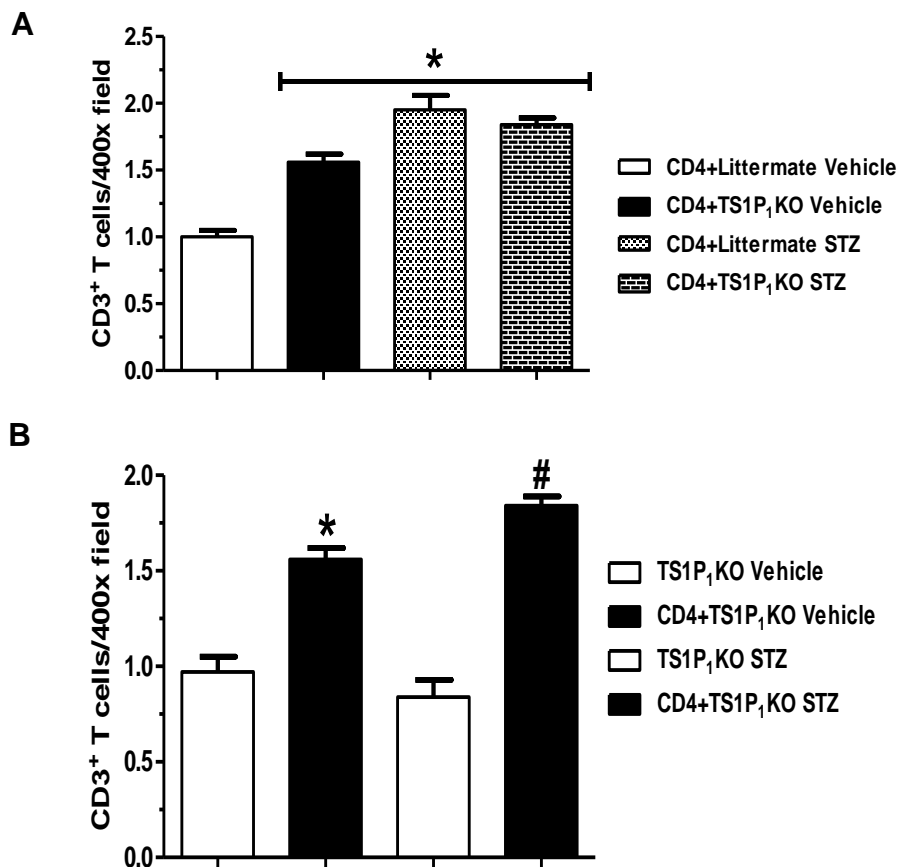


**Figure 4-18:** Quantification of infiltrated CD3<sup>+</sup> T cells in myocardium of CD4<sup>+</sup> T cells recipient littermate and TS1P<sub>1</sub>KO mice. **(A)** CD3<sup>+</sup> T cells number (cells per 400x magnification field) was significantly higher in TS1P<sub>1</sub>KO vehicle and TS1P<sub>1</sub>KO STZ mice heart section compared to CD4+littermate vehicle mice. \*P < 0.05 compared to CD4+littermate vehicle mice. **(B)** Comparison of CD3<sup>+</sup> T cells number in cardiac tissue between TS1P<sub>1</sub>KO mice with CD4<sup>+</sup> T cells transfer and TS1P<sub>1</sub>KO without CD4<sup>+</sup> T cells transfer. \*P<0.05 compared to TS1P<sub>1</sub>KO vehicle mice, #P<0.05 compared to TS1P<sub>1</sub>KO STZ mice. Results are from three independent experiments. The data is expressed as mean ± SEM.

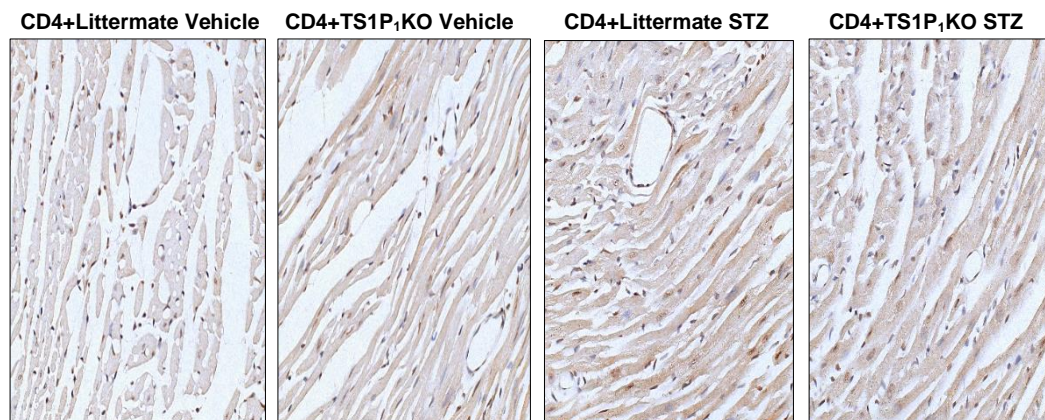


**Figure 4-19:** Immunohistochemical assessment of TGF beta 1 (TGF- $\beta$ 1) expression in CD4<sup>+</sup> T cells recipient littermate and TS1P<sub>1</sub>KO mice heart sections at the end of 11-weeks. CD4<sup>+</sup> T cells recipient TS1P<sub>1</sub>KO vehicle and TS1P<sub>1</sub>KO STZ mice heart sections have increased TGF- $\beta$ 1 expression after 11-week of experimental period as compared to littermate vehicle mice. Images are representative of three independent experiments. The magnification is 400x.

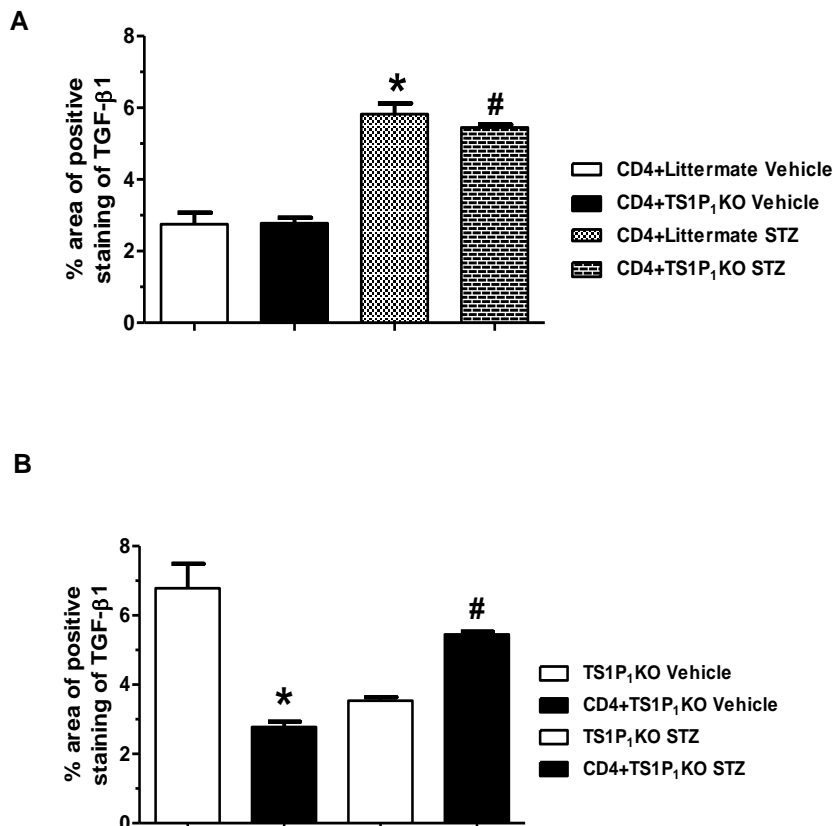


**Figure 4-20:** Quantification of TGF- $\beta$ 1 expression in myocardium of CD4<sup>+</sup> T cells recipient littermate and TS1P<sub>1</sub>KO mice. **(A)** TGF- $\beta$ 1 expression was significantly higher in littermate STZ (\*P<0.05) and TS1P<sub>1</sub>KO STZ (#P<0.05) mice heart section compared to CD4+littermate vehicle mice. TS1P<sub>1</sub>KO vehicle mice heart sections exhibited reduced TGF- $\beta$ 1 expression after CD4<sup>+</sup> T cell transfer. **(B)** Comparison of TGF- $\beta$ 1 expression in cardiac tissue between TS1P<sub>1</sub>KO mice with CD4<sup>+</sup> T cells transfer and TS1P<sub>1</sub>KO mice without CD4<sup>+</sup> T cells transfer. \*P<0.05 compared to TS1P<sub>1</sub>KO vehicle mice, #P<0.05 compared to TS1P<sub>1</sub>KO STZ mice. Results are from three independent experiments. The data is expressed as mean  $\pm$  SEM.

#### **4.3.9. CD4<sup>+</sup> T cells recipient diabetic TS1P<sub>1</sub>KO mice heart exhibited increased CD34 expression**

We evaluated CD34 expression by immunostaining in heart sections through computer assisted morphometric analysis. After CD4<sup>+</sup> T cells transfer TS1P<sub>1</sub>KO diabetic myocardium exhibited increased CD34 expression (5.53±0.33 % staining area vs. 2.97±0.17 % staining area, #P < 0.05, n= 3 experiments) than diabetic TS1P<sub>1</sub>KO mice without CD4<sup>+</sup> T cells transfer (Figure 4-21, 4-22A and 4-22B). Remarkably, CD4<sup>+</sup> T cells transfer reduced CD34 expression in TS1P<sub>1</sub>KO vehicle mice (2.77±0.43 % staining area vs. 6.52±0.47 % staining area, #P < 0.05, n= 3 experiments) than TS1P<sub>1</sub>KO vehicle mice without CD4<sup>+</sup> T cells transfer (Figure 4-21, 4-22A and 4-22B).

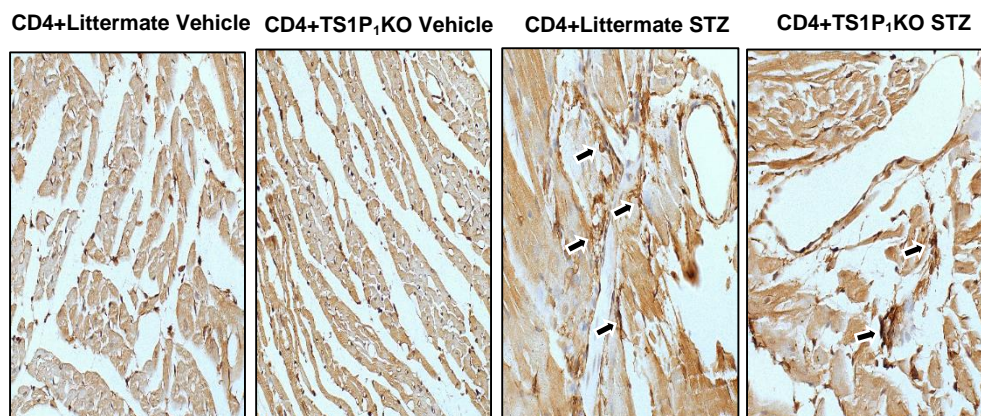


**Figure 4-21:** Immunohistochemical assessment of CD34 expression in CD4<sup>+</sup> T cells recipient littermate and TS1P<sub>1</sub>KO mice heart sections at the end of 11-weeks. (A) CD4<sup>+</sup> T cells recipient TS1P<sub>1</sub>KO STZ mice heart sections have increased CD34 expression after 11-week of experimental period. In contrast, CD4<sup>+</sup> T cells recipient TS1P<sub>1</sub>KO vehicle mice exhibited reduced CD34 expression in their myocardium. Images are representative of three independent experiments. The magnification is 400x.

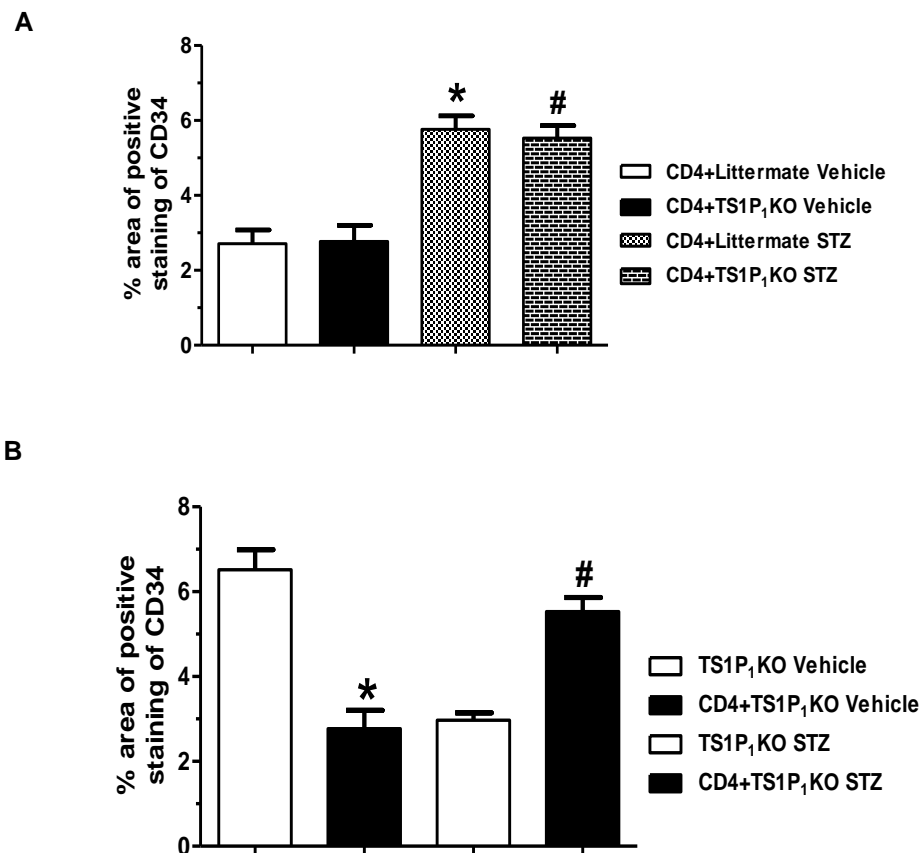


**Figure 4-22:** Quantification of CD34 expression in myocardium of CD4<sup>+</sup> T cells

recipient littermate and TS1P<sub>1</sub>KO mice. **(A)** CD34 expression was significantly higher in littermate STZ (\*P<0.05) and TS1P<sub>1</sub>KO STZ (#P<0.05) mice heart section compared to CD4+littermate vehicle mice. TS1P<sub>1</sub>KO vehicle mice heart sections exhibited reduced CD34 expression after CD4<sup>+</sup> T cells transfer. **(B)** Comparison of CD34 expression in cardiac tissue between TS1P<sub>1</sub>KO mice with CD4<sup>+</sup> T cells transfer and TS1P<sub>1</sub>KO mice without CD4<sup>+</sup> T cells transfer. \*P<0.05 compared to TS1P<sub>1</sub>KO vehicle mice, #P<0.05 compared to TS1P<sub>1</sub>KO STZ mice. Results are from three independent experiments. The data is expressed as mean ± SEM.

#### 4.4. Discussion

In this part of dissertation, we demonstrated that adoptive transfer of CD4<sup>+</sup> T cells from littermate mice to T cell specific S1P receptor 1 knockout (TS1P<sub>1</sub>KO) mice causes exacerbation in cardiac histology and augmentation of fibrosis area in TS1P<sub>1</sub>KO mice under long term diabetes. We found that CD4<sup>+</sup> T cells transfer to TS1P<sub>1</sub>KO mice increases infiltrating CD3<sup>+</sup> T cells number into myocardium that is associated with enhanced pro-fibrotic molecular (TGF-β1) and cellular (CD34) moieties expression in myocardium of TS1P<sub>1</sub>KO mice under chronic hyperglycemia.

In chapter 3, we have shown that T cell specific S1P receptor 1 genetic depletion results in profound deficiency of CD4<sup>+</sup> helper T cells and CD8<sup>+</sup> cytotoxic T cells in blood of TS1P<sub>1</sub>KO mice compared to littermate mice. We have demonstrated that TS1P<sub>1</sub>KO mice heart under long term streptozotocin (STZ)-induced type 1 diabetes exhibits cardioprotection and shows attenuated collagen deposition in myocardium with improved cardiac contractility compared to littermate diabetic mice. T lymphocytes under cardiac injury and inflammation, such as, myocardial infarction, hypertension, myocarditis, infiltrate in to the myocardium and participate in cardiac fibrotic remodeling and heart failure.<sup>36,73</sup> Thus, we evaluated the infiltrating CD3<sup>+</sup> T cells number in myocardium of diabetic littermate and TS1P<sub>1</sub>KO mice after 11-week experimental period. We have found that TS1P<sub>1</sub>KO mice heart tissue exhibited significantly less CD3<sup>+</sup> T cells invasion under chronic diabetes compared to littermate diabetic mice. Cardiac fibrosis is a complex, multifactorial, dynamic process in which diverse cellular and molecular interactions are involved.<sup>49,157,158</sup> We, therefore, evaluated the expression of transforming growth factor beta 1 (TGF-β1) and CD34 expressing fibrocytes infiltration into the

myocardium of littermate and TS1P<sub>1</sub>KO mice after 11-week experimental period. Our immunohistochemical studies showed that TGF- $\beta$ 1 and CD34 expressing cells expression were reduced markedly in diabetic TS1P<sub>1</sub>KO mice compared to diabetic littermate mice. Enhanced myocardial fibrosis causes ventricular wall stiffening, which underlies diastolic dysfunction with subsequent systolic dysfunction, if unresolved.<sup>46,159</sup> Therefore, we also evaluated the cardiac force of contraction in *ex-vivo* Langendorff's heart perfusion system in littermate and TS1P<sub>1</sub>KO mice after 11-weeks. We found that cardiac contractility was improved in diabetic TS1P<sub>1</sub>KO mice compared to diabetic littermate mice. Therefore, we demonstrated that genetic depletion of T cell S1P<sub>1</sub> receptor in mice results in circulatory T lymphocytes deficiency that is associated with cardioprotection and improved cardiac function in chronic diabetes. To this end, in this part of dissertation we further extended our investigation to evaluate the effects of naïve CD4<sup>+</sup> T cells transfer from littermate mice to TS1P<sub>1</sub>KO mice in context of cardioprotection and cardiac fibrosis under chronic hyperglycemia.

Among the two main subsets of T lymphocytes, CD4<sup>+</sup> helper T cells and CD8<sup>+</sup> cytotoxic T cells, CD4<sup>+</sup> helper T cells have been reported to be involved in fibrotic remodeling in different organs, including heart, lungs, kidney and liver.<sup>36,150,160,161,162</sup> CD4<sup>+</sup> T cells participate in fibrosis generation through several distinct molecular pathways, such as secretion of inflammatory cytokines that can stimulate collagen producing fibroblasts, increasing collagen cross-linking enzymes activity, such as lysyl oxidase (LOX) in heart tissue.<sup>70,163,164</sup> Enhancement of T helper subset 1 (T<sub>H</sub>1) cells increased total cardiac collagen content and cross-linked collagen in C57BL/6 mice heart, whereas in a hypertensive disease model T<sub>H</sub>2 cytokine predominant BALB/c mice

exhibited increased cardiac collagen content with augmented ventricular stiffness.<sup>69,70,72</sup> T<sub>H</sub>1 cytokine IFN- $\gamma$  and T<sub>H</sub>2 cytokine IL-4 have been shown to increase collagen cross-linking enzyme LOX activity in heart in normal physiological and inflammatory conditions, respectively.<sup>69,70,72,73</sup> In pressure overload transverse aortic constriction (TAC) murine model, mature lymphocytes lacking Rag2 knock-out (KO) mice heart tissue exhibited less LOX expression with attenuated fibrosis area after 6-week of TAC induction.<sup>75</sup> Splenic  $2 \times 10^7$  CD3<sup>+</sup> T cells from wild-type C57BL/6 mice to Rag2KO mice increases LOX enzyme expression and fibrotic area in heart sections substantially after TAC induction compared to only buffer recipient Rag2KO mice.<sup>75</sup> In another recent report, antibody induced neutralization of CD3 T cells activity showed cardioprotection in TAC induced heart failure model of mice as manifested by reduced fibrosis area and improved left ventricular function compared to only isotype treated mice after 4-weeks.<sup>76</sup> In TAC induced cardiac injury model, recruitment of T lymphocytes has been implicated with increased expression of adhesion molecules, such as ICAM-1, in cardiac endothelial cells.<sup>76</sup> Several approaches including T lymphocytes depletion and neutralization of T cells activation have been tested experimentally to protect heart from T cell invasion under chronic injury in order to reduce fibrosis.<sup>157</sup> To this end, in chapter 3, we for the first time showed that genetic depletion of T cell specific S1P<sub>1</sub> receptor induced altered T lymphocytes trafficking in systemic circulation associated with cardioprotection and reduction in fibrosis area under chronic hyperglycemia. However, the type of T lymphocytes important in cardiac fibrogenesis in diabetes associated hyperglycemia is not known decisively, and our studies in chapter 3 also did not elucidate the role of specific subset of T cells in diabetic myocardial fibrogenesis. To this end, in the present

study we showed that CD4<sup>+</sup> T cells reconstitution in TS1P<sub>1</sub>KO mice reverses the observed cardioprotection and antifibrotic effect under chronic diabetes.

In TS1P<sub>1</sub>KO mice, T lymphocytes have depleted S1P<sub>1</sub> expression due to T cell specific lymphocyte tyrosine kinase (Lck) promoter driven Cre-mediated recombination in coding region of S1P<sub>1</sub> gene.<sup>83</sup> S1P receptor 1 plays important role in T lymphocytes egress from primary and secondary lymphoid organs to circulation.<sup>85</sup> Genetic deficiency of S1P<sub>1</sub> in T cells inhibits T cells egress from lymphoid organs and sequesters them in primary lymphoid organ thymus.<sup>83</sup> Accordingly in chapter 3, we have shown that marked reduction of CD3<sup>+</sup> T cells in spleen and CD4<sup>+</sup>, CD8<sup>+</sup> T cells in blood of TS1P<sub>1</sub>KO mice. In the present chapter, we isolated CD4<sup>+</sup> T cells from littermate mice spleen and intravenously transferred to TS1P<sub>1</sub>KO mice. Our flow cytometry analysis showed 1.58-fold and 1.95-fold increase of CD4<sup>+</sup> T cells in blood of TS1P<sub>1</sub>KO vehicle and TS1P<sub>1</sub>KO STZ mice, respectively, compared to TS1P<sub>1</sub>KO vehicle and TS1P<sub>1</sub>KO STZ mice without CD4<sup>+</sup> T cells transfer after 11-weeks. CD4<sup>+</sup>Foxp3<sup>+</sup> T cells number also increased in spleen of both TS1P<sub>1</sub>KO vehicle and TS1P<sub>1</sub>KO STZ mice as measured after 11-week than without CD4<sup>+</sup> T cells transfer TS1P<sub>1</sub>KO vehicle and TS1P<sub>1</sub>KO STZ mice. Together the data indicate successful reconstitution of littermate CD4<sup>+</sup> T cells in to TS1P<sub>1</sub>KO mice in our present work. At the end of 11-week STZ-induced diabetic period, CD4<sup>+</sup> T cells recipient diabetic TS1P<sub>1</sub>KO STZ mice heart exhibited marked myocyte disorganization with increased interstitial and perivascular fibrosis, and reduced cardiac contractility compared to diabetic TS1P<sub>1</sub>KO mice without CD4<sup>+</sup> T cells transfer. Notably, diabetic TS1P<sub>1</sub>KO mice heart sections showed increased number of invading CD3<sup>+</sup> T cells number into myocardium compared to diabetic TS1P<sub>1</sub>KO mice without CD4<sup>+</sup> T cells

transfer at the end of 11-week diabetic period. Our immunohistological studies further revealed enhanced profibrotic TGF- $\beta$ 1 and CD34 expressing cells expression in diabetic TS1P<sub>1</sub>KO mice myocardium compared to diabetic TS1P<sub>1</sub>KO mice without CD4<sup>+</sup> T cells transfer. To this end, our findings revealed that CD4<sup>+</sup> T cells are an essential component in cardiac fibrogenesis under chronic hyperglycemia that provoke profibrotic molecular and cellular milieu in myocardium to increase fibrosis area leading to cardiac dysfunction.

Interestingly, administration of one million CD4<sup>+</sup> T cells into TS1P<sub>1</sub>KO vehicle mice increases CD4<sup>+</sup> T cells in circulation with increased presence of CD3<sup>+</sup> T cells in myocardium than TS1P<sub>1</sub>KO vehicle mice without CD4<sup>+</sup> T cells transfer. Strikingly, CD4<sup>+</sup> T cells recipient TS1P<sub>1</sub>KO vehicle mice myocardium showed reduced expression of TGF- $\beta$ 1 and CD34 expression with improved heart histology, reduced fibrosis area and significant improvement in cardiac contractility. In chapter 3, normoglycemic TS1P<sub>1</sub>KO vehicle mice myocardium showed exacerbated heart histology, increased fibrosis area and attenuated cardiac contractility whereas hyperglycemic TS1P<sub>1</sub>KO STZ mice myocardium showed cardioprotection with reduced fibrosis area and improved contractility. In present chapter, adoptive transfer of CD4<sup>+</sup> T cells to TS1P<sub>1</sub>KO mice reverses the cardioprotection in hyperglycemic TS1P<sub>1</sub>KO STZ mice and ameliorates fibrosis in normoglycemic TS1P<sub>1</sub>KO vehicle mice. These contrary results imply T lymphocytes have dual role in maintaining cardiac collagen homeostasis depending on the physiological conditions. TS1P<sub>1</sub>KO mice have reduced T lymphocytes in blood that increases circulatory B lymphocytes by two-fold as reported by Allende et al.<sup>83</sup> Notably, B lymphocytes generated auto-antibodies against heart derived antigens have been

implicated in cardiac dysfunction and fibrosis.<sup>146</sup> In this regard, it is noteworthy that in chapter 2 we found that diabetic Rag1 KO mice lacking both mature T and B lymphocytes exhibited reduced fibrosis area and improved cardiac contractility compared to diabetic wild-type C57BL/6 mice. Notably, normoglycemic Rag1 KO mice did not show enhanced fibrosis unlike in normoglycemic TS1P<sub>1</sub>KO vehicle mice heart. Hence, imbalance between T lymphocytes and B lymphocytes number in periphery could be a possible reason of increased fibrosis area in normoglycemic TS1P<sub>1</sub>KO vehicle mice heart. Increased presence of CD34 fibrocytes in normoglycemic TS1P<sub>1</sub>KO vehicle mice heart indicate the presence of inflammation as CD34 fibrocytes recruited at the site of tissue injury and inflammation. Notably, CD4<sup>+</sup> T cells recipient TS1P<sub>1</sub>KO vehicle mice spleen and blood showed 40.18% and 62% increase of regulatory CD4<sup>+</sup>Foxp3<sup>+</sup> T cells than TS1P<sub>1</sub>KO vehicle mice without CD4<sup>+</sup> T cells recipient at the end of 11-week experimental period.<sup>152</sup> Adoptive transfer of regulatory T cells in aortic constriction induced murine hypertension model reduced cardiac fibrosis area with reduced TGF-β1 expression in cardiac tissue.<sup>152</sup> In our present work, after CD4<sup>+</sup> T cells transfer to TS1P<sub>1</sub>KO mice, normoglycemic TS1P<sub>1</sub>KO vehicle mice have increased CD4<sup>+</sup>Foxp3<sup>+</sup> T cells in periphery that couples with reduced TGF-β1 and CD34 expression in myocardium with reduced fibrosis compared to TS1P<sub>1</sub>KO vehicle mice without CD4<sup>+</sup> T cells transfer. Regulatory CD4<sup>+</sup>Foxp3<sup>+</sup> T cells maintain immune tolerance in periphery by secreting immunosuppressive cytokines.<sup>68</sup> Hence, increased regulatory CD4<sup>+</sup>Foxp3<sup>+</sup> T cells after CD4<sup>+</sup> T cells transfer to TS1P<sub>1</sub>KO mice could be a possible reason for the reduced fibrosis in TS1P<sub>1</sub>KO vehicle mice.

Altogether, our findings indicate the dual role of CD4<sup>+</sup> T lymphocytes depending on normoglycemia and hyperglycemia. In normoglycemia, CD4<sup>+</sup> T cells presence in peripheral blood is necessary to maintain collagen homeostasis in heart, whereas in chronic hyperglycemia CD4<sup>+</sup> T cells potentiate collagen deposition by activating profibrotic signaling and enhancing proinflammatory cells recruitment to cardiac tissue. Thus, we demonstrated that CD4<sup>+</sup> T lymphocytes as an upstream provocative cellular component in myocardial fibrotic remodeling under chronic hyperglycemic conditions. Our CD4<sup>+</sup> T cells adoptive transfer experiment between littermate and TS1P<sub>1</sub>KO mice further demonstrated the necessity of S1P<sub>1</sub> mediated signaling in CD4<sup>+</sup> T cells trafficking in systemic circulation as well as in cardiac tissue to modulate cardiac fibrotic remodeling both in normal and pathological conditions.

#### **4.5. Conclusions**

The important findings of our present investigation are: (1) supplement of CD4<sup>+</sup> T cells increases myocardial fibrosis in TS1P<sub>1</sub>KO mice under chronic hyperglycemia with enhanced profibrotic milieu; (2) under normoglycemia CD4<sup>+</sup> T cells transfer to TS1P<sub>1</sub>KO mice protects cardiac histology and attenuates fibrosis area; (3) S1P receptor 1 is crucial for CD4<sup>+</sup> T lymphocytes trafficking that can be pharmacologically targeted to alter T lymphocytes trafficking to protect heart under diabetes.

## CHAPTER 5: SUMMARY

T lymphocytes are reported to be involved in cardiac fibrogenesis under cardiac inflammation and injury.<sup>73,77</sup> T cells participate in fibrosis generation by secreting cytokines, growth factors that facilitate profibrotic microenvironment development which stimulate collagen producing fibroblasts.<sup>36,163</sup> Activated fibroblasts, in turn, secrete excessive collagen into myocardium that ensues in fibrosis.<sup>36,165,166</sup> The activation and recruitment of T cells into the myocardium have been observed in hypertension, myocardial infarction, diabetes, pressure overload-induced cardiac injury.<sup>74,76,77,111,152</sup> To this end, enhanced T lymphocytes invasion has been detected in end stage heart failure patient myocardium compared to non-heart failure cardiac tissues.<sup>76</sup> Video microscopic studies revealed T lymphocytes from heart failure patients adhered in significantly higher numbers to activated vascular endothelial cells than T cells from non-heart failure volunteers, indicating subsequent T cells infiltration into the inflamed cardiac tissue.<sup>76</sup> To this end, reduction of T cells infiltration into the myocardium is considered as a potential translational target to protect the heart and reduce fibrosis in cardiovascular diseases.

To target T lymphocytes, the biology of these cells need to be taken in consideration. The activation, proliferation and migration of T lymphocytes to inflamed tissue are regulated through orchestrated innate immune cells i.e. antigen-presenting cells and T lymphocytes interaction in respective tissue draining secondary lymphoid organs i.e. lymph nodes.<sup>90</sup> This paradigm of T cells trafficking has been observed in experimental rodent heart failure and myocardial infarction model.<sup>77,157</sup> After induction of heart failure and myocardial infarction, increased numbers of antigen presenting cells i.e. dendritic cells and T lymphocytes have been detected in heart draining lymph

nodes.<sup>74,75,76</sup> The increased T cells number in heart draining lymph nodes was coupled to increased infiltration of T cells into the myocardium and increased cardiac fibrosis area. In line with these observations, an increased number of recent investigations have demonstrated that inhibition of T lymphocyte function reduces cardiac fibrosis and improves cardiac performance in heart failure and ischemic-reperfusion injury.<sup>77,157</sup> Several approaches, such as, antibody induced neutralization of T cells activation, depletion of T cells in transgenic mice, have been shown to reduce myocardial fibrosis with improved cardiac function.<sup>77,157</sup> To this end, experimental data is scarce to ameliorate cardiac fibrosis by modulating other aspects of T lymphocytes biology.

T lymphocytes trafficking from lymphoid organs to systemic circulation, i.e. blood, is an important aspect in immune response mediation. Naïve T lymphocytes continually recirculate between secondary lymphoid organs and systemic circulation.<sup>90</sup> Activation and proliferation of T lymphocytes occur in secondary lymphoid organs under appropriate microenvironment in response to inflammation, infection and injury. Upon activation, T lymphocytes trafficking from secondary lymphoid organs to periphery and the tissue leads to immune reaction in inflamed tissue. Epidemiological studies have shown increased presence of pro-inflammatory T cells in periphery of diabetic patient.<sup>78,79,110</sup> In experimental rodent diabetic model, enhanced T lymphocytes infiltration into the cardiac tissue has been observed with increased cardiac collagen content and ventricular stiffness.<sup>111</sup> Notably, the effects of T lymphocytes trafficking modulation in diabetes-induced fibrosis is not yet established. In our studies, we aimed to test our hypothesis that inhibition of T lymphocytes trafficking might protect diabetic heart and reduce myocardial fibrosis in chronic diabetes as discussed below.

In this dissertation, we have demonstrated that depletion of T lymphocytes in systemic circulation through modulating sphingosine 1-phosphate receptor 1 (S1P<sub>1</sub>) associated with reduced cardiac fibrosis and improved cardiac contractility in chronic diabetes. The depletion of T cells was achieved with both pharmacological agent – fingolimod (FTY70) and genetic approach – conditional knockout of T cell S1P<sub>1</sub> receptor. In chapter 2, we have shown that treatment with S1P<sub>1</sub> receptor modulator drug FTY720 substantially reduced CD4<sup>+</sup> and CD8<sup>+</sup> T cells number in peripheral blood of wild-type (WT) C57BL/6 mice compared to WT control and untreated diabetic mice. Chronic FTY720 treatment reduced invading CD3<sup>+</sup> T cells number into WT diabetic mice myocardium at the end of 11-week experimental period than untreated WT diabetic mice. In addition, FTY720 treated WT diabetic mice myocardium exhibited reduced expression of profibrotic TGF-β1 and fibroblast progenitor CD34 cells compared to untreated WT diabetic mice. The histology and morphometric analysis revealed that FTY720 improved heart histology and reduced cardiac fibrosis area in diabetic WT mice myocardium compared to untreated WT diabetic mice in chronic diabetes. Further, FTY720 treatment increased cardiac contractility of diabetic WT mice heart compared to untreated WT diabetic mice heart at the end of 11 weeks. We used recombination activating gene 1 knock-out (Rag1 KO) mice lacking mature B and T lymphocytes as a complementary genetic mouse strain of WT C57BL/6 mice. Diabetic Rag1 KO mice exhibited improved heart histology, less cardiac fibrosis and improved contractility compared to untreated WT diabetic mice. Our findings, thus, indicate that T lymphocytes play an important role

in fibrogenesis under diabetes. Paradoxically, we found that FTY720 treatment in Rag1 KO mice increased fibrosis area, deteriorated heart histology and attenuated cardiac contractility under diabetes. These contrary results between WT C57BL/6 and Rag1 KO mice after FTY720 treatment indicate that the drug might be enhancing other fibrotic pathways in absence of T lymphocytes under diabetes. Although FTY720 has high affinity towards binding with S1P<sub>1</sub> receptor, it can also activate other S1P receptors. FTY720 has been reported to bind on S1P<sub>3</sub> receptor on fibroblasts that causes transdifferentiation of these cells into collagen producing myofibroblasts. Therefore, the paradoxical results of FTY720 treatment in Rag1 KO mice set the premise to study S1P<sub>1</sub> mediated T cells trafficking effects in cardiac fibrogenesis by using a more precise genetic approach.

To this end, in chapter 3, we utilized genetic approach to study specifically S1P<sub>1</sub> loss-of-function effect on T lymphocytes trafficking to systemic circulation, and its associated effects in myocardial fibrosis generation in chronic diabetes. We generated conditional T cell specific S1P receptor 1 knock-out (TS1P<sub>1</sub>KO) mice through Cre-loxP approach. TS1P<sub>1</sub>KO mice exhibited marked reduction of CD4<sup>+</sup> and CD8<sup>+</sup> T cells in blood compared to littermate control mice. Under chronic diabetes, TS1P<sub>1</sub>KO mice heart sections exhibited significantly reduced invaded CD3<sup>+</sup> T cells with less fibrosis area compared to littermate mice. We further investigated the effects of reduced CD3<sup>+</sup> T cells into myocardium on profibrotic molecular and cellular milieu by immunohistochemistry. We demonstrated that diabetic TS1P<sub>1</sub>KO mice heart tissue had reduced expression of TGF-β1 and CD34 fibrocytes expression compared to diabetic littermate mice. These results indicate that T lymphocytes in diabetes is involved in myocardial fibrogenesis,

and inhibition of S1P<sub>1</sub> receptor associated altered T cells trafficking exerts cardioprotection in chronic diabetes. Paradoxically, TS1P<sub>1</sub>KO vehicle treated mice at the end of 11-week showed increased cardiac fibrosis area with deteriorated cardiac contractility compared to littermate vehicle mice. Although TS1P<sub>1</sub>KO vehicle mice myocardium had reduced CD3<sup>+</sup> T cells infiltration into myocardium, TGF-β1 and CD34 expression were increased. Our observations is consistent with the literature notion that fibrosis is a complex, multifactorial disease in which both systemic and cardiac resident cells can affect cardiac collagen homeostasis. Notably, in TS1P<sub>1</sub>KO mice blood, two times higher B lymphocytes number have been reported compared to littermate mice. To this end, B lymphocytes have been implicated to secrete autoantibodies that can cause myocytes apoptosis leading to fibrosis generation.<sup>146</sup> Programmed cell death-1 (PD-1) gene knock out mice developed severe form of cardiomyopathy with increased interstitial fibrosis.<sup>145</sup> PD-1 receptor is a negative immune regulator of lymphocytes proliferation, thus, genetic depletion of PD-1 results in increased deposition of IgG antibodies in myocardium. Notably, PD-1 KO mice generated in Rag2 KO mice background did not develop fibrosis indicating important contributions of lymphocytes in maintaining cardiac collagen homeostasis. In line with this finding, in chapter 2 we showed that diabetic Rag1 KO mice have reduced cardiac fibrosis area compared to diabetic WT mice. TS1P<sub>1</sub>KO mice have increased B lymphocytes in circulation, while have substantially reduced T lymphocytes in circulation compared to littermate mice. Imbalance between B and T lymphocytes number might be one of the possible reasons for increased cardiac fibrosis under normoglycemia in TS1P<sub>1</sub>KO mice. To this end, the results shown in chapter 4

demonstrated the effects of reconstitution of splenic CD4<sup>+</sup> T cells from littermate mice to TS1P<sub>1</sub>KO mice on cardiac fibrogenesis and cardiac function.

In chapter 4, we demonstrated that adoptive transfer of naïve CD4<sup>+</sup> T cells from littermate mice spleen exacerbated cardiac fibrosis area and reduced cardiac contractility in TS1P<sub>1</sub>KO mice in chronic diabetes. Infiltrating CD3<sup>+</sup> T cells numbers increased in myocardium of TS1P<sub>1</sub>KO mice after CD4<sup>+</sup> T cells transfer. Further, the reconstitution of CD4<sup>+</sup> T cells increased TGF-β1 and CD34 cell expression in diabetic TS1P<sub>1</sub>KO mice compared to diabetic TS1P<sub>1</sub>KO mice without CD4<sup>+</sup> T cells transfer. Notably, adoptive transfer of one million CD4<sup>+</sup> T cells from littermate mice to TS1P<sub>1</sub>KO mice improved heart histology, reduced cardiac fibrosis area and increased cardiac contractility under normoglycemia compared to normoglycemic TS1P<sub>1</sub>KO mice without TS1P<sub>1</sub>KO mice. We found that CD4<sup>+</sup> T cells transfer increased CD4<sup>+</sup> T cells number in blood and CD4<sup>+</sup>Foxp3<sup>+</sup> T cells number in spleen and blood of TS1P<sub>1</sub>KO vehicle mice compared to TS1P<sub>1</sub>KO vehicle mice without CD4<sup>+</sup> T cells transfer. TS1P<sub>1</sub>KO vehicle mice myocardium exhibited increased CD3<sup>+</sup> T cells presence in their myocardium compared to TS1P<sub>1</sub>KO vehicle mice without CD4<sup>+</sup> T cells transfer. Our immunohistochemistry studies showed that TGF-β1 and CD34 cells expression were reduced in TS1P<sub>1</sub>KO vehicle mice after CD4<sup>+</sup> T cells transfer indicating attenuated profibrotic microenvironment compared to TS1P<sub>1</sub>KO vehicle mice without CD4<sup>+</sup> T cells transfer. Our results, thus, indicate that CD4<sup>+</sup> T cells can play dual role in cardiac fibrosis depending normoglycemic and hyperglycemic conditions. Under normal physiological conditions CD4<sup>+</sup> T cells presence in periphery, i.e., blood, is necessary to maintain collagen homeostasis in cardiac tissue,

while in chronic diabetes CD4<sup>+</sup> T cells facilitate cardiac fibrosis generation by potentiating profibrotic signaling in myocardium.

Overall, following are the key findings in this dissertation:

- (1) T lymphocytes trafficking modulatory drug FTY720-induced CD4<sup>+</sup> and CD8<sup>+</sup> T cells reduction in systemic circulation is associated with cardioprotection and attenuated fibrosis area under chronic diabetes in WT C57BL/6 mice. Lack of T lymphocytes associated cardioprotection in diabetes was confirmed in Rag1 KO mice lacking mature lymphocytes. Contradictory results of FTY720 treatment in Rag1 KO diabetic mice indicate FTY720 can target other fibrotic signaling pathways in absence of T lymphocytes. (Chapter 2)
- (2) Conditional T cell specific S1P receptor 1 (S1P<sub>1</sub>) genetic ablation ensued in marked reduction of CD4<sup>+</sup> and CD8<sup>+</sup> T cells in blood and reduced infiltration of CD3<sup>+</sup> T cells in cardiac tissue under diabetes. Nonetheless, the presence of T lymphocytes in periphery is necessary to maintain collagen homeostasis in TS1P<sub>1</sub>KO mice as TS1P<sub>1</sub>KO mice under normoglycemic condition exhibited exacerbation of fibrosis. (Chapter 3)
- (3) Adoptive transfer of CD4<sup>+</sup> T cells reversed cardioprotection and increased fibrosis area in TS1P<sub>1</sub>KO mice under diabetes, while attenuated fibrosis and improved contractility in TS1P<sub>1</sub>KO normoglycemic mice. Thus, CD4<sup>+</sup> T cells might play dual role depending on peripheral immune compartment composition and pathological conditions in maintaining cardiac fibrosis. (Chapter 4)

In summary, we have demonstrated through pharmacological and genetic approaches that SIP<sub>1</sub> receptor mediated T cells trafficking to periphery is directly responsible for cardiac fibrosis development under chronic hyperglycemic conditions.

Alteration/depletion of T lymphocytes trafficking in periphery by modulating SIP<sub>1</sub> receptor is a novel, promising translational approach to ameliorate myocardial fibrosis, to protect the cardiac histology and improve cardiac contractility in chronic diabetes.

## CHAPTER 6: FUTURE PROSPECTS

Recent studies have shown T lymphocytes involvement in myocardial fibrogenesis in different cardiovascular diseases. To this end, the present study provides evidence that alteration/depletion of T lymphocytes trafficking to systemic circulation through modulation of S1P<sub>1</sub> receptor function is cardioprotective and attenuates cardiac fibrosis under chronic diabetes. Our findings give rise to exciting new research directions to ameliorate diabetic myocardial fibrogenesis as outlined below:

- (1) Although FTY720 treatment has reduced cardiac fibrosis in diabetic WT C57BL/6 mice, but increases fibrosis area in diabetic Rag1 KO mice (chapter 2). Rag1 KO mice lacks mature lymphocytes due to genetic deficiency of Rag1 gene necessary for mature lymphocytes development. FTY720 treatment increased fibrosis area in diabetic Rag1 KO mice. These results indicate FTY720 targets other fibrotic mechanisms which overrides cardioprotective effects of FTY720 in the absence of lymphocytes. Thus, mechanisms of FTY720 induced cardiac fibrosis in Rag1 KO mice under diabetes need to be studied further.
- (2) Genetic depletion of T lymphocytic S1P receptor 1 (S1P<sub>1</sub>) reduces T lymphocytes number substantially and exerts antifibrotic effect under chronic diabetes (chapter 3). The fate of T lymphocytic S1P<sub>1</sub> under high glucose level has not been investigated yet. The implications of S1P<sub>1</sub> mediated signaling in T lymphocytes infiltration to diabetic myocardium should be investigated further.
- (3) We have shown that adoptive transfer of CD4<sup>+</sup> T cells to TS1P<sub>1</sub>KO mice reverses the observed cardioprotection and increases fibrosis in diabetes (chapter 4). Notably, CD4<sup>+</sup> T cells can further differentiate into T<sub>H1</sub>, T<sub>H2</sub>, T<sub>regs</sub> and T<sub>H17</sub>

cells.<sup>68</sup> Thus, further studies on CD4<sup>+</sup> T cells differentiation in chronic diabetic mice and their effects in context of myocardial fibrosis is warranted.

- (4) In our present study, we primarily focused on the extent of CD3<sup>+</sup> T lymphocytes infiltration to myocardium and levels of expression of TGF- $\beta$ 1 and fibrocytes (CD34) invasion. We found that increased fibrosis area was coupled to increased CD34 cells in interstitial space of myocardium. This indicates a direct correlation between CD34 cells and the extent of myocardial fibrosis. Although our immunohistochemical studies detected localization of CD34 cells in myocardium, we did not elucidate the recruitment mechanism of these cells in diabetic myocardium. CD34 cells recruitment to the site of inflammation/injury from the blood occurs through chemokine-chemokine receptor interactions.<sup>61,62,63</sup> Thus, further studies are warranted to understand the chemokine receptor types expressed by diabetic myocardium that facilitates CD34 cells recruitment under inflammatory and profibrotic conditions, and how T lymphocytes modulate the chemokine receptors expression in myocardium, if any.

## REFERENCES

1. Diagnosis and classification of Diabetes Mellitus. American Diabetes Association. *Diabetes Care*. 2008; 31:S62-S67.
2. Grundy SM, Benjamin IJ, Burke GL, Chait A, Eckel RH, Howard BV, Mitch W, Smith SC, Sowers JR. Diabetes and cardiovascular disease: a statement for healthcare professionals from the American Heart Association. *Circulation*. 1999; 100:1134-1146.
3. Forbes JM, Cooper ME. Mechanisms of diabetic complications. *Physiol Rev*. 2013; 93:137-188.
4. Global status report on noncommunicable diseases 2014. Geneva, World Health Organization; 2012.
5. Global health estimates: deaths by cause, age, sex and country, 2000-2012. Geneva, World Health Organization; 2014.
6. National Diabetes Statistics Report: estimates of diabetes and its burden in the United States, 2014. Atlanta, Centers for Disease Control and Prevention, U.S. Department of Health and Human Services; 2014.
7. Mathers CD, Loncar D. Projections of global mortality and burden of disease from 2002 to 2030. *PLoS Med*. 2006; 3:e442.
8. Morrish NJ, Wang SL, Stevens LK, Fuller JH, Keen H. Mortality and causes of death in the WHO Multinational Study of Vascular Disease in Diabetes. *Diabetologia*. 2001; 44:S14-S21.

9. Rubler S, Dlugash J, Yuceoglu YZ, Kumral T, Branwood AW, Grishman A. New type of cardiomyopathy associated with diabetic glomerulosclerosis. *Am J Cardiol.* 1972; 30:595-602.
10. Kannel WB, Hjortland M, Castelli WP. Role of diabetes in congestive heart failure: the Framingham study. *Am J Cardiol.* 1974; 34:29-34.
11. Elliott P, Andersson B, Arbustini E, Bilinska Z, Cecchi F, Charron P, Dubourg O, Kuhl U, Maisch B, McKenna WJ, Monserrat L, Pankuweit S, Rapezzi C, Seferovic P, Tavazzi L, Keren A. Classification of the cardiomyopathies: a position statement from the European Society of Cardiology working group on myocardial and pericardial diseases. *Eur Heart J.* 2008; 29:270-276.
12. Poornima IG, Parikh P, Shannon RP. Diabetic cardiomyopathy: the search for a unifying hypothesis. *Circ Res.* 2006; 98:596-605.
13. Boudina S, Abel ED. Diabetic cardiomyopathy revisited. *Circulation.* 2007; 115:3213-3223.
14. Regan TJ, Lyons MM, Ahmed SS, Levinson GE, Oldewurtel HA, Ahmad MR, Haider B. Evidence for cardiomyopathy in familial diabetes mellitus. *J Clin Invest.* 1977; 60:884-899.
15. De Simone G, Devereux RB, Chinali M, Lee ET, Galloway JM, Barac A, Panza JA, Howard BV. Diabetes and incident heart failure in hypertensive and normotensive participants of the Strong Heart Study. *J Hypertens.* 2010; 28:353-360.
16. Bugger H, Bode C. The vulnerable myocardium: Diabetic Cardiomyopathy. *Hamostaseologie.* 2015; 35:17-24.

17. Ernande L, Derumeaux G. Diabetic cardiomyopathy: myth or reality. *Arch Cardiovasc Dis.* 2012; 105:218-225.
18. Di Bello V, Talarico L, Picano E, Di Muro C, Landini L, Paterni M, Matteucci E, Giusti C, Giampietro O. Increased echodensity of myocardial wall in the diabetic heart: an ultrasound tissue characterization study. *J Am Coll Cardiol.* 1995; 25:1408-1415.
19. Fang ZY, Yuda S, Anderson V, Short L, Case C, Marwick TH. Echocardiographic detection of early diabetic myocardial disease. *J Am Coll Cardiol.* 2003; 41:611-617.
20. Carugo S, Giannattasio C, Calchera I, Paleari F, Gorgoglione MG, Grappiolo A, Gamba P, Rovaris G, Failla M, Mancia G. Progression of functional and structural cardiac alterations in young normotensive uncomplicated type 1 diabetes mellitus. *J Hypertens.* 2001; 19:1675-1680.
21. Poirier P, Bogaty P, Garneau C, Marois L, Dumesnil JG. Diastolic dysfunction in normotensive men with well-controlled type 2 diabetes: importance of maneuvers in echocardiographic screening for preclinical diabetic cardiomyopathy. *Diabetes Care.* 2001; 24:5-10.
22. Di Bonito P, Moio N, Cavuto L, Covino G, Murena E, Scilla C, Turco S, Capaldo B, Sibilio G. Early detection of diabetic cardiomyopathy: usefulness of tissue Doppler imaging. *Diabet Med.* 2005; 22:1720-1725.
23. Shivalkar B, Dhondt D, Goovaerts I, Van Gaal L, Bartunek J, Van Crombrugge P, Vrints C. Flow mediated dilatation and cardiac function in type 1 diabetes mellitus. *Am J Cardiol.* 2006; 97:77-82.

24. Varga ZV, Giricz Z, Liaudet L, Hasko G, Ferdinandy P, Pacher P. Interplay of oxidative, nitrosative/nitrative stress, inflammation, cell death and autophagy in diabetic cardiomyopathy. *Biochim Biophys Acta*. 2015; 1852:232-242.
25. Fiorentino TV, Prioletta A, Zuo P, Folli F. Hyperglycemia-induced oxidative stress and its role in diabetes mellitus related cardiovascular diseases. *Curr Pharm Des*. 2013; 19:5695-5703.
26. Giacco F, Brownlee M. Oxidative stress and diabetic complications. *Circ Res*. 2010; 107:1058-1070.
27. Barnes PJ, Larin M. Mechanisms of disease-nuclear factor-kappa-B: a pivotal transcription factor in chronic inflammatory diseases. *N Engl J Med*. 1997; 336:1066-1071.
28. Bierhaus A, Schiekofe S, Schwaninger M, Andrassy M, Humpert PM, Chen J, Hong M, Luther T, Henle T, Kloting I, Morcos M, Hofmann M, Tritschler H, Weigle B, Kasper M, Smith M, Perry G, Schmidt AM, Stern DM, Haring HU, Schleicher E, Nawroth PP. Diabetes-associated sustained activation of the transcription factor nuclear factor-kappa B. *Diabetes*. 2001; 50:2792-2808.
29. Yamagishi SI, Yonekura H, Yamamoto Y, Katsuno K, Sato F, Mita I, Ooka H, Satozawai N, Kawakami T, Nomura M, Yamamoto H. Advanced Glycation End Products-driven Angiogenesis in Vitro. Introduction of the growth and tube formation of human microvascular endothelial cells through autocrine vascular endothelial growth factor. *J Biol Chem*. 1997; 272:8723-8730.

30. Okon EB, Chung AW, Rauniyar P, Padilla E, Tejerina T, McManus BM, Luo H, van Breemen C. Compromised arterial function in human type 2 diabetic patients. *Diabetes*. 2005; 54: 2415–2423.
31. Diamant M, Lamb HJ, Smit JWA, Roos AD, Heine RJ. Diabetic cardiomyopathy in uncomplicated type 2 diabetes is associated with the metabolic syndrome and systemic inflammation. *Diabetologia*. 2005; 48:1669-1670.
32. Westermann D, Rutschow S, Jäger S, Linderer A, Anker S, Riad A, Unger T, Schultheiss HP, Pauschinger M, Tschöpe C. Contributions of inflammation and cardiac matrix metalloproteinase activity to cardiac failure in diabetic cardiomyopathy: the role of angiotensin type 1 receptor antagonism. *Diabetes*. 2007; 56:641-646.
33. Westermann D, Van Linthout S, Dhayat S, Dhayat N, Schmidt A, Noutsias M, Song XY, Spillmann F, Riad A, Schultheiss HP, Tschöpe C. Tumor necrosis factor-alpha antagonism protects from myocardial inflammation and fibrosis in experimental diabetic cardiomyopathy. *Basic Res Cardiol*. 2007; 102:500-507.
34. Ares-Carrasco S, Picatoste B, Benito-Martin A, Zubiri I, Sanz AB, Sanchez-Nino MD, A. Ortiz, Egidio J, Tunon J, Lorenzo O. Myocardial fibrosis and apoptosis, but not inflammation, are present in long-term experimental diabetes. *Am J Physiol Heart Circ Physiol*. 2009; 297:H2109–H2119.
35. Lechleitner M, Koch T, Herold M, Dzien A, Hoppichler F. Tumour necrosis factor-alpha plasma level in patients with type 1 diabetes mellitus and its association with glycaemic control and cardiovascular risk factors. *J Intern Med*. 2000; 248: 67–76.

36. Kong P, Christia P, Frangogiannis NG. The pathogenesis of cardiac fibrosis. *Cell Mol Life Sci.* 2014; 71:549-574.
37. Fan D, Takawale A, Lee J, Kassiri Z. Cardiac fibroblasts, fibrosis and extracellular matrix remodeling in heart disease. *Fibrogenesis Tissue Repair.* 2012; 5:15.
38. Miki T, Yuda S, Kouzu H, Miura T. Diabetic cardiomyopathy: pathophysiology and clinical features. *Heart Fail Rev.* 2013; 18:149-166.
39. Van Linthout S, Seeland U, Riad A, Eckhardt O, Hohl M, Dhayat N, Richter U, Fischer JW, Bohm M, Pauschinger M, Schultheiss HP, Tschope C. Reduced MMP-2 activity contributes to cardiac fibrosis in experimental diabetic cardiomyopathy. *Basic Res Cardiol.* 2008; 103:319-327.
40. Schaper J, Speiser B. The extracellular matrix in the failing human heart. *Basic Res Cardiol.* 1992; 87:303-309.
41. Bosman FT, Stamenkovic I. Functional structure and composition of the extracellular matrix. *J Pathol.* 2003; 200:423-428.
42. Burlew BS, Weber KT. Cardiac fibrosis as a cause of diastolic dysfunction. *Herz.* 2002; 27:92-98.
43. Manabe I, Shindo T, Nagai R. Gene expression in fibroblasts and fibrosis: involvement in cardiac hypertrophy. *Circ Res.* 2002; 91:1103-1113.
44. Ahmed SH, Clark LL, Pennington WR, Webb CS, Bonnema DD, Leonardi AH, McClure CD, Spinale FG, Zile MR. Matrix metalloproteinases/tissue inhibitors of metalloproteinases: relationship between changes in proteolytic determinants of

- matrix composition and structural, functional, and clinical manifestations of hypertensive heart disease. *Circulation*. 2006; 113:2089-2096.
45. De Leeuw N, Ruiter DJ, Balk AH, De Jonge N, Melchers WJ, Galama JM. Histopathologic findings in explanted heart tissue from patients with end-stage idiopathic dilated cardiomyopathy. *Transpl Int*. 2001; 14:299-306.
46. Mewton N, Liu CY, Croisille P, Bluemke D, Lima JAC. Assessment of myocardial fibrosis with cardiovascular magnetic resonance. *J Am Coll Cardiol*. 2011; 57:891-903.
47. Pichler M, Rainer PP, Schauer S, Hoefler G. Cardiac fibrosis in human transplanted hearts is mainly driven by cells of intracardiac origin. *J Am Coll Cardiol*. 2012; 59:1008-1016.
48. Sabbah HN, Sharov VG, Lesch M, Goldstein S. Progression of heart failure: a role for interstitial fibrosis. *Mol Cell Biochem*. 1995; 147:29-34.
49. Fujii K, Nagai R. Contributions of cardiomyocyte-cardiac fibroblast-immune cell interactions in heart failure development. *Basic Res Cardiol*. 2013; 108:357.
50. Wu L, Derynck R. Essential role of TGF- $\beta$ 1 signaling in glucose-induced cell hypertrophy. *Dev Cell*. 2009; 17:35-48.
51. Rosenkranz S. TGF- $\beta$ 1 and angiotensin networking in cardiac remodeling. *Cardiovasc Res*. 2004; 63:423-432.
52. Dobaczewski M, Chen W, Frangogiannis NG. Transforming growth factor beta (TGF)-beta signaling in cardiac remodeling. *J Mol Cell Cardiol*. 2011; 51:600-606.

53. Biernacka A, Dobaczewski M, Frangogiannis NG. TGF-beta signaling in fibrosis. *Growth factors*. 2011; 29:196-202.
54. Li RK, Li G, Mickle DA, Weisel RD, Merante F, Luss H, Rao V, Christakis GT, Williams WG. Overexpression of transforming growth factor-beta 1 and insulin-like growth factor-1 in patients with idiopathic hypertrophic cardiomyopathy. *Circulation*. 1997; 96:874-881.
55. Border WA, Noble NA. Transforming growth factor  $\beta$  in tissue fibrosis. *N Engl J Med*. 1994; 331:1286-1292.
56. Smith JC. Mesoderm-inducing factors in early vertebrate development. *EMBO J*. 1993; 12:4463-4470.
57. Eghbali M. Cellular origin and distribution of transforming growth factor-beta in the normal rat myocardium. *Cell Tissue Res*. 1989; 256:553-558.
58. Kupfahl C, Pink D, Friedrich K, Zurbrugg HR, Neuss M, Warnecke C, Fielitz J, Graf K, Fleck E, Regitz-Zagrosek V. Angiotensin II directly increases transforming growth factor beta 1 and osteopontin and indirectly affects collagen mRNA expression in the human heart. *Cardiovasc Res*. 2000; 46:463-475.
59. Thompson NL. Transforming growth factor-beta 1 in acute myocardial infarction in rats. *Growth factors*. 1988; 1:91-99.
60. Volders PGA, Willems IEMG, Cleutjens JPM, Arends JW, Havenith MG, Daemen MJAP. Interstitial collagen is increased in the non-infarcted human myocardium after myocardial infarction. *J Mol Cell Cardiol*. 1993; 25: 1317-1323.

61. Bellini A, Mattoli S. The role of the fibrocyte, a bone marrow-derived mesenchymal progenitor, in reactive and reparative fibroses. *Lab Invest.* 2007; 87:858-870.
62. Reilkoff RA, Bucala R, Herzog EL. Fibrocytes: emerging effector cells in chronic inflammation. *Nat Rev Immunol.* 2011; 11:427-435.
63. Peng H, Herzog EL. Fibrocytes: emerging effector cell in chronic inflammation. *Curr Opin Pharmacol.* 2012; 12:491-496.
64. Bucala R, Spiegel LA, Chesney J, Hogan M, Cerami A. Circulating fibrocytes define a new leukocyte subpopulation that mediates tissue repair. *Mol Med.* 1994; 1:71-81.
65. Pilling D, Fan T, Huang D, Kaul B, Gomer RH. Identification of markers that distinguish monocyte-derived fibrocytes from monocytes, macrophages, and fibroblasts. *PLoS ONE.* 2009; 4:e7475.
66. Heart outcomes prevention evaluation study investigators. Effects of Ramipril on cardiovascular and microvascular outcomes in people with diabetes mellitus: results of the HOPE study and MICRO-HOPE substudy. *Lancet.* 2000; 355:253-259.
67. Zannad F, Alla F, Dousset B, Perez A, Pitt B. Limitation of excessive extracellular matrix turnover may contribute to survival benefit of spironolactone therapy in patients with congestive heart failure: insights from the randomized aldactone evaluation study (RALES). *Circulation.* 2000; 102:2700-2706.
68. Zhu J, Paul WE. CD4 T cells: fates, functions, and faults. *Blood.* 2008; 112:1557-1568.

69. Yu Q, Watson RR, Marchalonis JJ, Larson DF. A role for T lymphocytes in mediating cardiac diastolic function. *Am J Physiol Heart Circ Physiol*. 2005; 289:H643-651.
70. Yu Q, Vazquez R, Zabadi S, Watson RR, Larson DF. T-lymphocytes mediate left ventricular fibrillary collagen cross-linking and diastolic dysfunction in mice. *Matrix Biol*. 2010; 29:511-518.
71. Yuan W, Yufit T, Li L, Mori Y, Chen SJ, Varga J. Negative modulation of alpha1(I) procollagen gene expression in human skin fibroblasts: transcriptional inhibition by interferon-gamma. *J Cell Physiol*. 1999; 179:97-108.
72. Yu Q, Horak K, Larson DF. Role of T lymphocytes in hypertension-induced cardiac extracellular matrix remodeling. *Hypertension*. 2006; 48:98-104.
73. Wei L. Immunological aspect of cardiac remodeling: T lymphocyte subsets in inflammation-mediated cardiac fibrosis. *Exp Mol Pathol*. 2011; 90:74-78.
74. Hofmann U, Beyersdorf N, Weirather J, Podolskaya A, Bauersachs J, Ertl G, Kerkau T, Frantz S. Activation of CD4<sup>+</sup> T lymphocytes improves wound healing and survival after experimental myocardial infarction in mice. *Circulation*. 2012; 125:1652-1663.
75. Laroumanie F, Douin-Echinard V, Pozzo J, Lairez O, Tortosa F, Vinel C, Delage C, Calise D, Dutaur M, Parini A, Pizzinat N. CD4<sup>+</sup> T cells promote the transition from hypertrophy to heart failure during chronic pressure overload. *Circulation*. 2014; 129:2111-2124.

76. Nevers T, Salvador AM, Grodecki-Pena A, Knapp A, Vellazquez F, Aronovitz M, Kapur NK, Karas RH, Blanton RM, Alcaide P. Left ventricular T cell recruitment contributes to the pathogenesis of heart failure. *Circ Heart Fail.* 2015; 8:776-787.
77. Hofmann U, Frantz S. Role of lymphocytes in myocardial injury, healing, and remodeling after myocardial infarction. *Circ Res.* 2015; 116:354-367.
78. Prabhu SD. Cytokine-induced modulation of cardiac function. *Circ Res.* 2004; 95:1140-1153.
79. Tamariz L, Hare JM. Inflammatory cytokines in heart failure: role in aetiology and utility as biomarkers. *Eur Heart J.* 2010; 31:768-770.
80. Mann DL. Inflammatory mediators and the failing heart: past, present, and the foreseeable future. *Circ Res.* 2002; 91:988-998.
81. Pedicino D, Liuzzo G, Trotta F, Giglio AF, Giubilato S, Martini F, Zaccardi F, Scavone G, Previtiero M, Massaro G, Cialdella P, Cardillo MT, Pitocco D, Ghirlanda G, Crea F. Adaptive immunity, inflammation, and cardiovascular complications in type 1 and type 2 diabetes mellitus. *J Diabetes Res.* 2013; <http://dx.doi.org/10.1155/2013/184258>.
82. Zhao RX, Li WJ, Lu YR, Qin J, Wu CL, Tian M, He TY, Yi SN, Tang DQ, Sun L, Chen L. Increased peripheral proinflammatory T helper subsets contribute to cardiovascular complications in diabetic patients. *Mediators Inflamm.* 2014; <http://dx.doi.org/10.1155/2014/596967>.
83. Allende ML, Dreier JL, Mandala S, Proia RL. Expression of the sphingosine 1-phosphate receptor, S1P<sub>1</sub> on T-cells controls thymic emigration. *J Biol Chem.* 2004; 279:15396-15401.

84. Brinkmann V. Sphingosine 1-phosphate receptors in health and disease: mechanistic insights from gene deletion studies and reverse pharmacology. *Pharmacol Ther.* 2007; 115:84-105.
85. Rosen H, Goetzl EJ. Sphingosine 1-phosphate and its receptors: an autocrine and paracrine network. *Nat Rev Immunol.* 2005; 5:560-570.
86. Saba JD, Hla T. Point-counterpoint of sphingosine 1-phosphate metabolism. *Circ Res.* 2004; 94:724-734.
87. Spiegel S, Milstein S. Sphingosine-1-phosphate: an enigmatic signaling lipid. *Nat Rev Mol Cell Biol.* 2003; 4:397-407.
88. Camm J, Hla T, Bakshi R, Brinkmann V. Cardiac and vascular effects of fingolimod: mechanistic basis and clinical implications. *Am Heart J.* 2014; 632-644.
89. Garris CS, Blaho VA, Hla T, Han MH. Sphingosine-1-phosphate receptor 1 signalling in T cells: trafficking and beyond. *Immunology.* 2014; 142:347-353.
90. Owen JA, Punt J, Stranford SA, Jones PP. The immune response in space and time. In: *Kuby Immunology.* 7<sup>th</sup> ed. New York, NY: W. H. Freeman; 2013:451-484.
91. Brinkmann V, Davis MD, Heise CE, Albert R, Cottens S, Hof R, Bruns C, Prieschl E, Baumruker T, Hiestand P, Foster CA, Zollinger M, Lynch KR. The immune modulator FTY720 targets sphingosine 1-phosphate receptors. *J Biol Chem.* 2002; 277:21453-21457.

92. Brinkmann V, Billich A, Baumruker T, Heining P, Schmouder R, Francis G, Aradhye S, Burtin P. Fingolimod (FTY720): discovery and development of an oral drug to treat multiple sclerosis. *Nat Rev Drug Discov.* 2010; 9:883-897.
93. Paugh SW, Payne SG, Barbour SE, Milstein S, Spiegel S. The immunosuppressant FTY720 is phosphorylated by sphingosine kinase type 2. *FEBS Lett.* 2003; 554:189-193.
94. Skyes DA, Riddy DM, Stamp C, Bradley ME, McGuinness N, Sattikar A, Guerini D, Rodrigues I, Glaenzel AI, Dowling MR, Mullershausen F, Charlton SJ. Investigation the molecular mechanisms through which FTY720-P causes persistent S1P<sub>1</sub> receptor internalization. *Br J Pharmacol.* 2014; 171:4797-4807.
95. Chiba K, Yanagawa Y, Masubuchi Y, Kataoka H, Kawaguchi T, Ohtsuki M, Hoshino Y. FTY720, a novel immunosuppressant, induces sequestration of circulating mature lymphocytes by acceleration of lymphocyte homing in rats. I. FTY720 selectively decreases the number of circulating mature lymphocytes by acceleration of lymphocyte homing. *J Immunol.* 1998; 160:5037-5044.
96. Lenzen S. The mechanisms of alloxan- and streptozotocin-induced diabetes. *Diabetologia.* 2008; 51:216-226.
97. Uchigata Y, Yamamoto H, Kawamura A, Okamoto H. Protection by superoxide dismutase, catalase, and poly (ADP-ribose) synthetase inhibitors against alloxan- and streptozotocin-induced islet DNA strand breaks and against the inhibition of proinsulin synthesis. *J Biol Chem.* 1982; 257:6084-6088.

98. Yamamoto H, Uchigata Y, Okamoto H. Streptozotocin and alloxan induce DNA strand breaks and poly (ADP-ribose) synthetase in pancreatic islets. *Nature*. 1981; 294:284–286.
99. Sandler S, Swenne I. Streptozotocin, but not alloxan, induces DNA repair synthesis in mouse pancreatic islets in vitro. *Diabetologia*. 1983; 25:444–447.
100. Bugger H, Abel ED. Rodent models of diabetic cardiomyopathy. *Dis Model Mech*. 2009; 2:454-466.
101. Fuentes-Antras J, Picatoste B, Gomez-Hernandez A, Egido J, Tunon J, Lorenzo O. Updating experimental models of diabetic cardiomyopathy. *J Diabetes Res*. 2015; 656795:15. <http://dx.doi.org/10.1155/2015/656795>
102. McVerry BJ, Garcia J GN. Endothelial cell barrier regulation by sphingosine 1-phosphate. *J Cell Biochem*. 2004; 92:1075-1085.
103. Weyden LVD, Adams DJ, Bradley A. Tools for targeted manipulation of the mouse genome. *Physiol Genomics*. 2002; 11:133-164.
104. Sun Z. Overview of recent advances in molecular cardiology. *Can J Cardiol*. 2006; 22:235-240.
105. Sohal DS, Nghiem M, Crackower MA, Witt SA, Kimball TR, Tymitz KM, Penninger JM, Molkentin JD. Temporally regulated and tissue-specific gene manipulations in the adult and embryonic heart using a tamoxifen-inducible Cre protein. *Circ Res*. 2001; 89:20-25.

106. Strachan T, Read A. Genetic manipulation of animals for modeling disease and investigating gene function. In: *Human Molecular Genetics*. 4<sup>th</sup> ed. New York: Garland Science; 2011:639-673.
107. Bugger H, Abel DE. Molecular mechanisms of diabetic cardiomyopathy. *Diabetologia*. 2014; 57:660-671.
108. Li J, Zhu H, Shen E, Wan Li, Arnold MO, Peng T. Deficiency of Rac1 blocks NADPH oxidase activation, inhibits endoplasmic reticulum stress, and reduces myocardial remodeling in a mouse model of type 1 diabetes. *Diabetes*. 2010; 59:2033-2042.
109. Heerebeek LV, Hamdani N, Handoko ML, Falcao-Pires I, Musters RJ, Kupreishvili K, Ijsselmuiden AJ, Schalkwijk CG, Bronzwaer JG, Diamant M, Borbely A, Velden JVD, Stienen GJ, Laarman GJ, Niessen HW, Paulus WJ. Diastolic stiffness of the failing diabetic heart: importance of fibrosis, advanced glycation end products, and myocyte resting tension. *Circulation*. 2008; 117:43-51.
110. Giubilato S, Liuzzo G, Brugaletta S, Pitocco D, Graziani F, Smaldone C, Montone RA, Pazzano V, Pedicino D, Biasucci LM, Ghirlanda G, Crea F. Expansion of CD4<sup>+</sup>CD28<sup>null</sup> T-lymphocytes in diabetic patients: exploring new pathogenetic mechanisms of increased cardiovascular risk in diabetes mellitus. *Eur Heart J*. 2011; 32:1214-1226.
111. Becher PM, Lindner D, Frohlich M, Savvatis K, Westermann D, Tschope C. Assessment of cardiac inflammation and remodeling during the development of streptozotocin-induced diabetic cardiomyopathy *in vivo*: a time course analysis. *Int J Mol Med*. 2013; 32:158-164.

112. Haudek SB, Cheng J, Du J, Wang Y, Rodriguez JM, Trial J, Taffet GE, Entman ML. Monocytic fibroblast precursors mediate fibrosis in angiotensin-II-induced cardiac hypertrophy. *J Mol Cell Cardiol.* 2010; 49:499-507.
113. Mombaerts P, Iacomini J, Johnson RS, Herrup K, Tonegawa S, Papaioannou VE. Rag-1-deficient mice have no mature B and T lymphocytes. *Cell.* 1992; 68:869-877.
114. Matloubian M, Lo CG, Cinamon G, Lesneski MJ, Xu Y, Brinkmann V, Allende ML, Proia RL, Cyster JG. Lymphocyte egress from thymus and peripheral lymphoid organs is dependent on S1P receptor 1. *Nature.* 2004; 427:355-360.
115. Mandala S, Hajdu R, Bergstrom J, Quackenbush E, Xie J, Milligan J, Thornton R, Shei GJ, Card D, Keohane C, Rosenbach M, Hale J, Lynch CL, Rupprecht K, Parsons W, Rosen H. Alteration of lymphocyte trafficking by sphingosine 1-phosphate receptor agonists. *Science.* 2002; 296:346-349.
116. Zhang F, Xia Y, Yan W, Zhang H, Zhou F, Zhao S, Wnag W, Zhu D, Xin C, Lee Y, Zhang L, He Y, Gao E, Tao L. Sphingosine 1-phosphate signaling contributes to cardiac inflammation, dysfunction, and remodeling following myocardial infarction. *Am J Physiol Heart Circ Physiol.* 2015; doi:10.1152/ajpheart.00372.2015.
117. Li Z, Abdullah CS, Jin ZJ. Inhibition of PKC- $\theta$  preserves cardiac function and reduces fibrosis in streptozotocin-induced diabetic cardiomyopathy. *Br J Pharmacol.* 2014; 171:2913-2924.
118. Jin ZQ, Goetzl EG, Karliner JS. Sphingosine kinase activation mediates ischemic preconditioning in murine. *Circulation.* 2004; 110:1980-1989.

119. Xi L, Das A, Zhao ZQ, Merino VF, Bader M, Kukreja RC. Loss of myocardial ischemic preconditioning in adenosine A1 and bradykinin B2 receptors gene knockout mice. *Circulation*. 2008; 118:S32-S37.
120. Dong R, Liu P, Wee L, Butany J, Sole MJ. Verapamil ameliorates the clinical and pathological course of murine myocarditis. *J Clin Invest*. 1992; 90:2022-2030.
121. Klopfeisch R. Multiparametric and semiquantitative scoring systems for the evaluation of mouse model histopathology – a systematic review. *BMC Vet Res*. 2013; 9:123.
122. Lu J, Yao Y, Dai Q, Ma G, Zhang S, Cao L, Ren L, Liu N. Erythropoietin attenuates cardiac dysfunction by increasing myocardial angiogenesis and inhibiting interstitial fibrosis in diabetic rats. *Cardiovasc Diabetol*. 2012; 11:105.
123. Lan T, Bi H, Liu W, Xie X, Xu S, Huang H. Simultaneous determination of sphingosine and sphingosine 1-phosphate in biological samples by liquid chromatography-tandem mass spectrometry. *J Chromatogr B Analyt Technol Biomed Life Sci*. 2011; 879:520-526.
124. Schmidt H, Schmidt R, Geisslinger G. LC-MS/MS-analysis of sphingosine-1-phosphate and related compounds in plasma samples. *Prostaglandins other Lipid Mediat*. 2006; 81:162-170.
125. Like AA, Rossini AA. Streptozotocin-induced pancreatic insulinitis: new model of diabetes mellitus. *Science*. 1976; 193:415-417.
126. Lim H, Zhu YZ. Role of transforming growth factor- $\beta$  in the progression of heart failure. *Cell Mol Life Sci*. 2006; 63:2584-2596.

127. Liang J, Nagahashi M, Kim EY, Harikumar KB, Yamada A, Huang WC, Hait NC, Allegood JC, Price MM, Avni D, Takabe K, Kordula T, Milstien S, Spiegel S. Sphingosine-1-phosphate links persistent STAT3 activation, chronic intestinal inflammation, and development of colitis-associated cancer. *Cancer Cell*. 2013; 23:107-120.
128. Sobel K, Monnier L, Menyhart K, Bolinger M, Studer R, Nayler O, Gatfield J. FTY720 Phosphate Activates Sphingosine-1-Phosphate Receptor 2 and Selectively Couples to G $\alpha$ 12/13/Rho/ROCK to Induce Myofibroblast Contraction. *Mol Pharmacol*. 2015; 87:916-927.
129. Tschöpe C, Walther T, Escher F, Spillmann F, Du J, Altmann C, Schimke I, Bader M, Sanchez-Ferrer CF, Schultheiss HP, Noutsias M. Transgenic activation of the kallikrein-kinin system inhibits intramyocardial inflammation, endothelial dysfunction and oxidative stress in experimental diabetic cardiomyopathy. *FASEB J*. 2005; 19:2057-2059.
130. Peng X, Hassoun PM, Sammani S, McVerry BJ, Burne MJ, Rabb H, Pearse D, Tudor RM, Garcia JGN. Protective effects of sphingosine 1-phosphate in murine endotoxin-induced inflammatory lung injury. *Am J Respir Crit Care Med*. 2004; 169:1245-1251.
131. Shea BS, Brooks SF, Fontaine BA, Chun J, Luster AD, Tager AM. Prolonged exposure to sphingosine 1-phosphate receptor-1 agonists exacerbates vascular leak, fibrosis, and mortality after lung injury. *Am J Respir Cell Mol Biol*. 2010; 43:662-673.

132. Yin Z, Fan L, Wei L, Gao H, Zhang R, Tao L, Cao F, Wang H. FTY720 protects cardiac microvessels of diabetes: a critical role of S1P1/3 in diabetic heart disease. *PLoS One*. 2012; 7:e42900.
133. Kraft P, Gob E, Schuhmann MK, Gobel K, Deppermann C, Thielmann I, Herrmann AM, Lorenz K, Brede M, Stoll G, Meuth SG, Nieswandt B, Pfeilschifter W, Kleinschnitz C. FTY720 ameliorates acute ischemic stroke in mice by reducing thrombo-inflammation but not by direct neuroprotection. *Stroke*. 2013; 44:3202-3210.
134. Kovarik JM, Schmouder R, Barilla D, Wnag Y, Karus G. Single-dose FTY720 pharmacokinetics, food effect, and pharmacological responses in healthy subjects. *Br J Clin Pharmacol*. 2004; 57:586-591.
135. Park SI, Felipe CR, Machado PG, Garcia R, Skerjance A, Schmouder R, Silva HT, Pestana JOM. Pharmacokinetic/pharmacodynamic relationships of FTY720 in kidney transplant treatments. *Braz J Med Biol Res*. 2005; 38:683-694.
136. Keller CD, Gil PR, Tolle M, Giet MVD, Chun J, Radeke HH, Korting MS, Kleuser B. Immunomodulator FTY720 induces myofibroblast differentiation via the lysophospholipid receptor S1P<sub>3</sub> and Smad3 signaling. *Am J Pathol*. 2007; 170:281-292.
137. Allende ML, Yamashita T, Proia RL. G-protein-coupled receptor S1P<sub>1</sub> acts within endothelial cells to regulate vascular maturation. *Blood*. 2003; 102:3665-3667.
138. Truett GE, Heeger P, Mynatt RL, Truett AA, Walker JA, Warman JA, Warman ML. Preparation of PCR-quality mouse genomic DNA with hot sodium hydroxide and Tris (HotSHOT). *Biotechniques*. 2000; 29:52-54.
139. Westermann D, Van Linthout S, Dhayat S, Dhayat N, Escher F, Bucker-Gartner C, Spillmann F, Noutsias M, Riad A, Schultheiss HP, Tschope C. Cardioprotective and

anti-inflammatory effects of interleukin converting enzyme inhibition in experimental diabetic cardiomyopathy. *Diabetes*. 2007; 56:1834-1841.

140. Blaho VA, Hla T. An update on the biology of sphingosine 1-phosphate receptors. *J Lipid Res*. 2014; 55:1596-1608.

141. Liu G, Burns S, Huang G, Boyd K, Proia RL, Flavell RA, Chi H. The receptor S1P<sub>1</sub> overrides regulatory T cell-mediated immune suppression through Akt-mTOR. *Nat Immunol*. 2009; 10:769-777.

142. Liu G, Yang K, Burns S, Shrestha S, Chi H. The S1P<sub>1</sub>-mTOR axis directs the reciprocal differentiation of T<sub>H</sub>1 and Treg cells. *Nat Immunol*. 2010; 11:1047-1056.

143. Zhen Y, Sun L, Liu H, Duan K, Zeng C, Zhang L, Jin D, Peng J, Ding W, Zhao Y. Alterations of peripheral CD4<sup>+</sup>CD25<sup>+</sup>Foxp3<sup>+</sup> T regulatory cells in mice with STZ-induced diabetes. *Cell Mol Immunol*. 2012; 9:75-85.

144. Epelman S, Liu PP, Mann DL. Role of innate and adaptive immune mechanisms in cardiac injury and repair. *Nat Rev Immunol*. 2015; 15:117-129.

145. Nishimura H, Okazaki T, Tanaka Y, Nakatani K, Hara M, Matsumori A, Sasayama S, Mizoguchi A, Hiai H, Minato N, Honjo T. Autoimmune dilated cardiomyopathy in PD-1 receptor-deficient mice. *Science*. 291:319-322.

146. Cordero-Reyes AM, Youker KA, Torre-Amione G. The role of B-cells in heart failure. *Methodist Debaquey Cardiovasc J*. 2013; 9:15-19.

147. Mann DL. Inflammatory mediators and the failing heart: past, present, and the foreseeable future. *Circ Res*. 2002; 91:988-998.

148. Bolli MH, Abele S, Binkert C, Bravo R, Buchmann S, Bur D, Gatfield J, Hess P, Kohl C, Mangold C, Mathys B, Menyhart K, Muller C, Nayler O, Scherz M, Schmidt

G, Sippel V, Steiner B, Strasser D, Treiber A, Weller T. 2-imino-thiazolidin-4-one derivatives as potent, orally active S1P<sub>1</sub> receptor agonists. *J Med Chem.* 2010; 53:4198-4211.

149. Piali L, Froidevaux S, Hess P, Nayler O, Bolli MH, Schlosser E, Kohl C, Steiner B, Clozel M. The selective sphingosine 1-phosphate receptor 1 agonist Ponesimod protects against lymphocyte-mediated tissue inflammation. *J Pharmacol Exp Ther.* 2011; 337:547-556.

150. Barron L, Wynn TA. Fibrosis is regulated by Th2 and Th17 responses and by dynamic interactions between fibroblasts and macrophages. *Am J Physiol Gastrointest Liver Physiol.* 2011; 300:G723-G728.

151. Baldeviano GC, Barin JG, Talor MV, Srinivasan S, Bedja D, Zheng D, Gabrielson K, Iwakura Y, Rose NR, Cihakova D. Interleukin-17A is dispensable for myocarditis but essential for the progression to dilated cardiomyopathy. *Circ Res.* 2010; 106:1646-1655.

152. Kanellakis P, Dinh TN, Agrotis A, Bobik A. CD4(+) CD25(+)Foxp3(+) regulatory T cells suppress cardiac fibrosis in the hypertensive heart. *J Hypertens.* 2011; 29:1820–1828.

153. Kvakan H, Kleinewietfeld M, Qadri F, Park JK, Fischer R, Schwarz I, Rahn HP, Plehm R, Wellner M, Elitok S, Gratzke P, Dechend R, Luft FC, Muller DN. Regulatory T cells ameliorate angiotensin II-induced cardiac damage. *Circulation.* 2009; 119:2904–2912.

154. Tang TT, Yuan J, Zhu ZF, Zhang WC, Xiao H, Xia N, Yan XX, Nie SF, Liu J, Zhou SF, Li JJ, Yao R, Liao MY, Tu X, Liao YH, Cheng X. Regulatory T cells

ameliorate cardiac remodeling after myocardial infarction. *Basic Res Cardiol.* 2012; 107:232.

155. Niedermeier M, Reich B, Rodriguez Gomez M, Denzel A, Schmidbauer K, Gobel N, Talke Y, Schweda F, Mack M. CD4<sup>+</sup> T cells control the differentiation of Gr1<sup>+</sup> monocytes into fibrocytes. *Proc Natl Acad Sci U S A.* 2009; 106:17892-17897.

156. Owen JA, Punt J, Stranford SA. Receptors and signaling: B and T-cell receptors. In: *Kuby Immunology*. 7<sup>th</sup> ed. New York, NY: W. H. Freeman and Company; 2013:65-103.

157. Frieler RA, Mortensen RM. Immune cell and other noncardiomyocyte regulation of cardiac hypertrophy and remodeling. *Circulation.* 2015; 131:1019-1030.

158. Van Linthout S, Miteva K, Tschöpe C. Crosstalk between fibroblasts and inflammatory cells. *Cardiovasc Res.* 2014; 102:258-269.

159. Asbun J, Villarreal FJ. The pathogenesis of myocardial fibrosis in the setting of diabetic cardiomyopathy. *J Am Coll Cardiol.* 2006; 47:693-700.

160. Chiamonte MG, Donaldson DD, Cheever AW, Wynn TA. An IL-13 inhibitor blocks the development of hepatic fibrosis during a T-helper type 2-dominated inflammatory response. *J Clin Invest.* 1999; 104:777-785.

161. Wynn TA. Integrating mechanisms of pulmonary fibrosis. *J Exp Med.* 2011; 208:1339-1350.

162. Cieslik KA, Taffet GE, Carlson S, Hermosillo J, Trial J, Entman ML. Immune-inflammatory dysregulation modulates the incidence of progressive fibrosis and diastolic stiffness in the aging heart. *J Mol Cell Cardiol.* 2011; 50:248-256.

163. Russo I, Frangogiannis NG. Diabetes-associated cardiac fibrosis: cellular effectors, molecular mechanisms and therapeutic opportunities. *J Mol Cell Cardiol.* 2016; 90:84-93.
164. Wynn TA. Cellular and molecular mechanisms of fibrosis. *J Pathol.* 2008; 214:199-210.
165. Krenning G, Zeisberg EM, Kalluri R. The origin of fibroblasts and mechanism of cardiac fibrosis. *J Cell Physiol.* 2010; 225:631-637.
166. Leask A. Getting to the heart of the matter: new insights into cardiac fibrosis. *Circ Res.* 2015; 116:1269-1276.